Synthesis and studies on modified oligonucleotides for diagnostic and therapeutic applications

A thesis submitted to the Board of Mathematical, Physical and Life Sciences Division, Department of Chemistry in partial fulfilment for the degree of

Doctor of Philosophy

Chunsen Bai

Wolfson College, University of Oxford
Michaelmas Term 2022

Declaration

I, Chunsen Bai, declare that the thesis titled “Synthesis and studies on modified oligonucleotides for diagnostic and therapeutic applications” and the related research presented in this thesis was performed and written by the author under the supervision of Prof. Tom Brown at the University of Oxford. The research is original and has not been submitted in full or in part for any other degree at this or at any other university. The copyright of this thesis rests with the author.

Abstract

This thesis describes two different but related areas: intercalative thiazole orange (TO) probes and artificial DNA backbones. Thiazole orange (TO) is an asymmetric cyanine dye that is used to detect nucleic acids by fluorescence due to its intercalating characteristics, which results in an "on-off" fluorescent switch on binding to complementary nucleic acids. Modified nucleic acid backbones improve the half-lives of therapeutic oligonucleotides *in vivo* by conferring resistance to nuclease enzymic digestion. These two areas are both potentially important role in terms of diagnostic and therapeutic oligonucleotide properties.

The use of TO in various fluorogenic probe systems is described in this thesis. Phosphoramidite monomers based on a thymidine nucleoside with alkyne and amine modifications at the 5-position of the base, and with various lengths of amine linker (C3, C6) were designed for the orthogonal labelling of oligonucleotides at thymine sites. A single tube labelling technique was developed to functionalise the amino group via amide bond formation and the alkyne by CuAAC click chemistry (1,4-disubstituted 1,2,3-triazole formation). These new monomers were tested in oligonucleotide probes designed to facilitate fluorescence resonance energy transfer (FRET) between TO and a FRET acceptor/reporter dye (e.g. ROX) on binding to their complementary DNA or RNA targets. The steady state and time-resolved fluorescence properties of these modified oligonucleotides were investigated. Thermal duplex melting experiments revealed a beneficial increase in melting temperature (T_m) due to the presence of single or multiple

thiazole orange dyes, whereas the reporter dye caused duplex destabilisation. These new combination probes were used to detect a SARS-COV-2 sequence in a LAMP (Loop-mediated isothermal amplification) assay where they provided good specificity and high sensitivity.

The synthesis and properties of oligonucleotides modified with triazole-locked nucleic acids (TL-LNA) were studied with antisense applications in mind. Triazole backbones are charge neutral five-atom connections that have previously been shown to be duplex destabilising, hence inappropriate for antisense applications. I show that the thermal stability of oligonucleotides containing the TL backbone bound to complementary RNA targets is improved when the triazole is combined with a locked nucleic acid sugar on the 3´-side of the triazole ring. TL-LNA nucleoside phosphoramidite dimers were synthesised to make the required oligonucleotide sequences. LNA-TLs of the kind produced in this study have more favourable properties than previous TL modifications.

Acknowledgements

I would like to thank my supervisor, Professor Tom Brown, for his continuous support in my DPhil research studies. I appreciate very much that he was always helpful and patient when I had some difficulties in my research. It was truly a pleasure to work with him. I have to say many thanks to Dr. Afaf El-Sagheer because she always helped me to figure out some experimental problems in the lab and efficiently synthesised many oligonucleotides.

I was also lucky to go through my DPhil studies with the Brownies – my lovely labmates: Aaron, Alice, Ben, Brendan, Cameron, Cheng, Chole, Friedrich, Jack, Jinfeng, Jerry, Jagannath, Laura, Lilian, Nicolo, Phoebe, Piotr, Przemyslaw, Pui, Sebastian, Sven, Yssy, and Yutong. They always cheered me up when I was frustrated with my work. I have to specifically thank Piotr and Cheng – for publishing my first paper together; thanks to Alice and Ben for proofreading my thesis.

I am so grateful that I also have got some of my best friends at this time: Xu, Zhiwei, Yueqi, Anqi, Ally, Guanglong, Kenny, Wula, Alethea, Diudiu, Nadia, Patrick, Ziying etc. They were very supportive all the time and I learned a lot from them. I cannot be happier to have Sandy – my boyfriend with me to spend these years altogether. He is sweet, helpful, amazing all the time. Finally, I have to thank to my parents – Yun Shen and Jun Bai. I cannot appreciate more for all your nice care and support from home.

Publications

- Bai, C.; Klimkowski, P.; Jin, C.; Kuchlyan, J.; El-Sagheer, A. H.; Brown, T. A new phosphoramidite enables orthogonal double labelling to form combination oligonucleotide probes. *Org. Biomol. Chem.* **2022**, *20* (44), 8618-8622.

[a] https://www.rsc.org/journals-books-databases/author-and-reviewer-hub/authors-information/licences-copyright-permissions/#acknowledgements

Contents

Abbreviations

A	Adenine
Å	Angstrom
Abs	Absorbance
Ac	Acetate
aq.	aqueous
Ar	Aryl
ASO	Antisense oligonucleotide
a.u.	arbitrary units
br	broad
bp	base pair
Bn	Benzyl
BSA	*N*, *O*-bis(trimethylsilyl)acetamide
Bu	Butyl
Bz	Benzoyl
C	Cytidine
˚C	Degree Celsius
calc.	calculated
CD	Circular dichroism
conc.	concentrated
COSY	Correlation spectroscopy
CuAAC	Copper(I)-catalysed Azide-Alkyne Cycloaddition
d	doublet (NMR)
Da	Dalton(s)

dd	doublet of doublet (NMR)
dt	double triplet NMR)
DCM	Dichloromethane
DIPEA	Diisopropylethylamine
DMAP	4-dimethylaminopyridine
DMD	Duchenne muscular dystrophy
DMF	*N, N′*-dimethylformamide
DMP	Dess–Martin periodinane
DMSO	Dimethyl sulfoxide
DMTr	Dimethoxytrityl
DMTrCl	4,4′-dimethoxytrityl chloride
DNA	Deoxyribonucleic acid
EDTA	ethylendiaminetetraacetic acid
eq.	equivalent
ES	Electrospray
ESI	Electrospray ionization
EtOAc	Ethyl acetate
Et_2O	diethyl ether
EtOH	ethanol
FDA	Food and Drug Administration
G	Guanine
g	gram
h	hour
H-bond	Hydrogen bond
HIV	Human immunodeficiency virus

HPLC	High performance liquid chromatography
HRMS	High Resolution Mass Spectrometry
Hz	Hertz
ITCC	Indotricarbocyanine
LCMS	Liquid chromatography mass spectrometry
LNA	Locked nucleic acids
LRMS	Low Resolution Mass Spectrometry
M	molar concentration
m	multiplet (NMR)
mg	milligram
mL	milliliter
mm	millimetre
MeCN	acetonitrile
MeOH	methanol
MOE	2-Methoxyethyl
mRNA	messenger RNA
MS	Mass spectrometry
Ms	Mesyl group
MW	Molecular weight
m/z	mass/charge
NHS	*N*-hydroxysuccinimide
nm	nanometer
nM	nanomolar concentration
µM	micromolar concentration
µL	microlitre

NMR	Nuclear Magnetic Resonance
ON	Oligonucleotide
PCR	Polymerase chain reaction
PE	Petroleum ether
pH	negative logarithm of hydrogen ion concentration
Ph	Phenyl
PNA	Peptide nucleic acids
ppm	parts per million (NMR)
PPh_3	triphenylphosphine
PO	Phosphodiester
PS	phosphorothioate
q	quartet (NMR)
qPCR	Quantitative polymerase chain reaction
r.t.	room temperature
RNA	Ribonucleic acid
ROX	carboxyrhodamine
s	singlet (NMR)
T	Thymine
t	triplet (NMR)
TAMRA	5-Carboxytetramethylrhodamine
TBAF	Tetrabutylammonium fluoride
TBDMS	*tert*-butyldimethylsilyl
TBDPS	*tert*-butyldiphenylsilyl
TFA	Trifluoroacetic acid
THF	Tetrahydrofuran

THPTA	Tris(3-hydroxypropyltriazolylmethyl)-amine
td	triple doublet (NMR)
TEA	Triethylamine
TL	Triazole
TLC	Thin Layer Chromatography
T_m	Melting temperature
TMSOTf	Trimethylsilyl trifluoromethanesulfonate
U	Uridine
UV	Ultraviolet

Chapter 1

General Introduction

Chapter 1 – General Introduction

1.1 Nucleic acids

1.1.1 Primary structure of nucleic acids

Nucleic acids are very important biopolymers storing genetic information in living organisms. The two main classes of nucleic acids are deoxyribonucleic acid (DNA) and ribonucleic acid (RNA). They are made up of four different nucleotides which consist of a nitrogenous heterocyclic nucleobase, a pentose sugar and phosphate residue. The nucleobases can be classified into two types: bicyclic purines (adenine and guanine), and pyrimidines (cytosine, thymine and uracil). Adenine, cytosine and guanine are found in both DNA and RNA while thymine in DNA is replaced by uracil in RNA (Figure 1.1).[1]

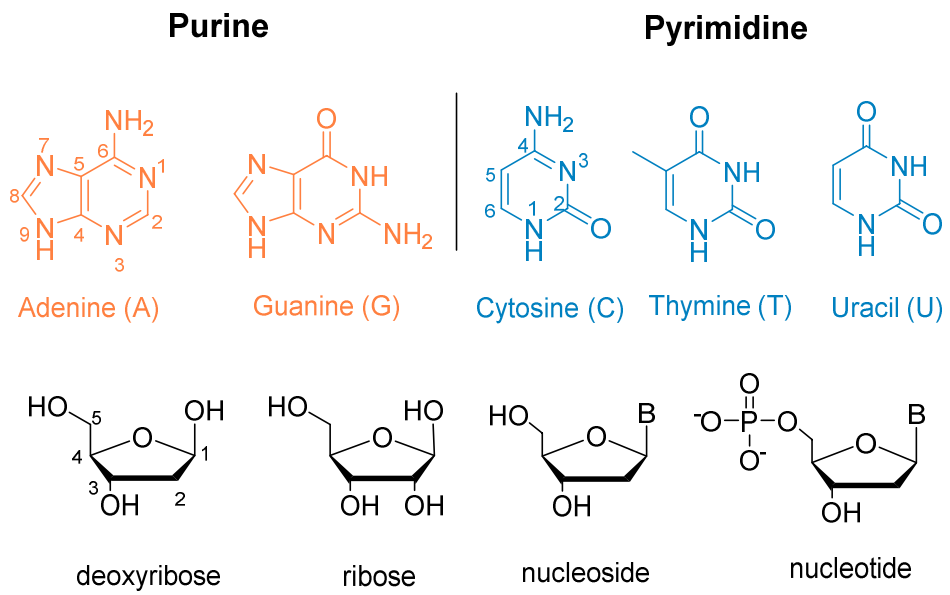

Figure 1. 1. Chemical structure of heterocyclic bases of nucleic acids, nucleoside and nucleotide. Purine: adenine (A), guanine (G); pyrimidine: cytosine (C), thymine (T) and uracil (U).

The pentose sugar in DNA is 2′-deoxy-D-ribose while in RNA it is D-ribose. Both are attached to the nucleobase via a -glycosidic bond which links the carbon C-1′of the sugar to the N-1 of pyrimidines or N-9 of purines. The heterocyclic base attached to the sugar C-1′-atom can either lie on the same face of the sugar ring as the 5′-OH group (β-anomer) which is the structure in natural DNA, or on the opposite face (α-anomer). Also, nucleobases can rotate around the glycosidic bond developing two extreme *syn*- and *anti*-conformations (Figure 1.2). However, the anti-conformation is more common in natural nucleotides owing to steric hindrance from the sugar moiety in the *syn*-conformation.[2]

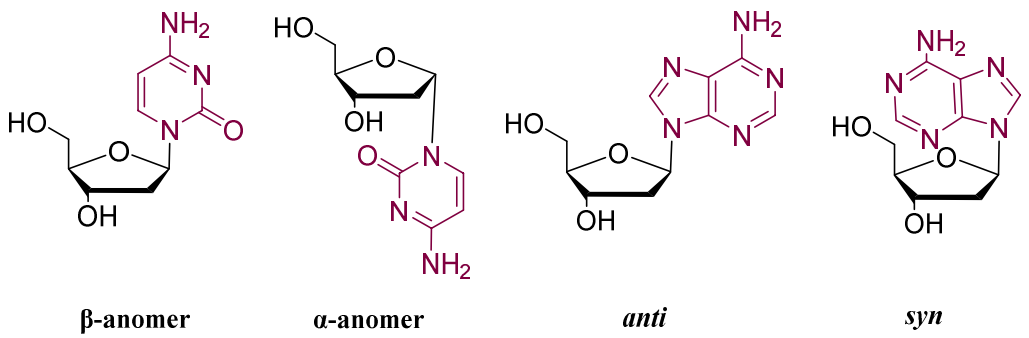

Figure 1. 2. Chemical structures of nucleoside α- and β-anomers, and *syn*- and *anti*-conformations.

Regarding the pentose sugar confirmation, the 2′-OH group has a great effect on the sugar conformation (pucker). Puckers that push atoms above the ring on the same face as the 5′-position are defined as *endo*, whereas puckers on the opposing face are described as *exo*. DNA adopts mainly the S-type (Southern) conformation with the C-2′ *endo* puckering of the deoxyribose, whereas RNA adopts mostly the N-type (Northern) conformation with C-3′ *endo* ribose puckering to reduce ring strain, in turn reducing the energy of the system.

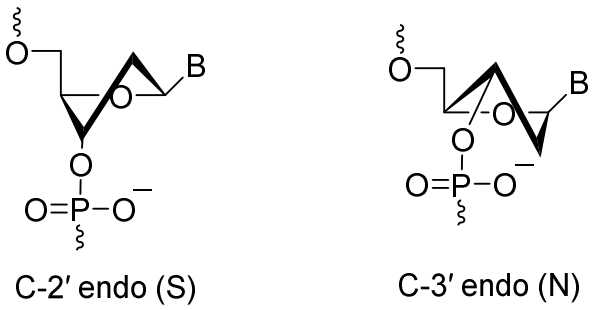

Figure 1. 3. 2′- *endo* (S) and 3′-*endo* (N) pucker (conformations) of deoxyribose.

The primary sequence of DNA is the order in which the nucleotides are arranged. The primary structure of nucleic acids (single-strand form) has directionality, and the specific nucleobase sequence is conventionally written from the 5′- to 3′-direction.

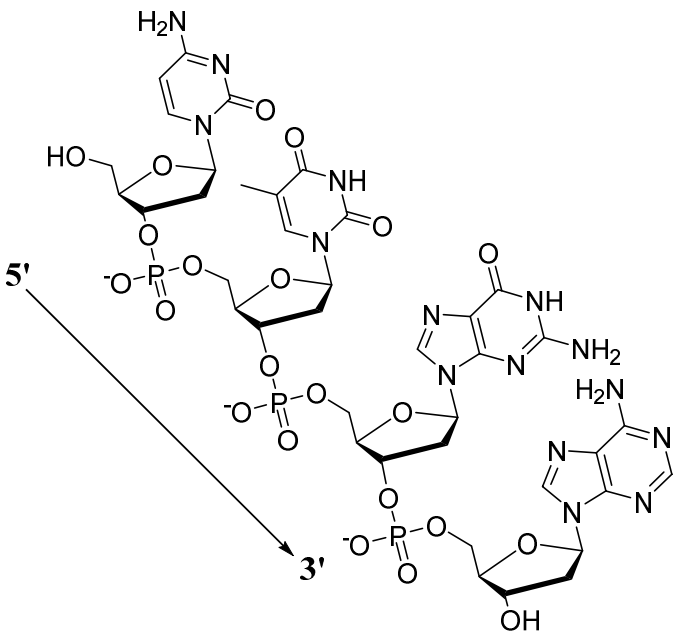

Figure 1. 4. Primary structure of oligonucleotides. The example shown here is a single-stranded DNA with the sequence 5′-CTGA-3′.

1.1.2 Secondary and tertiary structure of nucleic acids

In 1949 Chargaff et al. have found that the ratio of purines to pyrimidines in DNA in cells was always 1:1 and that the molar amount of adenine always equalled to the amount of thymine, and the same for guanine and cytosine. This important analysis implied that these nucleotides were pairing together in some way.[3] Afterwards, Maurice Wilkins and Rosalind Franklin did X-ray diffraction studies on DNA fibres, which led them to propose that the DNA duplex was helical, and that the precise form depends on the humidity.[1, 4, 5]

With access to Franklin′s data, James Watson and Francis Crick suggested that the structure of DNA was a double helix[6] and that the two strands were antiparallel, i.e. one strand was 5′ - 3′ and the other was 3′ - 5′. These two complementary nucleic acid strands are joined together via hydrogen bonds and π-stacking between nucleobases. They showed that nucleobase A pairs with T whereas C pairs with G (called “Watson-Crick base pairs”). Many other types of base pairing such as Hoogsteen base pairs (e.g. in triplexes) and wobble base pairs (in mismatched bases and tRNA) have also been observed.[7] (Figure 1.5). Each base pair in the double helix is separated by approximately 3.4 Å and one full helical turn is 34 Å in vertical height, so it consists of 10-11 bases per full helical turn. As noted by Watson and Crick, the exterior of the DNA helix consists of deoxyribose sugars attached by phosphate backbones (phosphodiesters), which hold a formal negative charge under physiological conditions (pH 7.4).[6]

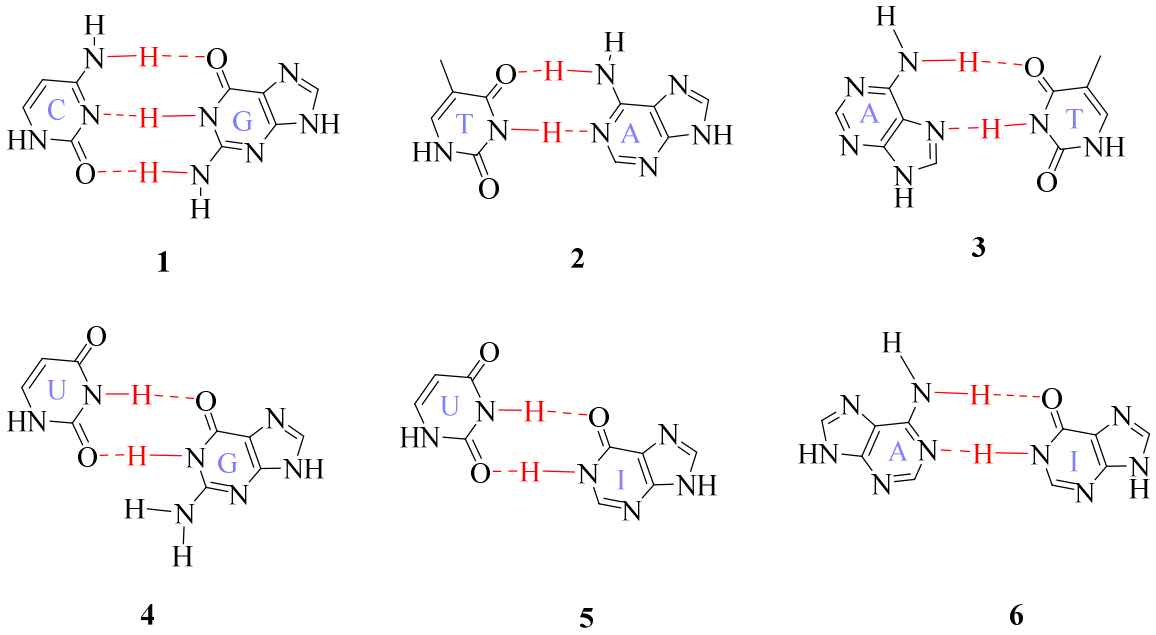

Figure 1. 5. Watson–Crick base pairing for C-G (**1**) and T-A (**2**). Hoogsteen base pairing for A-T (**3**). Wobble pairings for U-G (**4**), U-I (**5**) and A-I (**6**)

There are two common conformations in double stranded nucleic acids, the A-form and the B-form (Figure 1.6). Apart from these two conformations, another conformation was discovered later (the Z-form) which does not commonly exist in nucleic acids.[1, 8] A- and B-DNA are both right-handed helices and the Z-form is left-handed. B-DNA is the most common form found in DNA at neutral pH and physiological conditions while the A-form is the most common form of RNA.

The major groove and minor groove are almost the same in depth in B-DNA as the base pairs are positioned directly on the helix axis, but the major groove is wider compared to the minor groove. These grooves provide binding opportunities for other molecules. Large molecules such as proteins interact primarily in the major groove[9] and small molecules

commonly interact in the minor groove.[10] The helix diameter is 20 Å. The sugars have the C2′-*endo* pucker and all the glycosides adopt the *anti*-conformation (Figure 1.6 B).[1] The A-form helix (Figure 1.6 A) is wider and vertically compressed with 11 base pairs in each full turn of 28 Å, with an inter-base distance of 2.55 Å. The A-form has a very narrow and deep major groove, while its minor groove is wide and shallow. The furanose sugars have a C3′-*endo* pucker and the glycosylic bonds are in the *anti*-conformation. [11]

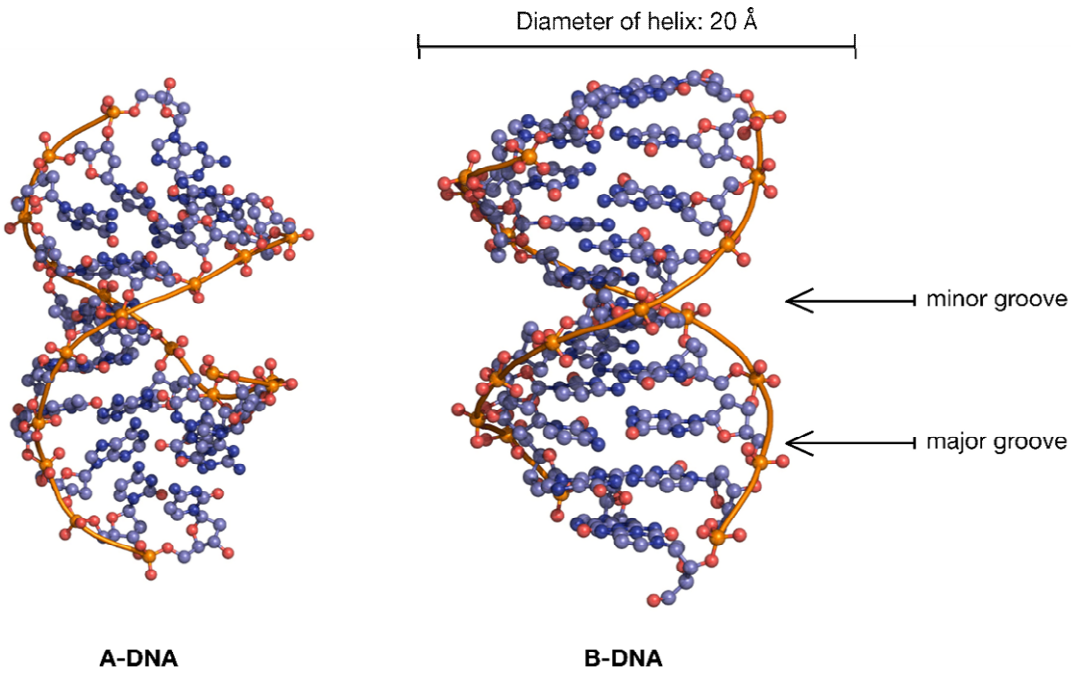

Figure 1. 6. A-type and B-type DNA conformations. Figure taken from[12] with permission.

1.2 Solid-phase synthesis of oligonucleotides

There are several methods of oligonucleotide synthesis including the H-phosphonate and phosphotriester methods described by A. M. Michelson and Alexander R[13, 14], the solid-

phase approach developed by Robert Letsinger[15] and the phosphoramidite method pioneered by Marvin Caruthers[16] which was universally adopted and massively broadened the applications of oligonucleotides. Solid-phase oligonucleotide synthesis is usually performed in the 3′- to 5′- direction unlike the 5′ to 3′ direction in enzymatic synthesis of oligonucleotides. The most common approach to oligonucleotide synthesis uses phosphoramidite monomers as building blocks which need to be prepared with the required protecting groups to allow for controlled oligonucleotide coupling on the solid-phase oligonucleotide synthesis cycles and avoidance of side-reactions. (Figure 1.7).[17, 18]

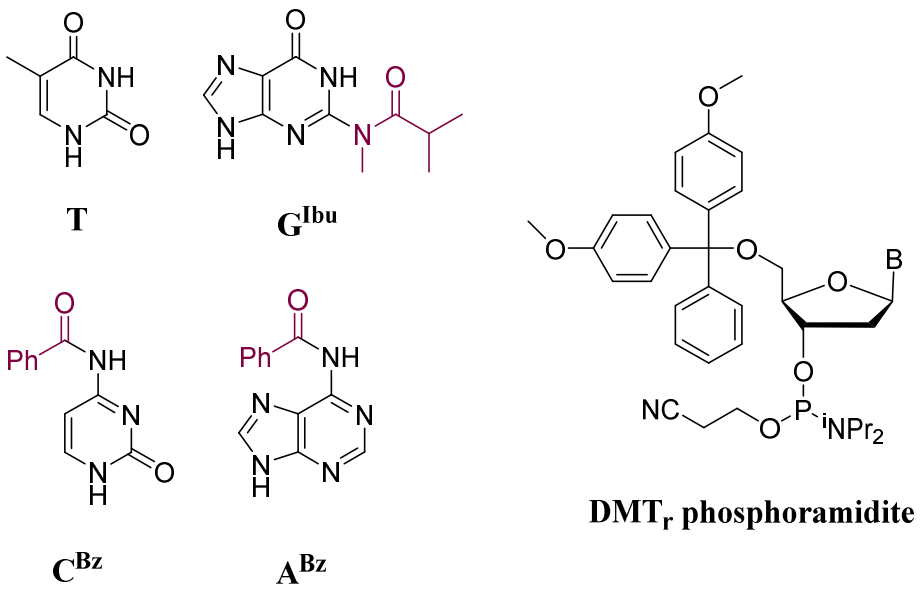

Figure 1. 7. Common phosphoramidite building blocks used for solid phase synthesis. The key structural features are: the 3′-phosphoramidite group that will form the phosphate linkage, the 5′-DMTr-hydroxyl protecting group and the nucleobases with protected primary amines.

Apart from these protected nucleobases the 5′-hydroxyl group in the phosphoramidite needs temporary protection with the DMTr group to avoid uncontrolled polymerisation in

the coupling reaction. One nucleotide is added during a single synthetic cycle and each synthetic cycle consists of a number of steps that are presented in (Figure 1.8). The first cycle starts with a single 5′-DMTr-protected nucleoside monomer which is attached to the resin. This monomer is detritylated using trichloroacetic acid (TCA) to remove the 5′-DMTr-group and expose the 5′-hydroxyl for the subsequent coupling step. Before the phosphoramidite can be coupled to the resin bound monomer, it must first be activated by protonation of the diisopropylamino group. Nucleophilic attack from the 5′-hydroxyl to phosphorus then promotes the loss of the di-isopropylamine leaving group, forming a phosphate (phosphodiester) linkage between two monomers. An excess of phosphoramidite monomer is used to guarantee a good coupling yield and unreacted phosphoramidite is washed out of the resin. This is a key advantage of solid phase synthesis. Some of the 5′-hydroxyl groups will not react in the coupling step, even though the coupling efficiency is >99%. These unreacted 5′-hydroxyl groups can react in the next cycle and produce a shorter by-product sequence which is missing a nucleotide. This constitutes a deletion mutation which is highly undesirable. Therefore, this unwanted extension of unreacted oligonucleotide chains can be partially prevented by introducing a capping step after the coupling step to block further extension of these OH-groups. Capping is performed by mixing two capping reagents on the synthesiser: N-methylimidazole and acetic anhydride *N*-methylimidazole activate the acetic anhydride

which acetylates 5′-hydroxyl group. The 5′-capped acylated oligonucleotide will not be coupled in the following cycles.

After the coupling and capping, the phosphite-triester P^{+3} oxidation state is acid sensitive and cannot survive the detritylation step. Oxidation of phosphorus is therefore performed by using iodine with a small amount of water under slightly basic conditions. The oxidised P^{+5} is stable to acid. The cycle is then repeated to make the desired sequence. Removal of the DMTr-group produces an orange cation that can be monitored at 495nm to measure coupling efficiency. On completion of oligonucleotide assembly, the succinyl linkage between the oligonucleotide and the resin, and the nucleobase and phosphate 2-cyanoethyl protecting groups are cleaved by concentrated aqueous NH_3 in a sealed tube at 55 ˚C for 5 hours. This provides the oligonucleotide in solution ready for purification.

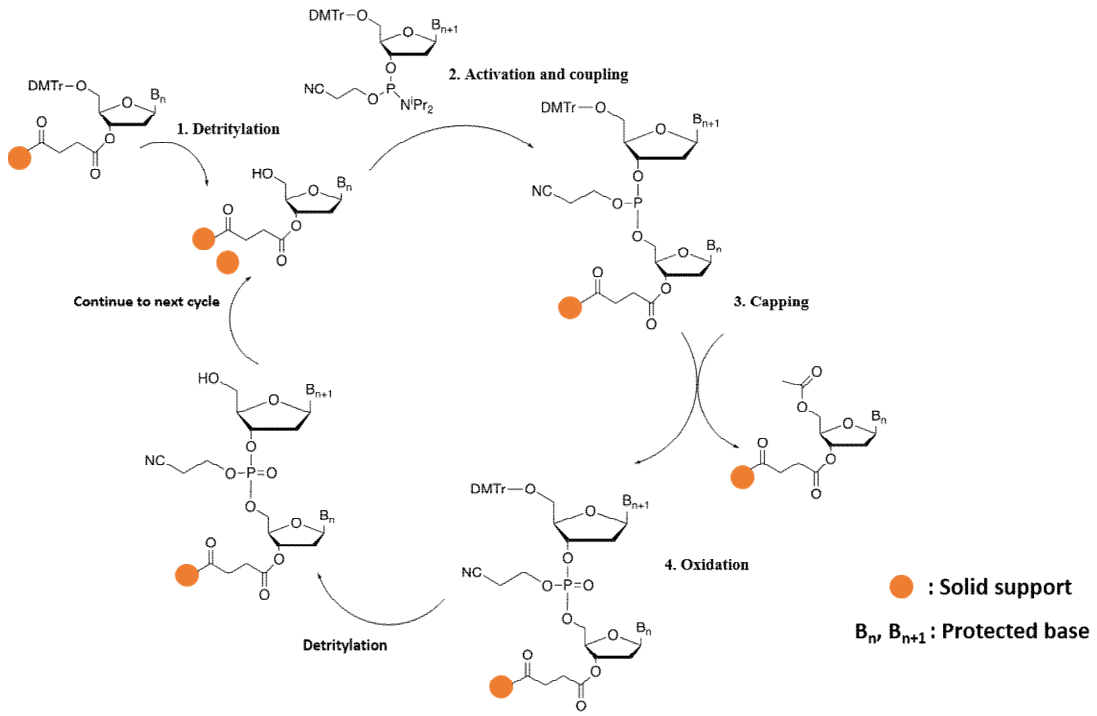

Figure 1. 8. Solid phase synthesis cycle using phosphoramidite monomers; n = residue number.

RNA synthesis is similar to DNA synthesis; the main difference is that the 2′-hydroxyl group of RNA must be protected during the solid-phase synthesis process because RNA readily undergoes strand migration between the 2′ and 3′-positions of the sugar, and chain cleavage also occurs. The most common protecting groups for the 2′-hydroxyl group in RNA synthesis are *tert*-butyldimethylsilyl (TBDMS) and 2′-thiomorpholine-4-carbothioate (TC). The protecting group for the 2′-OH has to be removed at the end of the RNA synthesis and base/phosphate deprotection. The TBDMS group can be removed by triethylamine trihydrofluoride (NEt_3.3HF). The TC group can be efficiently deprotected by ethylenediamine but TC phosphoramidite monomers are much more expensive than TBDMS monomers.

The protecting groups used for the heterocyclic bases (A, G, C) in RNA synthesis are slightly different from those used in DNA synthesis. The *tert*-butylphenoxyacetyl group can be removed under relatively mild conditions (Figure 1.9). The coupling efficiency in RNA synthesis is lower and coupling time must be extended relative to the conditions of DNA synthesis due to the steric hindrance of the bulky 2′- hydroxyl protecting group which slows down the phosphoramidite coupling reaction. The capping in RNA synthesis cycles is done using *tert*-butylphenoxyacetic anhydride (not acetic anhydride) in order to prevent exchange of the acyl based protecting groups for acetyl. After solid phase synthesis the RNA is treated in a milder solution of EtOH: NH_3 (1:3, v/v) at 55 ˚C for 2.5 hours for cleavage from the resin and protecting removal.

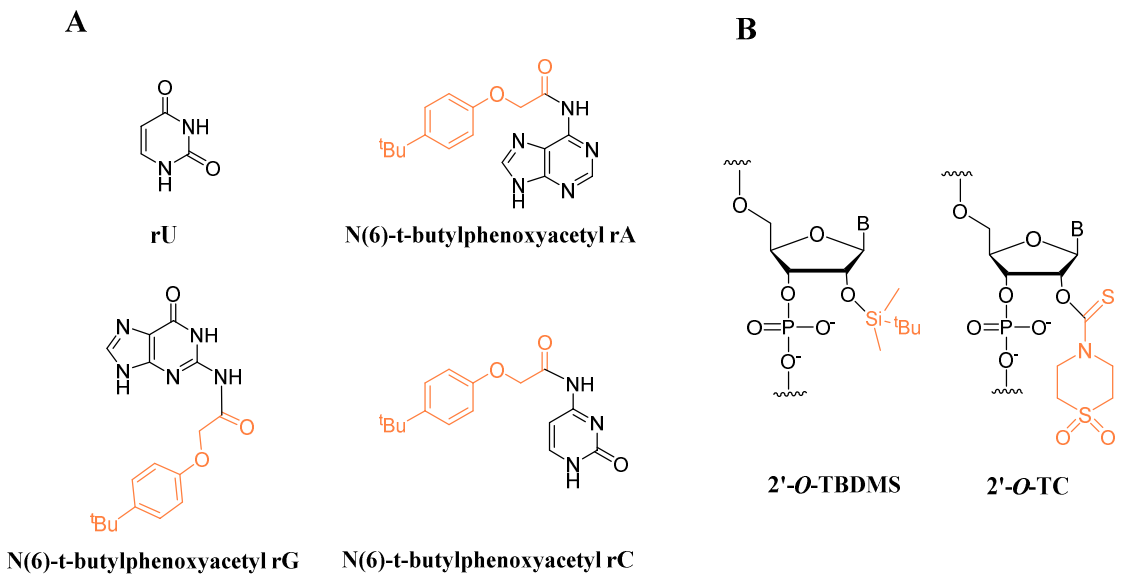

Figure 1. 9. A. Chemical structures of protected nucleobases; **B.** Chemical structures of 2′-protecting groups including *Tert*-butyldimethylsilyl (TBDMS) and Thiomorpholine-4-carbothioate (TC).

1.3 Ligation of oligonucleotides

The practical limit of solid-phase oligonucleotide synthesis is around 200 bases in length due to the imperfect efficiency of the chemical processes, and eventual blockage of the resin pores which have a limit of around 3000 angstroms in diameter. Larger pores lead to degradation of the resin particles. If longer modified oligonucleotides are required they can be made by ligation of shorter ones. There are two general methods to ligate oligonucleotides, enzymatic ligation and chemical ligation. Ligation can be carried out between two single-stranded sequences held together by a complementary splint or two "staggered end" double stranded sequences which provide mutual templating. Ligase enzymes require specific buffer conditions and temperatures and perfect Watson-Crick base pairs, whereas modified backbones such as triazole and carbamate linkages[19, 20] can be ligated by chemical reactions under different conditions. Some artificial backbones (e.g. triazoles) can be read through by DNA polymerases.[21]

1.3.1 Enzymatic ligation

There are two types of structure at the terminal regions of double stranded sequences: blunt ends and sticky ends. Blunt ends have no overhanging complementary bases hence do not benefit from Watson-Crick base pairs for the ligation reaction. Ligases generally require sticky end owing to the Watson-Crick interactions between overhanging single strands. They can work on blunt ends but with lower yields. Sticky-end ligation is obviously more precise, and more efficient.

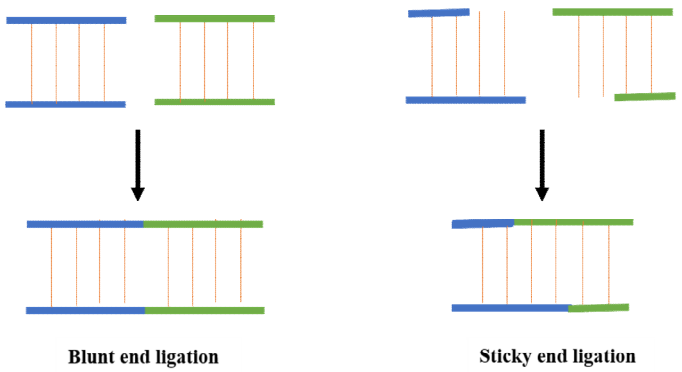

Figure 1. 10. Ligation of double stranded oligonucleotide sequences.

1.3.2 Chemical ligation using the CuAAC reaction

Click chemistry has become more and more important area in biophysical and chemical biology research currently. The Nobel Prize in Chemistry 2022 was awarded to Carolyn R. Bertozzi, Morten Meldal and K. Barry Sharpless "for the development of click chemistry and bioorthogonal chemistry". Sharpless and Meldal have laid the foundation for a functional form of chemistry – click chemistry – in which molecular building blocks snap together quickly and efficiently. Bertozzi has taken click chemistry to a new dimension and started utilising it in living organisms.[22] The general concept of click chemistry is that two specific molecules can be efficiently joined together under mild conditions. [23] There is a robust chemical reaction in click chemistry named the copper(I)-catalysed azide-alkyne cycloaddition (CuAAC) which only generates the 1,4-disubstituted triazole product.[24] The CuAAC reaction has some outstanding advantages like fast reaction rate, great regioselectivity, high yield and it can be performed in aqueous conditions at room temperature, which makes it extremely useful and handy for oligonucleotides ligation.

Modified oligonucleotides with complementary azide and alkyne groups can be clicked together using the CuAAC reaction. In general, $CuSO_4$ is used as a source of copper but the Cu^{2+} needs to be reduced to a Cu^{1+} for facilitating the cycloaddition. Thus, sodium ascorbate is added as the reductant. Also, the reagent mixture should be degassed to remove oxygen in the solution by argon bubbling, and a ligand such as tris(3-hydroxypropyltriazolylmethyl)-amine (THPTA) acts to stabilise copper in its Cu(I) oxidation state and accelerate the click reaction.

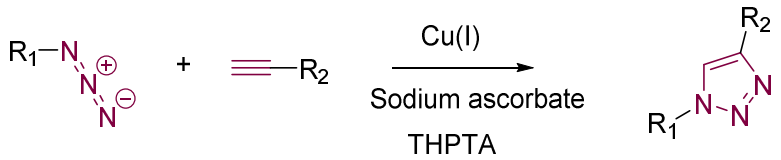

Figure 1. 11. Cu(I) catalysed azide-alkyne cycloaddition reactions and products.

1.4 Fluorescent labelling of modified oligonucleotides

There are various florescence labelling strategies for modified DNA or RNA for use in biochemical and biomedical research. Modified oligonucleotides need to be labelled with specific dyes, for instance, intercalators or fluorescent dyes, which can be widely applied in areas like antisense therapeutics, gene detection and diagnostics. Currently a number of efficient chemical methods are commonly used for florescent labelling including amine-active ester coupling, the copper-catalysed azide-alkyne cycloaddition reaction and the solid-phase phosphoramidite approach. However, the phosphoramidite approach needs ultra-mild reaction conditions during all the steps in the oligonucleotide solid phase

synthesis cycle and the subsequent deprotection as many fluorophores phosphoramidite monomers are light sensitive and chemically sensitive.

1.4.1 Amine-active ester coupling

The amine-active ester coupling reaction involves a primary amino group and an activated ester such as an N-hydroxysuccinimide (NHS) ester to form a stable amide bond (Figure 1.12 B). The reaction is performed under basic conditions at a pH ranging from 7.2 to 9. N-hydroxysuccinimide (NHS) esters of fluorophores are commercially available or can be synthesised using coupling reagents like carbodiimides (e.g. DCC)[25], uronium reagents (e.g. HATU)[26], or phosphonium reagents (e.g. PyBOP).[27]

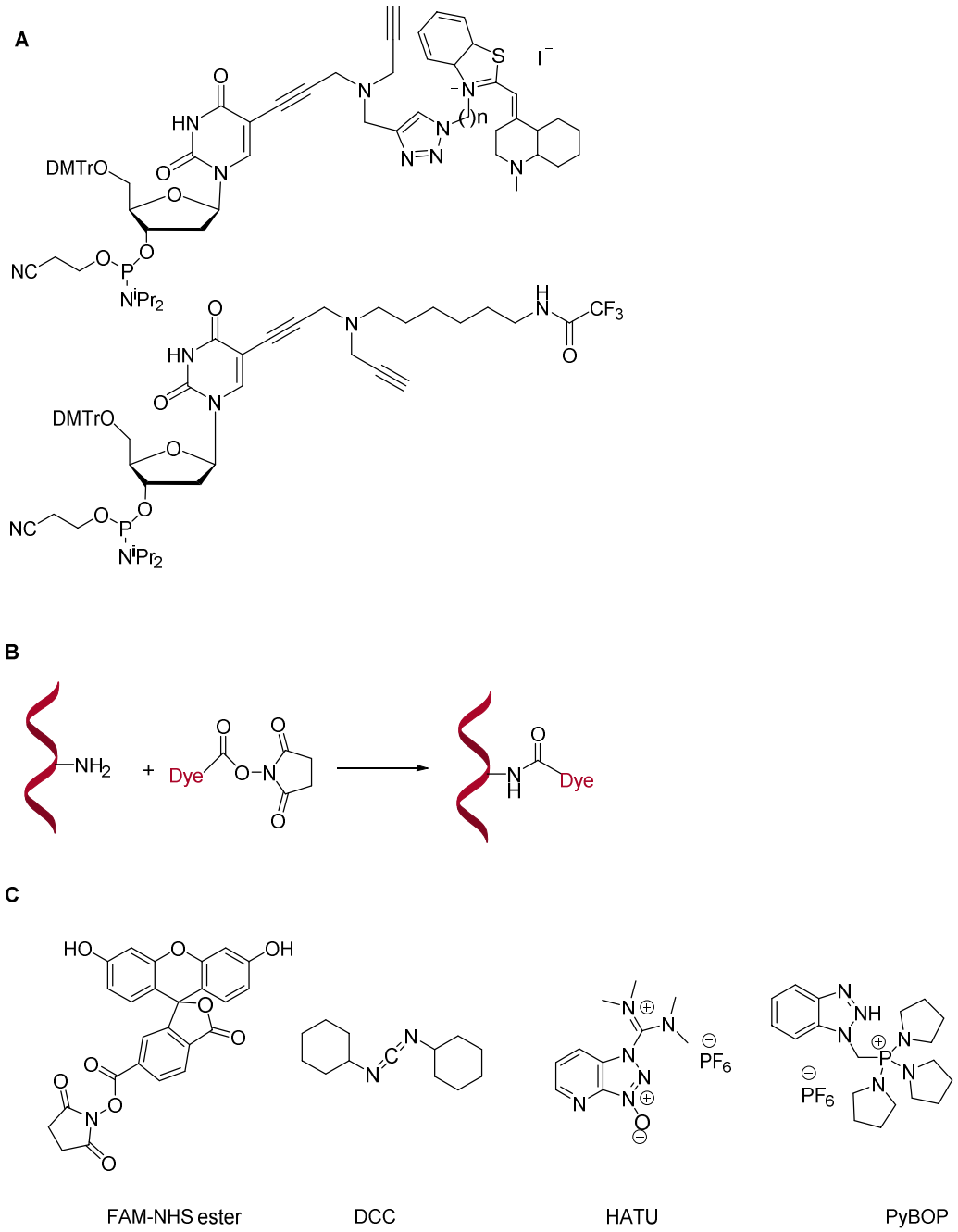

Figure 1. 12. A. Top: Example of fluorescent dye phosphoramidite monomer (thiazole orange dT); Bottom: Example of phosphoramidite monomer with amino group modification; **B.** Amine-active ester coupling reaction; **C.** Chemical structures of one example of a dye NHS ester and amide coupling reagents.

1.4.2 Click oligonucleotide labelling via the CuAAC reaction

Click labelling via the CuAAC reaction is one of the most common used methods of labelling oligonucleotides. It requires one moiety with alkynyl group and the other moiety with azide group (Figure 1.13). Fluorescent labelling can be performed in an efficient and fast way and monomer phosphoramidites with alkynyl group attached to the nucleobases can be easily incorporated into oligonucleotides during solid phase synthesis cycles.

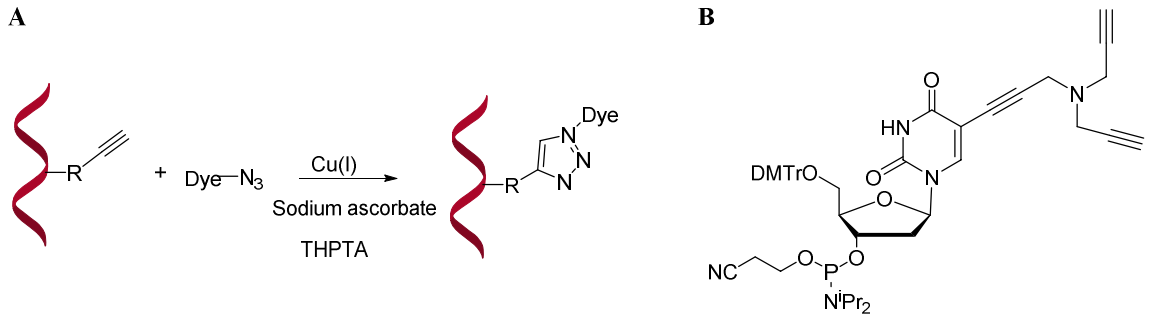

Figure 1. 13. A. Copper-catalysed azide-alkyne cycloaddition reaction; **B.** An example of a phosphoramidite monomer with alkynyl moieties.

1.5 Fluorescence

1.5.1 Fluorescence theory

Fluorescence is the emission of light by a substance that has absorbed light or other electromagnetic radiation, and is a form of luminescence. It involves absorption of a photon ($h\nu_A$) by the fluorophore that is excited from its ground state (S_0) to one of the higher vibrational states of S_1 (or S_2, excited singlet states) and this step happens within 10^{-15} s. There is an internal conversion (IC) in the next 10^{-12} s during which the molecule undergoes non-radiative relaxation to the lowest vibrational state of electronically excited

states (S_1). Afterwards the molecule returns to ground state (S_0) by emission of a photon ($h\nu_F$). Emission only occurs from the lowest vibrational level of the excited singlet states (S_1) and is independent of the excitation wavelength based on Kasha′s rule.[28] Emission (Figure 1.14, red) has lower energy compared to absorption (Figure 1.14, blue) because of internal conversion (IC) and relaxation which explains why emission is observed at a longer wavelength than absorption. The difference between the maxima of the absorption and emission is called the Stokes′ shift.[29]

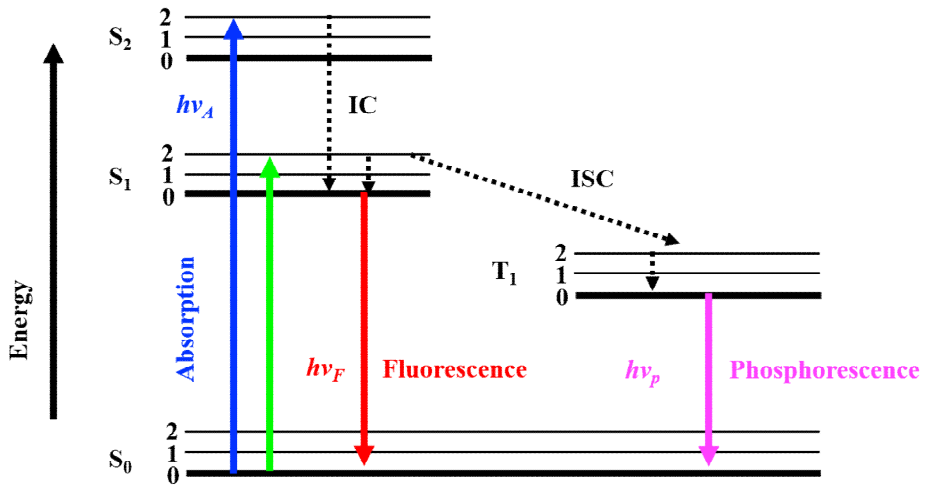

Figure 1. 14. Jabłoński energy level diagram illustrating the pathway of an excited electron. $h\nu_A$: photon absorption; $h\nu_F$: photon emitted in the fluorescence phenomenon; $h\nu_P$: phosphorescence photon; S_0: ground state; S_1 and S_2: excited singlet states; T_1: excited triplet state; 0, 1, 2: vibrational levels; IC: internal conversion; ISC: intersystem crossing.

1.5.2 Förster fluorescence resonance energy transfer (FRET)

Förster (Fluorescence) resonance energy transfer (FRET) is a mechanism describing energy transfer between two light-sensitive molecules. Its mechanism involves

a donor fluorophore in an excited electronic state, which may transfer its excitation energy to a nearby acceptor chromophore in a non-radiative fashion through long-range dipole-dipole interactions.[30] The theory supporting energy transfer is based on the concept of treating an excited fluorophore as an oscillating dipole that can undergo an energy exchange with a second dipole having a similar resonance frequency. Therefore, FRET can happen only when the emission spectrum of donor fluorophore overlaps with the absorbance spectrum of the acceptor (Figure 1.15 B). The ruling principle of the FRET phenomenon is based on the spatial overlap of donor and acceptor molecular orbitals, which requires both molecules to be in close proximity. After FRET the donor′s fluorescence intensity is reduced and the acceptor′s emission intensity is boosted. (Figure 1.15 A).

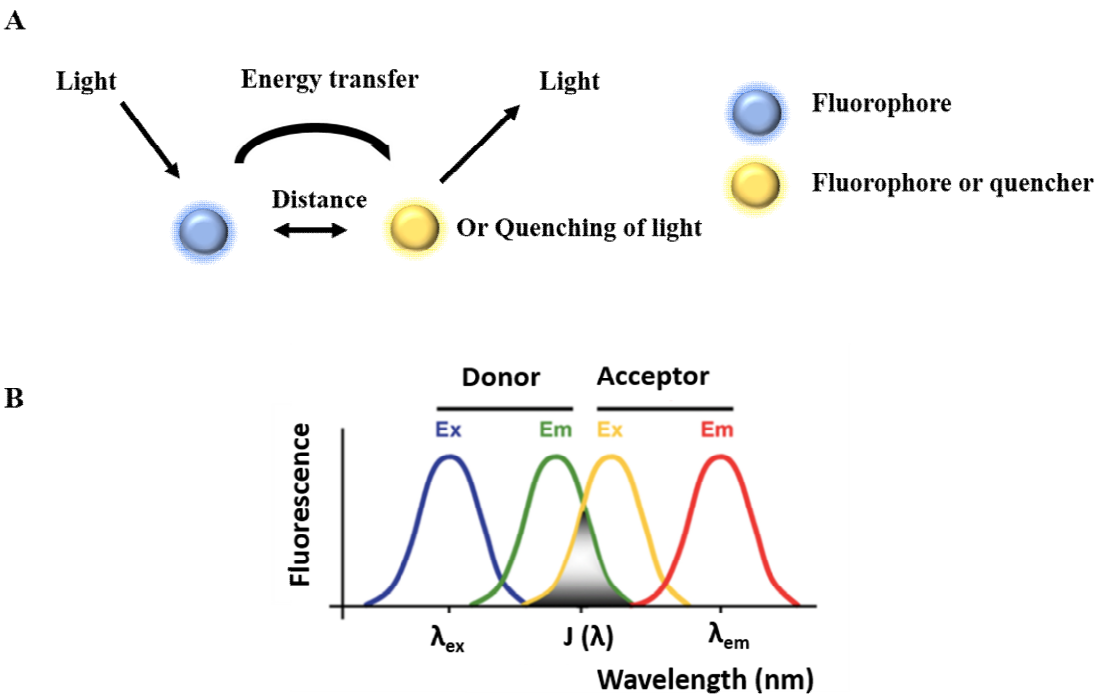

Figure 1. 15. A: Illustration of fluorescence resonance energy transfer (FRET); B: Schematic representation of spectral overlap.

The efficiency of this process strongly depends on the donor-to-acceptor separation distance (r) and the Förster distance (R_0)[31] between the donor and acceptor (Figure 1.16 A). The efficiency of the process is 50% when the distance between molecules is equal to the Förster distance (typically 40-60 Å, Figure 1.16 B), which allows for distance measurements between molecules. FRET efficiency also depends on the relative orientation of the donor emission and acceptor absorption dipole (κ^2, Figure 1.16 C). If the isotropic reorientation of molecules requires a time shorter than the excited lifetime of the donor, the average value for κ^2 is then assumed to be equal to 2/3[32] which also allows the measurement of distances in double stranded DNA.[33, 34]

A $E = \dfrac{Ro^6}{Ro^6 + r^6}$

B $R_o = 0.211\ (\kappa^2 n^{-4} Q_D J(\lambda))^{1/6}$

C $\kappa^2 = (\cos\theta A - 3\cos\theta B \cos\theta C)^2$

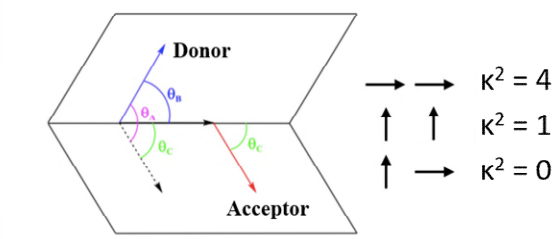

Figure 1. 16. Schematic of the dipole orientation angles in FRET between a donor and an acceptor. E: the efficiency of FRET (**A**). $\mathbf{\Phi_D}$ is the fluorescence quantum yield of the donor in the absence of the

acceptor, κ^2 is the dipole orientation factor, ***n*** is the refractive index of the medium and ***J(λ)*** is the overlap integral of the donor emission and acceptor absorbance spectra (**B**). The orientation factor κ^2 (**C**). **θA** is the angle between the emission transition dipole of the donor and the transition absorption dipole of the acceptor.

1.6 Fluorescent hybridization probes

Fluorescent hybridization probes have played an important role in gene detection, gene imaging and diagnostics and fluorescence has been widely used in biological studies of proteins and nucleic acids.[35-37] Also, fluorescence labelled oligonucleotides can be used to detect genetic variations in DNA and to identify single nucleotide polymorphisms (SNPs) due to the high sensitivity of the technique.[36] Fluorescent hybridization probes may be used with fluorescence melting analysis and/or real-time polymerase chain reaction (PCR) to detect SNPs and mutations. Due to the reduced stability caused by a single nucleobase substitution, insertion, or deletion, fluorescent probes hybridised to fully complementary targets are distinguished from their mismatched counterparts. These oligonucleotide probes usually contain a fluorophore and a quencher. The fluorophore is quenched before hybridization through collisional or FRET mechanisms, and it is deactivated once it binds to the complementary strand. Below are two examples of fluorescent hybridization probes and an illustration of their mechanism (molecular beacons[38-40] and HyBeacons[41-43]).

1.6.1 Molecular beacons

Molecular beacons were first reported in 1996.[39] They are single-stranded nucleic acids that are labelled with a fluorophore at one end and a quencher at the other end. A loop

portion of the probes is designed so that it is complementary to the target sequence (15–30 nucleotides long), as well as two arm sequences (5–7 nucleotides long) that are complementary to each other.[31, 44] A stem-loop structure can be formed within the oligonucleotide (Figure 1.17), allowing the fluorophore and quencher to remain in close proximity to one another. An annealing process to the complementary target causes the stem-loop to open, separating the fluorophore from the quencher, which generates strong emission.[45, 46]

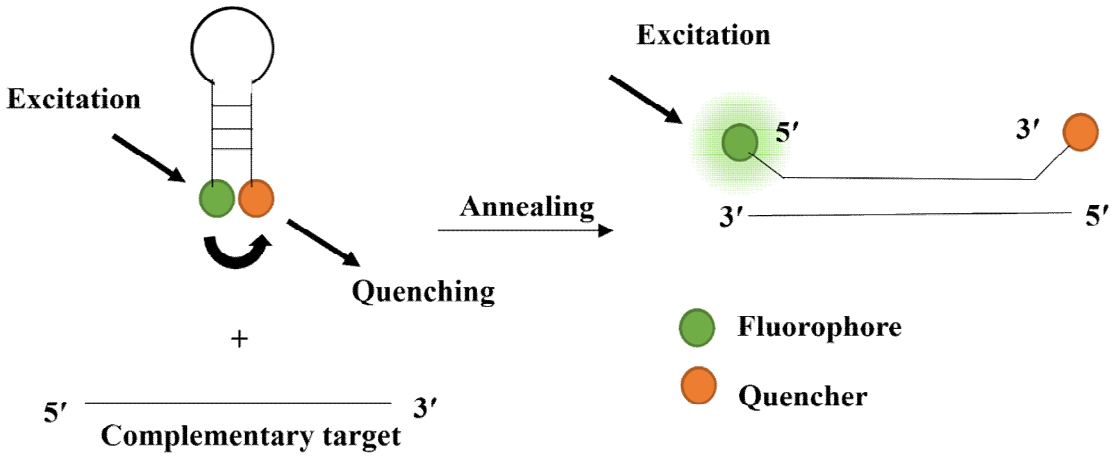

Figure 1. 17. Schematic representation of molecular beacon interacting with the target sequence. On their own, molecular beacons are non-fluorescent due to fluorescence quenching. Once hybridised to the target, a rigid duplex is formed that separates the fluorophore and quencher, and restores fluorescence.

1.6.2 HyBeacon probes

HyBeacon probes are single-stranded oligonucleotides that contain two or more fluorophores attached covalently to one or more internal nucleotide positions, either the major groove or the minor groove. High fluorescence is observed when these probes are

hybridised to complementary DNA targets, whereas low fluorescence is observed when they are in their unstructured single-stranded state due to quenching of intrinsic fluorescence (Figure 1.18). A HyBeacon probe hybridizes to a fully complementary target sequence more efficiently than a mutant target (which contains mismatched base pairs). The method can be used to detect and identify single nucleotide polymorphisms (SNPs)[47], short tandem repeats (STRs),[43] as well as allele discrimination and mutation detection. Through real-time PCR, HyBeacons are used in a number of diagnostic applications.[42, 43] Six HyBeacon probes have been used simultaneously to analyze mutations in a six-channel system that analyzes DNA fluorescence melting for genetic analysis of cystic fibrosis mutations.[41]

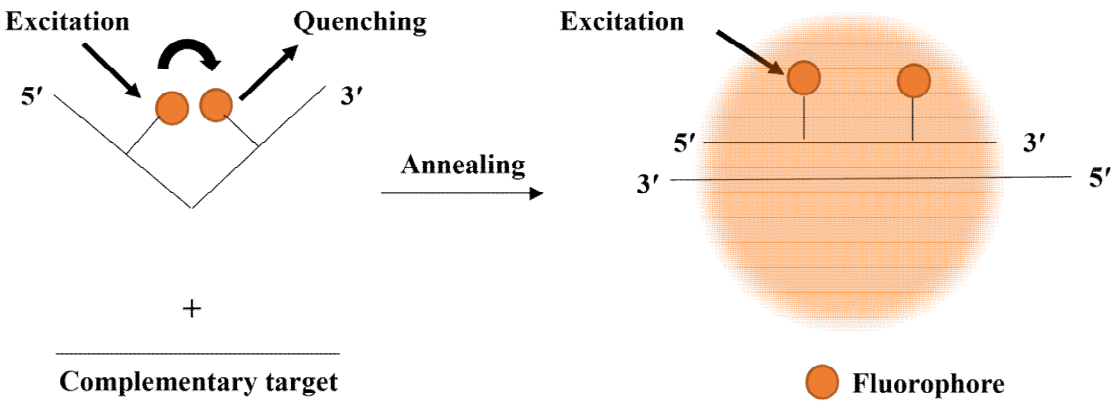

Figure 1. 18. Schematic representation of HyBeacon probe interacting with the target sequence. On their own, the molecules are only weakly fluorescent due to internal fluorescence quenching. Once hybridised to the target, a rigid duplex is formed that separates the fluorophores, thereby restores fluorescence.

1.6.3 Thiazole orange intercalation probes

1.6.3.1 Thiazole orange

Despite the wide application of hybridization probes,[41, 47] simple fluorescence-labelled nucleic acid probes can give undesirably strong fluorescent backgrounds, partly because of failed hybridization or excess probes binding to biological material in an indiscriminate manner. Even at modest concentrations, excessive fluorescence can create false-positive signals, obstructing highly sensitive studies like live cell imaging of RNA or genomic DNA. As a result, novel nucleic acid probes, particularly fluorophores, must be developed to improve fluorescence sensitivity and selectivity. Thiazole orange (TO) and its derivatives, which have been intensively studied and utilized in a variety of applications, including the detection of complementary DNA,[48, 49] RNA,[50-52] triplexes,[53, 54] and G-quadruplexes, from the asymmetric cyanine dye family[55, 56] are a prospective contender.

Asymmetric cyanine dyes are a valuable class of fluorophores that are made up of two heteroaromatic fragments joined together to allow complete conjugation.[57] Thiazole orange is one of these dyes (TO, Figure 1.19). It has a methine bridge between a benzothiazole and quinoline moiety. TO is an effective photophysical dye for DNA binding since it is nearly non-fluorescent in solution but emits approximately 18,900 times more when bound to DNA or RNA duplexes.[49, 58, 59] This is owing to TO intercalation between the base pairs, which reduces rotation around the methine bridge joining the two aromatic systems, resulting in a planar completely conjugated system. The unbound dye, on the other hand, is not fully conjugated and suffers from non-radiative degradation when irradiated.[60]

Studies of their direct covalent attachment to nucleic acids have been driven by these intriguing features. The TO derivatives TO_B and TO_Q (Figure 1.19), which are attached via one of the two endocyclic nitrogen atoms, can be used.[58] The nitrogen atom in quinoline faces the DNA minor groove, whereas the nitrogen atom in benzothiazole faces the major groove.[61] Privat et al.[50, 62] found that when TO_Q was directed into the minor groove of DNA duplexes, the TO_Q-DNA conjugates had better stability and fluorescence. An NMR analysis of a TO dimer (i.e. TOTO) intercalating into the DNA duplex through the minor groove with the quinoline ring situated between two purine bases supports this conclusion. When TO_B was oriented towards the major groove, however, it produced more fluorescence and better stability.[58] This may be due to the dihedral angle of the chromophore and linker along the methine bridge; TO_B has a smaller dihedral angle (69.0°), but TO_Q has a dihedral angle of roughly 170.7° and is less stable.[58] Furthermore, when TO_B was inserted at the 5-position of thymidine, the oligonucleotides produced less fluorescence in the absence of a complementary strand and larger fluorescence quantum yields when hybridised to their targets than TO_Q-DNA probes.[63]

1.6.3.2 Incorporation of TO into nucleic acids

The endocyclic nitrogen of quinoline (TO_Q) or the benzothiazole moiety can covalently link thiazole orange to nucleic acid probes (TO_B). When TO_B was directed into the major groove and TO_Q was directed into the minor groove,[50, 58, 62] studies on the relationship between attachment and binding to the phosphodiester backbone revealed a higher fluorescence signal and a greater increase in T_m (duplex melting temperature), which is consistent with TOTO dimer studies.[64] This could be due to the dihedral angle between the

methine bridge and the linker, TO_B having a smaller angle (B = 69.0°) than TO_Q (Q = 170.7°)[58] (Figure 1.19) and so providing better stacking between base pairs. Post-synthetically or during solid phase synthesis, TO and its derivatives can be added to the nucleobase, sugar, or phosphodiester backbone of oligonucleotide probes. It′s worth noting that the Okamoto et al. modified nucleobase (Figure 1.20 A) uses two TO dyes. In the unbound state, this TO-pair produces an H-aggregate, which reduces the fluorescence signal. This aggregation is broken when it binds to the target, resulting in a strong fluorescence signal. 'Exciton-Controlled Hybridization-sensitive fluorescence Oligonucleotide′ (ECHO) probes is the name given to these probes. The resulting F_{ds}/F_{ss} is roughly 30-fold and the probes can be used to monitor intracellular RNA levels.[65-68]

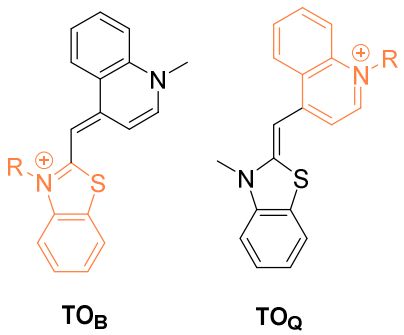

Figure 1. 19. Chemical structures of thiazole orange (TO_B, TO_Q) analogues. R: alkyl group TO_B: the linker is attached at the endocyclic nitrogen of the benzothiazole ring, TO_Q: the linker is attached at the endocyclic nitrogen of the quinoline ring.

Qiu et al. created a novel method in which TO is combined with a second reporter dye on the thymidine base. The FRET (Figure 1.20 B) has the benefit of shifting the fluorescence emission to the second dye while also taking advantage of TO′s intercalating

characteristics. After binding to the DNA targets, fluorescence responses of up to 19.5 times were achieved.[69] Modification of the sugar gives a 'TO nucleotide′ (Figure 1.20 C).[70] Promising fluorescent properties were observed in terms of sensing small interfering RNAs when there was a CuAAC-mediated attachment of TO to the 2′-position of the sugar of thymidine via the quinoline moiety (Figure 1.20 D).[71]

Privat et al. modified the phosphodiester backbone, which resulted in mild fluorescence responses. Differences in fluorescence (F_{ds}/F_{ss}) were mild in another work in which TO was coupled to the DNA phosphodiester backbone (Figure 1.20 E) via its quinoline moiety;[58] 2.4-fold for the TO-minor groove isomer and 0.8-fold for the TO-major groove isomer (Figure 1.20 E S_p). When TO was directed into the main groove of DNA via its benzothiazole moiety, there was a 2.7-fold increase in fluorescence upon duplex formation and a 1.3-fold increase when TO was directed into the minor groove (Figure 1.20 E R_p). Surface based detection was enabled by TO modifications at the 5′-phosphate of an oligonucleotide probe and covalent attachment of the probe to the surface of a biosensor (Figure 1.20 F).[72]

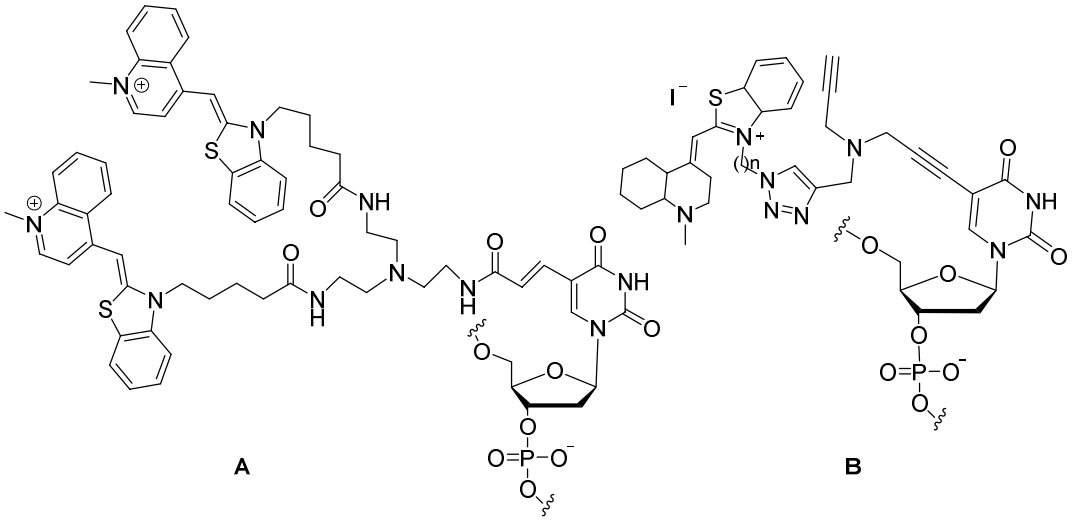

A

B

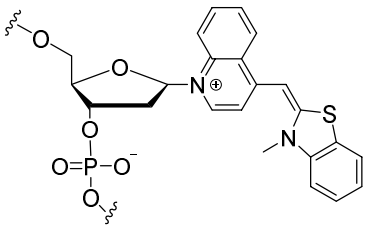

C

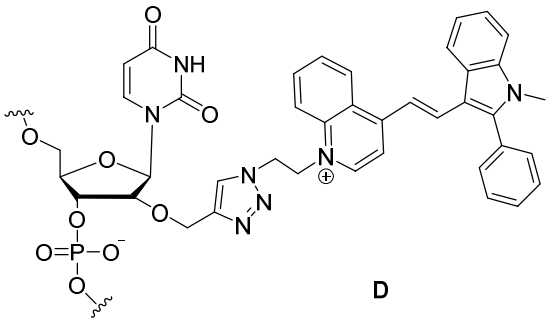

D

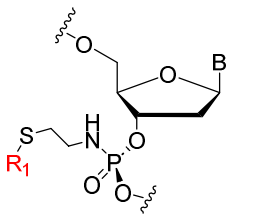

R1=

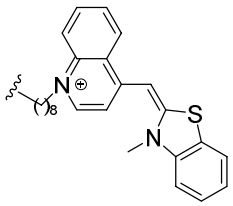

E

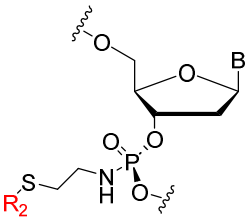

R2=

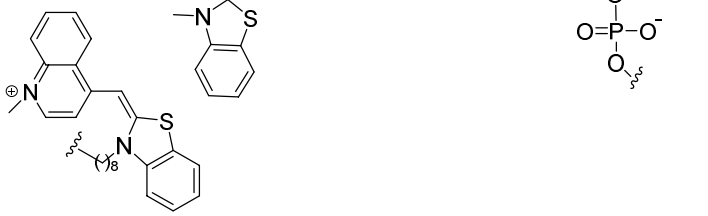

F

Figure 1. 20. Examples of TO modified oligonucleotide-based probes. A: Double attachment of TO to the T- nucleobase (ECHO probes); B: incorporation of TO with a reporter dye on a thymidine; C: modified sugar TO with attached; D: modified nucleobase with TO attached to the sugar; E: internal modification of phosphodiester backbone; F: modification of 5′ phosphate with TO.

1.7 Modifications of backbone linkage

1.7.1 Phosphorothioate and Triazole modification

The canonical bond between oligonucleotide monomers is the phosphodiester backbone (PO) (Figure 1.21). It is a five-bond linkage with sp^3 centres that are flexible. The phosphate atom is at the centre of the backbone, surrounded by two bridging and two non-bridging oxygens. The phosphate backbone is the consequence of biological co-evolution with enzymes that form, alter, and cleave the linkage to complete an oligonucleotides biological lifecycle.[73] The phosphate backbone can be altered to improve thermal stability, resistance to enzyme degradation, and cellular uptake.[74]

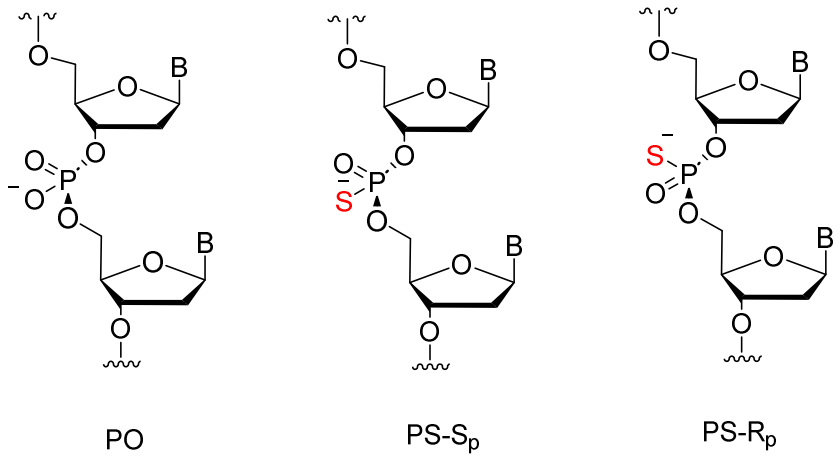

Figure 1. 21. Structures of phosphate derived backbones in oligonucleotides including, phosphodiester (PO) and Phosphorothioates (PS). Addition of a non-bridging sulphur creates a chiral centre and two enantiomeric forms (S_p and R_p).

Phosphorothioates (PS) are structurally similar to phosphodiesters and are one of the most researched modified backbones (Figure 1.21).[75] The main difference between these two backbones is that the phosphorothioate has a sulphur instead of a non-bridging oxygen. It was shown that adding sulphur to adenosine 5′-mono phosphorothioate (AMPS) gave substantial phosphatase resistance when compared to the standard alternative, adenosine 5′-monophosphate (AMP).[76] Although adding sulphur to make phosphorothioates improves their resistance to nuclease breakdown,[77, 78] there are certain disadvantages. The oligonucleotide duplex structure is destabilised by phosphorothioates because of its larger atomic radius. Furthermore, it is difficult to control stereochemistry during synthesis,[79] and it is still unknown which configuration is optimum in therapeutic applications, or whether complex combinations are required for specific applications.[80]

The modified backbone species discussed in this thesis is triazole (TL, chapter 4). (Figure 1.22) and there are another two common modified backbones which share some similar characteristics; amide and carbamate (Figure 1.22).

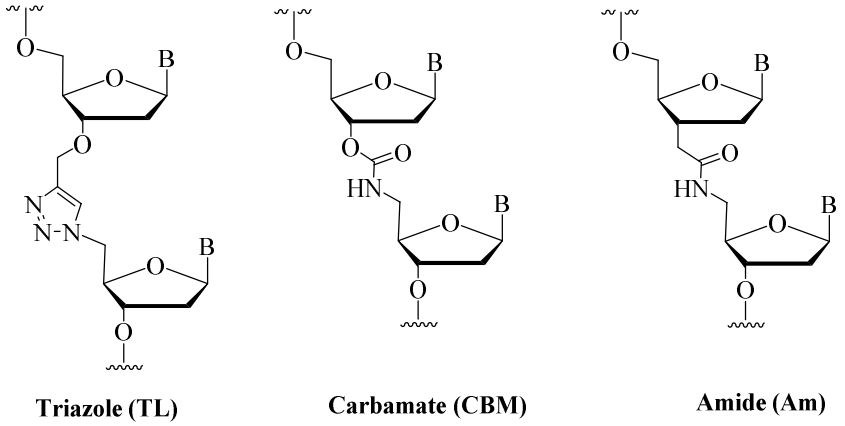

Figure 1. 22. Structure of modified backbones featured in this work, triazole (TL), carbamate (CBM) and amide (Am).

Modified backbones are very resistant to nuclease breakdown in general. Phosphatases, for example, have evolved to be highly specialised enzymes that exclusively cleave the P-O bond of a canonical phosphodiester. The addition of a modified backbone that is devoid of phosphate structure or charge prevents the backbone from being cleaved, extending the biological half-life. The changed backbone structure is the defining feature that determines its properties in oligonucleotides. Backbones that are either too short or too long disrupt the structure of a duplex, causing hydrogen bonding or base stacking to become unstable. Backbones that best mimic the phosphodiester provide the most stable duplexes. Charge neutrality is one of the key advantages of redesigned backbones. The delivery of a nucleic acid through cellular barriers is a major obstacle for oligonucleotide therapies.[81] The cell membrane is made up of a negatively charged hydrophilic surface and a charge-neutral hydrophilic interior.[82] This means that polyanionic phosphodiesters in conventional oligonucleotides have limited absorption into cells. Charge neutral backbones, such as

carbamates and amide, lower the oligonucleotide′s negative charge, enhancing membrane permeability and cellular uptake.[83]

The triazoles artificial backbone linkages in DNA and RNA have been thoroughly investigated. For example, Fujino and Isobe et al. described triazole linkage 1 (Figure 1.23 **A**) with improved stiffness, which was used to make a DNA analogue in which every native phosphate backbone was replaced by a triazole.[84, 85] El-Sagheer et al. published a triazole linkage 2 (Figure 1.23 **B**) in 2011 that destabilises duplexes in the same way as triazole linkage 1.[21, 86] Triazole linkage 2 is, on the other hand, relatively simple to chemically synthesise via the CuAAC process. Remarkably, this triazole backbone linkage is read accurately by DNA polymerase in the polymerase chain reaction (PCR) and is functional in Escherichia coli..[21, 87] Afterwards the authors reported that DNA strands with triazole linkage 2 can be transcribed by T7-RNA polymerase to produce RNA in high yield.[88] Birts et al. used a click-linked gene expressing the fluorescent protein mCherry to validate the biocompatibility of this artificial DNA connection in human cells in 2014.[87] The biocompatibility of the triazole linkage 2 was further demonstrated by the one-pot chemical synthesis of a 335 base-pair iLOV fluorescent protein gene with eight triazoles at chemical ligation sites, which was functional in vitro and in E. coli.[89] Taemaitree et al. recently discovered that an artificial triazole linkage works in crucial sections of single guide RNA (sgRNA), enabling efficient target DNA breakage in vitro and gene editing in cells.[90]

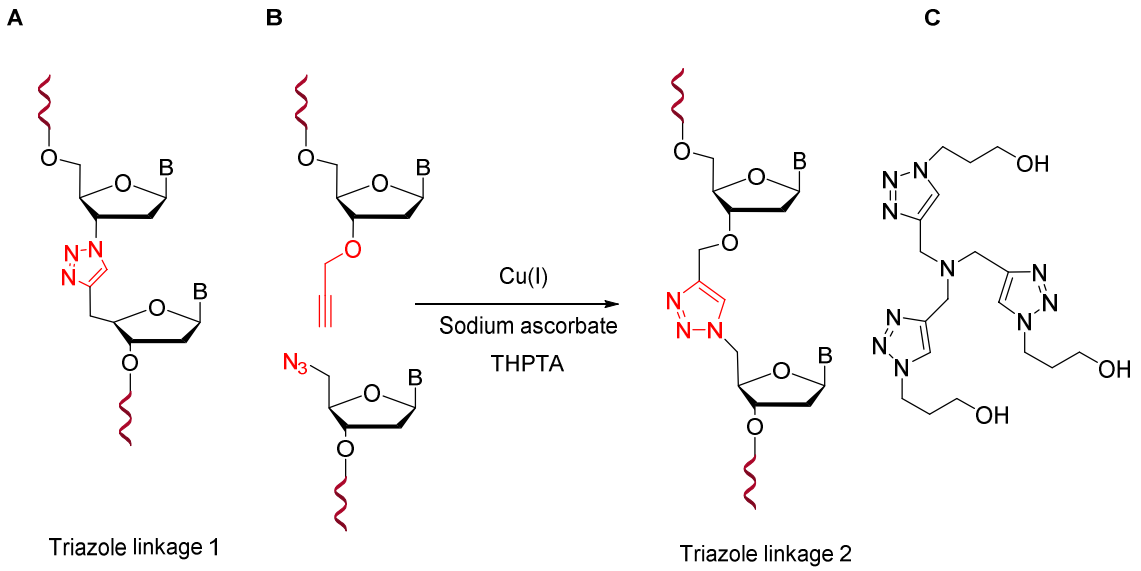

Figure 1. 23. A. Structure of a triazole linkage 1; **B.** CuAAC reaction of linear oligonucleotides containing 5′-azide/3′-alkyne modifications to generate triazole linkage 2; **C.** Chemical structure of the THPTA ligand. B = DNA bases.

In general, no single artificial backbone is ideal for all applications; instead, distinct backbones should be chosen for each purpose. The biocompatibility of a changed backbone is influenced by factors such as connection length, flexibility, and charge neutrality. These may usually be improved further by combining them with other alterations such 2′-*O*-methyl sugars, locked nucleic acids, or base changes.[91] Modified backbones could be useful in the development of oligonucleotide medicines, DNA libraries, and diagnostic agents. Although they have significant limitations, the ability to combine them with a variety of other modifications allows them to be tuned for improved performance.

1.7.2 Locked nucleic acid modification

T. Imanishi et al.[92, 93] and J. Wengel et al.[94, 95] developed locked nucleic acids (LNAs), which were 2′-4′-bicyclic nucleic acids (Figure 1.24). The nucleic acid flexibility is limited by the structure of these modified sugars, which lock the sugar into a 3′-*endo* conformation.[96, 97] LNAs have a high affinity for RNA targets and the capacity to increase duplex stability when integrated into oligonucleotides due to their preference for the 3′-*endo* conformation. Although enhanced binding is normally beneficial, excessive duplex stabilisation can result in non-specific target binding. As a result, LNA oligonucleotides must be specially engineered to balance their thermodynamic properties in order to allow for selective targeting while avoiding potentially toxic off-target effects.[98, 99] LNA has a wide range of applications and has been used in antisense gapmers sequences[84] as well as suitable substrates for enzymatic labelling.[100, 101] It has been demonstrated to be compatible with polymerases and has been employed in PCR amplification[102], and more recently, LNA has been used in CRISPR RNAs, where it was found to improve Cas9 endonuclease specificity when compared to RNA controls.[103]

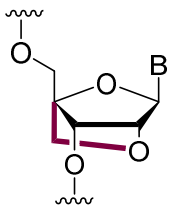

Figure 1. 24. Structure of the bicyclic ring fused Locked nucleic acid (LNA).

1.8 Antisense oligonucleotides

1.8.1 Mechanism of action of ASOs

Mutations in genomic DNA cause genetic disorders. These illnesses can be passed down from one generation to the next (hereditary) or they can develop spontaneously. The ′mutation′ can be as simple as a single base change in a gene, a more extensive gene alteration, as complex as multifactorial alterations in several genes (possibly resulting in the formation of an additional chromosome), or the deletion of sections or all of a chromosome. A gene mutation can result in the creation of an abnormal or harmful protein, or it can entirely cease the production of a protein, preventing it from performing its job. Severe genetic illnesses are relatively uncommon, as are effective medicines and cures.

The use of antisense oligonucleotides is one of the most common strategies in gene therapy research (ASO).[104-106] By acting on the genetic material of the cell, the antisense oligonucleotide approach uses fragments of DNA or RNA as medicinal agents to treat genetic problems.[107] Zamecnik and Stephenson were the first to recognise the potential of oligodeoxynucleotides as antisense agents in 1978.[108] It differs from traditional treatment techniques, in which a drug binds to an enzyme or receptor, causing the enzyme or receptor′s function to be modulated. Antisense oligonucleotides are DNA or RNA strands that are 15 to 30 nucleotides long. Their sequences bind to specific areas of messenger RNA (mRNA) or non-coding RNA via Watson-Crick base pairing. This hybridisation process interferes with the translation of the genetic code, preventing the creation of the desired protein. This is accomplished in two main ways. First, an ASO can activate RNase

H which cleaves the mRNA in ASO:mRNA heteroduplexes (Figure 1.25). This induces mRNA degradation, which prohibits the protein from being produced further. If the ASO:mRNA duplex does not activate RNase H, the ASO can inhibit the translation process through steric blockage of ribosome. The activation of RNase H has been found to be the more common method of the two.[109]

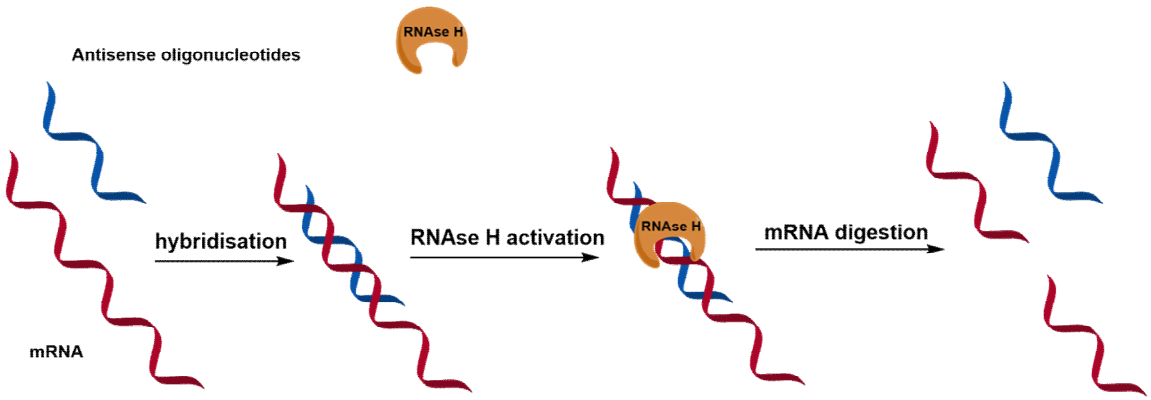

Figure 1. 25. RNase-H induced antisense oligonucleotide mechanism.

Exon-skipping or splice-switching is another antisense oligonucleotide mechanism. Splice-switching oligonucleotides control the splicing of pre-mRNA[110]. They repair faulty RNA and restore protein production, or they give rise to novel protein variants with altered characteristics, by doing so. Exon-skipping and splice-switching are induced by the ASO, which targets the exon-intron junction or splice site in pre-mRNA and disrupts the normal assembly of the spliceosome on the exon, redirecting the splicing route and causing the targeted exon to be skipped (Figure 1.26).[110]

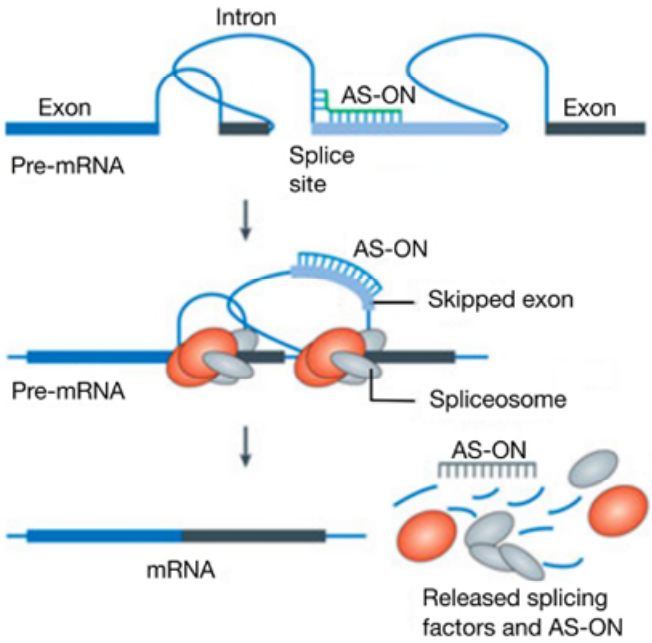

Figure 1. 26. Exon skipping mechanism. Figure used with permission of Dr. Ryszard Cole.[110]

Although antisense techniques are promising in theory, there are a number of issues that must be addressed before ASOs may be used as therapeutic candidates. Given the highly structured nature of RNA, identifying an accessible location for stable duplex formation with the ASO is a major problem .[111] In addition, foreign ONs are rapidly degraded in biological fluids by a wide spectrum of naturally occurring nuclease enzymes, hence the ASO must be modified to be resistant to nuclease degradation. Finally, a sufficient level of cellular uptake of the ASO along with the desired intracellular localization must be accomplished. Natural canonical oligonucleotides have to undergo a number of changes in order to meet these requirements. There are three categories of modification: nucleobase, sugar, and phosphate backbone alterations. (Figure 1.27). Some sequences should also be

avoided when designing ASOs. Intermolecular G-quartets can form from four consecutive guanosine residues, lowering the ′active′ concentration of ONs.[112] Also, CpG dinucleotide steps are more commonly present in viral or bacterial DNA and may interact to the TLR9 protein, they can stimulate immunological responses in mammalian systems.[113]

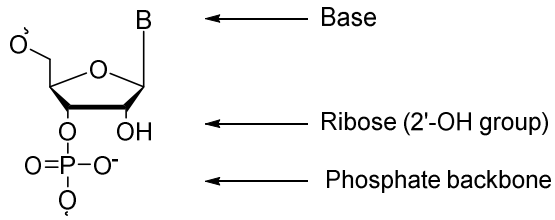

Figure 1. 27. Sites for chemical modification of oligonucleotides

RNA interference (RNAi) is probably the most promising and effective target mechanism for antisense applications (Figure 1.28). Pre-miRNAs are transported from the nucleus into the cytosol and processed by an endoribonuclease called Dicer.[109] Double-stranded RNA binds to Dicer, which cleaves it into 22-mer fragments. Another protein complex, RISC that contains Argonaut protein, binds these fragments. One of the RNA strands is eliminated but the other remains bound to the RISC complex and serves as a probe to detect mRNA molecules. When an mRNA molecule can pair with the RNA fragment on RISC, it is cleaved and degraded. The gene producing this mRNA has been silenced.[114]

Being an endogenous mechanism, RNAi presents a versatile tool that can be adapted to many needs. By introduction of exogenic miRNA known as small interfering RNA (siRNA), sequences can be used to target many genes of interest. The mechanistic details have been well defined, and a range of RNA modifications can be used to enhance siRNA

efficacy. Eric Rozners and co-workers have made significant progress in the use of amide backbones for siRNA both in the guide and passenger strands.[115] Modification to the siRNA is important as it allows for improvement of biological efficacy, particularly if it enhances oligonucleotide delivery or target specificity.[116]

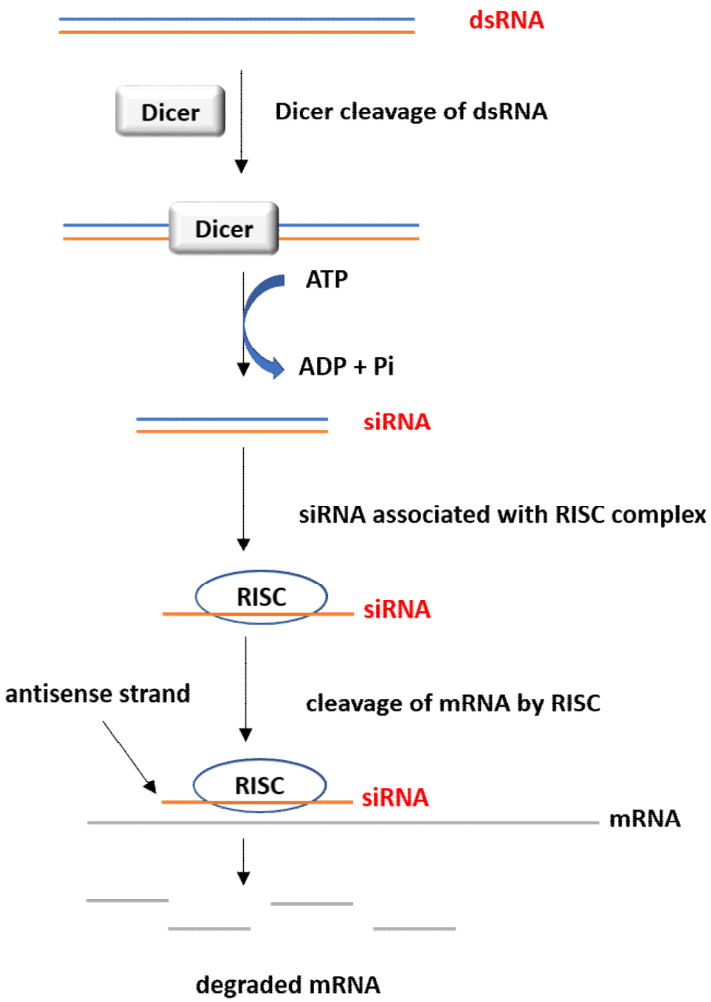

Figure 1. 28. Mechanism of RNA interference.

1.8.2 First generation antisense oligonucleotides

Backbone modifications in ′first generation′ antisense oligonucleotides focused on replacing non-bridging oxygen atoms in the phosphate group with sulphur atoms (Figure 1.29). Phosphorothioate backbones (PS) were originally synthesised in the 1960s by Eckstein and colleagues by a single replacement of oxygen with sulphur.[117, 118] A phosphorothioate oligonucleotide is a complicated mixture of diastereomers because the phosphorus atom is a chiral centre in DNA. Individual phosphorothioate groups have the Rp or Sp configuration after chemical production of PS oligonucleotide.[119] They have only minor structural changes from the parent phosphodiester backbone, and they bind to enzymes with similar affinities to phosphodiester oligonucleotides, according to X-ray crystallography and NMR investigations.[120-122]

Matsukura et al. and Agrawal et al. were the first to use PS DNA in antisense oligonucleotides to inhibit HIV-1 replication.[123, 124] In biological media, unmodified oligonucleotides have a half-life of about 1 hour, whereas their PS equivalents have a half-life of 100 times longer, indicating increased nuclease resistance.[125, 126] While the Sp diastereomer was totally resistant to enzymatic hydrolysis, Brautigam and Steitz reported in 1998 that the Rp phosphorothioate linkage was only slightly more durable than the unmodified phosphodiester version.[127] The nuclease enzyme complexed with a phosphodiester and Rp phosphorothioate oligonucleotide have substantial structural similarities, according to X-ray crystallography.[122] The sulphur atom in the Sp PS oligonucleotides, on the other hand, displaces the two metal ions in the nuclease active site that are required for enzymatic activity, preventing RNase H destruction.[127] Unfortunately,

phosphorothioate oligonucleotides have a stronger non-sequence specific interaction with some proteins that bind to polyanions, such as heparin, than do phosphodiesters.[128] Binding to plasma proteins, on the other hand, can shield ONs from filtration and improve their pharmacokinetic profile. Finally, when compared to natural counterparts, PS oligonucleotides show a lower affinity for complementary mRNA by about 0.5 °C (melting temperature of heteroduplex) per nucleotide. [110, 129]

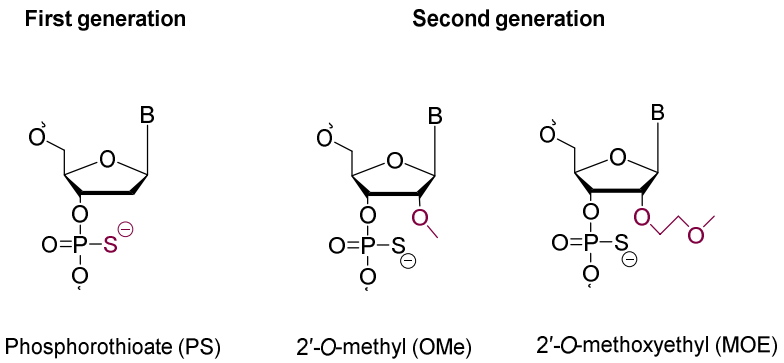

Figure 1. 29. First and second generation of antisense oligonucleotides.

1.8.3 Second generation antisense oligonucleotides

Antisense oligonucleotides of the "second generation" were developed to solve the problems phosphorothioates cause by incorporating alkyl modifications at the 2′ position of the ribose sugar to improve the hybridization characteristics of the ON to its target. 2′-*O*-methyl (OMe) and 2′-*O*-methoxyethyl (MOE) RNAs are the most commonly employed modifications (Figure 1.30).[130, 131] In comparison to PS oligonucleotides, these ONs preserve nuclease resistance while also having higher hybridization affinity and reduced toxicity.[132] The 2′-modification, on the other hand, suppresses RNase H pathway activation,

so RNase-H does not cleave the RNA target. Gapmers were created to solve the problem of RNase H inactivation.[133]

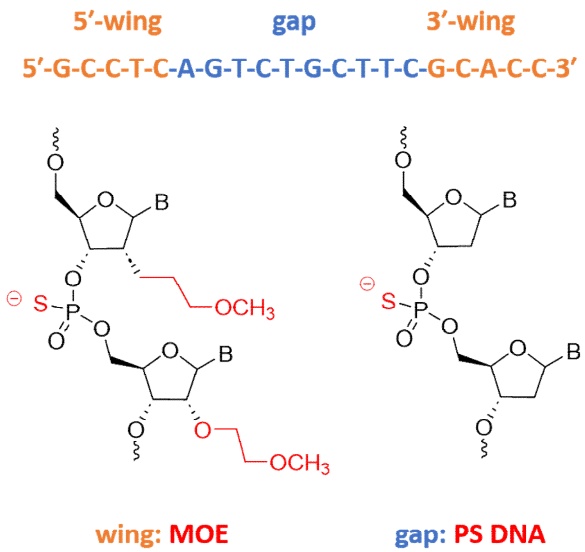

Figure 1. 30. Structure of antisense oligonucleotide gapmer.

Phosphorothioates are present in the middle of the oligonucleotide strand, with 2′-modified nucleotides at the 3′ and 5′ ends (Figure 1.30).[132, 134] RNase H can bind to the core region of the oligonucleotide and degrade the RNA target, and the termini improve enzymatic and thermal duplex stability. Although this improves the design, the central region of the ASO is more sensitive to endonuclease degradation than the termini, hence this design has an inherent constraint.

1.8.4 Third generation antisense oligonucleotides

Antisense oligonucleotides of the "third generation" and their mimetics have recently been developed to improve target affinity, pharmacokinetics, nuclease resistance, and cellular

uptake. Peptide nucleic acids (PNAs),[135, 136] N3′-P5′phosphoroamidates (NPs), locked nucleic acids (LNAs), and morpholino oligonucleotides (MF) are among the most effective of this generation of ONs, which incorporate more extensive changes on the phosphate backbone as well as the ribose sugar (Figure 1.31).

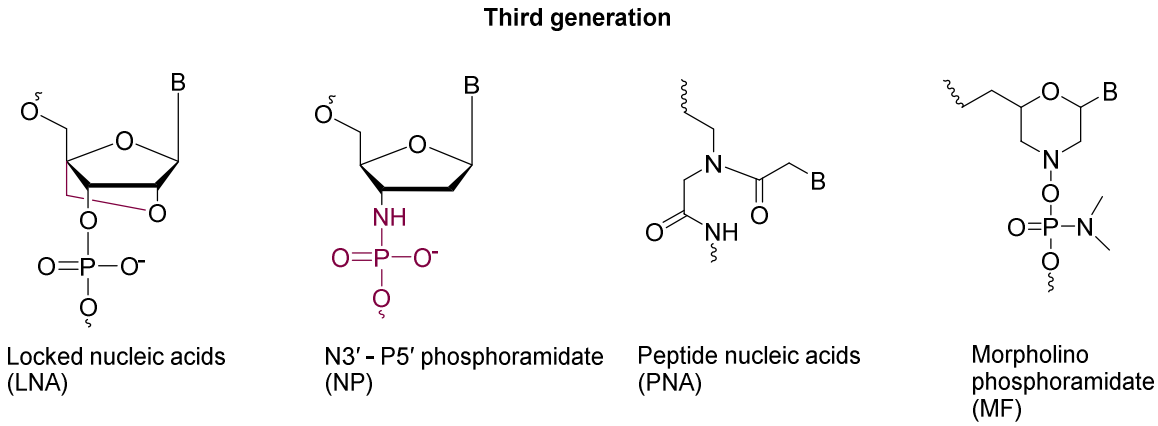

Figure 1. 31. Third generation of antisense oligonucleotides.

One of these ′third′ generation designs is N3′ - P5′ phosphoramidates (NPs), in which the 3′-hydroxyl in the phosphodiester backbone is replaced by a 3′-amino group (Figure 1.31).[137] NPs are resistant to nucleases and have a strong affinity for complementary RNA.[138] *In vivo*, their antisense activity was found to suppress the expression of the c-myc gene.[139] NPs physically interfere with mRNA translation or promote exon skipping and they work through steric obstruction rather than RNase H activation.

PNAs, which were first introduced in 1991 by Nielsen and colleagues, have polyamide rather than deoxyribose phosphate backbones (Figure 1.31).[140, 141] They are made with commercially available monomers protected with t-Boc or Fmoc utilising typical

automated solid-phase peptide synthesis procedures.[142, 143] PNA is a good structural mimic of DNA, and when Watson-Crick base pairing is used, it forms very stable duplexes with complementary DNA and RNA.[142, 144, 145] However, because PNA is electrostatically neutral, it is poorly absorbed by cells and, like DNA, requires the use of a delivery vehicle, such as cell penetrating peptides, to promote cell membrane penetration.[146, 147] There have been several examples of antisense PNA causing gene expression to be downregulated.[148-150] Although it is known that PNA-RNA duplexes do not activate RNase H, they could be very valuable in splicing modulation procedures[151, 152]due to quick elimination through the kidneys,[153] a short serum half-life, and restricted tissue bioavailability. Simple changes, such as cationic peptide conjugates, are being employed to address these difficulties.[154]

Summerton initially described morpholino oligonucleotides (MF oligomers) in 1985.[155] They are non-ionic DNA analogues with a morpholino moiety in place of the ribose sugar and a phosphoramidate backbone in place of the phosphodiester backbone (Figure 1.31). They have high aqueous solubility due to their excellent base stacking, which apparently allows the hydrophobic bases to be effectively shielded from the polar solvent.[155, 156] Nucleases in serum have no effect on MF oligomers.[157] They act by steric obstruction/splicing regulation and do not activate RNase H enzymes.[158] MFs are unlikely to bind serum proteins due to their uncharged backbone, resulting in decreased toxicity. Their propensity for hybridization to RNA is similar to that of natural DNA:RNA duplexes, although it is lower than that of PNA, NP, or LNA modified nucleic acids.[159]

1.8.5 FDA approved antisense drugs and clinical trials

Mipomersen, which acts via the RNase-H pathway and has 2′-MOE wings and a phosphorothioate backbone, is used to treat homozygous familial hypercholesterolemia. Mipomersen was first rejected by the FDA due to its severe liver toxicity, but it was approved in 2013 and is currently available for specific instances.[160, 161] Nusinersen (spinraza) (Figure 1.32) is an exon-skipping oligonucleotide used to treat spinal muscular atrophy (SMA) and was approved by the FDA in 2016. It has a 2´-*O*-methoxyethyl phosphorothioate backbone, and is a mixture of diastereomers at phosphorus. It does not restore the function of the faulty SMN1 gene but induces survival motor neuron (SMN) protein expression from SMN2 genes with an exon 7-skipping mutation.[162, 163] Another ASO that uses PS linked nucleotides in combination with MOE sugars is Inotersen (Figure 1.32). It is used to treat hereditary transthyretin amyloidosis and was authorised in 2018.[164]

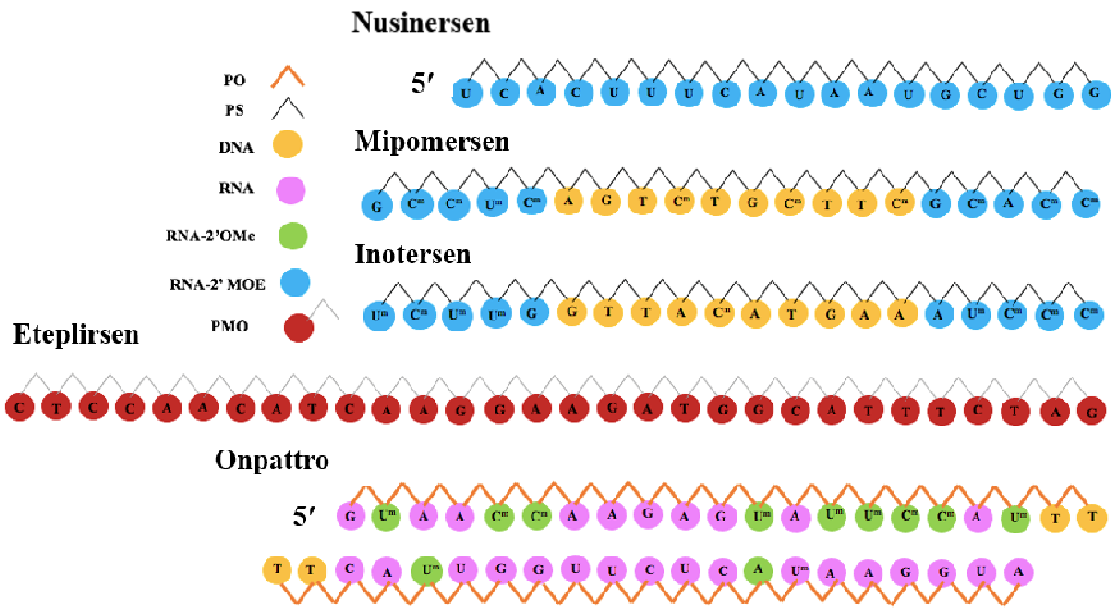

Figure 1. 32. FDA approved antisense oligonucleotides with backbone and sugar modifications. PO = phosphodiesters, PS = phosphorothioates, OMe = 2′-*O*-methyl RNA, 2′-MOE = 2′-(2-methoxy ethyl), PMO = Phosphorodiamidate morpholino, ^{m} = methylation on the nucleobase at the 5-position.

Eteplirsen (Figure 1.32) was the first PMO medicine to be approved in the United States, and the FDA expedited its approval. Eteplirsen promotes exon skipping by binding to enhancer sites within pre-RNA, which is significant for the treatment of Duchenne′s muscular dystrophy because it allows for frame shift correction and production of a shortened dystrophin protein that restores partial function.[165, 166]

Onpattro is a first in class short interfering RNA (siRNA) drug and it is a double stranded siRNA encapsulated in a lipid nanoparticle for delivery to intracellular compartments of hepatocytes where transthyretin is produced (Figure 1.32).[167] It is a liposome formulation containing a slightly modified siRNA encapsulated with lipid excipients and delivery is by intravenous infusion composed of ionizable cationic lipids (DLin-MC3-DMA), phospholipid (DSPC), cholesterol, and polyethylene glycol-modified lipids (PEG2000-C-DMG), combined by rapid mixing under acidic conditions, followed by a pH-dependent fusion process.[168, 169] It treats polyneuropathy in people with hereditary transthyretin-mediated amyloidosis.[170]

Inclisiran is also an siRNA therapy that targets/degrades PCSK9 mRNA. PCSK9 is derived almost entirely from the liver, hence, therapeutic approaches that target and reduce hepatic production of PCSK9 offer an important therapy. Targeted delivery into liver cells by $(GalNac)_3$ - attached at the 3´-end of the sense strand (Figure 1.33).[171, 172] Specific binding

of the GalNAc ligand to asialoglycoprotein receptors (ASGPR) enables targeted uptake of inclisiran into hepatocytes[173]. Following uptake into hepatocytes, the antisense strand of inclisiran (which specifically corresponds to human PCSK9 mRNA) is integrated into the RNA-induced silencing complex, directing the catalytic breakdown of PCSK9 mRNA and thus preventing PCSK9 protein translation.[174]

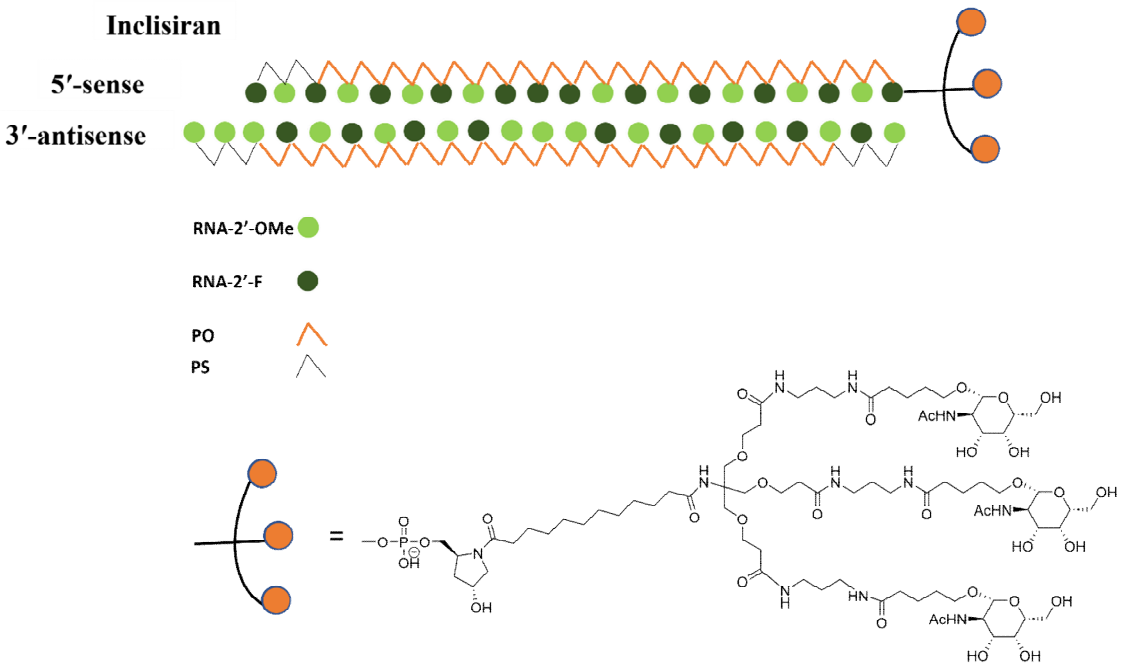

Figure 1. 33. Structure of Inclisiran. The sense strand is conjugated with a triantennary N-acetylgalactosamine (GalNAc) ligand to enable targeting of hepatocytes via the asialoglycoprotein receptor (ASGPR).

1.9 Research aims

The overall aim of this thesis is: 1) to develop and synthesise new combination oligonucleotide probes; 2) to design and incorporate artificial DNA backbones into

oligonucleotides and to assess their properties for various applications. The specific aims of this work are:

Chapter 2 – To synthesise a new phosphoramidite which enables orthogonal double labelling to form combination oligonucleotide probes. The steady state and time-resolved fluorescence and duplex thermal stability properties of these labelled combination oligonucleotide probes will be investigated.

Chapter 3 – To assess the capability of these new combination oligonucleotide probes that aim to detect a SARS-COV-2 sequence in a LAMP (Loop-mediated isothermal amplification) assay.

Chapter 4 – To develop synthetic procedures for the synthesis of triazole-LNA dimer phosphoramidites, to incorporate these dimers into oligonucleotides, and to assess the biophysical properties of triazole-LNA modifications for potential antisense applications.

Chapter 2

Synthesis, site-selective labelling and properties of combination probes for DNA and RNA detection

Chapter 2 – Synthesis, site-selective labelling and properties of combination probes for DNA and RNA detection

2.1 Introduction

Clinical diagnostics often involves the analysis of genomic DNA, mRNA and non-coding RNA in which fluorogenic probes have played an important role in detecting specific DNA or RNA sequences for diagnostics applications.[175] Fluorogenic oligonucleotide probes are nucleic acid-based biosensors that respond to targets by a change in fluorescence. In general, such probes consist of a modified synthetic DNA or RNA strand for sequence-specific target recognition and a signal transduction element to report on the interaction with their target.[35, 36] Various fluorogenic oligonucleotide probe designs have been used to detect and image bioanalytes, including mRNA, with excellent specificity and sensitivity.[37, 175]

Molecular Beacons (MBs) and HyBeacon probes are typical examples; MBs are hairpin-shaped single-stranded oligonucleotides with a fluorophore at one end and a quencher at the other (Figure 1.17).[39] Due to the intramolecular quenching of the fluorophore, MBs have weak or negligible fluorescence emission in their hairpin-state. However, upon hybridization with their targets, MBs switch from a hairpin to a rigid linear structure which separates the fluorophore from the quencher, producing strong fluorescence emission. HyBeacon probes are single-stranded oligonucleotides that contain one or more fluorophores covalently attached to internal nucleotides (Figure 1.18). Collisional

quenching occurs when these probes are single-stranded and fluorescence is 'turned on' on hybridisation with their complementary DNA target (Figure 1.18).[42, 43]

Thiazole orange (TO) is a fluorescent DNA binding molecule that has been used for the detection of nucleic acids.[176-183] Fluorescence increase upon target hybridisation is caused by restriction of rotation about the methine bridge of TO when it intercalates into a double-stranded DNA or RNA.[184] The applications of thiazole orange in fluorescent sensing of biomolecules have recently been reviewed.[185] Covalent attachment of thiazole orange to oligonucleotide probes has also been well studied.[54, 183, 186-194]

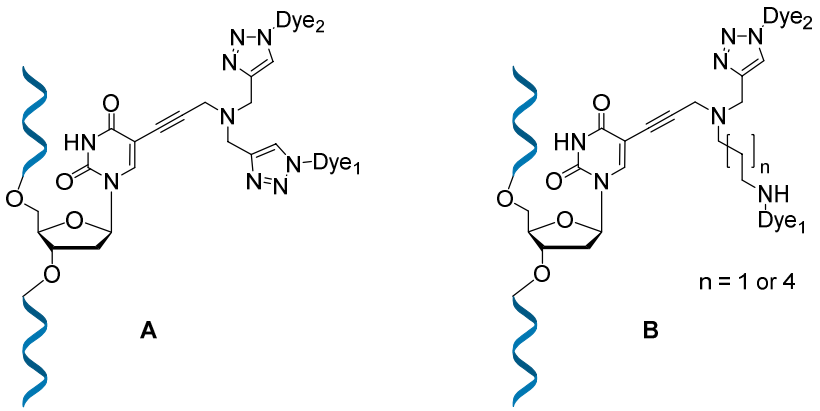

Figure 2. 1. Structure of combination probe (A) and new approach (B).

Recently Prof. Brown's group reported combination probes composed of TO and a reporter dye attached to the same thymidine base for RNA detection (Figure 2.1 A).[195] The fluorescence of the single-stranded probe is switched off by collisional quenching between TO and the adjacent reporter dye. Upon binding to the target strand, TO intercalates via the major groove of the duplex and becomes separated from the reporter fluorophore. As

a consequence, the probe emits a strong fluorescent signal due to excitation of TO and fluorescence resonance energy transfer (FRET) to the reporter fluorophore (Figure 2.2 a). The combination of TO and a bright reporter dye provides a low single-stranded fluorescence background and strong double-stranded signal. A particular advantage of these combination probes is stabilisation of the probe-target duplex by TO-intercalation.

Ikeda et al. coupled FRET with a second energy transfer process, excitonic interaction by synthesising probes that contained an internal doubly TO-labelled nucleotide and a terminal Cy5 reporter dye. The authors demonstrated that their exciton-controlled hybridization-sensitive fluorescent oligonucleotide probes (ECHO) could monitor distribution of poly(A) RNA in the nucleoplasm *in vitro* and fixed cells.[182] Improving limit of detection while maintaining favourable F_{ds}/F_{ss} ratio is highly desirable for visualization of mRNA within a complex tissue.[178] A plausible solution to this issue was demonstrated by PNA-based TO-FIT probes with various reporter dyes. The best results were obtained with Alexa594, NIR664 and ITCC that quench the fluorescence of TO and reporter dyes both in ss and ds state simultaneously increasing the $F_{ds}/F_{ss,}$ ratio.[179] Recent results suggest that a DNA based FIT design is superior for cellular applications compared to the PNA design.[196] A combination probe (Figure 2.1 A) with two incorporations of the modification with ATTO647N as the reporter dye was used to detect the R516G locus of the CFTR gene, and detection of the G-mutant by fluorescent melting studies.[10] Its favourable properties such as good F_{ds}/F_{ss} (up to 19.5-fold) arise from the collisional quenching of the dyes in the unbounded state, which upon binding to the target, TO intercalates and an efficient FRET based signal is obtained while providing increased thermal stability due to

intercalation of TO. The main drawback of this method is demanding synthesis of the TO-thymidine modification as well as high polarity of the phosphoramidite monomer and need for ultra-mild protective groups on standard nucleotide monomers due to the sensitivity of thiazole orange to ammonia, both of which limit wider application of this approach.[69]

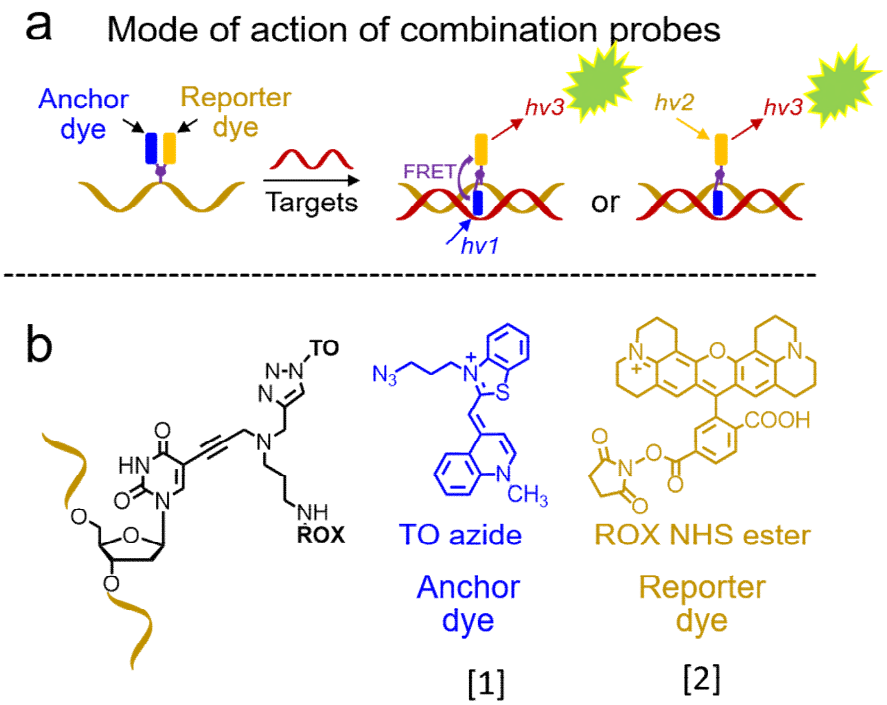

Figure 2. 2. (**a**) Mechanism of action of oligonucleotide combination probes for fluorescence detection of target nucleic acids. (**b**) Chemical structures of combination probes developed in this work, the thiazole orange anchor dye (TO) and FRET reporter dye (ROX).

The work in this thesis describes an improved synthesis of combination probes involving chemospecific functionalization with TO [**1**] and fluorescent dyes such as ROX [**2**] (Figure 2.2 b).[197] To achieve this, we have developed a new AP-C3/AP-C6 dT phosphoramidite

monomer containing an alkyne and a trifluoroacetyl (TFA)-protected amine. Multiple incorporations of the modified nucleotide in combination probes leads to excellent fluorescence on hybridization with the complementary target, while TO also reverses the detrimental effect on duplex stability caused by the reporter dye. We also show that combination probes composed of 2′-*O*-methyl ribosyl nucleotides have good duplex stability and high fluorescence when bound to RNA targets.

2.2 Synthesis of new modified dT monomer for combination probes

To site-selectively label oligonucleotides with TO azide and ROX NHS ester, AP-C3 and AP-C6 dT phosphoramidites were synthesised according to Figure 2.3. The only structural difference between these two monomers is the length of aminoalkyl linkage; one includes three carbon atoms and the other includes six carbon atoms. This bifunctional handle, with an alkyne and an amine was chosen so that it could be reacted sequentially in an amide coupling with an NHS-ester and with an azide in a copper catalysed cycloaddition (CuAAC). These reactions are orthogonal, and proceed in aqueous solution with high yield and selectivity. To synthesise the required monomer [**7**], 3-aminopropan-1-ol was reacted with ethyl trifluoroacetate to protect the amine with TFA protection in good yield (n=1, 97%; n=4, 68%),[198] and the alcohol of compound **3** was oxidized to aldehyde using Dess-Martin periodinane reagent (n=1, 51%; n=4, 89%).[199] Then, compound **4** was reacted with dipropargylamine and $NaBH(OAc)_3$ to provide compound **5** with two alkyne groups in high yield (n=1, 95%; n=4, 98%). Compound **5** was coupled with 5-iodo-5′-DMT-deoxythymidine [**13**] to give compound **6** (n=1, 59%; n=4, 54%) which was converted to AP-C3 dT phosphoramidite monomer (compound **7**) using a standard phosphitylation

protocol (n=1, 72%; n=4, 61%). Choice of the propargyl group was based on the previous monomer where the length of the amine linker was similar.[10]

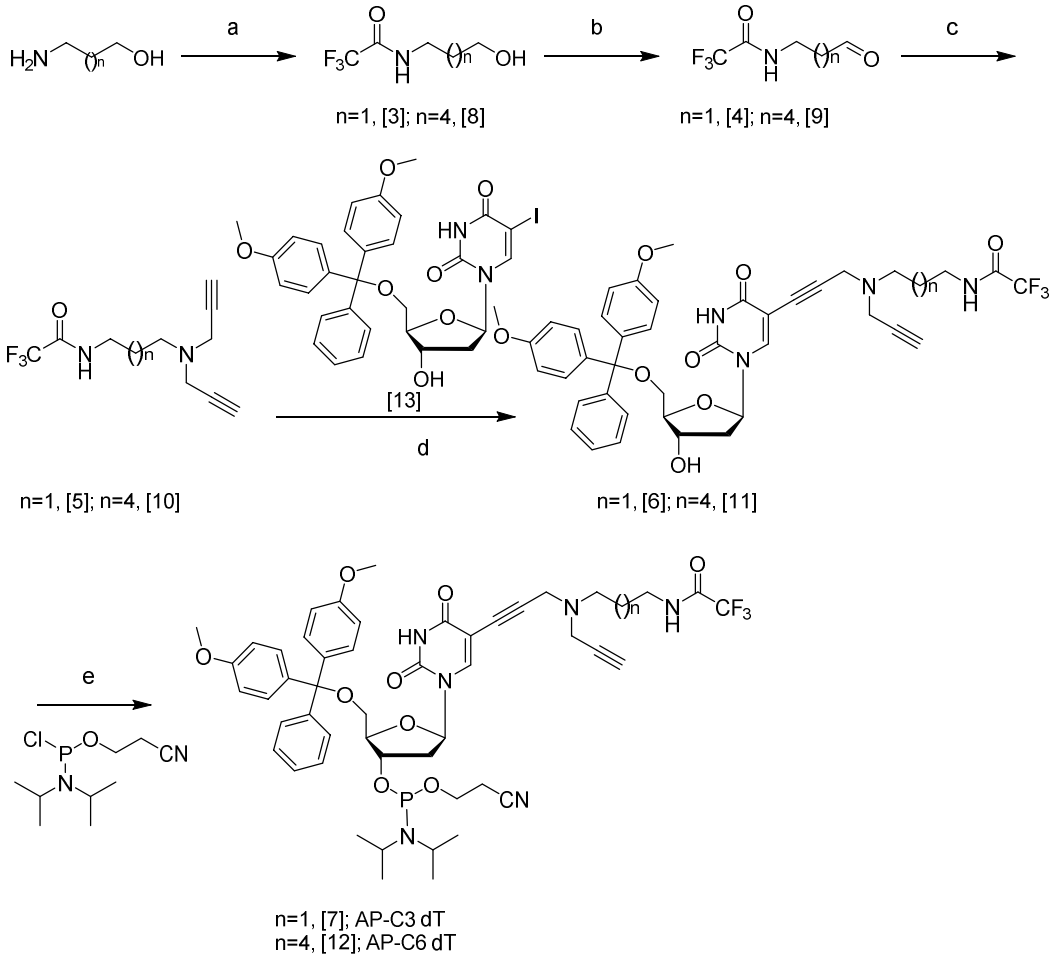

Figure 2. 3. Synthesis of **AP-C3 dT** (n = 1) monomer, reagents and conditions: (a) Ethyl trifluoroacetate, 3 h, 0 °C – r.t., 97%; (b) Dess-Martin periodinane, CH_2Cl_2, 0 °C – r.t., 2 h, 51%; (c) Dipropargylamine, $NaHB(OAc)_3$, CH_2Cl_2, r.t., 2 h, 95%; (d) 5-iodo-5′-DMTr-deoxythymidine, $PdCl_2(PPh_3)_2$, CuI, DMF, NEt_3, r.t., 12 h, 59%; (e) 2-Cyanoethyl N,N-diisopropylchlorophosphoramidite, DIPEA, CH_2Cl_2, r.t., 1.5 h, 72%.; Synthetic of **AP-C6 dT** (n = 4), reagents and conditions : (a) Ethyl trifluoroacetate, RT, 2.5 h, 68%; (b) Dess-Martin periodinane, CH_2Cl_2, 0°C – r.t., 2 h, 89%; (c) dipropargylamine, $NaHB(OAc)_3$, CH_2Cl_2, r.t., 2 h, 98%; (d) 5-iodo-5′-

DMTr-deoxythymidine, $PdCl_2(PPh_3)2$, CuI, NEt_3, DMF, r.t., 24 h, 54%; (e) 2-Cyanoethyl *N*, *N*-diisopropylchlorophosphoramidite, DIPEA, CH_2Cl_2, r.t., 1.5 h, 61%.

2.3 Novel combination probes design

Next both monomers were incorporated into probe sequences by automated standard solid phase oligonucleotide synthesis (Table S1-S5). A DNA probe (22-mer) sequence derived from previous work[69] was used for a comparison with the old design of combination probes and short (10-mer) RNA probe sequence was used for optimisation of TO attachment position (TO_{B6}-NHS and TO_{B3}-N_3) in terms of fluorescence response. Attachment to the nucleobase by the benzothiazole moiety was chosen as we previously found that attaching the thiazole orange to the 5-position of uracil by the quinoline moiety gives less stable oligonucleotides.[183]

Single, double and triple incorporations of the monomer into probe sequences were performed, because it was predicted that multiple incorporations would provide favourable photophysical properties, as has been shown previously with the double propargyl monomer (Figure 2.1 A).[69] Azide dyes were incorporated via the CuAAC reaction. The reporter dye 6-ROX-NHS (RX) was chosen as spectral overlap with TO results in a bright signal.[69] TO_{B6}-NHS labelled was carried out using protocols in the Brown group.[183] Due to the orthogonal labelling abilities of AP-C3 and AP-C6, dye combinations of TO, 6-ROX and TO/6-ROX were synthesised in order to investigate the interaction between the intercalating anchor (TO) and the reporter dye. These probes were purified by HPLC after labelling reactions and purity was analysed by HPLC-MS (Figure 2.5).

Oligonucleotides containing single, double and triple incorporations of AP-C3 dT were synthesised on an ABI 394 DNA synthesiser and deprotected in concentrated aqueous ammonia at 55 °C for 5 hours (standard conditions). After purification by high-performance liquid chromatography (HPLC), the oligonucleotides were characterized by electrospray mass spectrometry (ES^-). The data in Table S1 demonstrates the successful incorporation of AP-C3 dT into DNA. Next, the AP-C3 dT-modified oligonucleotides were labelled with TO_{B3} azide [**1**] and separately with ROX NHS ester [**2**]. For TO-labelling, AP-C3 dT-modified oligonucleotides were coupled with TO_{B3} azide [**1**] in triethylammonium acetate (TEAA) buffer catalysised by CuI:THPTA (tris(3-hydroxypropyltriazolylmethyl)-amine) to produce 1,4-substituted 1,2,3-triazole linkages.

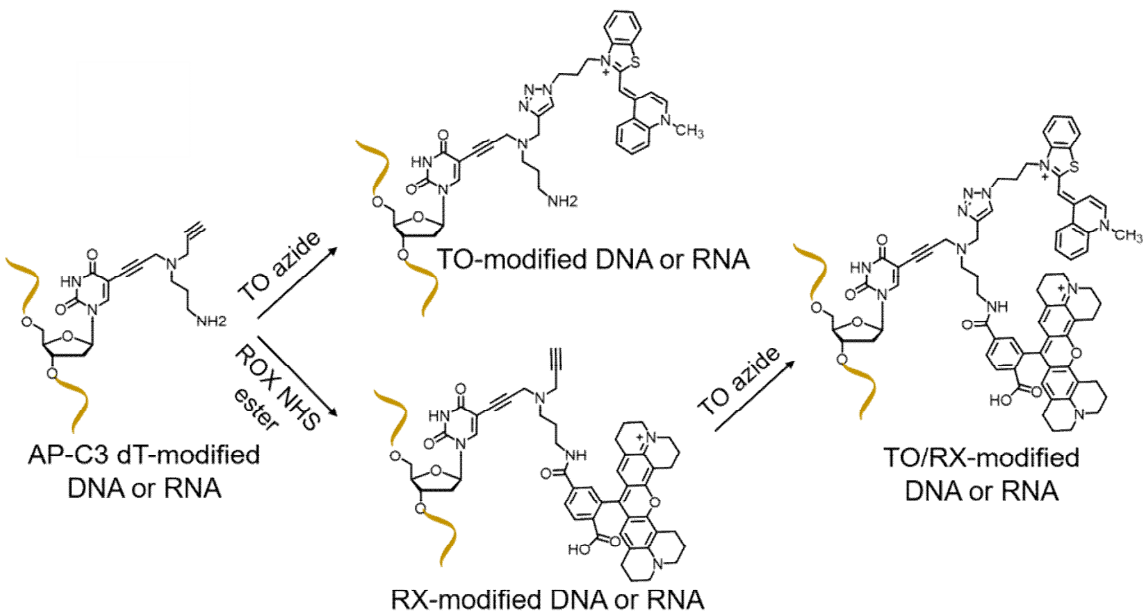

Figure 2. 4. Labelling of oligonucleotides with TO and ROX dyes.

For labelling the amino function with ROX (amide formation), AP-C3 dT-modified DNA was reacted with ROX NHS ester [**2**] in bicarbonate buffer at 37 °C for 3 hours. RX-labelled oligonucleotides were further incubated with TO_{B3} azide [1] to produce TO/RX-dual-labelled oligonucleotides (Figure 2.4). Both labelling steps proceeded in near quantitative yield as monitored by HPLC (Figure S1). When the reactions were completed, the unreacted dyes were removed by NAP gel-filtration and the labelled oligonucleotides were purified by reversed-phase HPLC. The post-purification analytical HPLC chromatograms and mass spectra of the dye-labelled oligonucleotides indicate high purity as a consequence of efficient site-selective labelling with TO or ROX dyes at the AP-C3 dT sites (Figures 2.5). All labelling reactions of AP-C6 dT-modified DNA were performed in an identical way to that of AP-C3 dT-modified DNA.

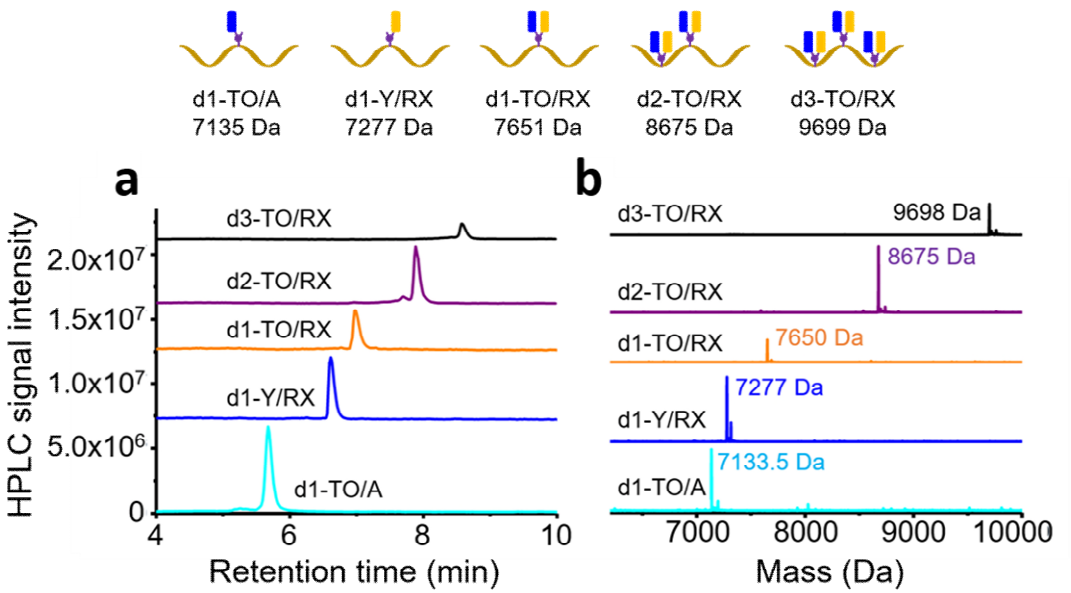

Figure 2. 5. Characterization after site-selective labelling of oligonucleotides with TO and ROX dyes. (**a**) HPLC chromatograms and (**b**) mass spectra of the oligonucleotides containing TO and ROX dyes.

Oligonucleotide sequences: d1: 5′-CGCTTCXGTATCTATATTCATC; d2: 5′-CGCTTCXGTATCTAXATTCATC; d3: 5′-CGCTXCTGTAXCTATAXTCATC, where X=labelled AP-C3 dT.

2.4 Fluorescence studies of AP-C3/C6 combination probes

Short AP-C3 and AP-C6 dT modified oligonucleotides were labelled with TO_{B3} azide and TO_{B6} NHS ester to see different performance on hybridization to the respective DNA and RNA targets (Table S5). The steady-state fluorescence indicates that TO_{B3}-labelled AP-C3 probes can emit higher fluorescence than TO_{B6}-labelled AP-C3 probes on binding with targets which may be related to the duplex conformation or entropic factors (F_{ds}/F_{ss} for ORN5-TO_{B3} = 17.9, ORN5-TO_{B6} = 10.2) at λ_{ex} = 510 nm.

Having confirmed the efficient site-selective labelling of AP-C3 dT-modified oligonucleotides with TO and ROX dyes, we further studied the fluorescence response of TO/RX-labelled probes when bound to complementary DNA and RNA oligonucleotides. As described above, TO is a DNA intercalator that shows bright fluorescence emission after intercalating into duplexes[200] due to restricted rotation at its methine bridge. Consistent with this, single TO-labelled DNA (d1-TO/A) shows enhanced fluorescence emission after hybridization with its complementary DNA target (Figure 2.6 a, black lines). However, no significant change in the fluorescence emission of RX-labelled probe (d1-Y/RX) was observed upon hybridization with the DNA target (Figure 2.6 a, blue lines). For the TO/RX combination probes, weak fluorescence emission was observed in the single strand. However, upon hybridization with target DNA, the single labelled probe

showed a slight increase in fluorescence at the maximum emission wavelength of ROX (red lines in Figure 2.6 a). Comparing the single (d1-TO/RX), double (d2-TO/RX) or triple (d3-TO/RX) incorporations of the TO/RX functionalised nucleotide indicated that the triple incorporation shows far greater fluorescence enhancement after hybridization to complementary DNA with a ratio of > 16.7-fold in ds/ss RX fluorescence. This is an interesting and useful observation, suggesting possible uses in real-time PCR. In addition, d3-TO/RX is also effective in detecting a complementary RNA target (Figure 2.6 d, Figure S2). These results demonstrate that DNA combination probes with multiple additions of the labelled AP C3-dT monomer (probes d2-TO/RX and d3-TO/RX) are highly effective in the fluorescence detection of complementary nucleic acids.

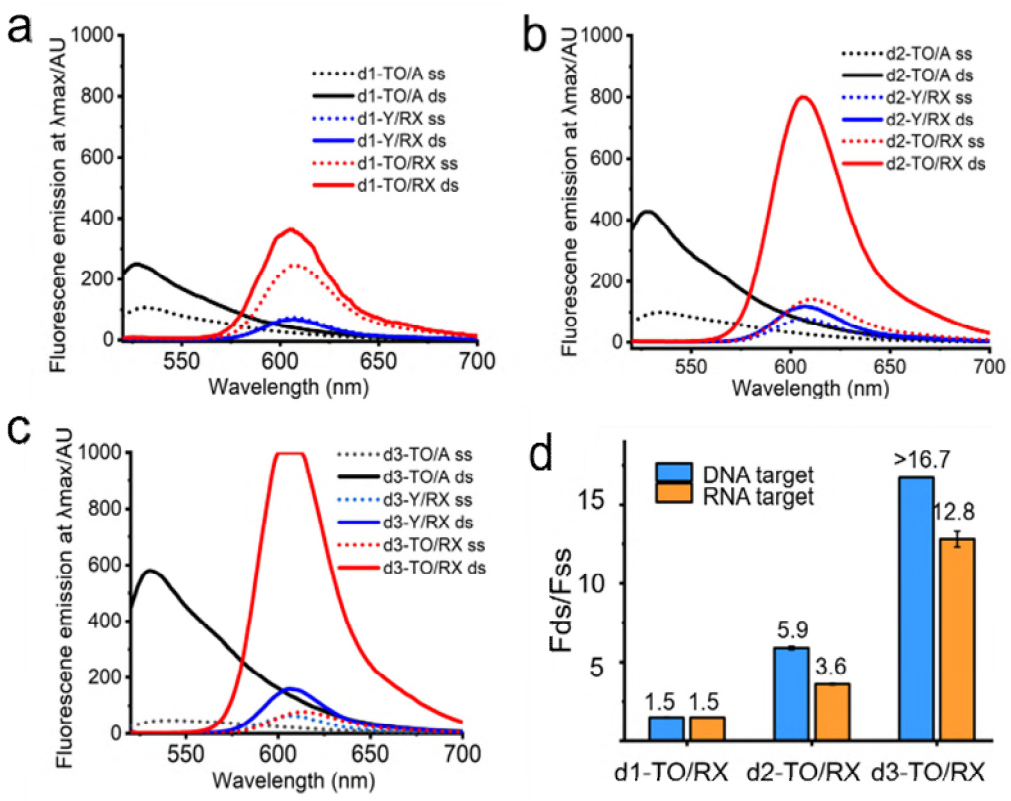

Figure 2. 6. Fluorescence spectra of TO, RX or TO/RX probes bound to DNA target. (**a**) Fluorescence spectra of 0.25 µM single TO, RX or TO/RX-labelled DNA probes to 0.275 µM DNA target. (**b**) Fluorescence spectra of 0.25 µM double TO, RX or TO/RX-labelled DNA probes to 0.275 µM DNA target. (**c**) Fluorescence spectra of 0.25 µM triple TO, RX or TO/RX-labelled DNA probes to 0.275 µM DNA target. Solid red curve shows saturation of detector (Table S6). (**d**) Fold-change in fluorescence intensity of TO/RX-labelled DNA probes before and after hybridization with complementary DNA (blue columns) or RNA (orange columns). ss: single strand. ds: double strand. Conditions: 10 mM phosphate buffer, 200 mM NaCl, pH 7.0. Oligonucleotide sequences are shown in Table S1. Data points were measured in triplicate.

2.5 UV and fluorescence melting studies of AP-C3 combination probes

2.5.1 Thermal stability studies on matched and mismatched targets

Thermal stability (melting temperature), as measured by the temperature of dissociation of nucleic acid duplexes, is an important factor when designing oligonucleotide probes as it relates to the affinity of an oligonucleotide for it target).[201] The intercalation properties of TO when conjugated to a nucleobase are known to increase duplex stability.[49, 69, 183] We studied the thermal stability of DNA probes containing TO, RX and TO/RX modifications against DNA and RNA targets to determine the effects of the labels on duplex stability (Table 2.1, left). We have performed both UV melting and fluorescence melting because we had to measure T_m of unmodified oligonucleotides by UV melting and make good comparison with TO, ROX, TO/ROX labelled DNA probes. The duplexes labelled with TO show improved stability which can be attributed to the intercalation of TO. In principle, a greater number of TO moieties should induce greater duplex thermal stability, and

this was indeed the case, with an increase of around 8.9 °C for three TO-incorporations compared to only single incorporation. Labelling of ROX decreases the melting temperature of the duplexes, whether or not they contain TO, probably because in the single strand the ROX dye can bury itself in the hydrophobic environment of the coiled DNA strand created by the aromatic nucleobases, whereas in the rigid duplex it is exposed to the aqueous environment, making duplex formation more entropically unfavourable. As a result, RX-only labelled duplexes show low thermal stability compared to TO/RX dual-labelled duplexes (drop of 3.5 °C for three RX-incorporations). This decrease of T_m is clearly dependent on the reporter dye, which could be altered by careful evaluation of dye and attachment to minimize this effect in future work.[69]

Table 2. 1. Fluorescence and UV-derived melting temperatures of DNA (left) and 2′-OMe RNA probes (right) hybridised to complementary targets. Samples were made up to 0.4 μM oligonucleotide probes against 0.44 μM targets in buffer (NaH_2PO_4, 10 mM; NaCl 200 mM) at pH 7.0. The samples were initially denatured by heating to 85 °C at 1 °C min^{-1} then cooled to 25 °C at 1 °C min^{-1} and fluorescence was recorded every 0.1 °C. Oligonucleotide sequences: d1: 5′-CGCTTCXGTATCTATATTCATC; d2: 5′-CGCTTCXGTATCTAXATTCATC; d3: 5′-CGCTXCTGTAXCTATAXTCATC, where X=labelled dT.

Probe	T_m/°C (DNA target)	T_m/°C (RNA target)	Probe	T_m/°C (DNA target)	T_m/°C (RNA target)
d1-Y/A	63.7(UV)	61.9(UV)	r1-Y/A	45.5(UV)	63.5(UV)
d2-Y/A	64.7(UV)	63.5(UV)	r2-Y/A	46.8(UV)	63.1(UV)
d3-Y/A	65.6(UV)	63.8(UV)	r3-Y/A	48.7(UV)	63.4(UV)
d1-TO/A	64.5(FL)	64.0(FL)	r1-TO/A	49.0(FL)	66.0(FL)
d2-TO/A	69.5(FL)/71.2(UV)	65.5(FL)	r2-TO/A	53(FL)/53.8(UV)	67(FL)/68.3(UV)
d3-TO/A	74.5(FL)	69.0(FL)	r3-TO/A	51.0(FL)	62.0(FL)
d1-TO/RX	60.5(FL)	59.5(FL)	r1-TO/RX	48.0(FL)	65.0(FL)
d2-TO/RX	56.0(FL)	54.0(FL)	r2-TO/RX	45.0(FL)	63.0(FL)
d3-TO/RX	51.5(FL)	51.5(FL)	r3-TO/RX	53.0(FL)	50.0(FL)
d1-Y/RX	57.0(FL)	57.5(FL)	r1-Y/RX	47.5(FL)/48.7(UV)	65.5(FL)/66.3(UV)

d2-Y/RX	52.0(FL)	54.0(FL)	r2-Y/RX	36.5(FL)	60.5(FL)
d3-Y/RX	48.0(FL)	52.0(FL)	r3-Y/RX	24.0(FL)/25.9(UV)	51.0(FL)

We also investigated the duplex stability of d1-TO/A (DNA probe labelled with single TO only) and d1-TO/RX A (DNA probe labelled with single TO and ROX) probes against targets containing a single-nucleotide mismatch. All DNA duplexes and DNA/RNA targets with a G:T mismatch opposite to TO, or with an A:C mismatch five-bases away from TO, gave lower melting temperatures than the fully complementary double strands (Table 2.2). For example, the T_m of the duplex between d1-TO/RX and its DNA target is 60.5 °C, compared to 55 °C for its G:T mismatch, and 48.5 °C for its A:C mismatch DNA target. These results indicate that combination probes can discriminate clearly between matched and mismatched targets.

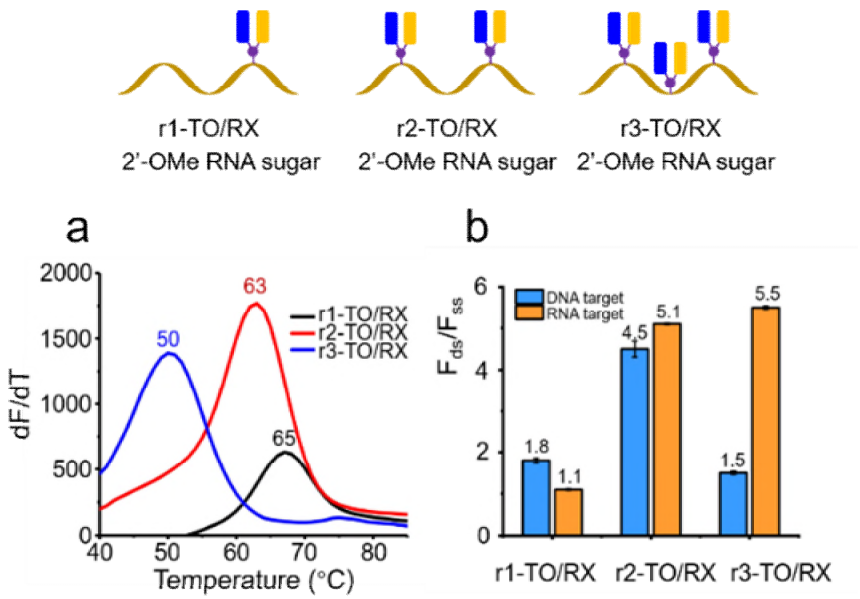

Figure 2. 7. Thermal stability and fluorescence of TO/RX-functionalised 2′-OMe RNA probes when bound to complementary targets. (**a**) Fluorescence melting temperature of 0.4 µM single, double and

triple TO/RX-incorporated 2′-OMe RNA probes bound to 0.44 μM RNA target. (**b**) Ratios of fluorescence intensity of 0.25 μM TO/RX-incorporated 2′-OMe RNA probes before and after hybridization with 0.275 μM DNA or RNA targets when the excitation wavelength is 510 nm. Conditions: 10 mM phosphate buffer, 200 mM NaCl, pH 7.0. Oligonucleotides sequences are shown in Table S2. Data points were measured in triplicate.

Given that the biomedical applications of fluorogenic oligonucleotides probes require high fluorescence as well as stability against enzymatic degradation in biological fluids, we constructed combination probes containing nucleotides that stabilise oligonucleotides against degradation *in vivo*. Probes composed of 2′- modifications are known to possess this property, and have been employed in the clinical development of therapeutic oligonucleotides.[202, 203] We synthesised 2′-OMe RNA probes containing AP-C3 dT (1, 2 and 3 additions), labelled them with TO and ROX and investigated the properties of the resulting 2′-OMe RNA combination probes (Figure 2.7). The 2′-OMe RNA probes with single (r1-TO/RX), double (r2-TO/RX) and triple (r3-TO/RX) incorporations of TO and ROX (Table S2) all displayed good duplex stability when hybridized with an RNA target, 65 °C for r1-TO/RX, 63 °C for r2-TO/RX and 50 °C for r3-TO/RX (Figure 2.7 a and Table 2.1, right). However, in the case of r3-TO/A and r3-TO/RX, the presence of three TO moieties did not improve duplex stability against DNA or RNA compared to two TO moieties (r2-TO/A). This indicates that there should be a minimum separation between the TO intercalators for them to produce the optimum increase in duplex stability and emphasises the extreme duplex destabilisation due to the presence of the ROX dye which is evident from the low melting temperature of r3-Y/RX. The very low stability of the 2′-*O*-methyl RNA probes against a DNA target is striking, and suggests that careful sequence

design could lead to TO/RX probes that are highly selective for RNA over DNA. Both r2-TO/RX and r3-TO/RX showed clear enhancement of fluorescence emission after hybridization with their RNA target (Figure 2.7 b, Figure S4). However, only a 1.5-fold increase of fluorescence intensity of r3-TO/RX after hybridization with its complementary DNA target was observed (Figure 2.7 b, Figure S3). This suggests that in the DNA-RNA hybrid structure, the AP-C3 modifications in the triply modified base are too close, allowing fluorescence quenching to occur.

Table 2. 2. Fluorescence melting temperatures of single TO and TO/RX labelled probes hybridised to fully complementary and specific single mismatched targets. Measurement was performed with probe concentration of 0.4 µM and target concentration of 0.44 µM in 10 mM Na-phosphate buffer, 200 mM NaCl, pH 7.0. Samples were initially denatured by heating to 85 °C at 1 °C min^{-1} then cooled to 25 °C at 1 °C min^{-1}. Fluorescence emission was recorded every 0.1 °C in TET channel (Excitation wavelength: 515 nm-535 nm; Emission wavelength: 560 nm- 580 nm) and ROX channel (Excitation wavelength: 560 nm-590 nm; Emission wavelength: 610 nm- 650 nm). Oligonucleotides sequences were shown in Table S1 and S2.

Probe	T_m/°C (DNA target)	T_m/°C (G:T mismatch DNA target)	T_m/°C (A:C mismatch DNA target)	T_m/°C (RNA target)	T_m/°C (G:T mismatch RNA target)	T_m/°C (A:C mismatch RNA target)
d1-TO/A	64.5	54.0	48.0	64.0	57.5	53.5
d1-TO/RX	60.5	55.0	48.5	59.5	53.5	48.0
r1-TO/A	49.0	43.0	34.0	66.0	61.0	53.0
r1-TO/RX	48.0	44.0	31.5	65.0	63.5	55.0

2.5.2 Combination probes in real time-PCR-based applications

It was demonstrated that combination probes can be used in real time-PCR-based applications. (Figure 2.8). This will enable target analyte concentrations to be determined, and the post-PCR melting temperature of the probe-amplicon duplex to be analysed for point mutation detection.[204] The analyte is the PCR product made from a region of a

2665mer RNA template made by in vitro transcription from plasmid pcDNA3.1-hAsCpf1 (Addgene, plasmid number #69982, kindly gifted by Dr. Feng Zhang). We used this RNA template for a ligation reaction (confidential) and ligated DNA strand was used for one PCR. We have used this PCR product as our second PCR template and TO labelled probe for detection. The TO-intercalator increases the stability of the probe-target duplex allowing shorter PCR probes to be used with consequently superior mismatch/mutation detection. In support of this we have shown that mismatch discrimination with the new combination probes is excellent (Table 2.2).

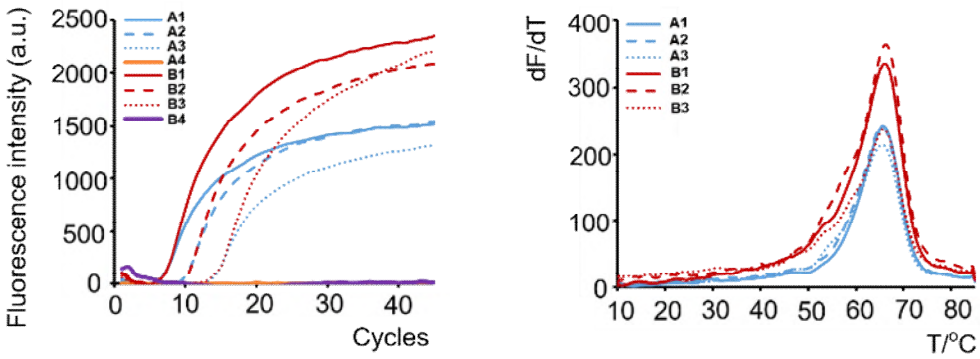

Figure 2. 8. RT-qPCR (left) of TO/RX probe and fluorescence melting curve (right) of PCR product. A represents 0.15 µM of probe and B represents 0.30 µM of probe. 1-3 represent 1.5 nM, 0.15 nM and 0.015 nM of template. 4 indicates no template (negative control). Oligonucleotide sequence information and details of target DNA are shown in Table S3. Data points were measured in triplicate.

2.6 Fluorescence lifetime studies of AP-C3 combination probes

Time-resolved fluorescence measurements were carried out to study the modulations in the fluorescence decay kinetics of TO labelled probes d1-TO/A, d2- TO/A, d3-TO/A, r1-

TO/A, r2-TO/A and r3-TO/A on hybridization to DNA and RNA targets (Figure 2.9). The lifetime of all probes are bi-exponential in nature with one long lived (τ2) and one short lived lifetime (τ1). Fluorescence decays for TO labelled probes (recorded at 1 μM) both in the absence and presence of targets are shown in Figure 2.9. It is hypothesised that the short lifetimes are due to relatively unrestricted rotation of TO around the methine bridge and the long lifetimes are attributed to TO in a more constrained environment due to hybridisation with target DNA or RNA.[205] In presence of DNA and RNA target, the average lifetime of each construct is enhanced in line with the steady-state fluorescence measurements. The ratios of lifetimes in the double strand compared to single strands are generally slightly higher for RNA than DNA targets, suggesting that TO is more constrained/planar in an A-like helix than a B-form helix.

With target DNA or RNA, the contribution of short-lived lifetime (τ1) is diminished (50% for DNA target and 33% for the RNA) which reflects strong hybridization of the probes with targets (Table S12). The short-lived lifetime shows a rather constant value (0.81-1.70 ns) but long lifetime shows increment in presence of targets (4.97 ns from 3 ns). The amplitude of long lifetime rises up to 67% for each case in presence of targets from almost 30%, indicating the constrained motion of TO restrict due to presence of DNA and RNA targets. The ratio of lifetime for hybrid stand (double stand of DNA/RNA) and single stand probe ($<\tau>_{ds/ss}$) are essential to comparison the sensitivity of the probes towards target. The ratios are higher for the RNA target than the DNA target and more increment is observed for the 2′-OMe-RNA probes. In case of one TO labelled 2′-OMe probe the values are 2.48 for RNA target and 1.79 for DNA target. The observed results reflect that

our probes design was more sensitive for RNA targets and the probes will be useful for RNA specific detection in cellular levels. (Figure 2.9).

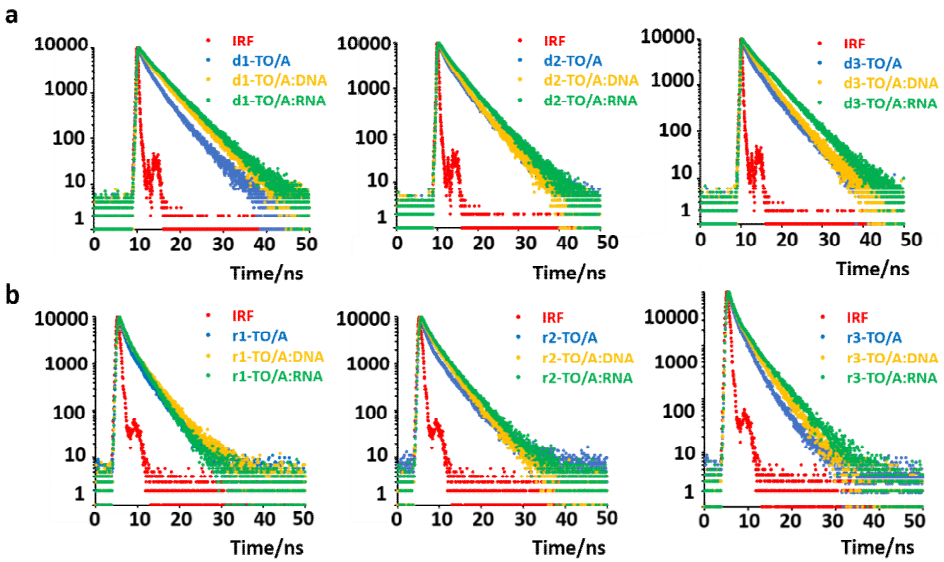

Figure 2. 9. Fluorescence decay of TO-labelled AP-C3 dT probes. a. d1-TO/A, d2-TO/A, d3-TO/A and b. r1-TO/A, r2-TO/A, r3-TO/A. 1 µM of probe was hybridised to 1.1 µM of complementary DNA and RNA target. Samples were excited at 475 nm and fluorescence decays were measured at 530 nm. Buffer is 10 mM Na-phosphate, 200 mM NaCl, pH = 7.0. Data points were measured in triplicate.

2.7 Conclusions

In conclusion, this work describes a method to efficiently label single thymidine sites in oligonucleotides with two different fluorophores, one of which is also a duplex-stabiliser. To achieve this, a new AP-C3 dT phosphoramidite monomer containing a terminal alkyne and a TFA-protected primary amine has been developed for the labelling of oligonucleotides with a thiazole orange anchor dye and a ROX reporter dye. The approach takes advantage of the orthogonality of the CuAAC click and amide bond formation

reactions which enables multiple TO and ROX labelled oligonucleotides to be produced, and a high density of labels to be introduced into short oligonucleotides. Thermal duplex stability and fluorescence studies demonstrate that TO/RX combination probes can detect nucleic acid targets with highly favourable signal-background-ratios. To enhance resistance against the enzymatic degradation that is encountered in a cellular environment, 2′-OMe RNA combination probes were synthesised and showed good duplex stability and excellent fluorescence properties on binding to complementary RNA targets. Future work will involve optimisation of the length and nature of the linkers between the nucleobase and the fluorescent labels, and attaching thiazole orange to AP-C3 by the quinoline moiety rather than benzthiazole to determine if this offers any advantages in terms of fluorescence or duplex stability. Finally, the use of AP-C3 dT to introduce multiple alkyne and amine moieties into oligonucleotides will be advantageous in other applications where densely-labelled oligonucleotides are required. For such applications many small molecule azides and NHS esters are commercially available, including affinity ligands, as well as alternative intercalators and reporter dyes.

Chapter 3

New combination probes applied to LAMP for COVID-19 diagnostics

Chapter 3 – New combination probes applied to LAMP for COVID-19 diagnostics

3.1 Introduction

COVID-19 (coronavirus disease 2019), which is caused by the SARS-CoV-2 virus, is still rapidly spreading, mutating, and causing tremendous problems worldwide.[206] Rapid and robust diagnostic assays for COVID-19 infections are limiting spread of the virus, but despite this, cheap and sensitive tests are still needed. Most countries are performing real-time polymerase chain (RT-qPCR) in centralised laboratories, which requires sophisticated equipment and skilled technicians. Assays based on isothermal amplification require simpler instrumentation, so are particularly attractive at the point of care and where finances are limited.

Loop mediated isothermal amplification (LAMP) is a nucleic acid amplification assay which has outstanding sensitivity and specificity[207] and does not require expensive instruments. The method involves a DNA polymerase and a set of at least four oligonucleotide primers which can recognize distinct sequences on the target DNA (Figure 3.1). LAMP is initiated with an inner primer containing sequences of the sense and antisense strands of the target DNA. An outer primer then triggers strand displacement synthesis to release ssDNA. This works as a template for DNA elongation by using the second inner and outer primers that hybridize to the other end of the target sequence to produce a stem–loop DNA structure. In subsequent LAMP cycling one inner primer hybridizes to the loop on the product and initiates displacement DNA synthesis, producing

the original stem–loop DNA and a new stem–loop DNA.[208] LAMP recognizes the target by six distinct sequences initially and by four distinct sequences afterwards, explaining the high selectivity for COVID-19 detection. During the first few steps all four primers are used, but afterwards during the cycling reaction only the inner primers are used for strand displacement DNA synthesis. The inner primers are called the forward inner primer (FIP) and the backward inner primer (BIP), respectively[209].

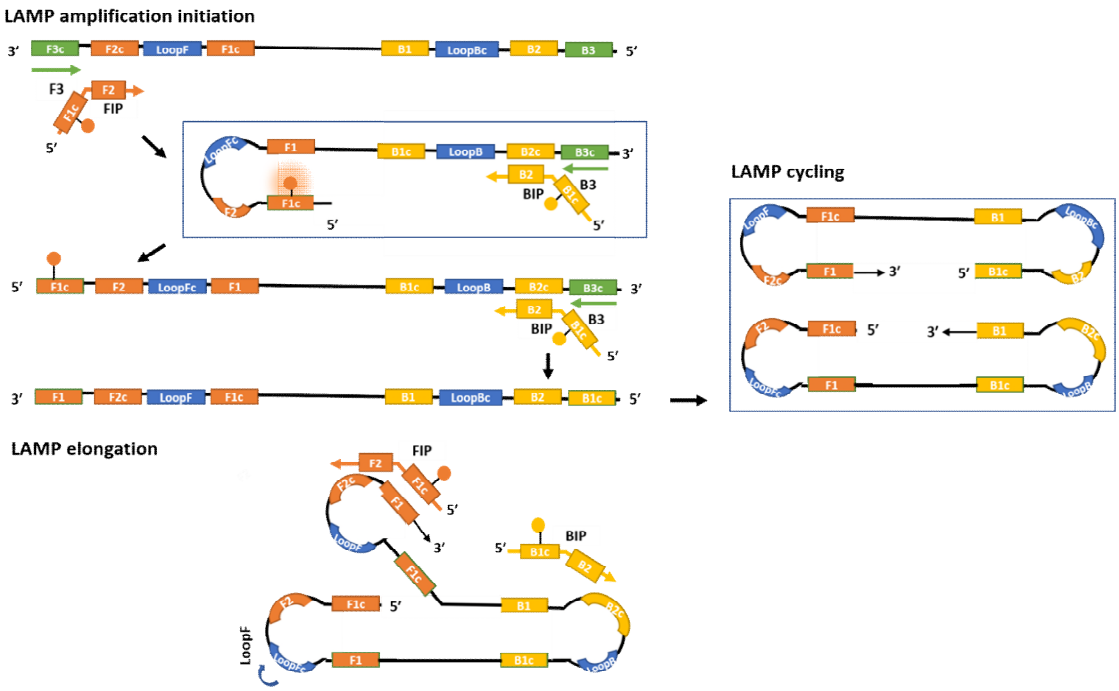

Figure 3. 1. LAMP isothermal DNA amplification mechanism.

Another new technique for quickly detecting SARS-CoV-2, the virus that causes COVID-19, has been developed. The method is isothermal, meaning it can operate at a constant temperature, and does not require reverse transcription to convert RNA to DNA. Instead, it uses a unique process of forming a hybrid RNA/DNA molecule that can be selectively

cleaved to generate a short DNA trigger, which is then rapidly amplified using exponential amplification. By combining the RNA-to-DNA conversion and amplification steps into a single reaction, the RTF-EXPAR assay can detect very low levels of SARS-CoV-2 RNA in under 10 minutes using fluorescence measurement.[210]

The combination of LAMP and fluorescent dyes potentially provides high sensitivity and specificity for COVID-19 testing and can significantly reduce the assay time. To that end, we have used a real time fluorescent method with both an intercalating TO dye and a fluorescent reporter TA [**16**] (fluorescence assay in real time) (Figure 3.2) to mediate detection via LAMP amplification. The primers can be labelled with TO only or they can be labelled with TO and TAMRA at the same thymidine to perform in the LAMP as combination probes. The specificity can be improved by the intercalation of TO which has been discussed in Chapter 2.

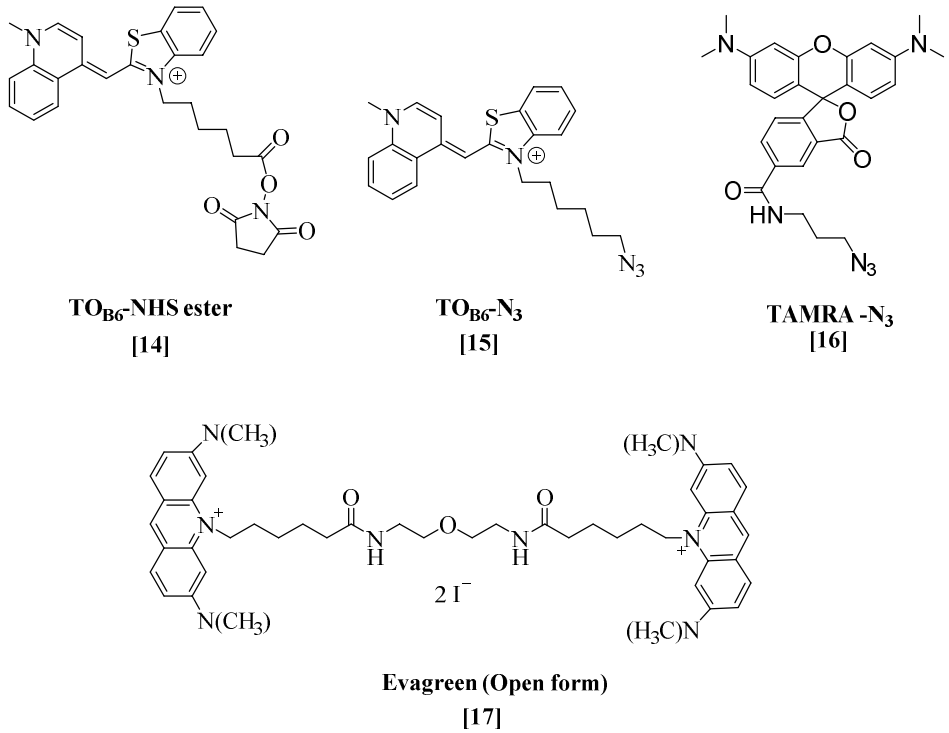

Figure 3. 2. Structure of TO_{B6}-NHS ester, TO_{B6}-N_3, TAMRA-N_3 and EvaGreen (open form).

3.2 FIP and BIP sequence and primer pairs design

We have synthesised oligonucleotides probes labelled with TO_{B6}-NHS ester [**14**], TO_{B6} azide [**15]** and also combination probes labelled with TO_{B6}-NHS [**14**] and TAMRA azide [**16**]. These probes consist of different pairs of forward inner primers (FIP) and backward inner primers (BIP) designed to develop a fast and accurate COVID-19 LAMP assay.

Please see below and Table 3.1.

Sequences of COVID-19 Penn-RAMP primers used by El-Tholoth et al., (2020). [211] These primers target the open reading frame 1ab (ORF1ab) gene of the SARS-COV-2 RNA. Primer Sequence (5′ – 3′): (X= AP-C6 dT)

F3: TGCTTCAGTCAGCTGATG

B3: TTAAATTGTCATCTTCGTCCTT

FIP-d1: TCAGTACTAGTGCCXGTGCCCACAATCGTTTTTAAACGGGT;

FIP-d2: TCAGXACTAGTGCCXGTGCCCACAATCGTTTTTAAACGGGT;

BIP-d1: TCGTATACAGGGCXTTTGACATCTATCTTGGAAGCGACAACAA;

BIP-d2: TCGXATACAGGGCXTTTGACATCTATCTTGGAAGCGACAACAA;

Loop F: CTGCACTTACACCGCAA

Loop B: GTAGCTGGTTTTGCTAAATTCC

Table 3. 1. Table of primer pairs used in LAMP assays for COVID-19 detection. Sequences and mass of primers were shown in Table S13.

Primer Pairs	Forward inner primer	Backward inner primer
P1	F-unmodified	B-unmodified
P2	F-d1-Y/TO	B-unmodified
P3	F-unmodified	B-d1-Y/TO
P4	F-d1-Y/TO	B-d1-Y/TO
P5	F-d2-Y/TO	B-unmodified
P6	F-unmodified	B-d2-Y/TO
P7	F-d2-Y/TO	B-d2-Y/TO
P8	F-d2-TO/A	B-unmodified
P9	F-unmodified	B-d2-TO/A
P10	F-d2-TO/A	B-d2-TO/A
P11	F-d1-TA/TO	B-unmodified
P12	F-unmodified	B-d1-TA/TO
P13	F-d2-TA/TO	B-unmodified
P14	F-unmodified	B-d2-TA/TO

Note: in probe names, F= forward primer, B= backward primer, d = DNA oligo, number = probe number, A = unlabelled amine, Y = unlabelled alkyne, TO = labelled with thiazole orange, TA = labelled with TAMRA, TA/TO = labelled with thiazole orange and TAMRA.

3.3 Results and discussion

3.3.1 Primer pairs labelled with TO only

The primer pair without dye labelling (P1) acts as the positive control when used in combination with EvaGreen [**17**] for fluorescence detection. EvaGreen is a next-generation DNA-binding dye that is ideal for quantitative real-time PCR (RT-qPCR) and many other applications where high sensitivity is required, along with the ability to do sensitive melting curve analysis. (Table 3.2).

However, EvaGreen can be intercalated into any target DNA/RNA, making it non-specific in terms of sequence detection. An intercalating dye with high specificity would be particularly useful. As discussed in chapter 2, oligonucleotide probes labelled with TO can detect specific target DNA/RNA sequences. Also, AP-C6 probe labelled with TO only has shown better fluorescence against DNA target than AP-C3 probe labelled with TO only when excitation wavelength was 510 nm (Table S10). With this in mind, we synthesised AP-C6 modified monomer phosphoramidite (Figure 2.3) and incorporated the modified monomer into oligonucleotides by solid-phase oligonucleotide synthesis. Initially we put double incorporations of the AP-C6 modified monomer into the oligonucleotides, which were used as primers in LAMP to see if such TO-labelled primers are compatible with LAMP.

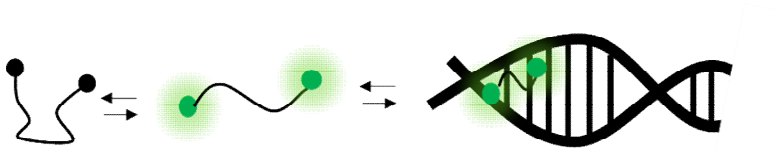

Figure 3. 3. The fluorescence emission signalling mechanism of EvaGreen. The chemical structure of its open form is shown in Figure 3.2.

We labelled the FIP and BIP primers with TO_{B6} NHS ester and TO_{B6} azide which consisted of various primer pairs (P5 - P10) for LAMP. Compared to unmodified primers, fluorescence was found to be more intense in TO-containing pairs, albeit with a delay in detection (Figure 3.4), and with P5 having the highest fluorescence intensity. This might be explained by an extended form of FIP and BIP with a dumbbell structure (Figure 3.1). The amplification elongation needs to separate the dumbbell structure formed by FIP and BIP to single strands, and since TO can stabilise duplex structures this could be more difficult as compared to unmodified strands. Therefore, we performed the melting studies for each fluorophore-labelled primer (Table 3.2). The elongation stage may be detrimentally affected by stable dumbbell structures when FIP and BIP are both labelled with TO_{B6}-NHS ester.

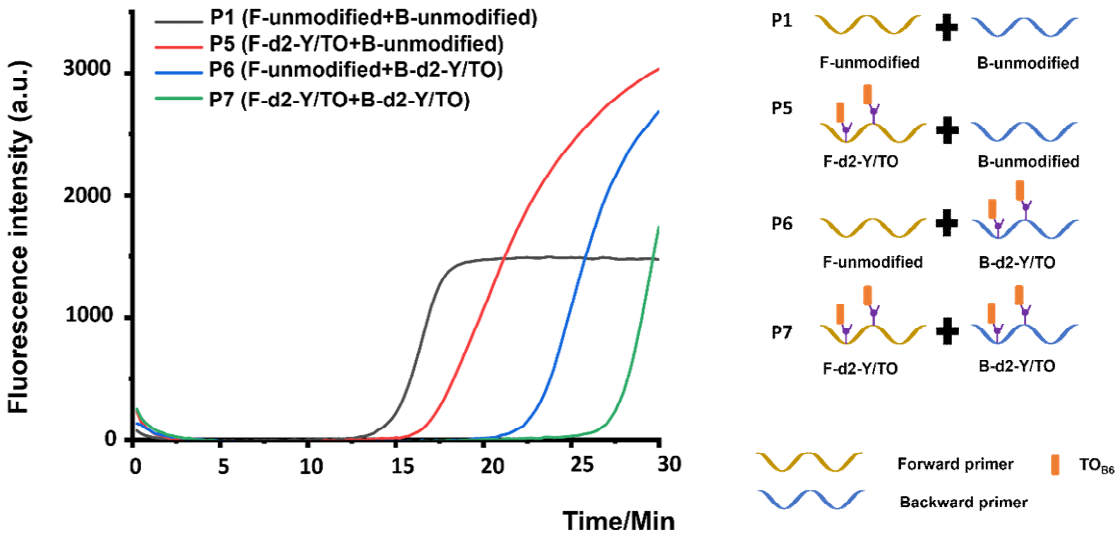

Figure 3. 4. LAMP amplification of positive control (P1) (with EvaGreen, grey line) and P5 - P7 (red line, blue line, green line). 2.0 µL extracted RNA template was added in the mixture of 7.5 µL of 2X LAMP master mix (a blend of dNTPs, Bst 2.0 WarmStart DNA Polymerase and WarmStart RTx Reverse Transcriptase in an optimized LAMP buffer solution), 1.5 µL of 10X primer mix (16 µM), 1.5 µL of FIP (16 µM), BIP (16 µM) and 2 µL H_2O into 50 µL PCR tubes. The mixture was vortexed and centrifuged for 30 seconds. The PCR tubes were incubated at 65 °C. LAMP was undertaken using a BioRad CFX96 Real-Time PCR Instrument, with CFX Manager software (BioRad), monitoring in the following channels: TET channel (excitation range 515–535 nm, detector range 560–580 nm), Primers′ sequences were shown in Table S13.

Apart from TO_{B6}-NHS labelled primers we also labelled primers with TO_{B6} azide for comparison due to orthogonal labelling on an APC6 monomer. Different primer pairs (P8-P10) were labelled with TO_{B6} azide at 65°C and they were found to need similar amplification time as TO_{B6}-NHS labelled primer pairs (Figure S5). To investigate if the stability of dumbbells structure has an impact on the amplification we put single incorporations of the AP-C6 modified monomer into the oligonucleotide. With this in mind

we labelled the FIP and BIP with TO_{B6}-NHS ester which consisted of various primer pairs (P2 - P4) for LAMP amplification.

P3 needed the least amplification time to detect COVID-19 in LAMP while P2 and P5 needed slightly more time, with both around 15 mins. P6 showed higher fluorescence intensity than P2 and P3 but it required longer amplification time compared to P2, P3 and P5, suggesting that the stability of dumbbell structure may have an impact on the amplification (Figure 3.5).

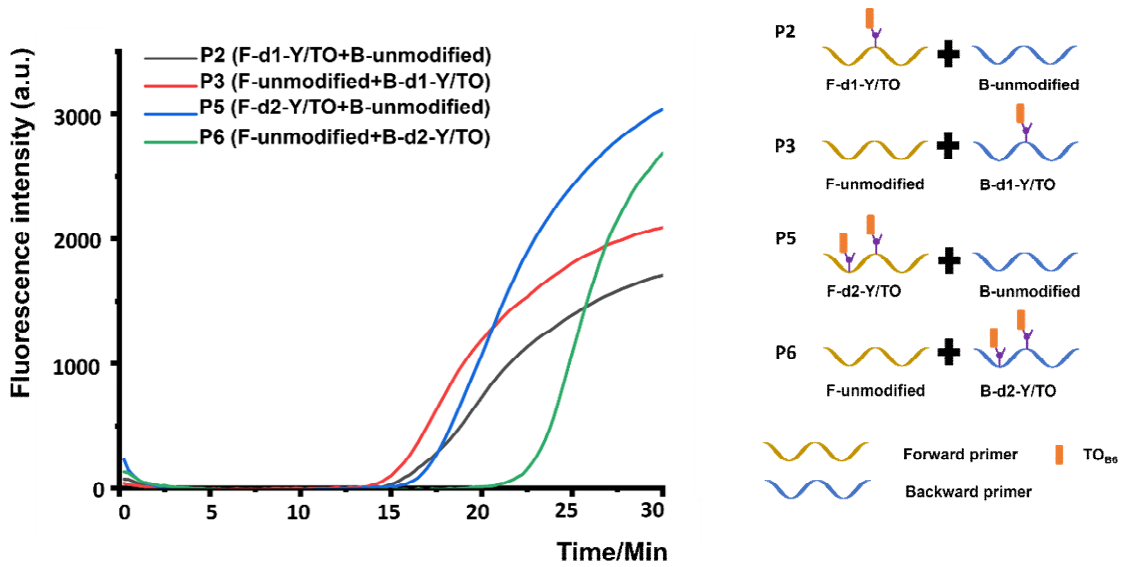

Figure 3. 5. LAMP amplification of P2 (grey), P3 (red), P5 (blue), P6 (green). 2.0 µL extracted RNA template was added in the mixture of 7.5 µL of 2X LAMP master mix (a blend of dNTPs, Bst 2.0 WarmStart DNA Polymerase and WarmStart RTx Reverse Transcriptase in an optimized LAMP buffer solution), 1.5 µL of 10X primer mix (16 µM), 1.5 µL of FIP (16 µM), BIP (16 µM) and 2 µL H_2O into 50 µL PCR tubes. The mixture was vortexed and then centrifuged for 30 seconds. The PCR tubes were incubated at 65 °C. LAMP was undertaken using a BioRad CFX96 Real-Time PCR Instrument, with CFX Manager software (BioRad), monitoring in the following channels: TET channel (excitation range

515–535 nm, detector range 560–580 nm), Primers′ sequences were shown in Table S13. Data points were measured in triplicate.

3.3.2 Primer pairs labelled with TO and TAMRA

As discussed in Chapter 2, combination probes can be labelled with many different pairs of dyes on the same nucleobase, with TO as a fluorogenic anchor and the other bright fluorophore as a reporter. This logic can also be applied to LAMP primers which would be non-fluorescent in the unhybridised form due to efficient quenching. Once the labelled primers are hybridizing with target oligonucleotides Förster resonance energy transfer (FRET) between the dyes will occur and fluorescence will be observed. In addition to TAMRA, other bright dyes including ATTO647N and Alexa 647 can emit higher intensity fluorescence via FRET and the amplification could be detected by different emissions channels simultaneously. Multiplex detection is useful when detecting multiple viruses, for instance, Influenza, Rhinovirus etc.

We labelled FIP and BIP containing single and double incorporations of the AP-C6 modified monomer with TO_{B6}-NHS and TAMRA azide. Afterwards various primer pairs (P11-P14) were used in LAMP with P12 (an unmodified FIP with single TAMRA/TO label in the BIP) showing the shortest amplification time among these combinational probe primer pairs. As discussed in Chapter 2, TO dyes can help to stabilise the duplex structure and the other reporter dyes will destabilise it. The melting temperature of P12 is slightly higher than P13 and P14 but showed better LAMP. This can be explained on the basis that the melting temperature of combination probe primers against DNA target were all lower

than the LAMP reaction temperature (65°C) such that the stability of dumbbell structure in LAMP amplification would not be a main factor but the steric hindrance. Therefore, the P11 and P12 needed less time than P13 and P14.

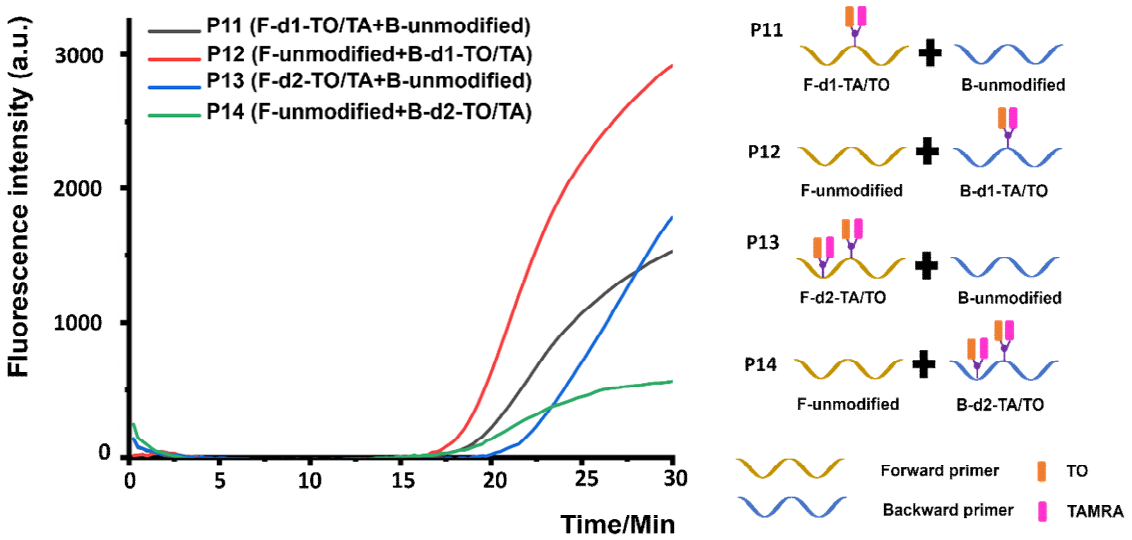

Figure 3. 6. LAMP amplification results of P11-P14 at 65°C. 1.0 µL extracted RNA template was added in the mixture of 7.5 µL of 2X LAMP master mix (a blend of dNTPs, Bst 2.0 WarmStart DNA Polymerase and WarmStart RTx Reverse Transcriptase in an optimized LAMP buffer solution), 1.5 µL of 10X primer mix (16 µM), 1.5 µL of FIP (16 µM), BIP (16 µM) and 2 µL H_2O into 50 µL PCR tubes. The mixture was vortexed, and then centrifuged for 30 seconds. The PCR tubes were incubated at 65 °C. LAMP was undertaken using a BioRad CFX96 Real-Time PCR Instrument, with CFX Manager software (BioRad), monitoring in the following channels: FRET channel (excitation range 450–490 nm, detector range 560–580 nm). Primers′ sequences were shown in Table S13.

LAMP is usually performed at 65°C but reaction temperature can be optimized with the various dye labelled primers used. Firstly, the P3 was used to optimize the LAMP temperature from 45°C to 65°C. (Figure 3.7 a) and we found LAMP worked well at 61.6°C, 63.8°C and 65°C. P1, P3, P12 were used to perform at this gradient temperature

in order to develop the best primer pair used in LAMP for COVID-19 detection which required least amplification time. We can clearly observe that all three primer pairs worked best at 63.8°C (Figure 3.7 b). Also, the TO only labelled primer pair P3 and TAMRA/TO labelled primer pair P12 both showed quicker amplification compared to unmodified primer pair (Positive control).

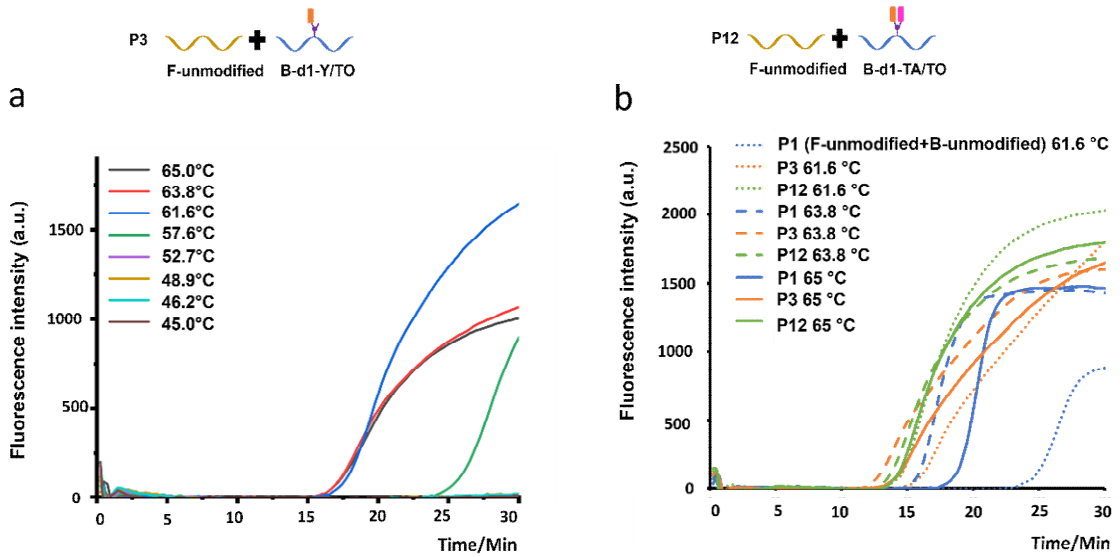

Figure 3. 7. a. LAMP amplification results of P3 at a gradient temperature from 45°C to 65°C **b.** LAMP amplification results of P1, P3, P12 at a gradient temperature from 61.6 °C to 65°C. 1.0 µL extracted RNA template was added in the mixture of 7.5 µL of 2X LAMP master mix (a blend of dNTPs, Bst 2.0 WarmStart DNA Polymerase and WarmStart RTx Reverse Transcriptase in an optimized LAMP buffer solution), 1.5 µL of 10X primer mix (16 µM), 1.5 µL of FIP (16 µM), BIP (16 µM) and 2 µL H_2O into 50 µL PCR tubes. The mixture was vortexed, and then centrifuged for 30 seconds. The PCR tubes were incubated at the different gradient temperatures above. LAMP was undertaken using a BioRad CFX96 Real-Time PCR Instrument, with CFX Manager software (BioRad), monitoring in the following channels: TET channel (excitation range 515–535 nm, detector range 560–580 nm); FRET channel (excitation range 450–490 nm, detector range 560–580 nm). Primers′ sequences were shown in Table S13.

3.4 Melting temperature studies of various modified primers

LAMP is an innovative variation of Polymerase Chain Reaction (PCR) which is widely used to rapidly make millions to billions of copies of a specific DNA sample, allowing exceedingly small samples of DNA to be amplified. LAMP proceeds in three enzymatically catalysed and coordinated steps: initiation, elongation, and termination (Figure 3.1). For elongation, the polymerase can work only when the dumbbell structure becomes separated. Also, the double dye labelled primers had more steric hindrance compared to single dye labelled primers when it came to the elongation stage. These two factors can explain why various pairs of primers performed with different efficacy.

For primers labelled with single TO only, the TO was intercalated into the oligonucleotides which could stabilize the duplex structure. We performed melting temperature (T_m) studies by fluorescence melting and UV melting (Table 3.2). The table showed P3 (F-unmodified: B-d1-Y/TO) has the lowest T_m (69.39 ^{o}C), which can explain why P3 had quickest amplification. Also, we found that single TO only labelled primers had lower T_m than double TO only labelled primers and so they can have quicker amplification (Figure 3.5). When using TO-labelled primers with a reporter dye (such as TAMRA), the reporter dye destabilises the duplex, probably due to entropic effects (the dye prefers not to be in a hydrophilic environment). As a result, the T_m of TO and TAMRA labelled primers were lower than that of unmodified primers (Table 3.2). BIP with TAMRA/TO had the highest T_m, and is closest in T_m to the unmodified primer. When the process of amplification is not limited by the separation of double strands, single TAMRA/TO labelled primers (P11, P12) had quicker detection than the double TAMRA/TO labelled primers (P13, P14) potentially

indicating that steric hindrance caused by labelled dyes may also slow down the LAMP amplification for COVID-19 detection (Figure 3.6).

Table 3. 2. Fluorescence and UV-derived melting temperatures of various primers labelled with TO only and TAMRA/TO against with DNA target. Measurement was performed with probe concentration of 0.4 µM and target concentration of 0.44 µM in 10 mM Na-phosphate buffer, 200 mM NaCl, pH 7.0. Samples were initially denatured by heating to 85 °C at 1 °C min^{-1} then cooled to 25 °C at 1 °C min^{-1}. Fluorescence emission was recorded every 0.1 °C in TET channel (Excitation wavelength: 515 nm-535 nm; Emission wavelength: 560 nm- 580 nm) and FRET channel (excitation range 450–490 nm, detector range 560–580 nm). Primers sequences were shown in Table S13.

Primers	T_m on CFX	T_m by UV melting	Primers	T_m on CFX	T_m by UV melting
FIP+TO	68.4	72.05	FIP+TAMRA/TO	61.8	60.54
FIP+2TO	74.2	74.81	FIP+2TAMRA/TO	56.4	56.10
BIP+TO	68.2	69.39	BIP+TAMRA/TO	62.6	61.25
BIP+2TO	72.2	72.98	BIP+2TAMRA/TO	58.6	60.84
Unmodified FIP	n.d.	66.13	Unmodified BIP	n.d.	65.61

3.5 Conclusions

The new combination probe and TO labelled probe principles have been successfully applied to the forward inner primer and backward inner primer modifications for a LAMP assay to detect COVID-19. Oligonucleotides containing single and double incorporations of the AP-C6 monomer have been synthesised as inner primers for use in LAMP. These inner primers were labelled with various dyes via NHS labelling and the CuAAC click reaction. Double TO only and double TAMRA/TO labelled primers (P5-P6, P8-P9, P13-P14) required more amplification time than single dye-labelled primers (P2-P3, P11-P12) for COVID-19 detection due to their duplex stability and potential steric hindrance during the elongation stage. Also, P3 (F-unmodified: B-d1-Y/TO) showed the quickest

amplification in the LAMP assays and P12 (F-unmodified: B-d1-TAMRA/TO) also performed better than the positive control P1 (F-unmodified: B-unmodified). There is potential for further optimization, and good reason to pursue this line of research: compared to RT-qPCR, LAMP could be more convenient and affordable for use in developing countries.

Chapter 4

Synthesis and biophysical properties of triazole-locked nucleic acids for antisense therapeutics

Chapter 4 – Synthesis and biophysical properties of triazole-locked nucleic acids for antisense therapeutics

4.1 Introduction

Antisense oligonucleotides (ASOs) are synthetic oligonucleotide (ON) analogues which target complementary RNA via Watson-Crick base pairing. Thus, they can affect gene expression and regulate protein production by sequence-specific hybridization. Although the potential in therapeutics is great, intact ASOs are not efficiently delivered into cells due to enzymatic degradation and poor cellular uptake. Various backbone and ribose modifications have been applied in the design of ASOs to resolve these undesirable properties. Important ribose C2 modifications include 2′-O-methylation (2′OMe), 2′-(2-methoxyethyl) (2′-MOE), 2′-fluoro (2′F) and a locked nucleic acid (LNA) (Figure 4.1).

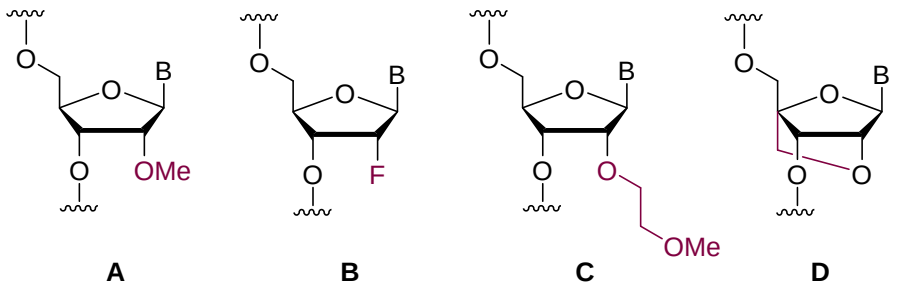

Figure 4. 1. Common modifications used in antisense templates, A = 2′-*O*-Methyl, B = 2′-Fluoro, C = 2′-*O*-(2-Methoxyethyl) (2′-MOE), D = Locked nucleic acid (LNA).

The 2′-OMe alteration was one of the earliest sugar modifications and ocurs normally in some RNAs post translation *in vivo*.[212] Inclusion of 2′-OMe in ASOs, increases their

affinity for RNA,[213] and resistance to degradation by nucleases.[214] However, it is not compatible with RNase H cleavage of the RNA target. Other modifications have also been investigated, such as the 2′-fluoro and 2′-(2-methoxyethyl) (2′-MOE), which gives improved target selectivity compared to 2′-OMe and great nuclease stability.[215]

Triazoles are a possible alternative linkage in therapeutic ONs, however triazole-containing ASOs often suffer from poor duplex stability with target RNA.[20, 216, 217] Triazole-containing ASOs can be obtained using modified dinucleotides phosphoramidites, synthesised using a copper catalysed alkyne-azide cycloaddition (CuAAC) reaction as a key step. The triazole linkage (TL) is attractive for use in ASOs for applications involving diagnostic tools and therapeutic agents because triazole linkages (Figure 4.2) can induce increased nuclease resistance and also they reduce the overall anionic charge, which has been proposed to improve cellular uptake.

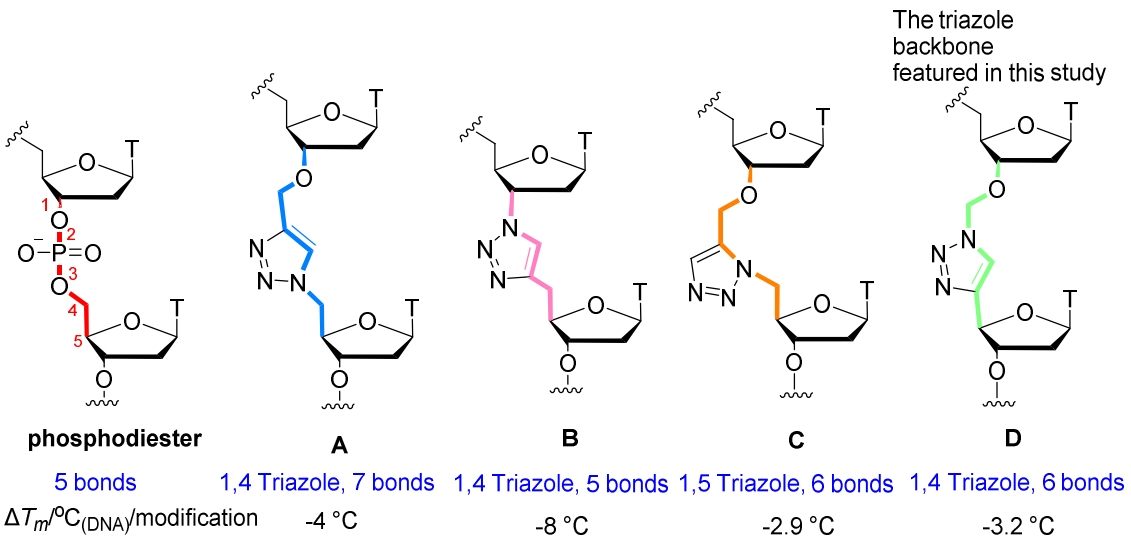

Figure 4. 2. Examples of triazole linkages, their inter-sugar spacing (shown in bold bond) counted as the number of bonds, and their influence on duplex stability against DNA target. A) Biocompatible triazole first reported by Zerrouki et al.; B) Triazole reported by Isobe et al.; C) Triazole reported by Ysobel et al.; D) Triazole reported by Varizhuk et al..

A recent study by Baker et al. compared the biophysicial properties of 1,4 and 1,5 triazoles A, B C and D, shown in Figure 4.2.[218] 1,5-Triazoles can be synthesised by replacing the copper catalyst for ruthenium. A 1,4-triazole linkage containing 7 atoms (Figure 4.2 A) was first synthesised by Zerrouki et. al..[219] Although the backbone is slightly destabilising (-4 °C/mod) it has good biocompatibility,[220] can be easily synthesised, and has a commercially available precursor alkyne phosphoramidite. Isobe et. al.[85] incorporated a 1,4-triazole linkage with 5 bonds (Figure 4.2 B). Thermal investigation of this backbone indicated that the linkage was exceedingly duplex destabilizing when consolidated into oligonucleotides (-8 °C/mod), most likely due to the positioning of the triazole towards the 5′-end of the backbone and the short nature of this backbone. It was found that the 1,4-triazole (Figure 4. 2 D) had the most favourable properties in ASOs for RNA targets, with similar duplex stability (T_m -0.4 °C/mod) to the unmodified ON.[221]

Triazole (TL)-linked oligonucleotides generally exhibit poor binding affinity to complementary RNA. This has hampered their use in antisense therapies, where strong duplex thermal stability and mismatch discrimination are required. Based on the seminal work by Wengel,[222] LNA displays superb binding affinity to target RNA strands and can stabilise duplexes by up to +7 °C per LNA modification which can help TL-modified ONs to bind to their RNA target with affinity similar to unmodified ONs.[95, 222] Our group has

previously introduced a combination of LNA with a DNA backbone mimic comprised of a six-atom triazole linkage which improves duplex stability compared to the unmodified ONs.[217]

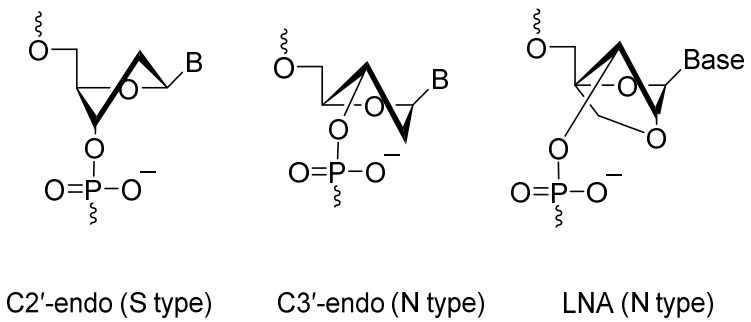

Figure 4. 3. The C2′-*endo* and C3′-*endo* sugar ring conformations present in nucleic acids and the molecular structure of locked nucleic acid (LNA), which shows the locked C3′-*endo* sugar conformation. (From left to right: C2′-*endo*, C3′-*endo*, LNA).

NMR, CD spectroscopy, and X-ray crystallography have all been used to determine the structures of LNA-DNA and LNA-RNA duplexes. The Watson and Crick base pairing, nucleobases in anti-orientation, base stacking, and a right-handed helical shape are all common properties of native nucleic acid duplexes. LNA increases the A-like conformational character according to structural analysis; the NMR data revealed that as the population of N-type sugar puckers in the hybrid grows, it forces an A-like geometry that grows with increasing LNA content.[97, 223] This is attributed to the LNA-induced structural perturbation of the DNA nucleotides in the LNA-containing strand which attain an N-type sugar pucker, which contrasts with the equilibrium between the N- and S- type sugar conformations in the native DNA-RNA duplex (Figure 4.3). Overall LNA is a highly

promising modification for therapeutic oligonucleotide drugs. When incorporated into ASOs it provides good sequence discrimination and work by Wengel highlights that with careful design LNA oligonucleotides can be potent and non-toxic.[99] Efficacy of ASOs is not only limited to RNase H induction of RNA target degradation, studies have also provided evidence for good *in vivo* activity of LNA oligonucleotides as steric blockers and in RNAi.[224, 225]

4.2 Aims and objectives

This chapter describes the design and synthesis of LNA-triazole dinucleotide phosphoramidites, their incorporation into DNA utilizing standard solid phase synthesis, and preliminary biophysical studies.

It is hypothesised that the combination of the LNA modification, for improved thermodynamic stability, and the triazole linkage, for increased cell uptake and nuclease resistance, will result in improved therapeutic properties. Three different TL-LNA-linked dinucleotide phosphoramidites (Figure 4.4 B) will be synthesised and incorporated in the ONs which will be analysed using ultraviolet melting hybridisation studies to evaluate the best modification, and structural analysis by circular dichroism spectroscopy.

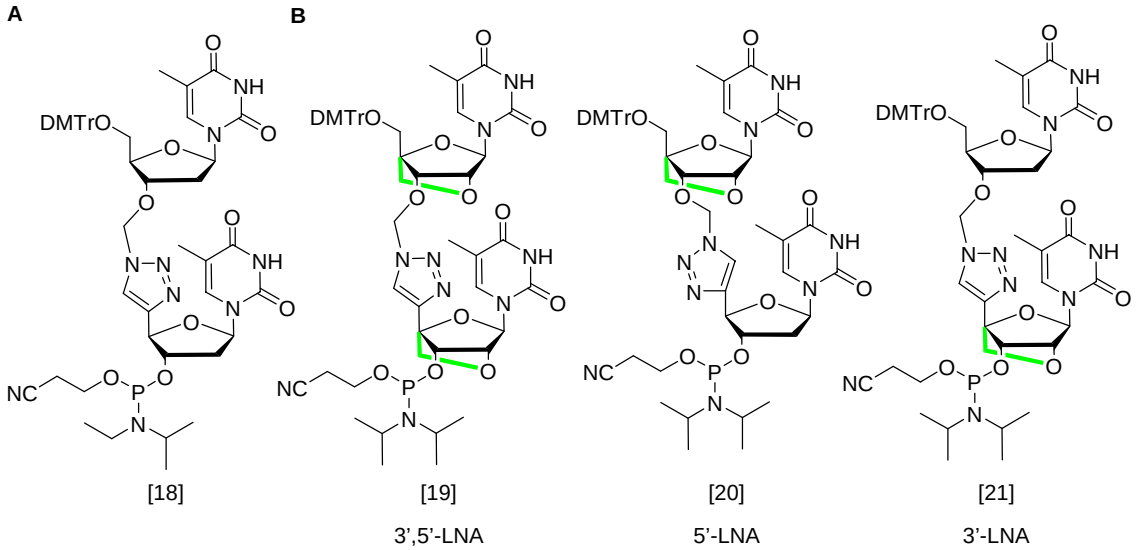

Figure 4. 4. The chemical structure of phosphoramidite building blocks used in this study: A) DNA-DNA TT dimer phosphoramidite; B) LNA-DNA, DNA-LNA, LNA-LNA TT dimer phosphoramidite.

4.3 Synthesis of LNA-TL-linked dinucleotide phosphoramidites

The triazole-linked dinucleotides described in this chapter were synthesised by reacting a 3′-azido thymidine and a 5′-alkynyl thymidine under CuAAC reaction conditions. LNA was incorporated at either the 3′-end of the TL, the 5′-end of the TL, or to both sides flanking the modified TL-backbone (Figure 4.4 B). Four different monomers were required for the synthesis of the LNA-TL-linked dinucleotide phosphoramidites designed in Figure 4.5. The four monomers required included 3′-azidomethyl LNA thymine (**22**), 5′- ethynyl LNA thymidine (**23**), 3′-azidomethyl thymidine (**24**) and 5′-ethynyl thymidine (**25**).

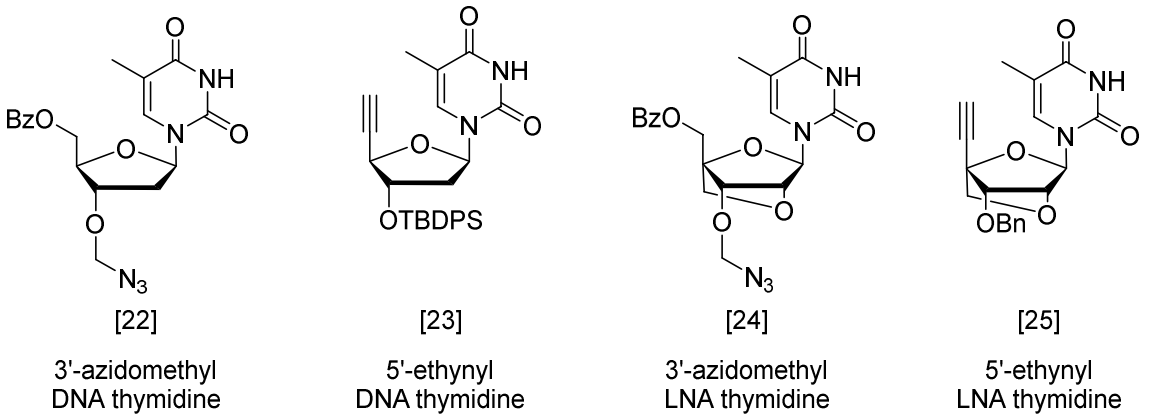

Figure 4. 5. Chemical structure of four different modified monomers.

4.3.1 Synthesis of 3′-azidomethyl thymidine

The synthesis route of 3′-azidomethyl thymidine (**22**) started with thymidine as previously described (Figure 4.6).[221] Firstly, the 5′-OH was protected by a benzoyl group at 4^{o}C because the 3′-OH can also react with benzoyl chloride at higher temperatures. In order to obtain the 3′-azidomethyl nucleoside the 3′-OH was activated by a mixture of DMSO, acetic acid and acetic anhydride to give the 3′-methylthiomethyl nucleoside. There was a side product (3′-OAc) which compromised the yield (62%). However, we were able to obtain the desired 3′-methylthiomethyl thymidine. Then bromine and 20 % aqueous LiN_3 were added in turn to afford 3′-azidomethyl DNA thymidine (**22**) for use in click reactions after chromatographic purification.

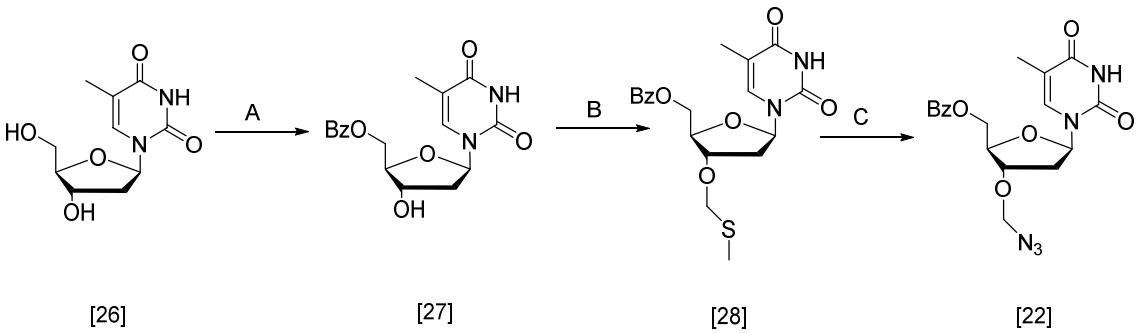

[26] [27] [28] [22]

Figure 4. 6. A. BzCl, imidazole, DMF, 4 °C to r.t., 3 h, 76%; B. DMSO, Ac_2O, AcOH, r.t., 72 h, 62%; C. 1) Br_2, MeCN, 0 °C, 0.5 h 2) 20 % LiN_3 in H_2O, 65 °C, 2 h, 72%.

4.3.2 Synthesis of 5′-ethynyl thymidine

The synthesis of 5′-ethynyl thymidine (**23**) was achieved by introducing orthogonal protecting groups onto the two alcohols of thymidine (Figure 4.7). The 5′-hydoxyl was reacted with TBDMSCl at 4 °C in 88% yield, and subsequent protection of the 3′-OH with TBDPSCl gave **30** in 84% yield. Then the 5′-*O*-TBDMS group could be selectively deprotected in 75% acetic acid in THF at room temperature for 72 h to give compound **31** in 65% yield. This deprotection reaction gave a moderate yield as it did not go to completion even when left for a long time.

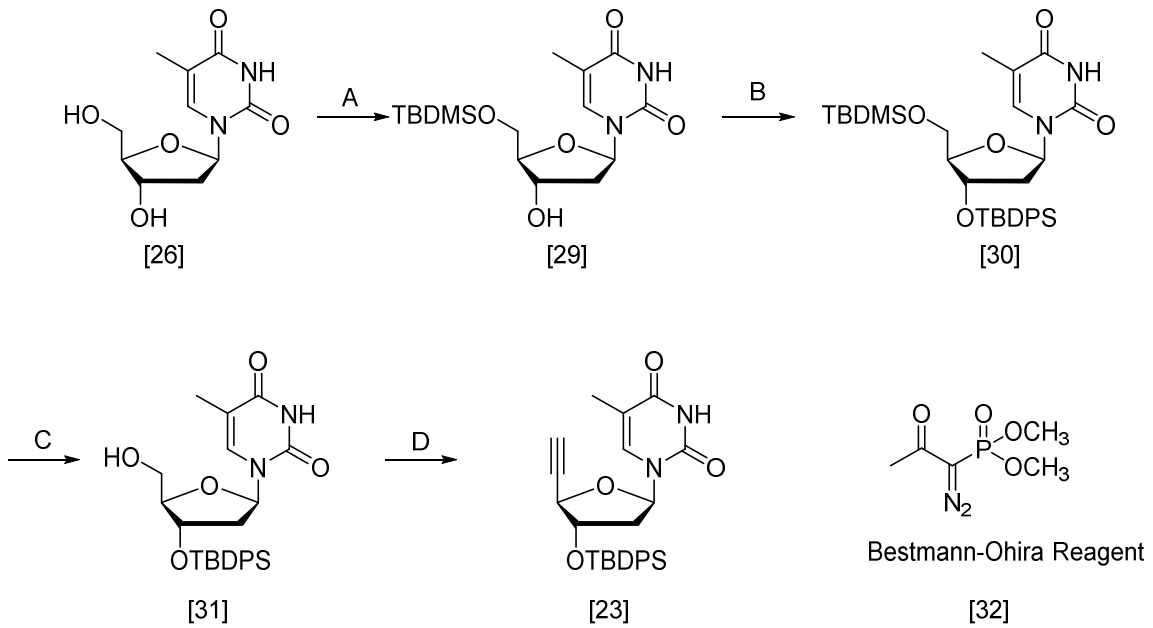

Figure 4. 7. A. TBDMSCl, imidazole, DMF, 4 °C to r.t., 3 h, 88%; B. TBDPSCl, imidazole, DMF, 16 h, r.t., 84%; C. Acetic acid/H_2O, 3:1(v/v), 65%; D. DMP, CH_2Cl_2, r.t., 3 h; Bestmann-Ohira Reagent, K_2CO_3, MeCN, MeOH, 4 h, 70%.

An alternative route to intermediate **31** was investigated in an attempt to increase the yield of the selective deprotection. It was predicted that a higher yield could be achieved if the orthogonal protecting groups chosen were not both silyl ethers. It was decided to investigate the use of a benzoyl ester as the protecting group on the 5′-OH (Figure 4.8). This synthesis route gives 3′-*O*-TBDPS-5′-OH thymidine with higher yield and shorter reaction time compared to the one in Figure 4.7. Benzoyl chloride was reacted with thymidine, and then subsequent protection of the 3′-OH with TBDPSCl gave **33** in 67% yield over 2 steps. The benzoyl ester was deprotected with potassium carbonate in methanol, in 85% yield, while the TBDPS group remained attached to 3′-OH (Figure 4.8). Following this sequence of steps, intermediate **31** was synthesised in 57% yield over 3 steps, which was superior to the previously mentioned route (48% over 3 steps).

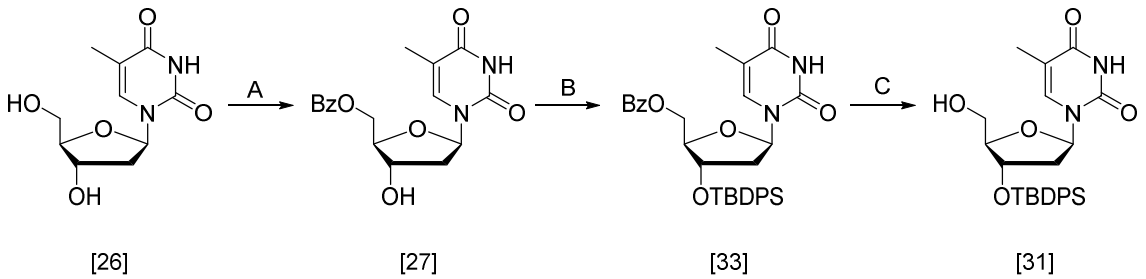

Figure 4. 8. A. BzCl, imidazole, DMF, 4 °C to r.t., 3 h, 76%; B. TBDPSCl, imidazole, DMF, 16 h, r.t., 88%; C. K_2CO_3, MeOH, overnight, r.t, 85%.

The 5′-OH was oxidized using Dess–Martin periodinane (DMP) in DCM to give the crude aldehyde that was used in the subsequent step without purification. Dess–Martin periodinane (DMP) oxidizes primary alcohols to aldehydes and secondary alcohols to ketones.[226, 227] Bestmann-Ohira Reagent was used to transform the crude aldehyde into a terminal alkyne in 70% yield over 2 steps according to paper of Varizhuk et. al..[228] This completed the synthesis of 5′-ethynyl thymidine (**23**), ready for coupling with 3′-azidomethyl LNA thymine for 5′-LNA dinucelotide synthesis.

4.3.3 Synthesis of 3′-azidomethyl LNA thymidine

The synthesis route (Figure 4.9) to protected 3′-azidomethyl LNA thymidine (**24**) started with 3-*O*-Benzyl-4-C-methanesulfonoxymethyl-5-methane-sulfonyl-1,2-*O*-isopropylidene-α-D-*erythro*-pentofuranose (**34**) following a sequence of steps described by Koshkin et al..[229] First, acetolysis and acetylation was achieved in a two-step reaction to obtain compound **35** in nearly quantitative yield without any chromatographic purification. Glycosyl acetates are common glycosyl donors in carbohydrate synthesis, and can be reacted with persilylated-nucleobases under conditions developed by Vorbruggen

and co-workers.[230-232] Then **35** was reacted with silylated thymine to give nucleoside **36** in 72% yield after chromatographic purification. Compound **36** was subsequently converted into **37** by deacetylation and a ring closing procedure after treatment with 2 M sodium hydroxide solution. In order to get 3′-azidomethyl nucleoside the 3′-OH was activated by a mixture of DMSO, acetic acid and acetic anhydride to give the 3′-methylthiomethyl nucleoside. Then bromine and 20 % aqueous LiN_3 were added in turn to afford 3′-azidomethyl LNA thymidine (**24**) for click reaction after chromatographic purification.

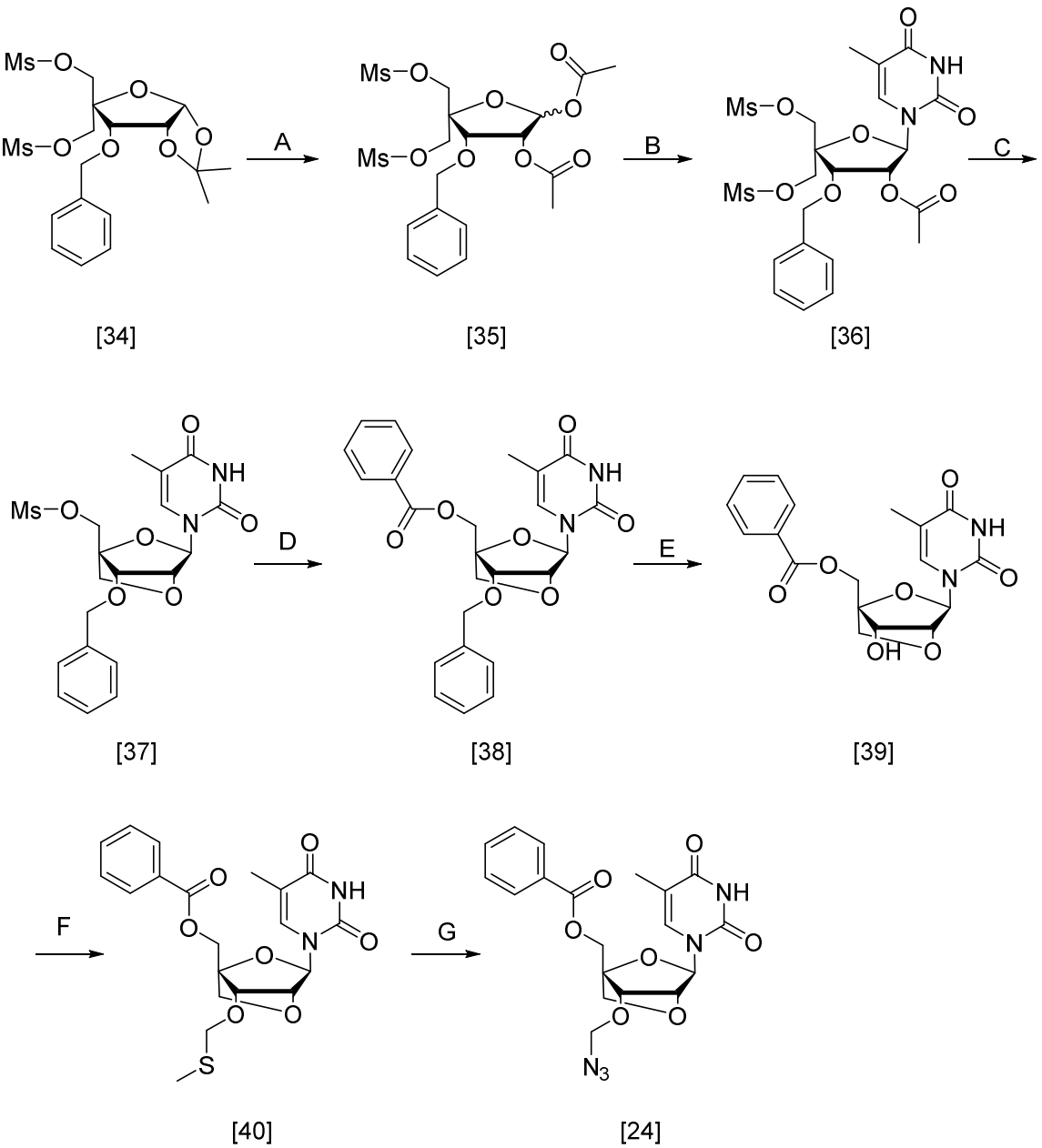

Figure 4. 9. A. 1) 80% Trifluoroacetic acid, 1 h 2) Ac_2O, pyridine, r.t., overnight, 95%; B. Thymine, *N*, *O*-Bis(trimethylsilyl)acetamide, Trimethylsilyl triflate, MeCN, 4 h, 72%; C. 2M NaOH, dioxane, water, 1 h, 92%; D. BzONa, DMF, 100 ^{o}C, 5 h, 88%; E. 20% $Pd(OH)_2$/C, ammonium formate, MeOH, reflux, 2 h, 77%; F. DMSO, Ac_2O, AcOH, r.t., 72 h, 42%; G. 1) Br_2, MeCN, 0 ^{o}C, 0.5 h 2) 20 % LiN_3 in H_2O, 65 ^{o}C, 2 h, 66%.

4.3.4 Synthesis of 5′-ethynyl LNA thymidine

The same general synthesis strategy developed for compound **23** was applied to synthesis of 5′-ethynyl LNA thymidine (**25**). DMP was used in an attempt to oxidize 3′-TBDPS-5′-OH LNA thymidine to the equivalent LNA aldehyde. However, the oxidation of 5′-OH LNA thymidine by DMP was unsuccessful and it was hypothesised that this was due to steric hinderance caused by the bulky 3′-*O*-TBDPS protecting group in addition to the LNA. An alternative protecting group on the 3′-OH was investigated (Figure 4.10). The synthesis of 5′-ethynyl LNA thymidine started with **38** and the benzoyl group was deprotected by a 2 M solution of sodium hydroxide in THF and water (v: v = 1:1) at room temperature. This time the oxidation of 5′-OH LNA thymidine by DMP was successful in the presence of the 3′-*O*-Bn protecting group and LNA sugar. The crude aldehyde was transformed by Bestmann-Ohira Reagent into the terminal alkyne (**25**) in 48% yield over 2 steps.

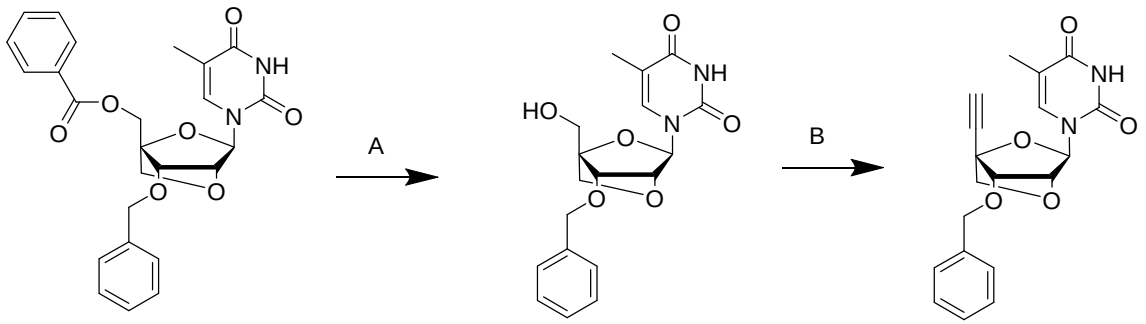

[38] [41] [25]

Figure 4. 10. A. 2 M NaOH, THF/H_2O, v/v=1:1, r.t, 1 h, 92%.; B. i. DMP, CH_2Cl_2, r.t.,3 h; ii. Bestmann-Ohira Reagent, K_2CO_3, MeCN, MeOH, r.t., 4 h, 48%.

4.3.5 Synthesis of the TL-dinucleotide phosphoramidites

4.3.5.1 Synthesis of the 3′-LNA TL-dinucleotides phosphoramidite

Comound **22** and **25** were reacted using catalytic $CuSO_4$ in the presence of a reductant, sodium ascorbate. The 5′-*O*-benzoyl group was removed by powered potassium carbonate in methanol (86% yield) and the 3′-*O*-benzyl group was deprotected by hydrogenation with 20% Pd $(OH)_2$/C and ammonium formate to produce compound **44** in 82% yield. Compound **44** is very polar and required multiple extractions by methanol in the reaction work up in order to obtain a decent yield.

The resulting 5′-alcohol was then reacted with 4,4′-dimethoxytrityl chloride in the presence of pyridine and compound **45** was isolated in 62% yield. Treatment of **45** with 2-cyanoethyl *N*, *N*-diisopropylchlorophosphoramidite in the presence of DIPEA and pyridine in dichloromethane for one hour at room temperature afforded target phosphoramidite **21** in 65% yield (Figure 4.11).

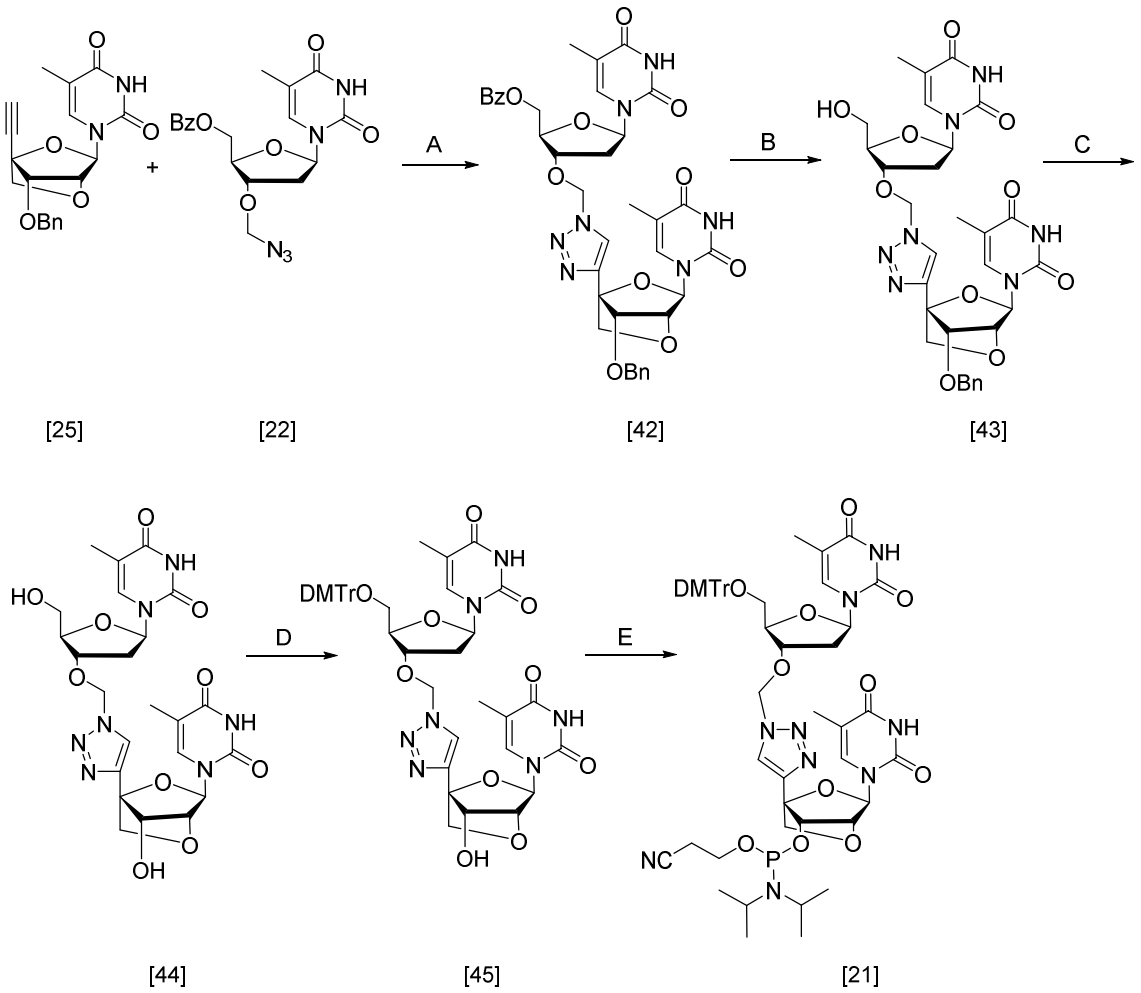

Figure 4. 11. A. $CuSO_4$, Na ascorbate, tetrahydrofuran (THF)/t-BuOH/H_2O (3:1:1), pyridine, r.t., 2 h, 74%; B. K_2CO_3, methanol, r.t., overnight, 86%; C. 20% $Pd(OH)_2/C$, ammonium formate, MeOH, reflux, 2 h, 82%; D. DMTrCl, dry pyridine, r.t., overnight, 62%; E. 2-cyanoethyl *N*, *N*-diisopropylchlorophosphoramidite, *N*, *N*-diisopropylethylamine (DIPEA), CH_2Cl_2, r.t., 1 h, 65%.

4.3.5.2 Synthesis of the 5′-LNA TL-dinucleotides phosphoramidite

The 5′-LNA TL dinucleotide phosphoramidite **20** was synthesised following the same reaction sequence as previously discussed. Compound **23** and **24** (Figure 4.5) were clicked together by a CuAAC reaction. The benzoyl ester protecting group was subsequently

hydrolysed using potassium carbonate in methanol. The TBDPS group was removed by TBAF dissolved in THF while the 4,4′-Dimethoxytrityl group was still attached to 5′-OH in preparation for the phosphitylation reaction. The 5′-LNA TL dinucleotide phosphoramidite (**20**) was then obtained after phosphitylation (64% yield) (Figure 4.12). This could be used for efficient incorporation of the corresponding dinucleotide analogue into ONs using standard solid phase phosphoramidite DNA synthesis methodology.

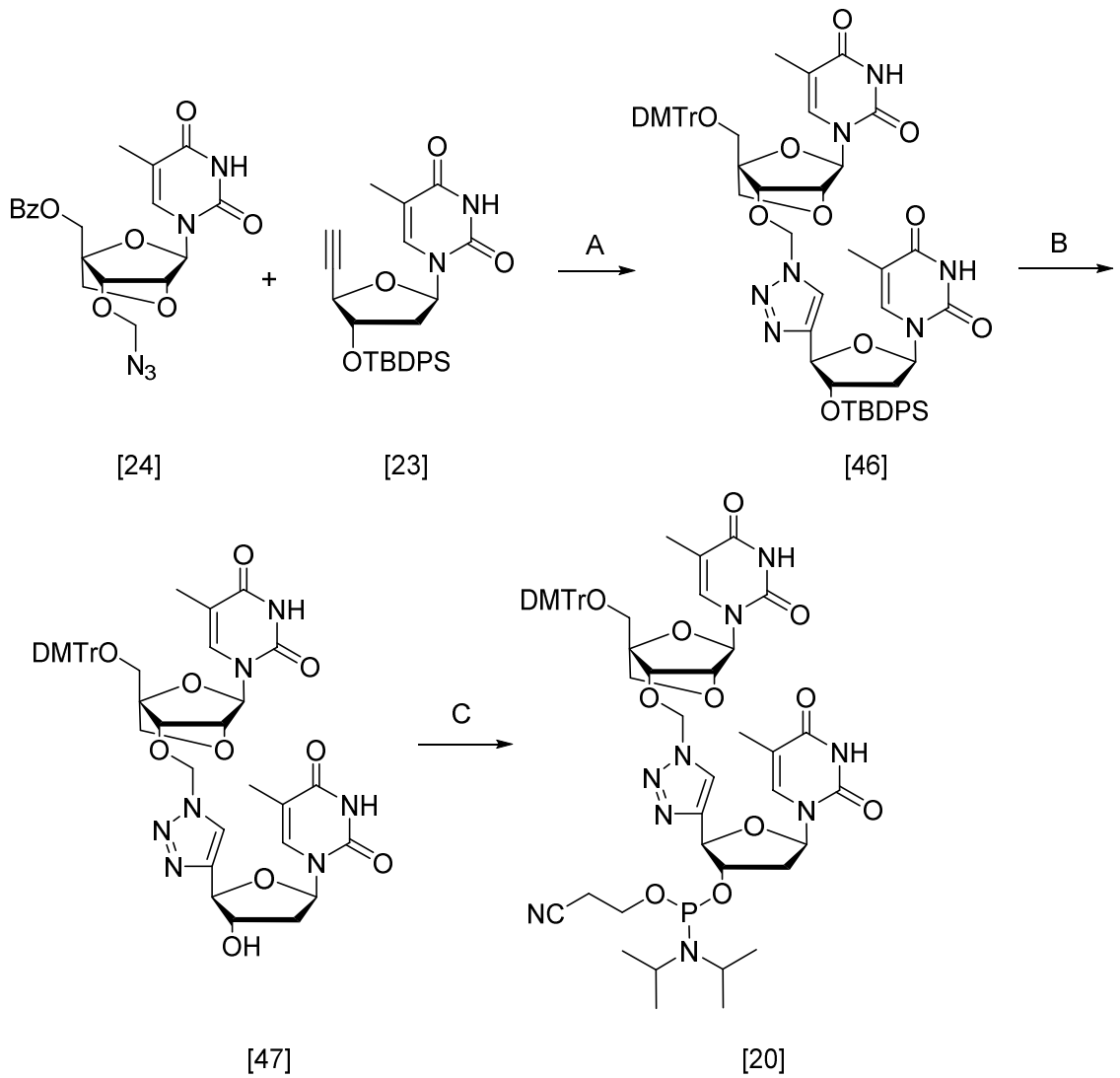

[24] [23] [46]

[47] [20]

Figure 4. 12. A. i. $CuSO_4$, Na ascorbate, tetrahydrofuran (THF)/t-BuOH/H_2O (3:1:1), pyridine, r.t., 2 h; ii. K_2CO_3, MeOH, r.t., overnight; DMTrCl, pyridine, r.t., overnight, 76%; B. TBAF, THF, r.t., 2 h; C. 2-cyanoethyl *N*, *N*-diisopropylchlorophosphoramidite, *N*, *N*-diisopropylethylamine (DIPEA), CH_2Cl_2, r.t., 1 h, 64%.

4.3.5.3 Synthesis of the 3′, 5′-LNA TL-dinucleotides phosphoramidite

The LNA-LNA dinucleotide phosphoramidite was synthesised following a similar synthetic route, starting with CuAAC reaction of compound **24** and **25** which gave **48** in 72% yield. Subsequent debenzylation under $Pd(OH)_2$/ammonium formate transfer hydrogenation conditions gave secondary alcohol **49** in 83% yield. Next, compound **50** was obtained after deprotection of the 5′-*O*-benzoyl group in low yield (12%) (Figure 4.13). This was due to loss of the product during the aqueous work-up because of the high water solubility of compound **50**. Unfortunately, the quantity obtained was not sufficient to continue with the synthesis. To avoid producing a highly polar intermediate, it was decided to introduce the 4,4′-dimethoxytrityl group prior to the hydrogenation. However, there was concern about the stability of the 4,4′-dimethoxytrityl ether under the elevated temperatures (65 ^oC) required for the transfer hydrogenation. A trial reaction was performed on 0.01 mmol scale at 65 ^oC for two hours. TLC analysis of the crude reaction indicated that the 4,4′-dimethoxytrityl group was still present after hydrogenation so the reaction was scaled-up.

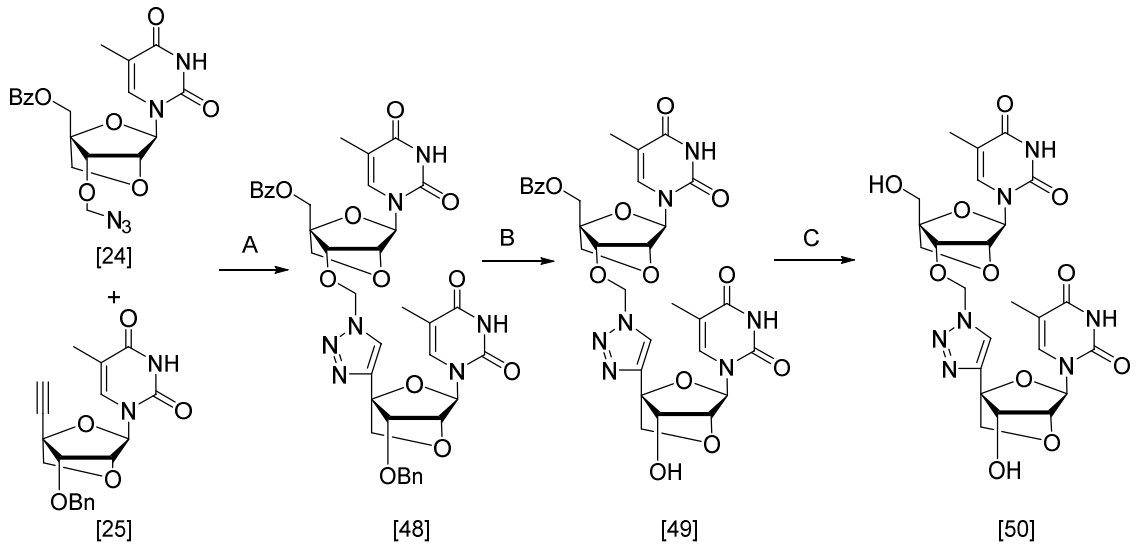

Figure 4. 13. A. $CuSO_4$, Na ascorbate, tetrahydrofuran (THF)/t-BuOH/H_2O (3:1:1), pyridine, r.t., 2 h, 72%; B. 20% $Pd(OH)_2$/C, ammonium formate, MeOH, reflux, 2 h, 83%; C. K_2CO_3, methanol, r.t., overnight, 12%;

Therefore, in the revised synthetic strategy the 5′-OH was protected with 4,4′-dimethoxytrityl after 5′-*O*-benzoyl group hydrolysis in the LNA-LNA dinucelotide (Figure 4.14). Next, the 3′-*O*-benzyl group was deprotected by hydrogenation while the 4,4′-dimethoxytrityl group was still attached to 5′-OH, which produced compound **52** in 39% yield over 4 steps, ready for phosphitylation to make the 3′, 5′-LNA dinucelotide phosphoramidite (**19**). Phosphitylation of intermediate **52** gave phosphoramidite **19** in 78% yield.

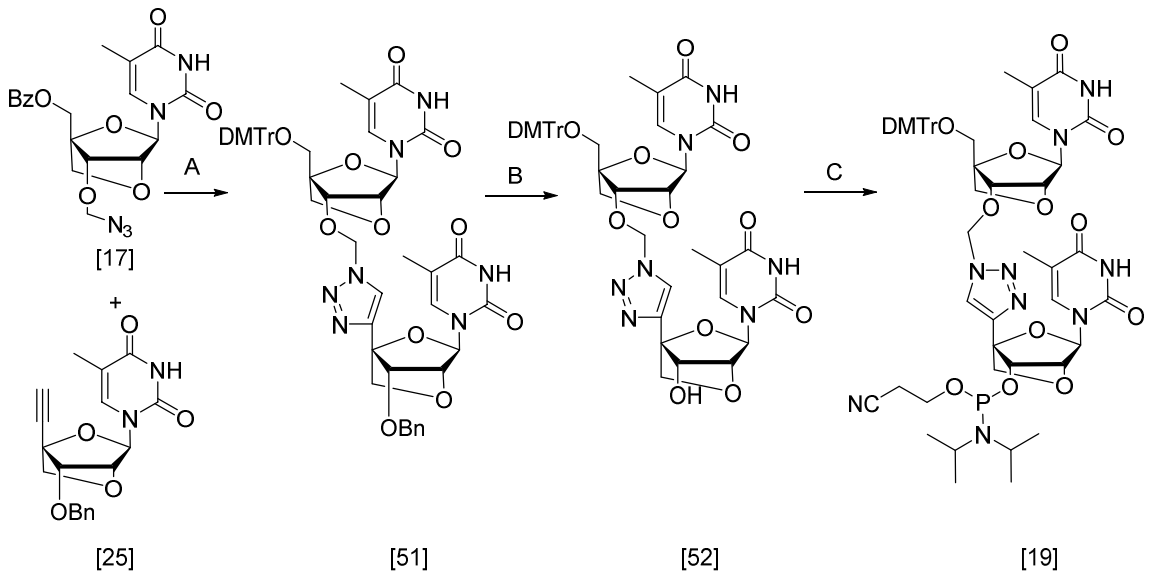

Figure 4. 14. A. i: $CuSO_4$, Na ascorbate, tetrahydrofuran (THF)/t-BuOH/H_2O (3:1:1), pyridine, r.t., 2 h; ii: K_2CO_3, methanol, r.t. overnight; iii: DMTrCl, pyridine, r.t., overnight, 54% B. 20% $Pd(OH)_2$/C, ammonium formate, MeOH, reflux, 2 h, 72%; C. 2-cyanoethyl *N*,*N*-diisopropylchlorophosphoramidite, *N*, *N*-diisopropylethylamine (DIPEA), CH_2Cl_2, r.t, 1 h, 78%.

4.4 Duplex stability studies of TL-Locked nucleic acid oligonucleotides

Phosphoramidites of compound **19, 20, 21** were used to synthesise the oligonucleotides (ONs) in Table 4.1 that were used for duplex stability studies and circular dichroism (CD) (Figure 4.15). LNA was added to either the 5′-side (ON B), 3′-side (ON A) or to both sides (ON C) of the triazole linkage. UV melting was used to determine the melting temperature (T_m) of ONs A-D on hybridization with DNA and RNA targets. As mentioned, before this TL-linked DNA (Figure 4.4 A) showed high binding affinity on hybridization with RNA target (T_m -0.4 °C compared to the unmodified ON[221]), and this will be used as a benchmark for novel TL-LNA oligonucleotides described in this thesis.

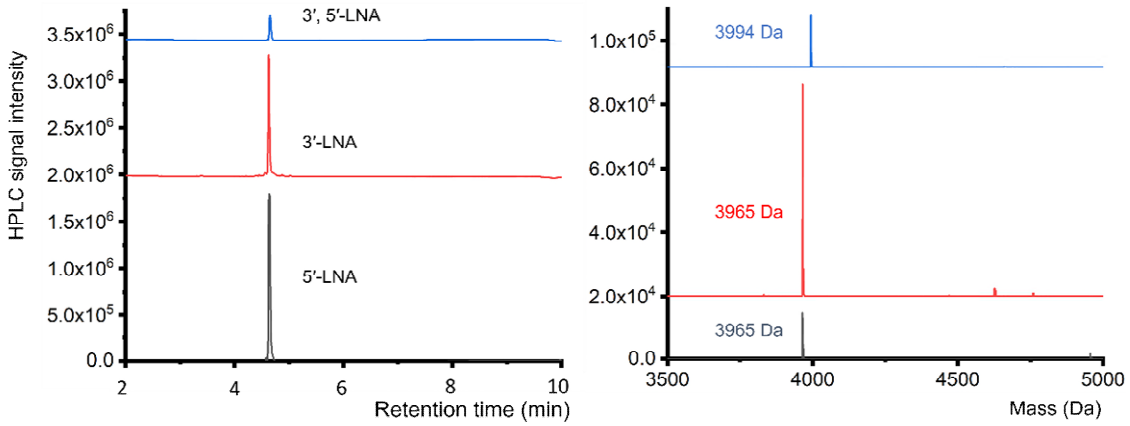

Figure 4. 15. HPLC chromatograms (left) and mass spectra (right) of the oligonucleotides containing triazole and LNA. Oligonucleotide sequences is shown in Table 4.1.

When targeting DNA sequences, the addition of 5′-LNA was observed to have a destabilizing effect in comparison to oligonucleotides without any modifications (ON E) or with only TL modifications (ON D). However, relocating the LNA to the 3′-end (ON A) resulted in the modification becoming stabilizing (Figure 4.16).

The duplex stability with complementary RNA was measured, and is deemed more important than ON-DNA duplex stability for therapeutic antisense oligonucleotides applications (Figure 4.17). Against RNA targets we found a difference in affinity when varying LNA position. 5′-LNA (ON B) formed the most destabilizing duplex with RNA target (ΔT_m -3.9 ^{o}C) compared to the unmodified ON E and TL only (ON D) oligonucleotides, which was in agreement with the literature[19, 217]. An explanation for this is because of the conformation of incorporated LNA sugars compared to that of the DNA sugars. In DNA, sugar conformation is variable but tends to the 2′-*endo* conformation.

The 2′-carbon is pushed out of the plane of the ring, into an envelope structure which reduces ring strain to lower conformational energy of the system. LNA being a 2′-4′-bicyclic ring system means it cannot have this conformation and instead tends to the 3′-*endo* conformation. The 3′-carbon pulls the backbone below it and puts strain on the linkage due to this. In the case of phosphodiester linkages, the duplex can mitigate this change with its sp^3 hybridised rotational flexibility, but this is not available for more constrained triazole, which is potentially destabilising the helix structure.

Table 4. 1. Thermal melting (T_m) data for triazole DNA: DNA and triazole DNA: RNA duplexes. Melting temperatures (T_ms) were determined using 3 mM of each ON at pH 7.0 in 10 mM phosphate buffer containing 200 mM NaCl. Δ*T*m means difference between modified ON and ON E (control). ^{L} = LNA nucleotide. t = triazole backbone. [a] Sequence of DNA target: GCTGCAAACGTCG. [b] Sequence of RNA target: GCUGCAAACGUCG.

ON	Triazole linkage	ON sequence (5′-3′)	DNA target[a]		RNA target[b]	
			T_m/°C	ΔT_m/°C	T_m/°C	ΔT_m/°C
A	3′-LNA	CGACG**TtT**^{L}TGCAGC	54.5	-7.4	58.4	-0.2
B	5′-LNA	CGACG**T**^{L}**tT**TGCAGC	52.0	-9.9	54.7	-3.9
C	3′, 5′-LNA	CGACG**T**^{L}**tT**^{L}TGCAGC	54.0	-7.9	59.0	+0.4
D	TL only	CGACG**TtT**TGCAGC	58.7	-3.2	57.8	-0.8
E	Phosphodiester	CGACG**TT**TGCAGC	61.9	0	58.6	0

The incorporation of single LNA-modified sugar on the 3′-end of the TL (ON-A) resulted in slightly improved duplex stability (ΔT_m -0.2 °C) compared to the ON without any LNA-modified sugars (ON-D, ΔT_m -0.8 °C, T_m and CD data of ON-D are from Ysobel *et. al*). This implies that when the LNA thymidine was on the 3′ side of the TL it causes some additional stabilising effect on DNA-RNA hybrids. This is not the case when the single

LNA incorporation is on the 5′-end of the TL (ON-B, ΔT_m -3.9 °C) as moving an LNA to the 3′-side means that the 3′-*endo* conformation is no longer acting on the modified backbone but instead on a phosphodiester linkage below it. Therefore, we now see the expected relative stabilisation compared to the triazole alone. The biggest difference between DNA and RNA targets was seen with the introduction of LNA to both sides of the triazole linkage. This also can be explained by the 3′-*endo* conformation of the LNA and its high affinity for RNA. In DNA:RNA duplexes, sugar conformation is pushed into the 3′-*endo* conformation.

The greatest improvement in ON-RNA duplex stability was observed when the LNA modification was on both 3′ side and 5′ side (ON C, ΔT_m +0.4 °C). Duplex stability with the RNA target has been increased by 1.2 °C compared to the ON D (triazole only) which suggests great potential in antisense oligonucleotide applications (Figure 4.17).

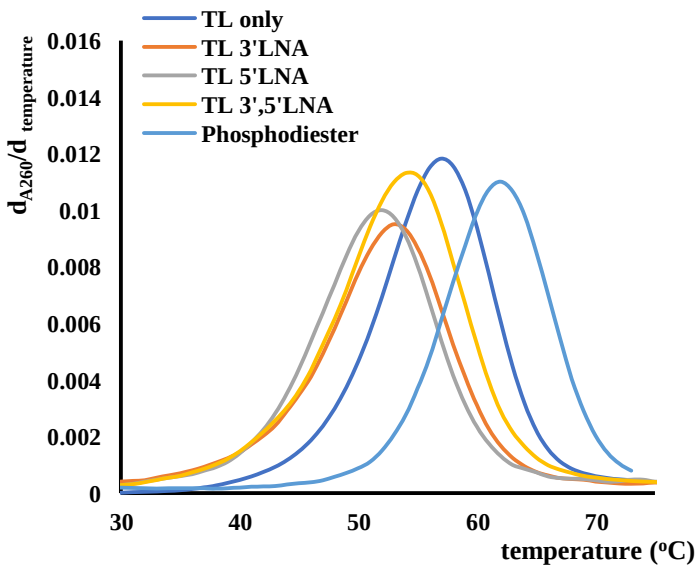

Figure 4. 16. UV melting studies of TL-LNA modified LNA-DNA duplexes (1st derivative of melting curve). Condition: 3 µM of oligonucleotides were added to 10 mM phosphate, 200 mM NaCl buffer, pH 7.0 and heated from 20–85 °C. T_m values were determined from an average of six ramps from a smoothed plot of dA/t. Both melting and annealing curves were used to determine T_m. Data points were measured in triplicate.

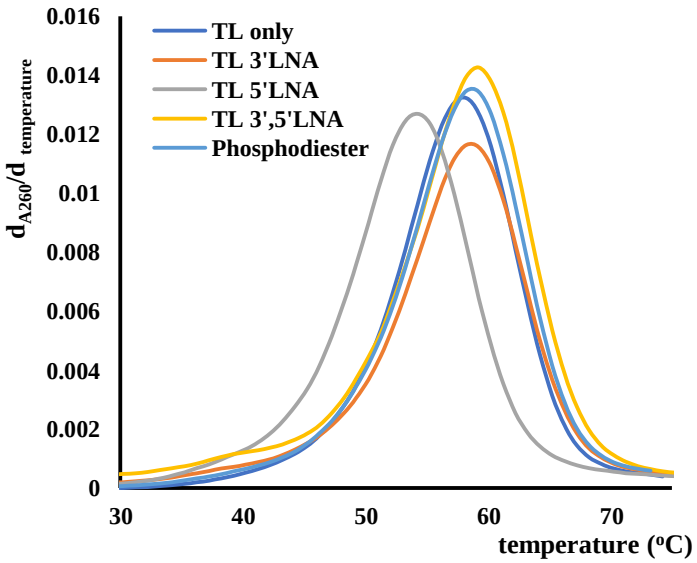

Figure 4. 17. UV melting studies of TL-LNA modified LNA-RNA duplexes (1st derivative of melting curve). Condition: 3 µM of oligonucleotides were added to 10 mM phosphate, 200 mM NaCl buffer, pH 7.0 and heated from 20–85 °C. T_m values were determined from an average of six ramps from a smoothed plot of dA/t. Both melting and annealing curves were used to determine T_m. Data points were measured in triplicate.

4.5 Circular dichroism studies of TL-Locked nucleic acid oligonucleotides

Circular dichroism (CD) was utilised to assess changes in global duplex structure by measuring polarised light absorption from 200–340 nm. The helical conformation is not

greatly affected, and structural alterations relative to the unmodified control are fairly minor, according to these findings. Transitions at 220, 255, and 280 nm characterise B-form structures in DNA-DNA duplexes (Figure 4.18). DNA-RNA hybrids form A-like duplexes with negative and positive peaks at 210 and 270 nm, respectively (Figure 4.19). When DNA-DNA and DNA-RNA hybrids are compared, it appears that LNA has more structural effects on DNA-DNA B-form duplexes. In unmodified DNA duplexes the deoxyribose sugar is C2′-*endo*, leading to a B-form helix. Conversely, LNA prefers a C3′-*endo* conformation characteristic of A-form RNA.[97] 5′-LNA had the greatest perturbating effect on the CD spectra (Figure 4.18) relative to the unmodified duplex and this is interesting as it is the 5′-LNA that gives the lowest T_m values. However, there was a synergistic effect on T_m of having both 5′- and 3′-LNA surrounding the triazole which is beneficial when targeting against RNA. This should be considered to be a preliminary structural investigation and in future work NMR and X-ray crystallographic studies will be attempted.

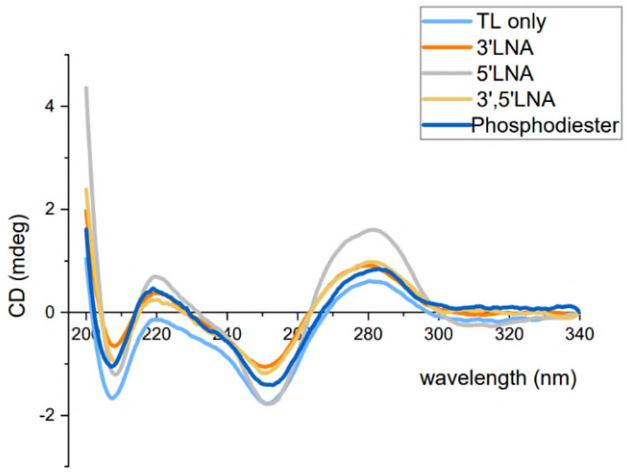

Figure 4. 18. Circular dichroism spectra of 3 µM TL-LNA modified oligonucleotides against DNA target in 10 mM phosphate, 200 nM NaCl buffer, pH 7.0. Spectra were averaged from four scans and smoothed to 20 points using a third order polynomial. For sequences see Table 4.1. Data points were measured in triplicate.

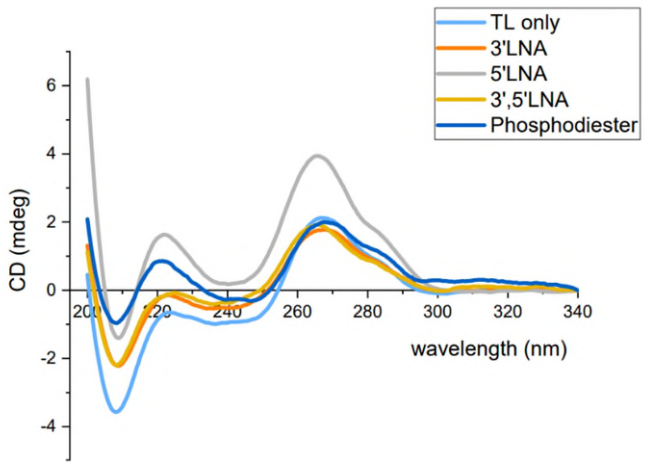

Figure 4. 19. Circular dichroism spectra of 3 µM TL-LNA modified oligonucleotides against RNA target in 10 mM phosphate, 200 nM NaCl buffer, pH 7.0. Spectra were averaged from four scans and smoothed to 20 points using a third order polynomial. For sequences see Table 4.1. Data points were measured in triplicate.

4.6 Conclusions

This chapter describes straightforward and efficient standard solid phase phosphoramidite DNA synthesis methodology to synthesise oligonucleotides containing triazole-LNA linkages, and the biophysical evaluation of these ONs to investigate the binding affinity to RNA targets for ASO therapeutic applications. Using the ′best′ triazole linkage described by Varizhuk et al. as a starting point,[221] this work has increased our understanding of the combined effects of LNA sugars and triazole linkages in ASOs on DNA: DNA and DNA: RNA duplex stability.

ON-D (triazole only) had high binding affinity to RNA targets compared to other triazole linkages reported by Varizhuk et al.[221] For this triazole backbone, the T_m of ON A (3′-LNA) was just +0.6 ^oC higher compared to ON D although ON B (5′-LNA) was moderately destabilizing. The T_m of ON C which the LNA sugars on both the 3′ side and 5′ sides of the triazole was increased +1.2 ^oC compared to the ON D and +0.4 ^oC compared to ON E (natural oligonucleotide). Therefore, the binding affinity for the RNA target has been improved by the LNA sugars (and the LNA-TL modification will resist digestion by nucleases in cells). Also, there might also be improved delivery of triazole-modified ON′s into cells due to their reduced overall negative charge. Taking the above properties into account, TL-LNA oligonucleotides could be future candidates for use in therapeutic, *in vivo* diagnostic, and *in vivo* imaging applications. To pursue this further, a considerable synthetic challenge will be faced in synthesising oligonucleotides with any of the four canonical bases (A, G, mC* and T) surrounding the LNA-triazole backbone. Synthesising all the required 16 dimers to make any sequence is a daunting task, and it will be more

realistic to carry out the triazole-forming click reactions during solid-phase oligonucleotide synthesis. This may also allow the synthesis of the corresponding 1,5 disubstituted triazole backbone by changing the catalyst in the click reaction.

The effects of multiple additions of LNA-triazole into antisense oligonucleotides (ASOs) also need to be investigated, as does the effects of combinations of LNA-triazole dimers, 2′-O-alkyl sugars and phosphorothioate backbones. This preliminary study has shown that such work will be potentially valuable in the therapeutic oligonucleotide field.

Chapter 5

Conclusions and future work

Chapter 5 – Conclusions and future work

In conclusion, a new phosphoramidite enables orthogonal double labelling to form combination oligonucleotide probes (AP-C3 and AP-C6, Chapter 2). Oligonucleotides labelled with thiazole orange intercalator and a reporter dye (ROX) on the same thymine base have been synthesized by taking advantage of the orthogonality of the CuAAC click and amide bond formation reactions. Multiple monomers can be added to produce heavily functionalised oligonucleotides. Thermal duplex stability and fluorescence studies demonstrate that TO/ROX combination probes can detect nucleic acid targets with highly favourable signal-background-ratios. To enhance resistance against the enzymatic degradation that is encountered in a cellular environment, 2′-OMe RNA combination probes were synthesised and showed good duplex stability and excellent fluorescence properties on binding to complementary RNA targets, indicating that this versatile platform has a lot of potential for cellular imaging, gene diagnostics, and gene detection applications.

Future work will involve optimisation of the length and nature of the linkers between the nucleobase and the fluorescent labels, and attaching thiazole orange to AP-C3 by the quinoline moiety rather than benzothiazole to determine if this offers any advantages in terms of fluorescence or duplex stability. 2′-*O*- methoxyethyl sugars will be used to reduce the fluorescence of the single-stranded form of thiazole orange oligonucleotides. The improvement provided by 2′-*O*-methyl sugars is possibly due to the methoxy group inhibiting the ability of the thiazole orange to stack on the nucleobases in the single strand

or create a single-stranded conformation that is less favourable for thiazole orange-nucleobase stacking. The 2′-*O*-methoxyethyl modification, being bulkier than methoxy, could give a further improvement. UV melting and steady state fluorescence of these probes should be performed to evaluate these modified probes.

The new combination probe and TO labelled probe principles have been successfully applied to the forward inner primer and backward inner primer modifications for a LAMP assay to detect COVID-19. These primers were labelled with various fluorescent dyes by CuAAC click and amide bond formation reactions. Different primer pairs were used in LAMP assays and P3 (F-unmodified: B-d1-Y/TO) showed the quickest amplification in the LAMP assays. P12 (F-unmodified: B-d1-TAMRA/TO) required slightly longer amplification time than P3 but still performed better than the positive control P1 (F-unmodified: B-unmodified) while its specificity can be significantly improved by the intercalation of TO. As the pandemic is still ongoing, it will be helpful to develop more sensitive and specific detection methods. Since the LAMP does not require costly reagents or specialised equipment such as RT-qPCR, it is more accessible and economical to most developing countries.

In Chapter 4 a straightforward and efficient standard solid phase phosphoramidite DNA synthesis methodology was applied to synthesise oligonucleotides containing triazole-LNA linkages. The biophysical properties of these ONs were evaluated to investigate the binding affinity to RNA targets for ASO therapeutic applications. A better understanding of the combined effects of LNA sugars and triazole linkages in ASOs on DNA was reached:

DNA and DNA: RNA duplex stability was reached after performing melting temperature and circular dichroism. The greatest improvement in ON-RNA duplex stability was observed when the LNA modification was on both 3′ side and 5′ side (ON C, ΔT_m +0.4 ^oC). This binding affinity on RNA target has been increased by 1.2 ^oC compared to the ON D (triazole only) which showed great potential in antisense oligonucleotide applications. TL-LNA oligonucleotides, as well as other combinations of LNA with artificial DNA backbones, could be future prospects for applications in diagnostic, therapeutic, and *in vivo* imaging, based on the above features.

Chapter 6

Experimental

Chapter 6 – Experimental

6.1 General synthetic procedures

All reagents were purchased from Sigma-Aldrich, Acros Organics, Invitrogen or Fisher Scientific and used without further purification. 3 Å Molecular sieves (beads, 4 – 8 mesh, Sigma-Aldrich) were used to dry MeOH and EtOH. Anhydrous CH_2Cl_2, DMF and MeCN were collected from a Grubbs-type SPS. Thin layer chromatography (TLC) was performed using Merck TLC silica gel 60 F254 plates (0.22 mm thickness, aluminium backed) and the compounds were visualized by irradiation at 254/365 nm and stained with *p*-anisaldehyde (*p*-anisaldehyde (11.5 mL), glacial acetic acid (4.8 mL), conc. sulphuric acid (15.7 mL) and 95% EtOH (423 mL)) or potassium permanganate ($KMnO_4$ (1.5 g), K_2CO_3 (10 g), and NaOH (10%, 1.25 mL) in H_2O (200 mL)). ^{1}H NMR spectra were measured at 400 MHz on a Bruker DPX400 (AVIIIHD 400) spectrometer or at 500 MHz on a Bruker AVIIIHD 500 spectrometer. ^{13}C NMR spectra were measured at 101 MHz on a Bruker DPX400 spectrometer or at 126 MHz on a Bruker AVIIIHD 500 spectrometer. ^{31}P NMR and ^{19}F NMR spectra were recorded on a Bruker AVIIIHD 400 spectrometer at 162 MHz and 376 MHz respectively. ^{1}H were internally referenced to the appropriate residual undeuterated solvent signal; ^{13}C NMR spectra referenced to the deuterated solvent. Assignment of the signals was aided by COSY (^{1}H - ^{1}H), HSQC-DEPT, HSQC (^{1}H - ^{13}C) and HMBC (^{1}H - ^{13}C) experiments. Aromatic carbon without attached proton was abbreviated with Ar and aromatic carbon with the proton attached was abbreviated Ar-H. Low-resolution mass spectra (LRMS) were recorded using electrospray ionisation (ESI^+

or ESI^-) on a Waters ZMD quadrupole mass spectrometer in HPLC grade methanol. High-resolution mass spectra (HRMS) were recorded in HPLC grade methanol using electrospray ionisation (EI) on a Bruker APEX III FT-ICR mass spectrometer.

6.2 Synthesised compounds

6.2.1 Synthesis of 2, 2, 2-trifluoro-*N*-(3-hydroxypropyl)acetamide

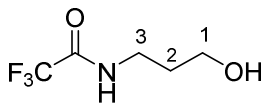

3

To stirred 3-aminopropanol (6.0 g, 79.9 mmol) was added ethyl trifluoroacetate (20.5 g, 144 mmol) dropwise under an argon atmosphere at 0 °C. The solution was stirred for 3 h, evaporated, followed by purification by column chromatography on silica gel (0-10% CH_3OH/CH_2Cl_2, v/v) to give the product compound **3** as a pale-yellow liquid (13.3 g, 77.7 mmol, 97%). Spectral data were in agreement with literature values.[198]

R_f = 0.60 (MeOH:CH_2Cl_2, v/v = 1:9), $KMnO_4$.

^{1}H NMR (400 MHz, $CDCl_3$): δ 7.80 (br s, 1H, NH), 3.72 (t, *J* = 5.6 Hz, 2H, H1), 3.47 (app. q, *J* = 6.0 Hz, 2H, H3), 3.19 (s, 1H, OH), 1.83 – 1.74 (m, 2H, H2);

^{13}C NMR (101 MHz, $CDCl_3$): δ 158.0 (q, *J* = 36.7 Hz, CO-CF_3), 116.1 (q, *J* = 287.3 Hz, CF_3), 60.7 (C1), 38.2 (C3), 30.6 (C2);

LRMS (ESI^-) *m/z* $[M-H]^-$ for $[C_5H_7F_3NO_2]^-$ calc. 170.1 found 170.1 (100%);

6.2.2 Synthesis of 2, 2, 2-trifluoro-*N*-(3-oxopropyl)acetamide

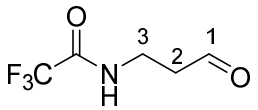

4

To a stirred solution of compound **3** (3.2 g, 18.7 mmol) in CH_2Cl_2 (60 mL) was added Dess-Martin periodinane (11.9 g, 28.1 mmol) under an argon atmosphere at 0 °C. The suspension was stirred for 2 h at room temperature, quenched with saturated $NaHCO_3$ (120 mL), Et_2O (120 mL) was added and the biphasic mixture was stirred for 20 min. A precipitate formed which was removed by filtration. The phases were separated and the aqueous phase was extracted with Et_2O (60 mL). The combined organic layers were washed with saturated NaCl (50 mL), dried with $MgSO_4$, filtered and evaporated. The crude product was purified by column chromatography on silica gel (0-60% EtOAc/PE 40-60, v/v) to give the product as a colourless liquid (1.6 g, 9.5 mmol, 51%). The product was used on the same day due to low stability. Spectral data of the compound were reported in $CDCl_3$.[199]

R_f = 0.43 (EtOAc: hexane, v/v = 2:3), $KMnO_4$.

^{1}H NMR (400 MHz, d_6-DMSO): δ 9.63 (t, *J* = 1.4 Hz, 1H, H1), 9.46 (s, 1H, NH), 3.49 – 3.42 (m, 2H, H3), 2.70 (td, *J* = 6.6, 1.4 Hz, 2H, H2);

^{13}C NMR (101 MHz, d_6-DMSO): δ 201.9 (C1), 156.7 (q, *J* = 36.2 Hz, C̲O-CF_3), 116.3 (q, *J* = 288.0 Hz, CF_3), 42.3 (C2), 33.7 (C3);

^{19}F NMR (376 MHz, d_6-DMSO): δ -74.5 (CF_3);

LRMS (ESI$^+$) *m/z* $[M-H]^-$ for $[C_5H_5F_3NO_2]^-$ calc. 168.0 found 168.0 (40%);

6.2.3 Synthesis of *N*-(3-(di(prop-2-yn-1-yl)amino)propyl)-2, 2, 2-trifluoroacetamide

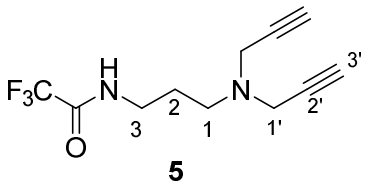

5

To a stirred solution of compound **4** (1.78 g, 10.5 mmol) and dipropargylamine (0.72 mL, 7.0 mmol) in an anhydrous CH_2Cl_2 (23 mL) under an argon atmosphere at room temperature, was added $NaBH(OAc)_3$ (2.97 g, 14.0 mmol). The solution was stirred for 2 h, quenched with saturated $NaHCO_3$ (10 mL) and stirred for 20 min. The mixture was extracted with CH_2Cl_2 (2 x 15 mL), the organic phase was washed with water, saturated aqueous NaCl. The organic layer was collected and dried with Na_2SO_4. The crude product was purified by column chromatography on silica gel (10%-70% EtOAc/PE 40-60, v/v) to give the product compound **5** as a white solid (1.63 g, 6.6 mmol, 95%).

R_f = 0.60 (MeOH:CH_2Cl_2, v/v = 1:9), $KMnO_4$.

^{1}H NMR (400 MHz, $CDCl_3$): δ 8.18 (br s, 1H, NH), 3.42 (app. q, *J* = 5.8 Hz, 2H, H3), 3.37 (d, *J* = 2.4 Hz, 4H, H1′), 2.71 (app. t, *J* = 2.7 Hz, 2H, H1), 2.19 (t, *J* = 2.4 Hz, 2H, H3′), 1.71 – 1.63 (m, 2H, H2);

^{13}C NMR (101 MHz, $CDCl_3$): δ 157.1 (q, *J* = 36.7 Hz, CO-CF_3), 117.4 (q, *J* = 287.9, CF_3), 77.9 (C2′), 73.6 (C3′), 51.5 (C1), 42.2 (C1′), 39.9 (C3), 24.4 (C2);

^{19}F NMR (376 MHz, $CDCl_3$): δ -76.10 (CF_3);

HRMS (ESI$^+$) *m/z* $[M+H]^+$ for $[C_{11}H_{14}F_3N_2O]^+$ calc. 247.1053 found 247.1052;

6.2.4 Synthesis of 5-propargylamino(*N*-propargyl-*N*-propyl-2, 2, 2-trifluoroacetamide)-5′-*O*-(4,4′-dimethoxy-tritryl)-2′-deoxythymidine

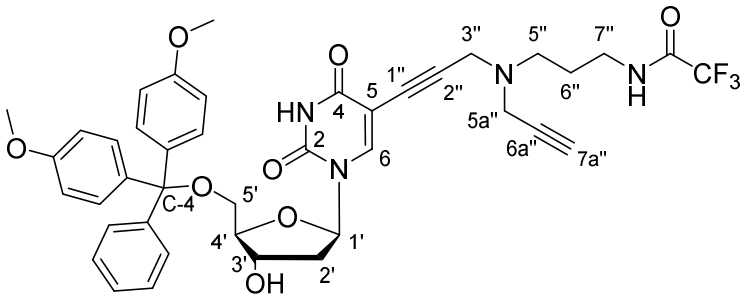

6

To a stirred solution of 5-iodo-5′-DMTr-deoxythymidine (4.20 g, 6.40 mmol), compound **5** (3.2 g, 12.8 mmol), $PdCl_2(PPh_3)_2$ (0.494 g, 0.704 mmol) and CuI (0.072 g, 0.378 mmol) in degassed DMF (60.6 mL) under an argon atmosphere at room temperature, degassed Et_3N (5.35 ml) was added. The mixture was stirred for 12 h, evaporated to dryness and the resulting residue was dissolved in EtOAc (100 mL). The organic layer was washed with an EDTA sodium salt solution (0.15 molar, 50 mL), H_2O (50 mL) and saturated NaCl (50 mL). The organic phase was dried with Na_2SO_4 and evaporated, followed by purification by chromatography on silica gel (17-100% EtOAc/CH_2Cl_2, v/v) to give the product as a pale-yellow foam (2.92 g, 3.76 mmol, 59%).

R_f = 0.20 (EtOAc:CH_2Cl_2, v/v = 7:3), *p*-anisaldehyde, UV.

^{1}H NMR (500 MHz, $CDCl_3$): δ 9.66 (s, 1H, NH-thymidine), 8.26 (t, *J* = 5.3 Hz, 1H, NH-chain), 8.12 (s, 1H, H6), 7.46 – 7.42 (m, 2H, Ar-H), 7.37 – 7.33 (m, 4H, Ar-H), 7.33 – 7.29 (m, 2H, Ar-H), 7.26 – 7.21 (m, 1H, Ar-H), 6.88 – 6.84 (m, 4H, Ar-H), 6.34 (t, *J* = 7.5 Hz, 1H, H1′), 4.56 – 4.52 (m, 1H, H4′), 4.11 (app. q, *J* = 3.1 Hz, 1H, H3′), 3.80 (s, 6H, OCH_3), 3.46 (dd, *J* = 10.8, 3.1 Hz, 1H, H5′a), 3.38 – 3.29 (m, 5H, H5′b, H3″ and H7″), 3.19 (d, *J*

= 2.5 Hz, 2H, H5a″), 2.56 – 2.51 (m, 3H, H2′a and H5″), 2.30 (ddd, *J* = 13.6, 7.6, 6.0 Hz, 1H, H2′b), 2.21 (t, *J* = 2.5 Hz, 1H, H7a″), 1.54 (app. p, *J* = 6.1 Hz, 2H, H6″).

^{13}C NMR (126 MHz, $CDCl_3$): δ 162.1 (C4), 158.6 (Ar), 157.2 (q, *J* = 36.5 Hz, C̲O-CF_3), 149.4 (C2), 144.5 (Ar), 142.3 (C6), 135.6 (Ar), 130.0 (Ar-H), 128.1 (Ar-H), 127.9 (Ar-H), 127.0 (Ar-H), 116.2 (q, *J* = 287.8 Hz, CF_3), 113.3 (Ar-H), 99.9 (C5), 88.8 (C2″), 87.0 (C-4), 86.6 (C4′), 85.7 (C1′), 78.6 (C6a″), 76.0 (C1″), 73.3 (C7a″), 72.2 (C3′), 63.4 (C5′), 55.3 (OCH_3), 50.8 (C5″), 43.1 (C3″), 42.7 (C5a″), 41.6 (C2′), 39.4 (C7″), 24.6 (C6″).

^{19}F NMR (376 MHz, $CDCl_3$): δ -75.91 (CF_3);

HRMS (ESI$^+$) *m/z* $[M+H]^+$ for $[C_{41}H_{42}F_3N_4O_8]^+$ calc. 775.2949 found: 775.2940;

6.2.5 Synthesis of 5-propargylamino(*N*-propargyl-*N*-propyl-2,2,2-trifluoroacetamide)-5′-*O*-(4,4′-dimethoxy-tritryl)-2′-deoxythymidine diisopropylamino cyanoethyl phosphoramidite

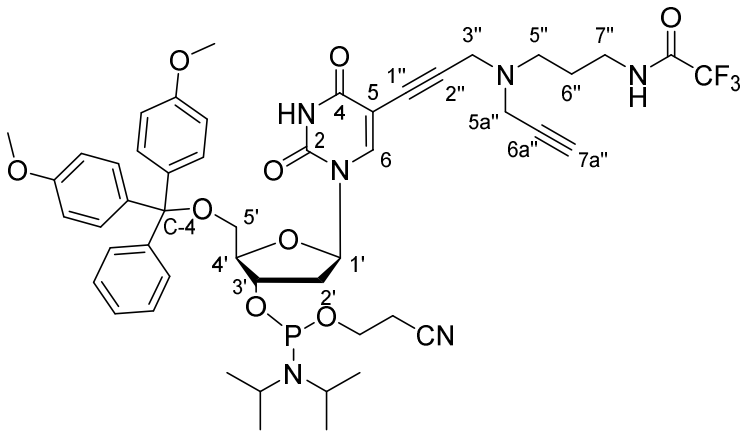

7

To a solution of compound **6** (2.01 g, 2.60 mmol) and anhydrous degassed DIPEA (1.27 mL, 7.28 mmol) in anhydrous degassed CH_2Cl_2 (60 mL) under an argon atmosphere, 2-cyanoethyl *N*, *N*-diisopropylchlorophosphoramidite (0.76 mL, 3.41 mmol) was added. The reaction was stirred for 1.5 h, quenched with degassed saturated KCl solution (30 mL) and the organic phase was passed through a layer of anhydrous Na_2SO_4 followed by evaporation to give a yellow foam. The crude product was purified by chromatography on silica gel (degassed 60-85% EtOAc/hexane, v/v) pre-equilibrated with pyridine, under an atmosphere of argon to give the product compound **7** as white foam (1.82 g, 1.87 mmol, 72%).

R_f = 0.31 and 0.48 for two isomers (EtOAc:hexane, v/v = 7:3), *p*-anisaldehyde, UV.

^{1}H NMR (400 MHz, $CDCl_3$) δ 8.31 (s, 1H, NH-chain), 8.08 (s, 0.5H, H6 isomer a), 8.04 (s, 0.5H, H6 isomer b), 7.39 – 7.33 (m, 2H, Ar-H), 7.30 – 7.20 (m, 6H, Ar-H), 7.19 – 7.10

(m, 1H, Ar-H), 6.80 – 6.73 (m, 4H, Ar-H), 6.23 (dt, *J* = 7.3, 5.9 Hz, 1H, H1′), 4.57 – 4.48 (m, 1H, H3′), 4.15 – 4.05 (m, 1H, H4′), 3.72 (s, 6H, OCH_3), 3.79 – 3.33 (m, 5H, H5′a and ^{i}Pr-CH and OCH_2CH_2-CN), 3.30 – 3.15 (m, 5H, H3′′and H5′b and H7′′), 3.06 (app. dd, *J* = 6.1, 2.4 Hz, 2H, H5a′′), 2.55 (t, *J* = 6.3 Hz, 1H, CH_2b-CN), 2.48 (ddd, J = 13.7, 5.9, 2.8 Hz, 1H, H2′a), 2.44 – 2.37 (m, 2H, H5′′), 2.35 (t, *J* = 6.3 Hz, 1H, CH_2a-CN), 2.25 (dt, *J* = 13.7, 7.3 Hz, 1H, H2′b), 2.11 (app. q, *J* = 2.4 Hz, 1H, H7a′′), 1.45 – 1.34 (m, 2H, H6′′), 1.12 – 1.07(m, 9H, ^{i}Pr-CH_3), 0.98 (d, *J* = 6.8 Hz, 3H, ^{i}Pr-CH_3).

^{31}P NMR (162 MHz, $CDCl_3$): δ 149.08 (s), 148.68 (s);

HRMS (ESI$^+$) *m/z* $[M+H]^+$ for $[C_{50}H_{59}F_3N_6O_9P]^+$ calc. 975.4028 found 975.4018;

6.2.6 Synthesis of *N*-(1-hydroxyhexyl)trifluoroacetamide

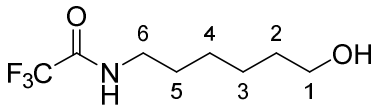

8

To a stirred 6-aminohexanol (4.00 g, 34.1 mmol) ethyl trifluoroacetate (5.70 mL, 47.7 mmol) was added dropwise under an argon atmosphere at room temperature. The solution was stirred for 2.5 h, evaporated, followed by purification by column chromatography on silica gel (20-100% EtOAc/CH_2Cl_2, v/v) to give the product as white solid (4.94 g, 23.2 mmol, 68%). Spectral data were in agreement with literature values.[214]

R_f = 0.57 (EtOAc:CH_2Cl_2, v/v = 8:2), $KMnO_4$.

^{1}H NMR (400 MHz, $CDCl_3$): δ 6.84 (br s, 1H, NH), 3.62 (td, *J* = 6.5, 3.3 Hz, 2H, H1), 3.34 (app. q, *J* = 6.8 Hz, 2H, H6), 1.90 (br s, 1H, OH), 1.63 – 1.50 (m, 4H, CH_2), 1.43 – 1.30 (m, 4H, CH_2);

^{13}C NMR (101 MHz, $CDCl_3$): δ 157.4 (q, *J* = 36.6 Hz, $\underline{C}O$-CF_3), 115.9 (q, *J* = 287.8 Hz, CF_3), 62.6 (C1), 39.8 (C6), 32.3 (CH_2), 28.8 (CH_2), 26.3 (CH_2), 25.2 (CH_2);

^{19}F NMR (376 MHz, $CDCl_3$): δ -75.97 (CF_3);

LRMS (ESI$^-$) *m/z* $[M-H]^-$ for $[C_8H_{13}F_3NO_2]^-$ calc. 212.1 found 212.1 (100%);

6.2.7 Synthesis of *N*-(1-oxohexyl)trifluoroacetamide

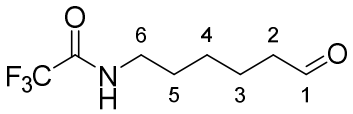

9

To a stirred solution of **8** (3.65 g, 17.1 mmol) in CH_2Cl_2 (100 mL) was added Dess-Martin periodinane (10.1 g, 23.9 mmol) under an argon atmosphere at 0 °C. The suspension was stirred for 2 h at room temperature, quenched with saturated $NaHCO_3$ (120 mL) and the Et_2O (120 mL) was added and the biphasic mixture was stirred for 20 min. Precipitate formed which was removed by filtration and phases were separated, the aqueous phase was extracted with Et_2O (60 mL). The combined organic layers were washed with saturated NaCl (50 mL), dried with $MgSO_4$ filtered and evaporated. The crude product was purified by column chromatography on silica gel (0-60% EtOAc/PE 40-60, v/v) to give the product as colourless liquid (3.21 g, 15.2 mmol, 89%). Spectral data of the compound were reported in $CDCl_3$.[215]

R_f = 0.49 (EtOAc:Hexane, v/v = 3:2), $KMnO_4$.

^{1}H NMR (400 MHz, d_6-DMSO): δ 9.67 (t, *J* = 1.6 Hz, 1H, H1), 9.39 (t, *J* = 6.5 Hz, 1H, NH), 3.17 (app. q, *J* = 6.5 Hz, 2H, H6), 2.43 (td, *J* = 7.2, 1.6 Hz, 2H, H2), 1.59 – 1.43 (m, 4H, CH_2), 1.32 – 1.20 (m, 2H, CH_2);

^{13}C NMR (101 MHz, d_6-DMSO): δ 203.8 (C1), 156.6 (q, *J* = 35.9 Hz, $\underline{C}O$-CF_3), 116.4 (q, *J* = 288.4 Hz, CF_3), 43.3 (C2), 39.4 (C6), 28.5 (CH_2), 26.1 (CH_2), 21.5 (CH_2);

^{19}F NMR (376 MHz, d_6-DMSO): δ -74.45 (CF_3);

LRMS (ESI$^-$) *m/z* $[M-H]^-$ for $[C_8H_{11}F_3NO_2]^-$ calc. 210.1 found 210.1 (100%);

6.2.8 Synthesis of *N*-(1-(*N, N*-dipropargyl)hexyl)trifluoroacetamide

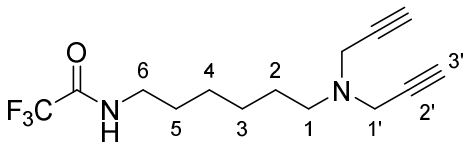

10

To a stirred solution of **9** (3.02 g, 14.3 mmol) and dipropargylamine (0.780 mL, 7.54 mmol) in a anhydrous CH_2Cl_2 (25 mL) under an argon atmosphere at r.t., was added $NaHB(OAc)_3$ (3.20 g, 15.1 mmol). The solution was stirred for 2 h, quenched with saturated $NaHCO_3$ (20 mL) and stirred for 20 min. The mixture was extracted with CH_2Cl_2 (2 x 15 mL), organic phase was washed with water, NaCl, dried with Na_2SO_4 filtered and evaporated. The crude product was purified by column chromatography on silica gel (5-50% EtOAc/PE 40-60, v/v) to give the compound **10** as a colourless liquid (2.13 g, 7.39 mmol, 98%).

R_f = 0.43 (MeCN:CH_2Cl_2, v/v = 1:9), $KMnO_4$.

^{1}H NMR (400 MHz, $CDCl_3$): δ 6.60 (br s, 1H, NH), 3.40 (d, *J* = 2.4 Hz, 4H, H1′), 3.33 (app. q, *J* = 6.8 Hz, 2H, H6), 2.35 – 2.47 (m, 2H, H1), 2.20 (t, *J* = 2.4 Hz, 2H, H3′), 1.61 – 1.52 (m, 2H, H5), 1.50 – 1.41 (m, 2H, H2), 1.37 – 1.30 (m, 4H, CH_2);

^{13}C NMR (101 MHz, $CDCl_3$): δ 157.2 (q, *J* = 36.7 Hz, CO-CF_3), 115.9 (q, *J* = 287.9 Hz, CF_3), 78.7 (C2′), 72.9 (C3′), 52.6 (C1), 42.1 (C1′), 39.9 (C6), 28.8 (C5), 27.1 (C2), 26.7 (CH_2), 26.4 (CH_2);

^{19}F NMR (377 MHz, $CDCl_3$): δ -75.94 (CF_3);

HRMS (ESI$^+$) *m/z* $[M+H]^+$ for $[C_{14}H_{20}F_3N_2O]^+$ calc. 289.1522 found 289.1521;

6.2.9 Synthesis of 5-propargylamino(*N*-propargyl-*N*-hexyltrifluoroacetamide) -5′-*O*-(4,4′-dimethoxytritryl)-2′-deoxythymidine

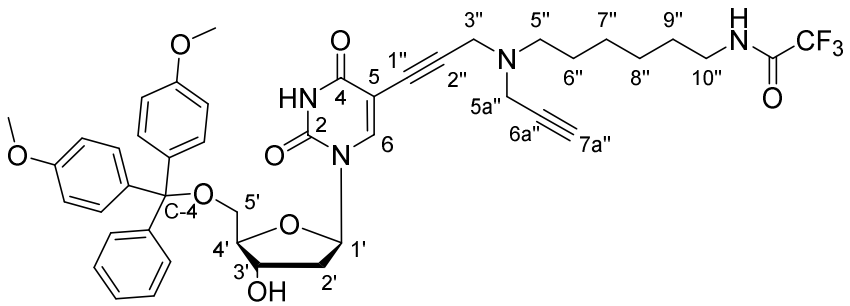

11

To a stirred solution of 5-iodo-5′-DMTr-deoxythymidine (0.50 g, 0.76 mmol), compound **10** (0.55 g, 1.9 mmol), $PdCl_2(PPh_3)_2$ (64 mg, 0.091 mmol) and CuI (9.0 mg, 0.047 mmol) in anhydrous degassed DMF (12 mL) under an argon atmosphere at r.t., anhydrous degassed NEt_3 (3.6 mL) was added. The mixture was stirred for 24 h, evaporated and redissolved in EtOAc (100 mL). The organic layer was washed with an EDTA solution (4%, 50 mL), H_2O (50 mL) and saturated NaCl (50 mL). The organic phase was dried with Na_2SO_4, filtered and evaporated, followed by purification by gel chromatography on silica gel (20-100% EtOAc/CH_2Cl_2, v/v) to give the product as a pale-yellow foam (0.33 g, 0.41 mmol, 54%).

R_f = 0.60 (MeCN:Toluene, v/v = 1:1), *p*-anisaldehyde, UV.

^{1}H NMR (500 MHz, $CDCl_3$): δ 9.59 (s, 1H, NH-thymidine), 8.01 (s, 1H, H6), 7.44 – 7.39 (m, 2H, Ar-H), 7.35 – 7.30 (m, 4H, Ar-H), 7.30 – 7.26 (m, 2H, Ar-H), 7.24 – 7.18 (m, 1H, Ar-H), 6.86 – 6.80 (m, 4H, Ar-H), 6.27 (t, *J* = 6.7 Hz, 1H, H1′), 4.50 (app. dt, J = 5.8, 3.1 Hz, 1H, H3′), 4.08 (app. q, *J* = 3.1 Hz, 1H, H4′), 3.77 (s, 6H, OCH_3), 3.41 – 3.27 (m, 6H, H3″ and H5′ and H10″), 3.20 (d, *J* = 2.5 Hz, 2H, H5a″), 2.51 – 2.40 (m, 3H, H2′a and H5″),

2.29 – 2.20 (m, 1H, H2′b), 2.15 (t, *J* = 2.5 Hz, 1H, H7a″), 1.54 (app. p, *J* = 7.0 Hz, 2H, H9″), 1.42 – 1.27 (m, 6H, H6″and H7″and H8″);

^{13}C NMR (126 MHz, $CDCl_3$): δ 162.0 (C4), 158.6 (Ar) 157.3 (q, *J* = 36.7 Hz, $\underline{C}O\text{-}CF_3$), 149.5 (C2), 144.5 (Ar), 142.2 (C6), 135.6 (Ar), 130.0 (Ar-H), 128.1 (Ar-H), 127.9 (Ar-H), 127.0 (Ar-H), 116.0 (q, *J* = 287.8 Hz, CF_3), 113.3 (Ar-H), 100.2 (C5), 89.4 (C2″), 87.0 (C-4), 86.5 (C4′), 85.7 (C1′), 79.0 (C6a″), 75.6 (C1″), 73.0 (C7a″), 72.2 (C3′), 63.5 (C5′), 55.3 (OCH_3), 52.1 (C5″), 43.0 (C3″), 42.4 (C5a″), 41.4 (C2′), 39.9 (C10″), 28.5 (C9″), 26.64, 26.47, 26.12 (C6″ – C8″);

^{19}F NMR (376 MHz, $CDCl_3$): δ -75.74 (CF_3);

HRMS (ESI$^+$) *m/z* $[M+H]^+$ for $[C_{44}H_{48}F_3N_4O_8]^+$ calc. 817.3419 found 817.3411;

6.2.10 Synthesis of 5-propargylamino(*N*-propargyl-*N*-hexyltrifluoroacetamide) -5′-*O*-(4,4′-dimethoxytritryl)-2′-deoxythymidine phosphoramidite

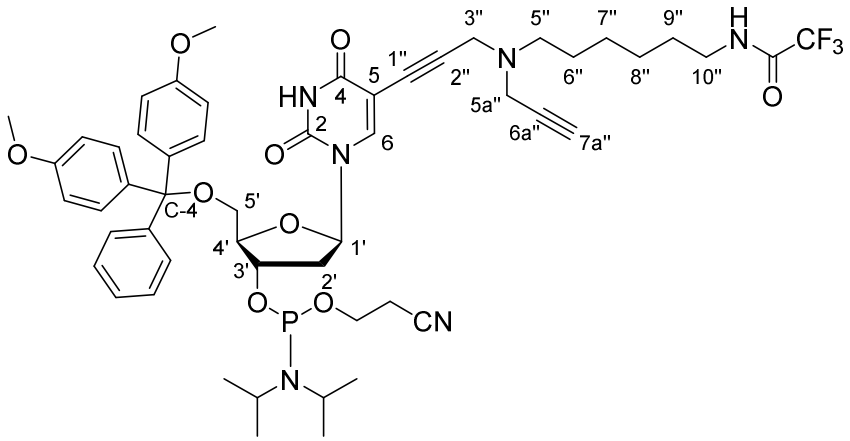

12

To a solution of **11** (0.27 g, 0.33 mmol) and anhydrous degassed DIPEA (0.16 mL, 0.93 mmol) under an argon atmosphere in anhydrous degassed CH_2Cl_2 (9.0 mL), was added 2-cyanoethyl *N*, *N*-diisopropylchlorophosphoramidite (0.10 mL, 0.46 mmol). The reaction was stirred for 1.5 h, quenched with argon saturated KCl solution (5 mL) and the organic phase was passed through a layer of anhydrous Na_2SO_4 followed by evaporation to give a yellow foam. The crude product was purified by gel chromatography on silica gel (degassed 60-75% EtOAc/Hexane, v/v) pre-equilibrated with pyridine, under an argon pressure to give the product compound **12** as white foam (0.20 g, 0.20 mmol, 61%).

R_f = 0.71 and 0.61 for two isomers (EtOAc:Hexane, v/v = 7:3), *p*-anisaldehyde, UV.

^{1}H NMR (400 MHz, $CDCl_3$): δ 8.77 (s, 1H, NH-thymidine), 8.06 (s, 0.5H, H6 isomer a), 8.02 (s, 0.5H, H6 isomer b), 7.47 – 7.39 (m, 2H, Ar-H), 7.38 – 7.24 (m, 6H, Ar-H), 7.24 – 7.15 (m, 1H, Ar-H), 6.90 – 6.79 (m, 4H, Ar-H), 6.33 – 6.22 (m, 1H, H1′), 4.61 – 4.54 (m, 1H, H3′), 4.22 – 4.13 (m, 1H, H4′), 3.79 (s, 6H, OCH_3), 3.88 – 3.36 (m, 6H, OCH_2CH_2-

CN and ^{i}Pr-CH and H10″), 3.36 – 3.25 (m, 4H, H3″ and H5′), 3.18 – 3.10 (m, 2H, H5a″), 2.62 (t, *J* = 6.3 Hz, 1H, CH_2a-CN), 2.58 – 2.49 (m, 1H, H2′a), 2.47 – 2.37 (m, 3H, CH_2b-CN and H5″), 2.33 – 2.24 (m, 1H, H2′b), 2.14 (app. q, *J* = 2.3 Hz, 1H, H7a″), 1.55 (app. p, *J* = 7.0 Hz, 2H, H9″), 1.41 – 1.23 (m, 6H, H6″ – H8″), 1.20 – 1.15 (m, 9H, ^{i}Pr-CH_3), 1.07 (d, *J* = 6.8 Hz, 3H, ^{i}Pr-CH_3);

^{31}P NMR (162 MHz, $CDCl_3$): δ 148.99 (s), 148.61 (s);

HRMS (ESI$^+$) *m/z* $[M+H]^+$ for $[C_{53}H_{65}F_3N_6O_9P]^+$ calc. 1017.4497 found 1017.4462;

6.2.11 Synthesis of 5′-*O*-benzoyl-thymidine

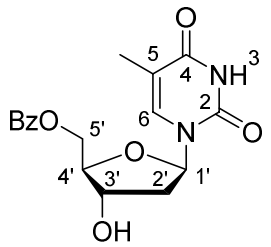

27

Thymidine (2.0 g, 8.2 mmol) was evaporated twice with 20 mL of anhydrous pyridine and then dissolved in 100 mL of anhydrous pyridine. Reaction was cooled at 0 °C and benzoyl chloride (1.0 mL, 8.6 mmol) was added to the reaction mixture. The mixture was stirred for 2 h at 0 °C under argon atmosphere. Reaction progress was monitored using TLC. After completion the mixture was evaporated to dryness. The obtained crude compound was purified by column chromatography (0-5% MeOH in CH_2Cl_2, v/v) to obtain compound **27** (2.3 g, 6.2 mmol, 76%). Characterisation data is consistent with literature.[233]

R_f = 0.50 (100% EtOAc)

^{1}H NMR (400 MHz, d_6-DMSO) δ 11.31 (s, 1H, H3), 8.03 – 7.95 (m, 2H, *o*-CH, Ph), 7.73 – 7.64 (m, 1H, *p*-CH, Ph), 7.55 (t, *J* = 7.7 Hz, 2H, *m*-CH, Ph), 7.39 (d, *J* = 1.4 Hz, 1H, H6), 6.21 (t, *J* = 6.9 Hz, 1H, H1′), 5.48 (d, *J* = 4.5 Hz, 1H, 3′-OH), 4.55 (dd, *J* = 12.0, 3.7 Hz, 1H, H3′), 4.41 (dt, *J* = 10.9, 5.4 Hz, 2H, H5′), 4.05 (dt, *J* = 5.2, 3.7 Hz, 1H, H4′), 2.30 – 2.11 (m, 2H, H2′), 1.59 (d, *J* = 1.2 Hz, 3H, 5-CH_3).

LRMS (ESI$^+$) (*m/z*): $[M+Na]^+$ for $[C_{17}H_{18}N_2NaO_6]^+$ cal. 369.1 found: 369.1 (100%).

6.2.12 Synthesis of 3′-*O*-methylthiomethyl-5′-*O*-benzoyl-thymidine

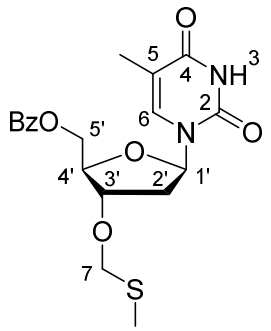

28

Compound **27** (2.3 g, 6.2 mmol) was dissolved in a mixture of DMSO (21.1 mL), acetic acid (4.3 mL), and acetic anhydride (14.0 mL). The mixture was stirred for 3 days at room temperature and then poured into cold saturated $NaHCO_3$ (200 mL) and stirred for 2 h more. The precipitate was filtered, washed on the filter with water, airdried, and compound was purified by silica gel column chromatography (0 – 75% EtOAc in PE 40-60, v/v) to give compound **28** as white foam (1.5 g, 3.8 mmol, 62%). Characterisation data is consistent with literature.[221]

R_f = 0.66 (75% EtOAc in PE 40-60, v/v).

^{1}H NMR (400 MHz, d_6-DMSO) δ 11.35 (s, 1H, H3), 8.04 – 7.96 (m, 2H, *o*-CH, Ph), 7.69 (ddt, *J* = 8.7, 6.9, 1.3 Hz, 1H, *p*-CH, Ph), 7.55 (td, *J* = 7.6, 1.1 Hz, 2H, *m*-CH, Ph), 7.42 (p, *J* = 1.5 Hz, 1H, H6), 6.17 (t, *J* = 7.1 Hz, 1H, H1′), 4.82 – 4.67 (m, 2H, H7), 4.59 – 4.51 (m, 2H, H3′ and H5′a), 4.47 (dd, *J* = 11.8, 5.1 Hz, 1H, H5′b), 4.26 (td, *J* = 4.7, 3.1 Hz, 1H, H4′), 2.37 – 2.30 (m, 2H, H2′), 2.10 (s, 3H, SCH_3), 1.60 (d, *J* = 1.2 Hz, 3H, 5-CH_3).

LRMS (ESI$^+$) (*m/z*): $[M+Na]^+$ for $[C_{19}H_{22}N_2NaO_6S]^+$ calc. 429.1 found: 429.1 (100%).

6.2.13 Synthesis of 3′-*O*- azidomethyl-5'-*O*-benzoyl-thymidine

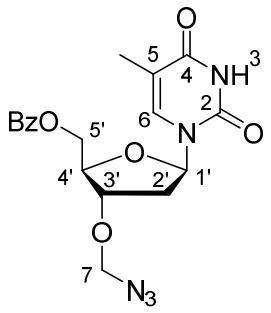

22

To a stirred solution of compound **28** (1.5 g, 3.8 mmol) in 60 mL of absolute CH_3CN was added Br_2 (0.20 mL, 3.8 mmol) dropwise at 0 °C. The mixture was stirred upon cooling for 30 min, and then lithium azide (0.93 g, 9.5 mmol) was added. The mixture foamed after the addition of lithium azide. The resulting suspension was mixed for 10 min upon cooling and then for 2 h at 60 °C. The solvent was evaporated under vacuum, and the residue was dissolved in CH_2Cl_2 (50 mL) and water (50 mL). The organic layer was separated, and the aqueous layer was extracted with CH_2Cl_2 (2 × 25 mL). The combined organic layers were washed with brine, dried over Na_2SO_4, filtered, and concentrated. The residue was purified by silica gel column chromatography in 0−75% EtOAc in PE 40-60 (v/v) to give compound **22** as a hard foam (1.2 g, 2.7 mmol, 72%). Characterisation data is consistent with literature.[221]

R_f = 0.64 (75% EtOAc in PE 40-60, v/v).

^{1}H NMR (400 MHz, d_6-DMSO) δ 11.35 (s, 1H, H3), 8.04 – 7.96 (m, 2H, *o*-CH, Ph), 7.68 (ddt, *J* = 7.9, 7.0, 1.3 Hz, 1H, *p*-CH, Ph), 7.61 – 7.50 (m, 2H, *m*-CH, Ph), 7.41 (q, *J* = 1.1 Hz, 1H, H6), 6.18 (t, *J* = 7.0 Hz, 1H, H1′), 4.96 – 4.82 (m, 2H, H7), 4.59 – 4.52 (m, 2H, H3′ and H5′a), 4.47 (dd, *J* = 12.0, 5.0 Hz, 1H, H5′b), 4.28 (dt, *J* = 5.0, 4.0 Hz, 1H, H4′), 2.43 – 2.35 (m, 2H, H2′), 1.60 (d, *J* = 1.2 Hz, 3H, 5-CH_3).

LRMS (ESI$^+$) (*m/z*): $[M+Na]^+$ for $[C_{18}H_{19}N_5NaO_6]^+$ calc. 424.1 found: 424.3 (100%).

6.2.14 Synthesis of 5′-*O*-(*tert*-Butyldimethylsilyl)-thymidine

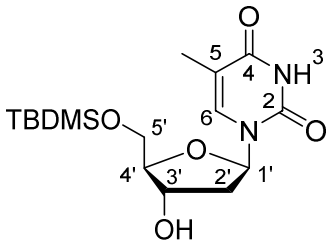

29

Imidazole (3.2 g, 45.5 mmol) was added to a stirred solution of thymidine (5.0 g, 20.6 mmol) in anhydrous DMF (72.0 mL) at 4 °C and stirred for 30 min. A solution of *tert*-butyldimethylsilyl chloride (3.4 g, 22.6 mmol) in anhydrous DMF (30 mL) was slowly added over 1 h and the reaction mixture was allowed to warm up to r.t. and stirred for another 3 h. The solvent was evaporated *in vacuo* and the residue dissolved in DCM (150 mL) and washed with H_2O (150 mL). The organic layer was dried over Na_2SO_4, filtered and evaporated. Column chromatography (0–100% EtOAc in PE 40-60, v/v) gave compound **29** as a white foam (6.8 g, 18.1 mmol, 88%). Characterisation is consistent with literature.[234]

R_f = 0.40 (5% MeOH in CH_2Cl_2, v/v);

^{1}H NMR (400 MHz, $CDCl_3$) δ 9.43 (s, 1H, NH), 7.53 (q, *J* = 1.1 Hz, 1H, H6), 6.39 (dd, *J* = 8.3, 5.6 Hz, 1H, H1′), 4.44 (ddt, *J* = 6.5, 4.5, 2.5 Hz, 1H, H3′), 4.06 (q, *J* = 2.5 Hz, 1H, H4′), 3.89 (dd, *J* = 11.3, 2.5 Hz, 1H, H5′), 3.82 (dd, *J* = 11.3, 2.5 Hz, 1H, H5″), 3.19 (d, *J* = 4.4 Hz, 1H, OH), 2.39 (ddd, *J* = 13.3, 5.6, 2.5 Hz, 1H, H2′), 2.17 – 1.99 (m, 1H, H2″),

1.90 (d, *J* = 1.2 Hz, 3H, 5-CH_3), 0.91 (s, 9H, 3 × CH_3-t-Bu), 0.10 (d, *J* = 2.7 Hz, 6H, $Si(CH_3)_2$);

LRMS (ESI$^+$) *m/z* $[M+Na]^+$ for $[C_{16}H_{28}N_2NaO_5Si]^+$ cal. 379.1 found 379.2 (100%);

6.2.15 Synthesis of 5'-*O*-(*tert*-butyldimethylsilyl)-3′-*O*-(*tert*-Butyldiphenylsilyl)-thymidine

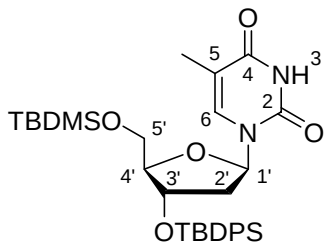

30

Imidazole (3.5 g, 51.6 mmol) was added to a stirred solution of compound **29** (6.8 g, 18.1 mmol) in anhydrous DMF (75 mL) and the solution was stirred at r.t. for 30 min. *tert*-Butyl(chloro)diphenylsilane (7.1 g, 25.8 mmol) was added and the reaction mixture was stirred at r.t. for 16 h. The solvent was evaporated *in vacuo* and the residue dissolved in EtOAc (100 mL) and washed with H_2O (100 mL). The organic layer was dried over Na_2SO_4, filtered and evaporated. Column chromatography (0–30% EtOAc in PE 40-60, v/v) gave compound **30** as a white solid (9.6 g, 15.2 mmol, 84%). Characterisation is consistent with literature.[234]

R_f = 0.82 (60% EtOAc in PE 40-60, v/v);

1H NMR (400 MHz, $CDCl_3$) δ 8.92 (s, 1H, NH), 7.75 – 7.55 (m, 4H, H-Ar), 7.49 – 7.35 (m, 7H, H6 and 6 × H-Ar), 6.50 (dd, *J* = 9.0, 5.4 Hz, 1H, H1'), 4.34 (dt, *J* = 5.7, 1.5 Hz, 1H, H3'), 3.99 (q, *J* = 2.0 Hz, 1H, H4'), 3.62 (dd, *J* = 11.4, 2.0 Hz, 1H, H5'), 3.13 (dd, *J* = 11.4, 2.0 Hz, 1H, H5''), 2.32 (ddd, *J* = 13.0, 5.4, 1.5 Hz, 1H, H2'), 1.87 (d, *J* = 1.2 Hz, 3H,

5-CH_3), 1.85 – 1.78 (m, 1H, H2"), 1.09 (s, 9H, t-Bu), 0.78 (s, 9H, t-Bu), -0.08 (s, 3H, $Si(CH_3)_2$), -0.12 (s, 3H, $Si(CH_3)_2$);

LRMS (ESI$^+$) *m/z* $[M+Na]^+$ for $[C_{32}H_{46}N_2NaO_5Si_2]^+$ cal. 617.2 found 617.2 (100%);

6.2.16 Synthesis of 3'-*O*-(*tert*-Butyldiphenylsilyl)-thymidine

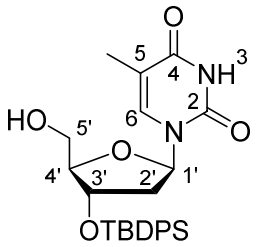

31

Compound **30** (9.6 g, 15.2 mmol) was dissolved in a solvent mixture of THF (30.2 mL) and AcOH/H_2O [3/1 (v/v), 120 mL] and stirred at r.t. for 72 h. The solvents were evaporated under reduced pressure and the residue was dissolved in CH_2Cl_2 (60 mL) and washed with saturated aq. $NaHCO_3$ (150 mL). The aqueous layer was extracted with CH_2Cl_2 (40 mL) and the combined org layers were dried over Na_2SO_4, filtered and evaporated. The crude was submitted to column chromatography (0–70% EtOAc in PE 40-60, v/v) to give compound **31** (4.8 g, 9.9 mmol, 65%). Characterisation data is consistent with literature.[234]

R_f = 0.23 (50% EtOAc in PE 40-60, v/v);

^{1}H NMR (400 MHz, $CDCl_3$) δ 8.68 (s, 1H, NH), 7.69 – 7.59 (m, 4H, H-Ar), 7.51 – 7.35 (m, 6H, H-Ar), 7.28 (d, *J* = 1.3 Hz, 1H, H6), 6.23 (dd, *J* = 7.8, 6.0 Hz, 1H, H1′), 4.45 (dt, *J* = 6.0, 3.0 Hz, 1H, H3′), 3.97 (q, *J* = 3.0 Hz, 1H, H4′), 3.63 (dt, *J* = 12.0, 3.0 Hz, 1H, H5′), 3.29 – 3.19 (m, 1H, H5′′), 2.27 (ddd, *J* = 13.4, 6.0, 3.0 Hz, 1H, H2′), 2.23 – 2.10 (m, 2H, H2′′ *and* OH), 1.84 (d, *J* = 1.3 Hz, 3H, 5-CH_3), 1.09 (s, 9H, t-Bu);

LRMS (ESI$^+$) *m/z* $[M+Na]^+$ for $[C_{26}H_{32}N_2NaO_5Si]^+$ cal. 503.2 found 503.2 (100%);

6.2.17 Synthesis of 5′-ethynyl-3′-*O*-(*tert*-Butyldiphenylsilyl) thymidine

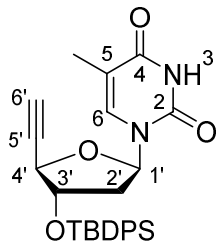

23

Compound **31** (2.7 g, 5.7 mmol) was dissolved in dry DCM (30.6 ml) and then Dess-Martin Periodinane (2.88 g, 6.8 mmol) was added. Transparent mixture was stirred for 2 h until it became white and cloudy. After this time reaction was quenched by addition of 60 ml of saturated solution of $NaHCO_3$ and $Na_2S_2O_3$. Then, another 30 ml of DCM was added. Organic layer was separated, and aqueous layer was extracted three times with EtOAc. Combined organic layers were dried over Na_2SO_4, filtered and evaporated under reduced pressure to give aldehyde crude as a white compound which was directed to the next step without purification.

Aldehyde crude and potassium carbonate (1.57 g, 11.4 mmol) were placed in an oven dried round bottom flask. Vacuum was applied and the flask was then filled with argon (repeated twice). Anhydrous methanol (75 mL) was added and the mixture was stirred at room temperature under an argon atmosphere for 30 min. Dimethyl (1-diazo-2-oxopropyl)phosphonate solution (10% in dry MeCN) (1.31 g, 6.84 mmol) was added to the faint grey turbid reaction mixture. The mixture was stirred at room temperature under an argon atmosphere for 4 hours. The reaction was monitored by TLC. The reaction

mixture was diluted with diethyl ether (125 mL) and washed with aqueous sodium bicarbonate (5%, 125 mL) and dried over Na_2SO_4, filtered and evaporated. The crude was submitted to column chromatography (0–70% EtOAc in PE 40-60, v/v) to give compound **23** (1.9 g, 4.0 mmol, 70%). Characterisation data is consistent with literature.[228]

R_f = 0.75 (50% EtOAc in PE 40-60, v/v);

^{1}H NMR (400 MHz, *d*$_6$-DMSO) δ 11.35 (s, 1H, H3), 7.66 – 7.57 (m, 4H, *o*-CH Ph TBDPS), 7.53 – 7.42 (m, 6H, *m*-CH, *p*-CH Ph TBDPS), 7.41 (q, *J* = 1.1 Hz, 1H, H6), 6.35 (t, *J* = 7.1 Hz, 1H, H4′), 4.57 (t, *J* = 2.1 Hz, 1H, H3′), 4.51 (dt, *J* = 5.0, 2.7 Hz, 1H, H3′), 3.77 (d, *J* = 2.2 Hz, 1H, H6′), 2.28 – 2.19 (m, 2H, H2′), 1.74 (d, *J* = 1.2 Hz, 3H, 5-CH_3), 1.04 (s, 9H, t-Bu).

LRMS (ESI$^+$) *m/z* $[M+H]^+$ for $[C_{27}H_{31}N_2O_4Si]^+$ cal. 475.2 found 475.3 (100%);

6.2.18 Synthesis of 5′-*O*-benzoyl-3′-*O*-(*tert*-Butyldiphenylsilyl) thymidine

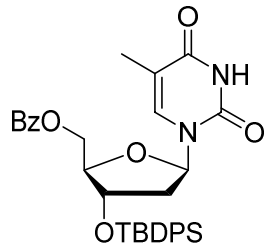

33

Imidazole (1.0 g, 15.1 mmol) was added to a stirred solution of compound **27** (2.0 g, 5.3 mmol) in anhydrous DMF (25 mL) and the solution was stirred at r.t. for 30 min. *tert*-Butyl(chloro)diphenylsilane (2.1 g, 7.5 mmol) was added and the reaction mixture was stirred at r.t. for 16 h. The solvent was evaporated *in vacuo* and the residue dissolved in EtOAc (30 mL) and washed with H_2O (30 mL). The organic layer was dried over Na_2SO_4, filtered and evaporated to give compound **33** as a white solid (9.6 g, 4.6 mmol, 88%). Compound **33** was used without purification for next step.

R_f = 0.68 (60% EtOAc in PE 40-60, v/v);

LRMS (ESI$^+$) *m/z* $[M+H]^+$ for $[C_{33}H_{37}N_2NaO_6Si]^+$ cal. 585.2 found 585.2 (100%);

6.2.19 Synthesis of 1,2-Di-*O*-acetyl-3-*O*-benzyl-4-*C*-methanesulfonoxy-methyl-5-*O*-methanesulfonyl-D-*erythro*-pentofuranose

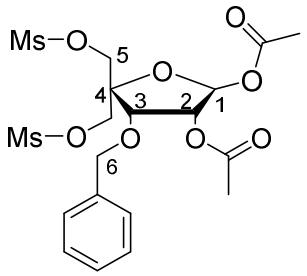

35

A solution of 3-*O*-Benzyl-4-*C*-methanesulfonoxymethyl-5-methane-sulfonyl-1,2-*O*-isopropylidene-α-D-*erythro*-pentofuranose (**34**) (20 g, 42.9 mmol) in 80% aqueous trifluoroacetic acid (125 mL) was stirred at room temperature for 1 h. The solvents were removed under reduced pressure, and the residue was dissolved in dichloromethane (250 mL) and washed with saturated $NaHCO_3$ (2 × 250 mL). The organic layer was dried (Na_2SO_4) and concentrated under reduced pressure to give a colorless oily intermediate. The intermediate was co-evaporated with anhydrous pyridine (2 × 60 mL), dissolved in anhydrous pyridine, and treated with Ac_2O (15 mL, 158.75 mmol) overnight. The reaction mixture was quenched by addition of saturated $NaHCO_3$ (300 mL) and washed with EtOAc (2 × 250 mL). The organic layers were combined, washed with brine (180 mL), dried with Na_2SO_4, and concentrated under reduced pressure to yield compound **35** (19.9 g, 39.0 mmol, 92%). The product was pure by NMR spectra and was used in the next step without further purification. Characterisation is consistent with literature.[229]

R_f = 0.42 (50% EtOAc in PE 40-60, v/v);

^{1}H NMR (400 MHz, $CDCl_3$) δ 7.38 – 7.29 (m, 5H, Ar-H), 6.17 (s, 1H, H1), 5.38 (d, *J* = 4.8 Hz, 1H, H2), 4.64 – 4.16 (m, 7H, H3 and 3 x CH_2), 3.01 (d, *J* = 2.6 Hz, 6H, 2 x CH_3-mesyl), 2.15 (s, 3H, CH_3-acetyl), 2.10 (s, 3H, CH_3-acetyl).

LRMS (ESI$^+$) *m/z* $[M+Na]^+$ for $[C_{22}H_{28}N_2NaO_{12}S_2]^+$ calc. 533.1 found 533.7 (100%);

6.2.20 Synthesis of 1-(2-*O*-Acetyl-3-*O*-benzyl-4-*C*-methanesulfonoxymethyl-5-*O*-methanesulfonyl-β-D-*erythro*-pentofuranosyl)-thymine

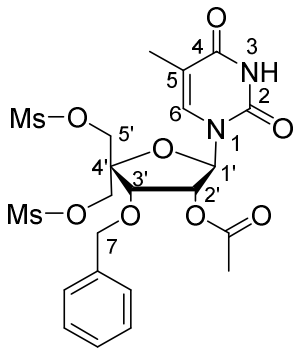

36

N, *O*-Bis(trimethylsilyl)acetamide (BSA) (70 mL, 283 mmol) was added to a mixture of compound **35** (19.9 g, 39.0 mmol) and thymine (6.1 g, 48.6 mmol) in anhydrous MeCN (100 mL). The reaction mixture was refluxed for 1 h to get a clear solution. Trimethylsilyl triflate (TMSOTf) (9.2 mL, 50.9 mmol) was added, and refluxing was continued further for 4 h. The solution was cooled to room temperature, diluted with CH_2Cl_2 (80 mL), and washed with saturated $NaHCO_3$ (2 × 100 mL). The organic layer was dried (Na_2SO_4), concentrated under reduced pressure, and the residue was purified by silica gel column

chromatography (0-10% MeOH/CH_2Cl_2, v/v) to give compound **36** (16.2 g, 28.1 mmol, 72%) as a white solid material. Characterisation is consistent with literature.[229]

R_f = 0.19 (50% EtOAc in PE 40-60, v/v);

^{1}H NMR (400 MHz, $CDCl_3$) δ 8.74 (s, 1H, H3), 7.40 – 7.30 (m, 5H, Ar-H), 7.07 (q, *J* = 1.2 Hz, 1H, H6), 5.71 (d, *J* = 3.4 Hz, 1H, H1′), 5.56 (dd, *J* = 6.5, 3.4 Hz, 1H, H2′), 4.68 (d, *J* = 6.5 Hz, 1H, H3′), 4.62 – 4.29 (m, 6H, 2 x CH_2 and H7), 3.02 (s, 3H, CH_3-mesyl), 3.00 (s, 3H, CH_3-mesyl), 2.11 (s, 3H, CH_3-acetyl), 1.92 (d, *J* = 1.2 Hz, 3H, 5-CH_3).

LRMS (ESI$^+$) *m/z* $[M+Na]^+$ for $[C_{22}H_{28}N_2NaO_{12}S_2]^+$ calc. 599.1 found 599.3 (100%);

6.2.21 Synthesis of 5′-*O*-methanesulfonyl-3′-*O*-benzyl-LNA thymidine

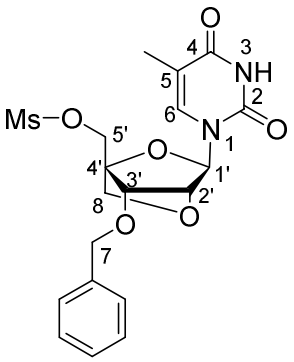

37

A solution of compound **36** (16.2 g, 28.1 mmol) in 1,4-dioxane/ H_2O (1/1 v/v; 72 mL) was added 2 M NaOH (72 mL). The mixture was stirred for 1 h at room temperature, diluted with saturated $NaHCO_3$ (100 mL), and extracted with CH_2Cl_2 (2 × 100 mL). The combined organic layers were dried (Na_2SO_4), concentrated under reduced pressure, and the residue was purified by silica gel column chromatography (0-10% MeOH/CH_2Cl_2, v/v) to give compound **37** (11.3 g, 25.8 mmol, 92%) as a white solid material. Characterisation is consistent with literature.[229]

R_f = 0.32 (5% MeOH in CH_2Cl_2, v/v);

^{1}H NMR (400 MHz, $CDCl_3$) δ 8.58 (s, 1H, H3), 7.41 (q, *J* = 1.3 Hz, 1H, H6), 7.33 (qq, *J* = 7.2, 2.3 Hz, 5H. Ar-H), 5.66 (s, 1H, H1′), 4.67 (d, *J* = 11.4 Hz, 1H, H7a), 4.62 – 4.50 (m, 4H, H7b, H2′ and H5′), 4.09 (d, *J* = 7.8 Hz, 1H, H8a), 3.92 (s, 1H, H3′), 3.88 (d, *J* = 7.8 Hz, 1H, H8b), 3.07 (s, 3H, CH_3-mesyl), 1.93 (d, *J* = 1.3 Hz, 3H, 5-CH_3).

LRMS (ESI$^+$) *m/z* $[M+H]^+$ for $[C_{19}H_{23}N_2O_8S]^+$ calc. 439.1 found 439.2 (100%);

6.2.22 Synthesis of 5′-*O*-benzoyl-3′-*O*-benzyl-LNA thymidine

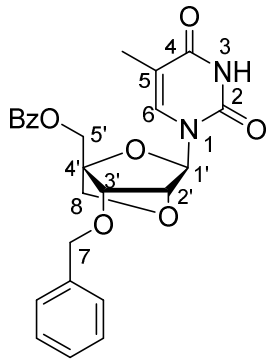

38

NaOBz (7.5 g, 51.8 mmol) was added to a solution of compound **37** (11.3 g, 25.8 mmol) in anhydrous DMF (560 mL). The mixture was stirred for 5 h at 100 °C, cooled to room temperature, and filtrated. The solvent was evaporated under reduced pressure, and the residue was suspended in EtOAc (200 mL), washed with H_2O (3 × 120 mL), dried (Na_2SO_4), and concentrated to a solid residue. Crystallization from EtOH afforded compound **38** (10.6 g, 22.8 mmol, 88%) as a white solid material. Characterisation is consistent with literature.[229]

R_f = 0.38 (60% EtOAc in PE 40-60, v/v);

^{1}H NMR (400 MHz, $CDCl_3$) δ 8.55 (s, 1H, H3), 8.05 – 7.92 (m, 2H, *o*-CH Ph BzO), 7.63 (ddt, *J* = 7.9, 7.0, 1.3 Hz, 1H, *p*-CH Ph BzO), 7.51 – 7.41 (m, 3H, H6 and *m*-CH Ph BzO), 7.23 - 7.28 (m, 5H, CH, Ph BnO), 5.64 (d, *J* = 0.7 Hz, 1H, H1′), 4.84 (d, *J* = 12.8 Hz, 1H, H7a), 4.73 (d, *J* = 11.8 Hz, 1H, H7b), 4.66 (s, 1H, H5′a), 4.59 (s, 0.5 H, H2′a), 4.55 (d, *J* = 2.2 Hz, 1H, H5′b), 4.52 (s, 0.5 H, H2′b), 4.18 (d, *J* = 7.8 Hz, 1H, H8a), 3.98 (d, *J* = 7.8 Hz, 1H, H8b), 3.91 (s, 1H, H3′), 1.59 (d, *J* = 1.3 Hz, 3H, 5-CH_3).

LRMS (ESI$^+$) *m/z* $[M+Na]^+$ for $[C_{25}H_{24}N_2NaO_7]^+$ calc. 487.2 found 487.3 (100%);

6.2.23 Synthesis of 5′-*O*-benzoyl -LNA thymidine

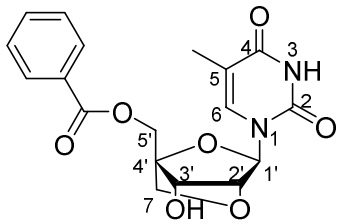

39

A mixture of compound **38** (2.5 g, 5.3 mmol), 20% $Pd(OH)_2/C$ (1.24 g) and ammonium formate (1.0 g, 16.6 mmol), was suspended in MeOH (15 ml). After refluxing for 2 h, the catalyst was filtered off on celite, and washed with MeOH. The combined organic layers were dried over Na_2SO_4, filtered and concentrated to a pale-yellow residue (1.5 g, 4.0 mmol, 77%). Compound **39** was used without purification for next step.

R_f = 0.47 (75% EtOAc in PE 40-60)

^{1}H NMR (400 MHz, d_6-DMSO): δ = 8.01-8.03 (m, 2H, BzO), 7.68-7.62 (m, 1H, BzO), 7.54-7.58 (m, 2H, BzO), 7.40 (d, 1H, *J* = 1.2 Hz, H6), 5.48 (s, 1H, H1′), 4.77 (d, 1H, *J* = 12.8 Hz, H7a), 4.70 (d, 1H, *J* = 12.8 Hz, H7b), 4.24 (s, 1H, H2′), 4.09 (s, 1H, H3′), 4.01 (d, 1H, *J* = 8.0 Hz, H5′a), 3.85 (d, 1H, *J* = 8.0 Hz, H5′b), 1.60 (s, 3H, 5-CH_3).

^{13}C NMR (101 MHz, d_6-DMSO): δ = 165.33 (C(O)Ph), 163.77 (C4), 149.89 (C2), 134.09 (C6), 133.70 (BzO), 129.25 (BzO), 128.94 (BzO), 108.68 (C5), 86.60 (C1′), 86.23 (C4′), 70.05 (C2′), 70.97 (C5′), 69.59 (C3′), 60.19 (C7), 11.99 (5-CH_3).

LRMS (ESI$^+$) *m/z* $[M+H]^+$ for $[C_{18}H_{19}N_2O_7]^+$ calc. 375.1 found 375.0 (100%);

6.2.24 Synthesis of 5′-*O*-benzoyl-3′-*O*-methylthiomethyl-LNA thymidine

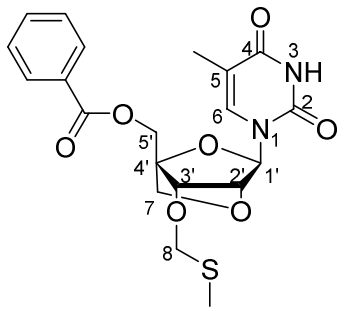

40

Compound **39** (1.5 g, 4.0 mmol) was dissolved in a mixture of DMSO (13.6 mL), acetic acid (2.8 mL), and acetic anhydride (9.1 mL). The mixture was stirred for 3 days at room temperature and then poured into cold saturated $NaHCO_3$ (150 mL) and stirred for 2 h more. The precipitate was filtered, washed on the filter with water, airdried, and compound was purified by silica gel column chromatography 0 – 75% EtOAc in PE 40-60, to give compound **40** as white foam (730.8 mg, 1.68 mmol, 42%).

R_f = 0.72 (75% EtOAc in PE 40-60).

^{1}H NMR (400 MHz, d_6-DMSO): δ = 11.43 (bs, 1H, H3), 8.03-8.07 (m, 2H, BzO), 7.72-7.73 (m, 1H, BzO), 7.55-7.59 (m, 2H, BzO), 7.36 (d, 1H, *J* = 1.2 Hz, H6), 5.53 (s, 1H, H1′), 4.87–4.67 (m, 4H, H7, H8), 4.61 (s, 1H, H2′), 4.31 (s, 1H, H3′), 3.97 (d, 1H, *J* = 8.1 Hz, H5′a), 3.90 (d, 1H, *J* = 8.1 Hz, H5′b), 2.05 (s, 3H, SCH_3), 1.55 (d, 3H, *J* = 1.2 Hz, 5-CH_3).

^{13}C NMR (101 MHz, d_6-DMSO): δ = 165.18 (C, BzO), 163.76 (C4), 149.83 (C2), 133.81 (C6), 133.77 (BzO *p*-CH, BzO), 129.21, 128.93 (*o*-CH, *m*-CH, BzO), 108.59 (C5), 86.73 (C1′), 85.42 (C4′), 76.66 (C2′), 74.00 (C3′), 73.89 (C8), 71.53 (C5′), 59.56 (C7), 13.12 (S-CH_3), 12.02 (5-CH_3)

HRMS (ESI$^+$): *m/z*, $[M+Na]^+$ for $[C_{20}H_{22}N_2NaO_7S]^+$ cal. 457.1038, found 457.1040.

6.2.25 Synthesis of 5′-*O*-benzoyl-3′-*O*-azidomethyl-LNA thymidine

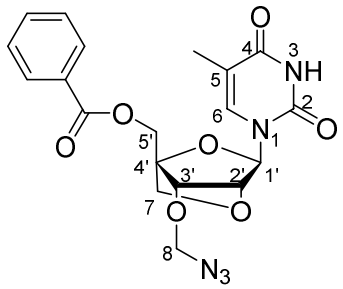

24

To a stirred solution of compound **40** (730.8 mg, 1.68 mmol) in 27.0 ml of dry MeCN, was added Br_2 (1.8 mmol, 87.6 µL) at 0 ^oC. The mixture was stirred upon cooling for 30 min, and then 20% aqueous solution of LiN_3 (1.08 ml, 4.24 mmol) was added. Resulting mixture was stirred for 3 h at 80 ^oC. The solvent was evaporated under vacuum, and the residue was dissolved in EtOAc (75 ml) and water (30 ml). The organic layer was separated, and then aqueous layer was extracted three times with EtOAc (3 x 50 ml). The combined organic layers were dried over Na_2SO_4, filtered and concentrated. The residue was purified by silica gel column chromatography in 0 – 80% EtOAc in PE 40-60 (v/v) to give product **24** as a white powder (486.8 mg, 1.1mmol, 66%).

R_f = 0.66 (75% EtOAc in PE 40-60, v/v).

^{1}H NMR (400 MHz, *d_6*-DMSO): δ = 11.41 (bs, 1H, H3), 8.02-8.06 (m, 2H, BzO), 7.70-7.72 (m, 1H, BzO), 7.54-7.58 (m, 2H, BzO), 7.34 (s, 1H, H6), 5.53 (s, 1H, H1′), 4.94 (1H, d, *J* = 8.3 Hz, H8a) 4.91 (d, 1H, *J* = 8.3 Hz, H8b), 4.82 (d, 1H, *J* = 13.1 Hz, H7a), 4.70 (d,

1H, *J* = 13.1 Hz, H7b), 4.57 (s, 1H, H2′), 4.29 (s, 1H, H3′), 4.00 (d, 1H, *J* = 8.0 Hz, H5′a), 3.93 (d, 1H, *J* = 8.0 Hz, H5′b), 1.56 (s, 3H, 5-CH_3).

^{13}C NMR (101 MHz, d_6-DMSO): δ = 165.25 (C, BzO), 163.89 (C4), 149.94 (C2), 133.92 (C6), 133.84 (BzO *p*-CH, BzO), 129.25, 129.00 (*o*-CH, *m*-CH, BzO), 108.70 (C5), 86.77 (C1′), 85.44 (C4′), 81.31 (C8), 77.37 (C2′), 75.82 (C3′), 71.45 (C5′), 59.62 (C7), 12.13 (5-CH_3)

HRMS (ESI$^+$): *m/z* for $[C_{19}H_{19}N_5NaO_7]^+$ cal. 452.1177 found 452.1177.

6.2.26 Synthesis of 3′-*O*-benzyl-LNA thymidine

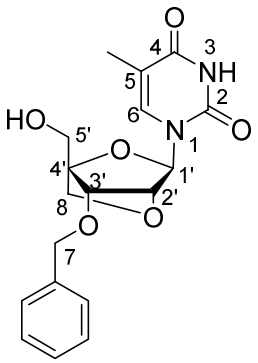

41

Finely powdered K_2CO_3 (0.29 g, 2.1 mmol) was added to a solution of compound **38** (2.0 g, 4.3 mmol) in 30 mL of absolute methanol, and the suspension was stirred for 12 h. The organic layers were dried over Na_2SO_4, filtered and concentrated. The solvent was removed under vacuum. The residue was purified by column chromatography (0−5% MeOH in CH_2Cl_2, v/v) to give compound **41** as a hard foam (1.4 g, 4.0 mmol, 92%). Characterisation is consistent with literature.[229]

R_f = 0.49 (75% EtOAc in PE 40-60, v/v)

^{1}H NMR (400 MHz, $CDCl_3$) δ 8.50 (s, 1H, H3), 7.43 (q, *J* = 1.2 Hz, 1H, H6), 7.37 – 7.28 (m, 5H, Ar-H Ph BnO), 5.65 (d, *J* = 0.8 Hz, 1H, H1′), 5.30 (s, 1H, 5′-OH), 4.68 (d, *J* = 11.6 Hz, 1H, H7a), 4.56 (d, *J* = 11.6 Hz, 1H, H7b), 4.53 (s, 1H, H3′), 4.06 (d, *J* = 7.9 Hz, 1H, H8a), 4.01 (dd, *J* = 12.6, 5.0 Hz, 1H, H5′a), 3.97 (d, *J* = 5.2 Hz, 1H, H5′b), 3.94 (s, 1H, H2′), 3.83 (d, *J* = 7.8 Hz, 1H, H8b), 1.90 (d, *J* = 1.2 Hz, 3H, 5-CH_3).

LRMS (ESI$^+$): *m/z*: $[M+H]^+$ for $[C_{18}H_{21}N_2O_6]^+$ cal. 360.1 found: 360.1.

6.2.27 Synthesis of 5′-ethynyl-3′-*O*-benzyl-LNA thymidine

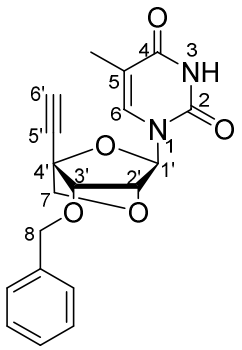

25

Compound **41** (1.4 g, 4.0 mmol) was dissolved in dry DCM (30.6 ml) and then Dess-Martin Periodinane (2.0 g, 4.8 mmol) was added. Transparent mixture was stirred for 2 h until it became white and cloudy. After this time reaction was quenched by addition of 45 ml of saturated solution of $NaHCO_3$ and $Na_2S_2O_3$. Then, another 20 ml of DCM was added. Organic layer was separated, and aqueous layer was extracted three times with EtOAc. Combined organic layers were dried over Na_2SO_4, filtered and evaporated under reduced pressure to give aldehyde crude as a white compound which was directed to the next step without purification.

Aldehyde crude and potassium carbonate (1.1 g, 8.0 mmol) were placed in an oven dried round bottom flask. Vacuum was applied and the flask was then filled with argon (repeated twice). Anhydrous methanol (60 mL) was added and the mixture was stirred at room temperature under an argon atmosphere for 30 min. Dimethyl (1-diazo-2-oxopropyl)phosphonate solution (10% in dry acetonitrile) (0.9 g, 4.8 mmol) was added to the faint grey turbid reaction mixture. The mixture was stirred at room temperature under

an argon atmosphere for 4 hours. The reaction was monitored by TLC. The reaction mixture was diluted with diethyl ether (100 mL) and washed with aqueous sodium bicarbonate (5%, 100 mL) and dried over Na_2SO_4, filtered and evaporated. The crude was submitted to column chromatography (0–70% EtOAc in PE 40-60, v/v) to give compound **25** (944.3 mg, 1.9 mmol, 48%).

R_f = 0.68 (50% EtOAc in PE 40-60, v/v);

^{1}H NMR (400 MHz, d_6-DMSO): δ = 11.41 (s, 1H, H3), 7.33-7.37 (m, 5H, BnO), 7.29 (d, 1H, *J* = 1.2 Hz, H6), 5.54 (s, 1H, H1′), 4.77 (d, 1H, *J* = 11.7 Hz, H7a), 4.72 (d, 1H, *J* = 11.7 Hz, H7b), 4.56 (s, 1H, H2′), 4.25 (s, 1H, H3′), 4.07 (s, 1H, H6′), 4.01 (1H, d, *J* = 8.0 Hz, H8a), 3.95 (1H, d, *J* = 8.0 Hz, H8b), 1.81 (3H, d, *J* = 1.2 Hz, 5-CH_3)

^{13}C NMR (101 MHz, d_6-DMSO): δ = 163. 74 (C4), 149.88 (C2), 137.47 (BnO, *para*), 134.34 (C6), 128.28, 127.74, 127.62 (BnO), 109.05 (C5), 86.88 (C1′), 82.36 (C6′), 79.50 (C3′), 77.10 (C5′), 76.86 (C2′), 74.88 (C4′), 74.06 (C8), 71.27 (C7), 12.28 (5-$\underline{C}H_3$)

HRMS (ESI$^+$) (*m/z*) $[M+Na]^+$ for $[C_{19}H_{18}N_2NaO_5]^+$ cal. 377.1108 found: 377.1108.

6.2.28 Synthesis of DNA-thymidine–TL-LNA-thymidine dimer

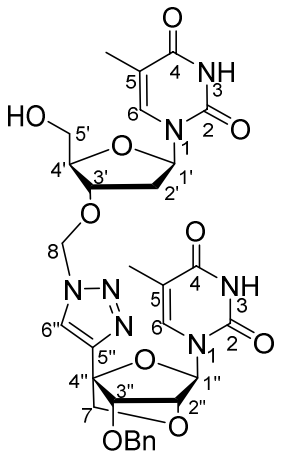

43

Compound **25** (346.7 mg, 0.73 mmol) and Compound **22** (264.7 mg, 0.66 mmol) were dissolved in THF/H_2O/t-BuOH (10 mL, 3:1:1, v/ v/v). To this solution was added pyridine (2−3 drops), $CuSO_4$ (1.5 mL, 7.5% aqueous, w/v), and sodium ascorbate (1.7 mL, 1 M aqueous). The reaction mixture was degassed with argon and stirred at room temperature for 2 h. The reaction was diluted with EtOAc (100 mL) and washed with H_2O (50 mL) and saturated aqueous solution of EDTA (3 × 50 mL). The combined aqueous phase was back extracted with EtOAc (50 mL) and the combined organic phase was dried (Na_2SO_4) and concentrated under reduced pressure. The residue was dissolved in 4 mL of absolute methanol and finely powdered K_2CO_3 (41.5 mg, 0.3 mmol) was added. The suspension was stirred for 12 h and the solvent was removed under vacuum. The residue was purified by silica gel column chromatography (0-100% EtOAc in PE 40-60) to give compound **33** as a hard foam (232.4 mg, 0.36 mmol, 54%).

R_f = 0.32 (75% EtOAc in PE 40-60, v/v);

^{1}H NMR (400 MHz, d_6-DMSO) δ 11.43 (s, 1H, H3, aT or eT), 11.29 (s, 1H, H3, aT or eT), 8.73 (s, 1H, H6″), 7.64 (d, *J* = 1.3 Hz, 1H, H6, aT or eT), 7.47 (d, *J* = 1.3 Hz, 1H, H6, aT or eT), 7.31 – 7.16 (m, 5H, Ar-H), 6.10 (dd, *J* = 8.3, 6.1 Hz, 1H, H1′), 5.94 – 5.83 (m, 2H, H8), 5.62 (d, *J* = 0.6 Hz, 1H, H1″), 5.13 (t, *J* = 5.1 Hz, 1H, 5′-OH), 4.64 (s, 1H, H7a), 4.59 (d, *J* = 11.7 Hz, 1H, OCH_2a-Bn), 4.49 (d, *J* = 11.7 Hz, 1H, OCH_2b-Bn), 4.39 (s, 1H, H7b), 4.36 (q, *J* = 4.0 Hz, 2H, H3′ and H3″), 4.19 (d, *J* = 8.2 Hz, 1H, H2″), 3.88 (q, *J* = 2.6 Hz, 1H, H4′), 3.59 – 3.45 (m, *J* = 4.6 Hz, 2H, H5′), 2.15 – 1.96 (m, 2H, H2′), 1.82 (d, *J* = 1.2 Hz, 3H, 5-CH_3, aT or eT), 1.76 (d, *J* = 1.2 Hz, 3H, 5-CH_3, aT or eT).

^{13}C NMR (101 MHz, d_6-DMSO) δ 164.14 (C4, aT or eT), 160.43 (C4, aT or eT), 150.45 (C2), 149.95 (C5″), 128.65 (C, BnO), 128.14 (*m*-CH, BnO), 127.42 (*o*-CH, *p*-CH, BnO), 121.62 (C6″), 116.53 (C5, aT or eT), 116.02 (C5, aT or eT), 105.79 (C1′), 105.29 (C1″), 99.62 (C3″), 99.11 (C2″), 94.61 (C4″), 91.06 (C4′), 90.55 (C7), 85.82 (O<u>C</u>H_2-Bn), 85.31 (C8), 64.81 (C5′), 61.05 (C5′), 60.54 (C3′), 31.80 (C2′), 12.20 (5-CH_3, aT and eT).

LR MS-ESI: m/z: $[M+H]^+$ for $[C_{30}H_{34}N_7O_{10}]^+$ calc. 652.2 found: 652.3 (100%).

Notes: aT means azidomethyl thymidine and **eT** means ethynyl thymidine.

6.2.29 Synthesis of DNA-thymidine–TL-LNA-thymidine dimer

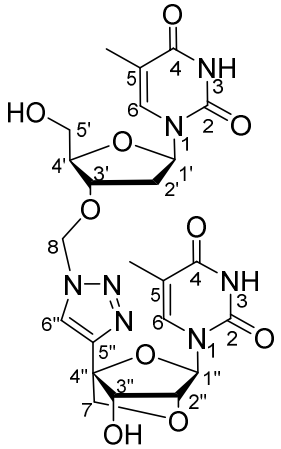

44

A mixture of compound **43** (232.4 mg, 0.36 mmol), 20% $Pd(OH)_2/C$ (115.6 mg), and ammonium formate (101.4 mg, 1.62 mmol), was suspended in MeOH (2.5 ml). After refluxing for 2 h, the catalyst was filtered off on celite, and washed with MeOH. The combined filtrates were concentrated to a white residue (168.6 mg, 0.3 mmol, 85%). Compound **44** was used without purification for next step.

R_f = 0.18 (100% EtOAc);

^{1}H NMR (400 MHz, d_6-DMSO) δ 11.35 (s, 2H, H3, aT and eT), 8.68 (s, 1H, H6″), 7.67 (d, *J* = 1.3 Hz, 1H, H6, aT or eT), 7.51 (d, *J* = 1.3 Hz, 1H, H6, aT or eT), 6.12 (dd, *J* = 7.8, 6.5 Hz, 1H, H1′), 5.92 (s, 1H, 3″-OH), 5.90 – 5.84 (m, 2H, H8), 5.56 (s, 1H, H1″), 5.19 (s, 1H, 5′-OH), 4.37 (dt, *J* = 5.0, 2.8 Hz, 1H, H3′), 4.33 (s, 1H, H7a), 4.32 (d, *J* = 2.6 Hz, 1H, H3″), 4.30 (s, 1H, H7b), 4.12 (d, *J* = 8.0 Hz, 1H, H2″), 3.91 (td, *J* = 3.8, 2.1 Hz, 1H, H4′), 3.55 (t, *J* = 4.3 Hz, 2H, H5′), 2.19 – 2.08 (m, 2H, H2′), 1.79 (dd, *J* = 20.1, 1.2 Hz, 6H, 5-CH_3, aT and eT).

^{13}C NMR (101 MHz, d_6-DMSO) δ 166.98 (C4, aT or eT), 162.01 (C4, aT or eT), 137.99 (C6, aT and eT), 132.32 (C5″), 121.63 (C6″), 113.19 (C5, aT and eT), 100.24 (C1′, C1″, C4″)), 87.45 (C4′), 86.94 (C2″), 79.24 (C8), 78.74 (C3′), 74.55 (C7), 74.04 (C3″), 63.08 (C5′), 36.37 (C2′), 12.51 (5-CH_3, aT and eT).

LR MS-ESI: m/z: $[M+H]^+$ for $[C_{23}H_{28}N_7O_{10}]^+$ calc. 562.2 found: 562.2 (100%).

Notes: aT means azidomethyl thymidine and **eT** means ethynyl thymidine.

6.2.30 Synthesis of 5′-*O*-(Dimethoxytrityl)-DNA-thymidine–TL–LNA-thymidine dimer

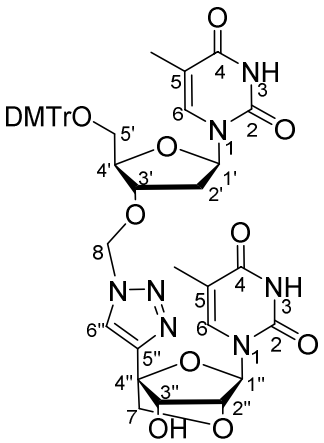

45

Compound **44** (168.6 mg, 0.3 mmol) was co-evaporated in dry pyridine (3 x 5.0 mL) and dissolved in dry pyridine (5.0 mL). To this was added DMTrCl (121.9 mg, 0.36 mmol) and stirred at room temperature for 20 h. This was then concentrated under reduced pressure and purified by silica column chromatography (0-5% MeOH in CH_2Cl_2, v/v) to produce compound **45** (155.6 mg, 0.18 mmol, 62%) as a white foam.

R_f = 0.40 (100% EtOAc);

^{1}H NMR (400 MHz, d_6-DMSO) δ 11.37 (s, 2H, H3, aT and eT), 8.67 (s, 1H, H6″), 7.51 (d, *J* = 1.4 Hz, 1H, H6, aT or eT), 7.47 (d, *J* = 1.3 Hz, 1H, H6, aT or eT), 7.36 – 6.86 (m, 13H, Ar-H), 6.15 (dd, *J* = 8.1, 6.1 Hz, 1H, H1″), 5.92 – 5.87 (m, 2H, H8), 5.55 (d, *J* = 0.6 Hz, 1H, H1′), 4.61 – 4.57 (m, 1H, H4′), 4.34 (s, 1H, H3″), 4.32 – 4.27 (m, 2H, H2″ and H3′), 4.09 – 4.01 (m, 2H, H7), 3.73 (d, *J* = 0.8 Hz, 6H, OCH_3), 3.18 (ddd, *J* = 51.2, 10.6,

3.6 Hz, 2H, H5′), 2.29 (dt, *J* = 18.0, 7.0 Hz, 2H, H2′), 1.77 (d, *J* = 1.2 Hz, 3H, 5-CH_3, aT or eT), 1.40 (d, *J* = 1.1 Hz, 3H, 5-CH_3, aT or eT);

^{13}C NMR (101 MHz, d_6-DMSO) δ 161.16 (C4, aT and eT), 135.08 ((C6, aT and eT) (C, PhOMe)), 129.65 (*o*-CH, PhOMe), 127.95 (C6″, (CH, Ph)), 113.31 (*m*-CH, PhOMe), 109.78 (C5, aT and eT), 86.09 (C DMTr), 82.24 (C4′, C4″), 75.79 (C2″, C3′, C8, C3″), 63.60 (C5′), 55.01 (OCH_3), 12.40 (5-CH_3, aT or eT), 11.58 (5-CH_3, aT or eT).

LRMS (ESI$^+$):(*m/z*): $[M+H]^+$ for $[C_{44}H_{46}N_7O_{12}]^+$ calc. 864.3 found 864.2 (40%).

Notes: aT means azidomethyl thymidine and **eT** means ethynyl thymidine.

6.2.31 Synthesis of 5′-*O*-(Dimethoxytrityl)-DNA-thymidine–TL–LNA-thymidine dimer phosphoramidite

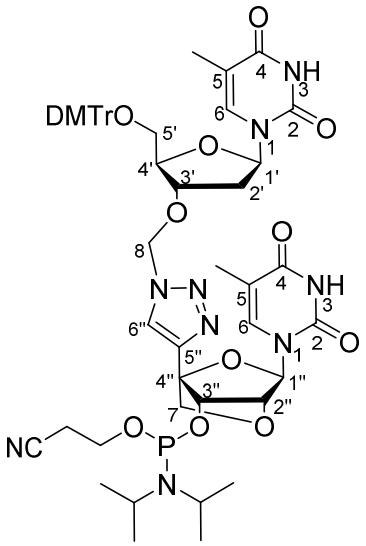

21

Compound **45** (155.6 mg, 0.18 mmol) was co-evaporated with degassed CH_2Cl_2 (3x 2.0 mL) and dissolved in dry degassed CH_2Cl_2 (5.0 mL). To this was added degassed DIPEA (78.4 µL, 0.45 mmol) followed by 2-Cyanoethyl *N, N*-diisopropylchlorophosphoramidite (48.0 µL) and stirred under argon for 1 h. The reaction was diluted in degassed CH_2Cl_2 (5.00 mL), washed with saturated KCl solution (10 mL) and dried over Na_2SO_4. The organic layer was concentrated and purified by silica column chromatography using degassed solvent (100% EtOAc) to give compound **21** as a white solid (124.5 mg, 0.12 mmol, 65%).

R_f = 0.58 (100% EtOAc);

^{31}P NMR (162 MHz, d_6-DMSO) δ 148.43, 148.40;

HRMS (ESI$^+$) (*m/z*): $[M+Na]^+$ for $[C_{53}H_{62}N_9NaO_{13}P]^+$ cal.1086.4097 found 1086.4098.

6.2.32 Synthesis of 5′-*O*-(Dimethoxytrityl)-LNA-thymidine–TL-3′-*O*-(*tert*-butyldiphenylsilyl)–DNA-thymidine dimer

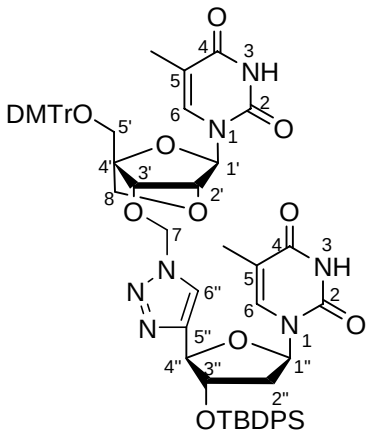

46

Compound **23** (243.4 mg, 0.55 mmol) and Compound **24** (313.6 mg, 0.66 mmol) were dissolved in THF/H_2O/t-BuOH (10 mL, 3:1:1, v/v/v). To this solution was added pyridine (2−3 drops), $CuSO_4$ (1.5 mL, 7.5% aqueous, w/v), and sodium ascorbate (1.7 mL, 1 M aqueous). The reaction mixture was degassed with argon and stirred at room temperature for 2 h. The reaction was diluted with EtOAc (100 mL) and washed with H_2O (50 mL) and saturated aqueous solution of EDTA (3 × 50 mL). The combined aqueous phase was back extracted with EtOAc (50 mL) and the combined organic phase was dried (Na_2SO_4) and concentrated under reduced pressure.

The crude residue was dissolved in dry methanol (5 mL) and added with finely powdered K_2CO_3 (38.0 mg, 0.27 mmol), and the suspension was stirred for 12 h. The organic layers were dried over Na_2SO_4, filtered and concentrated. Afterwards the concentrated residue

was co-evaporated in dry pyridine (3 x 5.0 mL) and dissolved in dry pyridine (2.5 mL). To this was added DMTrCl (244.0 mg, 0.72 mmol) and stirred at r.t. for 20 h. This was then concentrated under reduced pressure and purified by silica column chromatography (0−100% EtOAc in PE 40-60, v/v) to obtain compound **46** (460.2 mg, 0.42 mmol, 76%) as a white foam.

R_f = 0.36 (50% EtOAc in PE 40-60, v/v);

^{1}H NMR (400 MHz, *d_6*-DMSO) δ 11.50 (s, 1H, H3, aT or eT), 11.31 (s, 1H, H3, aT or eT), 8.07 (s, 1H, H6″), 7.64 – 6.80 (m, 25H, H6 and Ar-H), 6.41 – 6.32 (m, 1H, H1″), 5.87 (s, 2H, H7), 5.53 (s, 1H, H1′), 5.00 (d, *J* = 2.8 Hz, 1H, H4″), 4.57 (s, 1H, H3′), 4.53 (dd, *J* = 5.5, 2.9 Hz, 1H, H3″), 4.48 (s, 1H, 2′), 3.74 – 3.63 (m, 8H, H8 and OCH_3), 3.31 – 3.22 (m, 2H, H5′), 2.33 – 2.16 (m, 2H, H2″), 1.58 (dd, *J* = 3.3, 1.1 Hz, 6H, 5-CH_3, aT and eT), 1.00 (s, 9H, *t*-Bu).

^{13}C NMR (101 MHz, *d_6*-DMSO) δ 161.52 (C4, aT and eT), 148.76 (*p*-C, PhOMe DMTr), 139.26 (C, Ph DMTr, (*p*-CH, Ph DMTr)), 133.43 ((C6, aT and eT), (C, PhOMe DMTr), (CH, Ph_2Si)), 127.93 ((*o*-CH, Ph DMTr), (*m*-CH, Ph DMTr)), 121.80 (C6″), 114.55 (*m*-CH, PhOMe), 108.50 (C5, aT or eT), 88.66 (C4′, C1′, C1″), 88.16 (C, DMTr), 79.41 (C4″), 78.92 (C3″), 68.76 (C7), 64.58 (C5′), 54.95 (OCH_3), 26.61 (CH_3, *t*-Bu), 19.88 (C, *t*-Bu), 12.35 (5-CH_3, aT and eT).

LRMS (ESI$^+$) *m/z* $[M+H]^+$ for $[C_{60}H_{64}N_7O_{12}Si]^+$ calc. 1102.4 found 1102.3 (40%).

Notes: aT means azidomethyl thymidine and **eT** means ethynyl thymidine.

6.2.33 Synthesis of 5′-*O*-(Dimethoxytrityl)-LNA-thymidine–TL-DNA-thymidine dimer

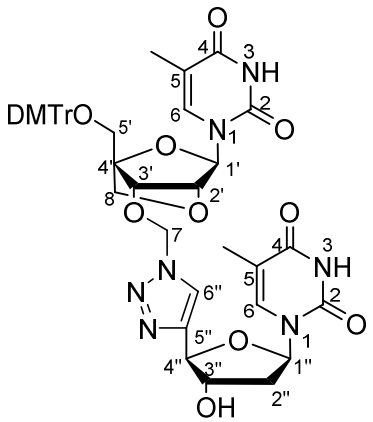

47

To a stirred solution of compound **46** (460.2 mg, 0.42 mmol) in dry THF (0.9 mL), 1 M solution of tetrabutylammonium fluoride in dry THF (0.9 mL) was added. The mixture was stirred for 2 h at room temperature, diluted with saturated $NaHCO_3$ (30 mL) and extracted with CH_2Cl_2 (3 x 40 mL). Combined organic layers were washed with water, dried over Na_2SO_4, filtered and concentrated. The residue was purified using column chromatography (0−100% EtOAc in PE 40-60, v/v) to obtain compound **47** (260.9 mg, 0.3 mmol, 72%) as a pale-yellow foam.

R_f = 0.57 (100% EtOAc)

^{1}H NMR (400 MHz, d_6-DMSO) δ 11.48 (s, 1H, H3, aT or eT), 11.32 (s, 1H, H3, aT or eT), 8.32 (s, 1H, H6″), 7.69 (d, *J* = 1.4 Hz, 1H, H6, aT or eT), 7.52 (d, *J* = 1.3 Hz, 1H, H6, aT or eT), 7.34 – 6.83 (m, 13H, Ar-H), 6.33 (dd, *J* = 8.1, 5.9 Hz, 1H, H1′), 5.92 (s, 2H, H7), 5.55 (s, 1H, 3″-OH), 5.52 (s, 1H, H1′), 4.87 (d, *J* = 2.6 Hz, 1H, H4″), 4.50 (d, *J* =

17.5 Hz, 2H, H2′ and H3′), 4.28 (s, 1H, H3″), 3.72 (s, 6H, OCH_3), 3.70 (s, 2H, H8), 3.34 – 3.23 (m, 2H, H5′), 2.36 (ddd, *J* = 13.6, 8.2, 5.6 Hz, 1H, H2″a), 2.17 (ddd, *J* = 13.3, 6.0, 2.9 Hz, 1H, H2″b), 1.63 (d, *J* = 1.1 Hz, 3H, 5-CH_3, aT or eT), 1.58 (d, *J* = 1.1 Hz, 3H, 5-CH_3, aT or eT).

^{13}C NMR (101 MHz, d_6-DMSO) δ 161.48 (C4, aT and eT), 158.13 (*p*-C, PhOMe DMTr), 150.52 (C2, aT and eT), 147.42 (C, Ph DMTr), 142.95 (C2″), 133.62 ((C6, aT and eT) (C, PhOMe DMTr)), 129.65 (*o*-CH, Ph DMTr), 125.34 ((*m*-CH, *p*-CH, Ph DMTr), (*o*-CH, PhOMe DMTr)), 118.82 (C6″), 113.33 (m-CH, PhOMe DMTr), 108.71 (C5, aT or eT), 108.70 (C5, aT or eT), 94.47 (C8), 89.43 (C1′, C1″, (C, DMTr) 85.43 (C4′, C4″), 75.39 (C7), 74.64 (C2′, C3′), 73.50 (C3″), 54.99 (OCH_3), 31.22 (C2″), 11.06 (5-CH_3, aT or eT), 11.01(5-CH_3, aT or eT).

LRMS (ESI$^+$) *m/z* $[M+H]^+$ for $[C_{44}H_{46}N_7O_{12}]^+$ cal. 864.3 found 864.3 (35%).

Notes: aT means azidomethyl thymidine and **eT** means ethynyl thymidine.

6.2.34 Synthesis of 5′-*O*-(Dimethoxytrityl)-LNA-thymidine–TL-DNA-thymidine dimer phosphoramidite

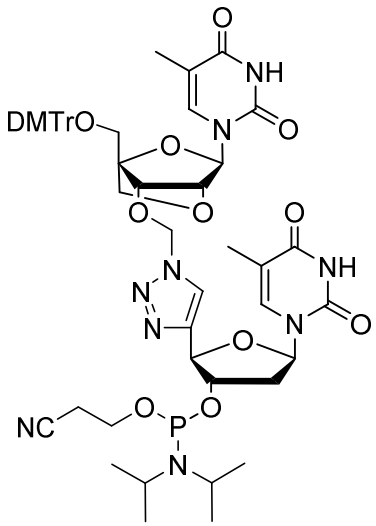

20

Compound **47** (260.9 mg, 0.3 mmol) was co-evaporated with degassed CH_2Cl_2 (3 x 2.0 mL) and dissolved in dry degassed CH_2Cl_2 (5.00 mL). To this was added degassed DIPEA (140 µL, 0.8 mmol) followed by 2-Cyanoethyl *N, N*-diisopropylchlorophosphoramidite (87.2 µL, 0.39mmol) and stirred under argon for 1 h. The reaction was diluted in degassed CH_2Cl_2 (5.00 mL), washed with saturated KCl solution (10.0 mL) and dried over Na_2SO_4. The organic layer was concentrated and purified by silica column chromatography using degassed solvent (EtOAc) to give compound **20** as a white solid (204.3 mg, 0.19 mmol, 64%).

R_f = 0.72 (100 % EtOAc);

^{31}P NMR (162 MHz, d_6-DMSO) δ 147.97, 148.03;

HRMS (ESI$^+$) ***m/z*****:** $[M+H]^+$ for $[C_{53}H_{63}N_9O_{13}P]^+$ cal. 1064.4277, found 1064.4279.

6.2.35 Synthesis of 5′-*O*-(Dimethoxytrityl)-LNA-thymidine–TL-3′-*O*-benzyl-LNA-thymidine dimer

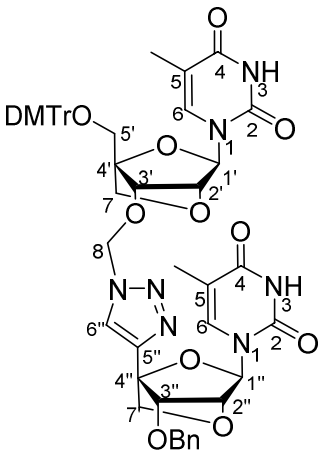

51

Compound **25** (116.8 mg, 0.33 mmol) and Compound **24** (197.3 mg, 0.46 mmol) were dissolved in THF/H_2O/t-BuOH (6 mL, 3:1:1, v/v/v). To this solution was added pyridine (2−3 drops), $CuSO_4$ (0.9 mL, 7.5% aqueous, w/v), and sodium ascorbate (1.2 mL, 1 M aqueous). The reaction mixture was degassed with argon and stirred at room temperature for 2 h. The reaction was diluted with EtOAc (60 mL) and washed with H_2O (30 mL) and saturated aqueous solution of EDTA (3 × 30 mL). The combined aqueous phase was back extracted with EtOAc (30 mL) and the combined organic phase was dried (Na_2SO_4) and concentrated under reduced pressure.

The crude residue was dissolved in dry methanol (3 mL) and added with finely powdered K_2CO_3 (22.8 mg, 0.16 mmol), and the suspension was stirred for 12 h. The organic layers

were dried over Na_2SO_4, filtered and concentrated. Afterwards the concentrated residue was co-evaporated in dry pyridine (3 x 3.0 mL) and dissolved in dry pyridine (1.5 mL). To this was added DMTrCl (146.4 mg, 0.4 mmol) and stirred at room temperature for 20 h. This was then concentrated under reduced pressure to obtain crude compound **51** (180.0 mg, 0.18 mmol, 54%) as a yellow foam.

R_f = 0.58 (100% EtOAc)

^{1}H NMR (400 MHz, *d_6*-DMSO) δ 11.50 (s, 1H, H3, aT or eT), 11.47 (s, 1H, H3, aT or eT), 8.66 (d, *J* = 2.2 Hz, 1H, H6″), 7.52 (d, *J* = 1.3 Hz, 1H, H6, aT or eT), 7.48 (d, *J* = 1.4 Hz, 1H, H6, aT or eT), 7.33 – 6.87 (m, 18H, Ar-H), 5.98 (s, 2H, H8), 5.53 (d, *J* = 6.7 Hz, 2H, H1′ and H1″), 4.59 (d, *J* = 4.2 Hz, 1H, OCH_2-Bn), 4.53 (d, *J* = 4.5 Hz, 1H, OCH_2-Bn), 4.49 (s, 1H, H7a), 4.44 (s, 1H, H7b), 4.38 (s, 1H, H7c), 4.36 – 4.32 (m, 1H, H3″), 4.31 (s, 1H, H7d), 3.98 – 3.95 (m, 1H, H2″), 3.76 – 3.73 (m, 2H, H2′ and H3′), 3.72 (s, 6H, OCH_3), 3.31 – 3.26 (m, 2H, H5′), 1.76 (d, *J* = 1.2 Hz, 3H, 5-CH_3, aT or eT), 1.61 – 1.58 (m, 3H, 5-CH_3, aT or eT).

^{13}C NMR (101 MHz, *d_6*-DMSO) δ 163.88 (C4, aT and eT), 163.85 (*p*-C, PhOMe DMTr), 149.96 (C2, aT or eT), 149.62 (C2, aT or eT), 137.59 (C, Ph DMTr), 137.56 (C, BnO), 136.12 ((C6, aT and eT) (C, PhOMe DMTr)), 129.67 (*m*-CH, Ph DMTr), 128.20 (*o*-CH, Ph DMTr), 128.17 (*m*-CH, Ph BnO), 128.03 (*p*-CH Ph BnO), 127.52 (*p*-CH Ph DMTr), 127.50 (*o*-CH, Ph BnO), 125.52 (C6″), 113.35 (*m*-CH PhOMe DMTr), 108.89 (C5, aT or eT), 108.84 (C5, aT or eT), 88.13 (C DMTr), 86.84 (C4″), 86.52 (C4′), 85.91(C2′, C3′),

85.76 (C2″, C3″), 81.48 (C7), 81.41(C7), 71.22 (<u>C</u>H_2-Bn), 55.01 (OCH_3), 12.49 (5-CH_3, aT or eT), 12.41 (5-CH_3, aT or eT).

LRMS (ESI$^+$) (*m/z*): $[M+H]^+$ for $[C_{52}H_{52}N_7O_{13}]^+$ cal. 982.3 found 982.4 (30%).

Notes: aT means azidomethyl thymidine and **eT** means ethynyl thymidine.

6.2.36 Synthesis of 5′-*O*-(Dimethoxytrityl)-LNA-thymidine–TL-LNA-thymidine dimer

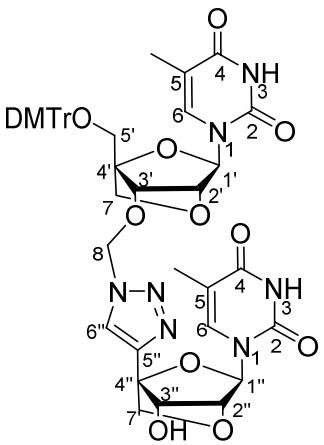

52

A mixture of compound **51** (180 mg, 0.18 mmol), 20% $Pd(OH)_2/C$, and ammonium formate (83 mg, 0.56 mmol), was suspended in MeOH (2.5 ml). After refluxing for 2 h, the catalyst was filtered off on celite, and washed with MeOH. The combined filtrates were concentrated to a pale-yellow residue. The residue was purified using column chromatography (0−100% EtOAc in PE 40-60, v/v) to obtain compound **52** (115 mg, 0.13 mmol, 72%) as a pale-yellow foam.

R_f = 0.23 (100% EtOAc)

^{1}H NMR (400 MHz, *d_6*-DMSO) δ 11.49 (s, 1H, H3, aT or eT), 11.43 (s, 1H, H3, aT or eT), 8.62 (s, 1H, H6″), 7.52 (d, *J* = 1.4 Hz, 1H, H6, aT or eT), 7.46 (d, *J* = 1.3 Hz, 1H, H6, aT or eT), 7.38 – 7.28 (m, 13H, Ar-H), 6.01 – 5.87 (m, 2H, H8), 5.84 (d, *J* = 4.7 Hz, 1H, 3″-O<u>H</u>), 5.54 (d, *J* = 1.6 Hz, 2H, H1′ and H1″), 4.53 (s, 1H, H7a), 4.45 (s, 1H, H7b), 4.33 (s, 1H, H7c), 4.26 (s, 1H, H7d), 4.24 (d, *J* = 2.3 Hz, 1H, H3″), 3.91 (d, *J* = 8.0 Hz, 1H, H2″), 3.76 – 3.70 (m, 2H, H2′ and H3′), 3.73 (s, 6H, OCH_3), 3.34 (d, *J* = 11.1 Hz, 1H, H5′a), 3.30 (d, *J* = 11.2 Hz, 1H, H5′b) 1.75 (d, *J* = 1.2 Hz, 3H, 5-CH_3, aT or eT), 1.61 (d, *J* = 1.2 Hz, 3H, 5-CH_3, aT or eT).

^{13}C NMR (101 MHz, *d_6*-DMSO) δ 164.32 (C4, aT or eT), 164.25 (C4, aT or eT), 158.63 (*p*-<u>C</u>, PhOMe), 150.43 (C2, aT or eT and C5″), 150.38 (C2, aT or eT), 140.20 (<u>C</u>, Ph and PhOMe, 135.38 (C6, aT or eT), 134.80 (C6, aT or eT), 130.11 (*o*-<u>C</u>H, PhOMe), 128.50 (*m*-<u>C</u>H, Ph), 127.99 (*p*-<u>C</u>H, *o*-<u>C</u>H, Ph), 125.81 (C6″), 113.83 (*m*-<u>C</u>H, PhOMe), 109.34 (C5, aT or eT), 109.23 (C5, aT or eT), 87.14 (C1′), 86.98 (C1″), 86.25 (C, DMTr), 82.72 (C4′, C4″), 73.00 (C2′, C2″, C3′, C3″, C5′, C7, C7′, C8), 55.49 (O<u>C</u>H$_3$), 55.38 (O<u>C</u>H$_3$), 12.94 (5-<u>C</u>H$_3$, aT or eT), 12.86 (5-<u>C</u>H$_3$, aT or eT).

LRMS (ESI$^+$) (*m/z*): $[M+Na]^+$ for $[C_{45}H_{45}N_7NaO_{13}]^+$ cal. 914.3 found 914.4 (100%).

Notes: aT means azidomethyl thymidine and **eT** means ethynyl thymidine.

6.2.37 Synthesis of 5′-*O*-(Dimethoxytrityl)-LNA-thymidine–TL-LNA-thymidine dimer phosphoramidite

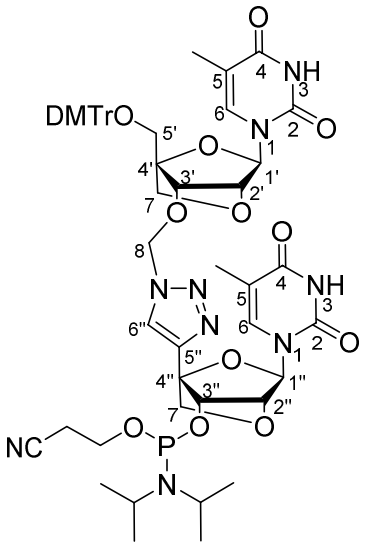

19

Compound **52** (115 mg, 0.13 mmol) was co-evaporated with degassed CH_2Cl_2 (3x 2.00 mL) and dissolved in dry degassed CH_2Cl_2 (5.00 mL). To this was added degassed DIPEA (56 μL, 0.32 mmol) followed by 2-Cyanoethyl *N, N*-diisopropylchlorophosphoramidite (35.0 μL) and stirred under argon for 1 h. The reaction was diluted in degassed CH_2Cl_2 (5.00 mL), washed with saturated KCl solution (10 mL) and dried over Na_2SO_4. The organic layer was concentrated and purified by silica column chromatography using degassed solvent (100% EtOAc) to give compound **19** as a white solid (109.2 mg, 0.10 mmol, 78%).

R_f = 0.45 (100% EtOAc);

^{31}P NMR (162 MHz, $CDCl_3$) δ 148.48, 148.42;

HRMS (ESI$^+$) (*m/z*)**:** $[M+Na]^+$ for $[C_{55}H_{62}N_9NaO_{14}P]^+$ cal. 1114.4046 found 1014.4050.

6.3. Synthesis and purification of oligonucleotides

6.3.1. Synthesis of DNA oligonucleotides

Standard DNA phosphoramidites, solid supports and additional reagents were purchased from Link Technologies and Applied Biosystems Ltd. Oligonucleotides were synthesised using an Applied Biosystems 394 automated DNA/RNA synthesiser using a standard 1.0 μmol phosphoramidite cycle of acid-catalyzed detritylation, coupling, capping and iodine oxidation. Stepwise coupling efficiencies and overall yields were determined by an automated trityl cation conductivity monitoring facility and in all cases were >98.0%. β-Cyanoethyl phosphoramidite monomers were dissolved in anhydrous acetonitrile to a concentration of 0.1 M immediately prior to use. The coupling time for normal A, G, C and T monomers was 35 s and the coupling time for the modified monomers (AP-C3 and AP-C6) was 360 s. Cleavage of the oligonucleotides from the solid support and deprotection was achieved by exposure to concentrated aqueous ammonia solution (1 h, R.T.) followed by heating in a sealed tube (5 h, 55 °C). After evaporation of the ammonia in vacuo, the fully deprotected oligonucleotides were purified by reverse-phase HPLC (RP-HPLC) on a Gilson system using a Luna 10 μm C8 100 Å pore Phenomenex 10x250 mm column with a gradient of acetonitrile (HPLC grade) in water (Sterile, Millipore system) with TEAA buffer (buffer A: 0.1 M triethylammonium acetate, pH 7.0; buffer B: 0.1 M triethylammonium acetate with 50% acetonitrile, pH 7.0; gradient: 0% to 100% buffer B over 20 min, flow rate: 4 mL/min) or TEAB buffer (buffer A: 0.1 M triethylammonium bicarbonate, pH 7.5; buffer B: 0.1 M triethylammonium bicarbonate,

pH 7.5, with 50% acetonitrile) were used (0% to 100% buffer B over 20 min). Elution was monitored by UV absorption at 260-299 nm. Oligonucleotides purified with TEAA buffers were desalted with GE Healthcare Life Sciences illustra NAP 25 then NAP 10 gel filtration columns. After RP-HPLC purification, all oligonucleotides were characterised by electrospray mass spectrometry using a Bruker microTOF II focus ESI-TOF MS or UPLC-MS Waters XEVO G2-QTOF instrument in ESI^- mode. Data were processed using MaxEnt or MassLynx v4.1

6.3.2. Synthesis of RNA oligonucleotides

2′-*O*-TBDMS (*Tert*-butyldimethylsilyl) protected RNA phosphoramidite monomers with t-butylphenoxyacetyl protection of the A, G and C nucleobases were used purchased from Sigma-Aldrich and used to assemble RNA oligonucleotides. Benzylthiotetrazole (BTT) was used as the coupling agent, t-butylphenoxyacetic anhydride as the capping agent and 0.1 M iodine as the oxidizing agent (Sigma-Aldrich). Coupling time of 10 min was used and coupling efficiencies of >97% were obtained. Cleavage of oligonucleotides from the solid support and protecting groups from the nucleobase and backbone were removed by exposure to concentrated aqueous ammonia: ethanol (v/v = 3:1) for 2 h at room temperature followed by heating in a sealed tube for 2 h at 55 °C.

6.3.3. Removal of 2′-*O*-TBDMS of RNA oligonucleotides

After cleavage from the solid support and removal of the protecting groups from the nucleobases and phosphodiesters in ammonia/ethanol as described above, oligonucleotides were concentrated to a small volume in vacuo, transferred to 15 mL plastic tubes and freeze dried (lyophilised). The residue was dissolved in DMSO (300 μL) and triethylamine

trihydrofluoride (300 μL) was added after which the reaction mixtures were kept at 65 °C for 2.5 h. Sodium acetate (3 M, 50 μL) and butanol (3 mL) were added with vortexing and the samples were kept at -80 °C for 30 min then centrifuged at 13000 rpm at 4 °C for 10 min. The supernatant was decanted and the precipitate was washed twice with ethanol (0.75 mL) then dried under vacuum. The fully deprotected oligonucleotides were purified in similar matter as DNA equivalents.

6.3.4. Removal of 2′-*O*-TC protecting groups on RNA oligonucleotides

600 μL of a 1:1 dry toluene: dry ethylenediamine (v/v) solution was slowly added to the RNA synthesis column with no agitation and incubated for 6 h at room temperature. The column was then washed twice with 1 mL dry toluene and dried with argon. RNA was eluted from the resin in the column by slowly pushing 1 mL water through the column and repeating with another 1 mL water.

6.3.5. Synthesis of 2′-OMe–RNA oligonucleotides

Phosphoramidites, solid supports and additional reagents were purchased from Link Technologies, the procedure was identical to the DNA oligonucleotides apart from extended coupling time, 10 min, for each step including modifications.

6.4. Labelling of oligonucleotides

6.4.1. NHS ester labelling

A solution of ROX NHS ester (20 eq. per modification) in DMF (80 μL) was added to an oligonucleotide (200 nmol) dissolved in carbonate buffer ($NaHCO_3/Na_2CO_3$, 0.5 M, pH =

8.75, 120 µL) and shaken for 3 h at 36 °C. The mixture was desalted by NAP gel filtration column and purified by RP-HPLC to obtain the desired labelled oligonucleotide.

6.4.2. General procedure of copper-click 1,3-dipolar cycloaddition (CuAAC)

To a solution of AP-C3 modified oligonucleotide (40 nmol, 1.0 eq.) in H_2O (600 µL), TEAA buffer (2 M, pH = 7.0; 200 µL), DMSO (590 µL) and stock of TO azide (10 nmol/µL in DMSO, 12 µL, 7.5 eq. per modification) and freshly prepared sodium ascorbate (0.9 mg/ 1.0 mL of H_2O; 200 µL) were vortexed together. Mixture was degassed by bubbling argon gas for 5 min followed by addition of Cu^{II}:THPTA (tris(3-hydroxypropyltriazolylmethyl)amine) complex (10 mM in 55%/45% DMSO/H_2O; 100 µL, Cu source: $CuSO_4$). Reaction was shaken for 3 hours at 30 °C, followed by ethanol precipitation with NaOAc (3 M) and was purified by reverse-phase HPLC with C8 column (RP-HPLC) to obtain pure product with full conversion.

6.5. Steady state fluorescence measurements

Fluorescence studies were performed on a Perkin Elmer LS50B luminescence spectrometer fitted with Perkin Elmer PTP-1 Peltier temperature controller. FLWinlabTempScan software was used with settings of 400 nm/s scan speed. For TO the emission wavelength was recorded from 510 nm to 700 nm, excitation wavelength 484 nm or 510 nm, gain high (900V), excitation slit width 7.0 nm, emission slit width 7.0 nm. For ROX the range of emission was 578 nm to 750 nm at excitation wavelength of 570 nm; the gain and slits width were identical as TO.

Experiment: samples were prepared in 300 µL cuvettes with 0.25 µM probe containing TO, 200 mM NaCl, 10 mM Na-phosphate buffer pH = 7.0 at 37 °C. Spectra were recorded for

the single-stranded oligonucleotide probe, and then titrated with 1.1 eq. of the desired target oligonucleotide and recorded again. F_{ds}/F_{ss} was calculated at the maximum emission wavelength (λ_{em}) of double strand probes (from 510 to 700 nm unless stated otherwise), each probe-target pair was recorded at least in duplicate and values are given in the charts as an averaged value.

6.6. UV Melting studies

UV melting measurements were made on a Varian Cary 4000 UV-Vis spectrophotometer with a Cary temperature controller. Cary Win UV Thermal software was used with an absorbance wavelength of 260 nm. Samples were analysed in 1 mL quartz cuvettes (1 cm path length) and were made to 1.0 μM oligonucleotide probe concentration (X = TO, RX, TO/RX strand) and 1.1 μM oligonucleotide target concentration in phosphate buffer (NaH_2PO_4, 10 mM, NaCl 200 mM at pH 7.0, unless stated otherwise). The samples were initially denatured by heating to 85 °C at 10 °C min^{-1} then cooled to 15 °C at -1 °C min^{-1} and then maintained at 15 °C for 2 min before heating to 85 °C at 1 °C min^{-1}. UV absorption was recorded every 0.1 °C. The melting temperature (T_m) values were derived from the derivatives of the melting curves and calculated at 260 nm using Cary Win UV Thermal application software. Four successive melting curves were measured and averaged.

6.7. RT-qPCR and Fluorescence melting studies

A polymerase master mix consisting of Vent (exo-) DNA polymerase (2 U/µL, 0.25 µL, NEB, cat. No. M0257S), ThermoPol buffer (10 x, 2 µL), heat-activated CleanAmp® dNTPs (10 mM, 0.4 µL, tebu-bio, cat. No. 040N-9506-2) and water (14.15 µL) was prepared in the 0.2 mL white 8-tube PCR strips (Bio-rad, cat. No. TLS0851). The mix was then added to a solution of d2(PCR)-TO/RX probe (10 uM, 0.3 µL/0.6 µL, to make a different probe concentration), forward primer (10 uM, 1.6 µL), reverse primer (10 uM, 0.3 µL) and diluted template (1 µL). Total reaction volume is 20 µL. After sealing the PCR tubes the reaction mixture was mixed thoroughly by vortexing and centrifuged before RT-qPCR amplification.

After initial thermal activation (120 s, 95 °C), 45 cycles of denaturation (15 s, 95 °C) and annealing/extension (60 s, 57.5 °C) were performed. At the end of each extension step, samples were excited at 560-590 nm and the emission at 610-650 nm was monitored. For melt curves analysis, samples were heated from 25 °C to 85 °C and fluorescence was recorded every 0.1 °C in ROX channel.

Fluorescence melting were undertaken using a BioRad CFX96 Real-Time PCR Instrument, with CFX Manager software (BioRad), monitoring in the following channels: TET channel (excitation range 515–535 nm, detector range 560–580 nm), ROX channel (excitation range 560–590 nm, detector range 610–650 nm). Reactions were run in 0.2 mL low-profile white 8-tube strips with optically clear lids (BioRad). Samples were made up to 0.4 µM oligonucleotide probes against 0.44 µM targets in buffer (NaH_2PO_4, 10 mM; NaCl 200

mM) at pH 7.0. The samples were initially denatured by heating to 85 °C at 1 °C min^{-1} then cooled to 25 °C at 1 °C min^{-1} and fluorescence was recorded every 0.1 °C in TET channel and ROX channel.

6.8. Fluorescence lifetime measurements

Fluorescence lifetime decays were determined with a time-correlated single photon counting (TCSPC) technique on a FS5 spectrofluorometer (Edinburgh Instruments). Picosecond pulsed diode laser (EPL-475) at 475 nm with 10 MHz repetition rate was used as excitation source for TO labelled samples. The cuvette holder (qpod, Quantum Northwest) was temperature controlled by a Peltier device (TC 125, Quantum Northwest) and decays were acquired at 298 K. The emission signals were monitored at 530 nm and collected with a magic angle. The instrument response function (IRF) was collected with an aqueous Ludox solution used to scatter the excitation light. Unless otherwise stated, data were accumulated until the number of counts in the channel with highest intensity reached 10 000. Our full-width half maxima (FWHM) of TCSPC apparatus was estimated about ~200 ps and all the picosecond fluorescence kinetics were reported after deconvolution using a Gaussian-shaped instrument response function (IRF). The emission decays were fit using the software (Fluoracle®) from Edinburgh Instruments assuming a multiexponential decay function, $I(t) = \sum_{i=1}^{n} \alpha_i exp(-t/\tau_i)$, where α_i is the amplitude and τ_i is the fluorescence lifetime of the i-th decay component. The maximum number of exponentials allowed by this software is four. For all measured decay traces, no more than three exponentials were needed to reasonably fit the data. The number of exponentials

required for each trace was determined by the quality of the fit, judged on the basis of the reduced chi-square χ^2 and the randomness of residuals. The mean lifetime was calculated by $<\tau> = \sum \alpha i\ \tau i$, using the lifetimes τi associated with the αi amplitudes.

6.9. Supplementary Figures and Tables

Table S. 1. Mass data on DNA probes with the AP-C3 dT modification labelled with dyes and appropriate targets. In the table TO stands for TO-N_3 attached via CuAAC and RX stands for ROX-NHS ester attached via amide bond formation.

Sequence	X =	Probe	Mass calculated	Mass found
ODN1 5′-CGCTTC**X**GTATCTATATTCATC	AP-C3	d1-Y/A	6761	6761
	AP-C3-(TO)	d1-TO/A	7135	7133
	AP-C3-(6-RX)	d1-Y/RX	7277	7276
	AP-C3-(TO/RX)	d1-TO/RX	7651	7651
ODN2 5′-CGCTTC**X**GTATCTA**X**ATTCATC	AP-C3	d2-Y/A	6895	6895
	AP-C3-(TO)	d2-TO/A	7643	7642
	AP-C3-(RX)	d2-Y/RX	7927	7929
	AP-C3-(TO/RX)	d2-TO/RX	8675	8675
ODN3 5′-CGCT**X**CTGTA**X**CTATA**X**TCATC	AP-C3	d3-Y/A	7029	7029
	AP-C3-(TO)	d3-TO/A	8151	8150
	AP-C3-(RX)	d3-Y/RX	8577	8579
	AP-C3-(TO/RX)	d3-TO/RX	9699	9698
5′-dCTATGATGAATATAGATACAGAAGCGTCAT	**DNA Target**	-	9262	9263
5′-rGAUGAAUAUAGAUACAGAAGCG	**RNA Target**	-	7136	7136
5′-dGATGAATATAGATACGGAAGCG	G:T mismatch DNA target	-	6856	6858
5′-dGATGAATATAAATACAGAAGCG	A:C mismatch DNA target	-	6824	6826
5′-rGAUGAAUAUAGAUACGGAAGCG	G:T mismatch RNA target	-	7151	7152
5′-rGAUGAAUAUAAAUACAGAAGCG	A:C mismatch RNA target	-	7119	7121

Note: in probe names, d = DNA oligo, r = RNA oligo, number = probe number, A = unlabelled amine, Y = unlabelled alkyne, TO = labelled with thiazole orange, RX = labelled with ROX, TO/RX = labelled with thiazole orange and ROX.

Table S. 2. Mass data on 2′-OMe long RNA probes with the AP-C3 dT modification labelled with dyes and appropriate targets. In the table TO stands for TO-N_3 attached via CuAAC and RX strand for ROX-NHS ester attached via amide bond formation.

Sequence (all 2′-OMe but X)	X =	Probe	Mass calculated	Mass found
5′-rCUUCUGUAUCUAUA**X**UC	AP-C3	r1-Y/A	5602	5605
	AP-C3-(TO)	r1-TO/A	5976	5977
	AP-C3-(RX)	r1-Y/RX	6119	6121
	AP-C3-(TO/RX)	r1-TO/RX	6493	6495
5′-rCU**X**CUGUAUCUAUA**X**UC	AP-C3	r2-Y/A	5720	5723
	AP-C3-(TO)	r2-TO/A	6468	6468
	AP-C3-(RX)	r2-Y/RX	6754	6756
	AP-C3-(TO/RX)	r2-TO/RX	7502	7502
5′-rCU**X**CUGUA**X**CUAUA**X**UC	AP-C3	r3-Y/A	5837	5841
	AP-C3-(TO)	r3-TO/A	6959	6959
	AP-C3-(RX)	r3-Y/RX	7388	7390
	AP-C3-(TO/RX)	r3-TO/RX	8510	8509
5′-dGAATATAGATACAGAAG	**DNA Target**	-	5275	5276
5′-rGAAUAUAGAUACAGAAG	**RNA Target**	-	5504	5505
5′-dGAGTATAGATACAGAAG	G:T mismatch DNA target	-	5291	5293
5′-dGAATATAATACAGAAG	A:C mismatch DNA target	-	5259	5261
5′-rGAGUAUAGATUCAGAAG	G:T mismatch RNA target	-	5521	5521
5′-rGAAUAUAAAUACAGAAG	A:C mismatch RNA target	-	5488	5489

Note: In probe names, d = DNA oligo, r = RNA oligo, number = probe number, A = unlabelled amine, Y = unlabelled alkyne, TO = labelled with thiazole orange, RX = labelled with ROX, TO/RX = labelled with thiazole orange and ROX.

Table S. 3. Mass data on oligonucleotide probe d2(PCR)-TO/RX and primers used in RT-qPCR. In the table TO stands for TO-N_3 attached via CuAAC and RX strand for ROX-NHS ester attached via amide bond formation.

Sequence	X =	Probe	Mass calculated	Mass found
5′-dA**X**GGCGCCATCCTGT**X**TGTGAAGA-propanol	AP-C3-(TO/RX)	d2(PCR)-TO/RX	9570	9571
5′-dGTCACTGGTCACAGATAGTAC;	-	Forward primer	6430	6431
5′-dCGTAGGTCAGACGTGAATAAG;	-	Reverse primer	6519	6520
5′-dCGTAGGTCAGACGTGAATAAGGAGAAGAACAATGGCGCCATCCTGTTTGTGAAGAACGGCCTGTACTATCTG;	-	PCR template	-	-

Note: in probe names, d = DNA oligo, number = probe number, TO = labelled with thiazole orange, RX = labelled with ROX, TO/RX = labelled with thiazole orange and ROX.

Table S. 4. Mass data on DNA probes with the AP-C3 dT modification labelled with dyes. In the table TO= TO-N_3 attached via CuAAC and RX strand for ROX-NHS ester attached via amide bond formation.

Sequence	X =	Probe	Mass calculated	Mass found
ODN4 5′-CGCTTC**X**GTATCTATATTCATC	AP-C6	d1[a]-Y/A	6803	6804
	AP-C6-(TO)	d1[a]-TO/A	7177	7176
	AP-C6-(6-RX)	d1[a]-Y/RX	7319	7319
	AP-C6-(TO/RX)	d1[a]-TO/RX	7693	7693
ODN5 5′-CGCTTC**X**GTATCTA**X**ATTCATC	AP-C6	d2[a]-Y/A	6980	6978
	AP-C6-(TO)	d2[a]-TO/A	7728	7726
	AP-C6-(RX)	d2[a]-Y/RX	8012	8012
	AP-C6-(TO/RX)	d2[a]-TO/RX	8760	8759
ODN6 5′-CGCT**X**CTGTA**X**CTATA**X**TCATC	AP-C6	d3[a]-Y/A	7157	7156
	AP-C6-(TO)	d3[a]-TO/A	8279	8279
	AP-C6-(RX)	d3[a]-Y/RX	8705	8704
	AP-C6-(TO/RX)	d3[a]-TO/RX	9827	9824

Note: In probe names, d = DNA oligo, [a] = AP-C6 dT modified oligo, number = probe number, A = unlabelled amine, Y = unlabelled alkyne, TO = labelled with thiazole orange, RX = labelled with ROX, TO/RX = labelled with thiazole orange and ROX.

Table S. 5. Mass data on short RNA probes with the AP-C3 dT and AP-C6 dT modification labelled with dyes. In the table TO_{B3} stands for TO_{B3}-N_3 and 5-RX stands for ROX-N_3 attached via CuAAC and 6-RX strands for ROX-NHS ester and TO_{B6} stands for TO_{B6}-NHS ester attached via amide bond formation.

Sequence	X =	Probe	Mass calculated	Mass found
5′-rGCAC**X**CUACG (all 2′OMe but X)	AP-C3	s-r1-Y/A	3378	3378
	AP-C3-(TO_{B3})	s-r1-TO/A	3752	3752
	AP-C3-(6-RX)	s-r1-Y/RX	3894	3895
	AP-C3-(TO_{B3}/6-RX)	s-r1-TO/RX	4268	4269
	AP-C3-(TO_{B6})	s-r1-Y/TO	3765	3765
	AP-C3-(5-RX)	s-r1-RX/A	3994	3995
	AP-C3-(5-RX/TO_{B6})	s-r1-RX/TO	4381	4381
5′-rGCAC**X**CUACG (all 2′OMe but X)	AP-C6	s-r1^a-Y/A	3420	3421
	AP-C6-(TO_{B3})	s-r1^a-TO/A	3794	3795
	AP-C6-(6-RX)	s-r1^a-Y/RX	3936	3937
	AP-C6-(TO_{B3}/6-RX)	s-r1^a-TO/RX	4310	4310
	AP-C6-(TO_{B6})	s-r1^a-Y/TO	3807	3806
	AP-C6-(5-RX)	s-r1^a-RX/A	4036	4037
	AP-C6-(5-RX/TO_{B6})	s-r1^a-RX/TO	4423	4423
5′-dCGTAGAGTGC	**Target**		3068	3068
5′-rCGUAGAGUGC	**Target**		3200	3200

Note: In probe names, d = DNA oligo, r = RNA oligo, ^{a} = AP-C6 dT modified oligo, number = probe number, A = unlabelled amine, Y = unlabelled alkyne, TO = labelled with thiazole orange, RX = labelled with ROX, TO/RX = labelled with thiazole orange and ROX.

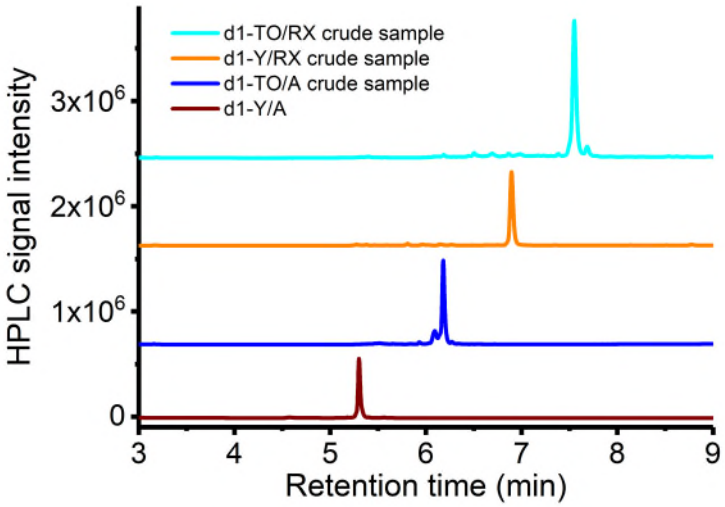

Figure S 1. HPLC chromatograms of d1-Y/A before (brown trace) and after reaction with TO azide (blue trace), ROX NHS ester (orange trace), and both ROX NHS ester and TO azide (cyan trace).

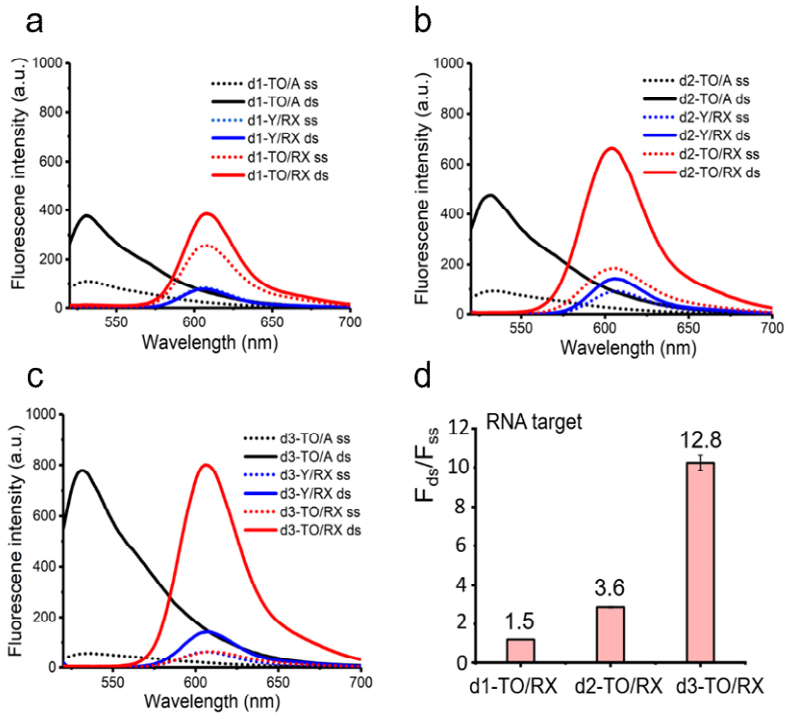

Figure S 2. Fluorescence spectra of TO, RX or TO/RX-functionalised DNA probes to RNA target when excitation wavelength was 510 nm. (a) Fluorescence spectra of 0.25 µM single TO, RX or TO/RX-functionalised DNA probes to 0.275 µM RNA target. (b) Fluorescence spectra of 0.25 µM double TO, RX or TO/RX-functionalised DNA probes to 0.275 µM RNA target. (c) Fluorescence spectra of 0.25 µM triple TO, RX or TO/RX-functionalised DNA probes to 0.275 µM RNA target. (d) Ratios of fluorescence intensity of TO/RX-functionalised DNA probes before and after hybridization with RNA target. Conditions: 10 mM Na-phosphate buffer, 200 mM NaCl, pH 7.0. Data points were measured in triplicate.

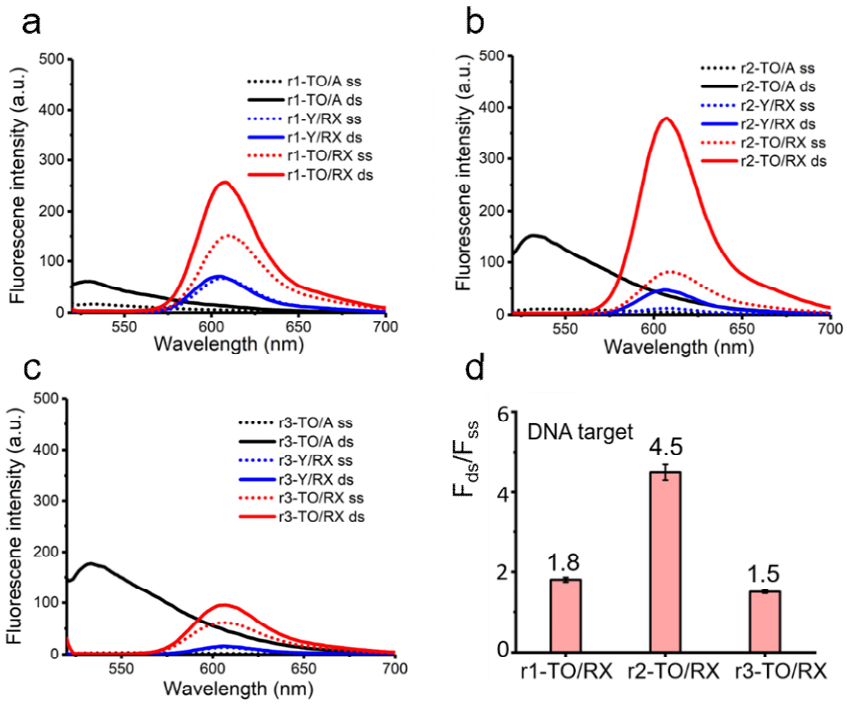

Figure S 3. Fluorescence spectra of TO, RX or TO/RX-functionalised 2′-OMe RNA probes to DNA target when excitation wavelength was 510 nm. (a) Fluorescence spectra of 0.25 μM single TO, RX or TO/RX-functionalised 2′-OMe RNA probes to 0.275 μM DNA target. (b) Fluorescence spectra of 0.25 μM double TO, RX or TO/RX-functionalised 2′-OMe RNA probes to 0.275 μM DNA target. (c) Fluorescence spectra of 0.25 μM triple TO, RX or TO/RX-functionalised 2′-OMe RNA probes to 0.275 μM DNA target. (d) Ratios of fluorescence intensity of TO/RX-functionalised 2′-OMe RNA probes before and after hybridization with DNA target. Conditions: 10 mM Na-phosphate buffer, 200 mM NaCl, pH 7.0. Data points were measured in triplicate.

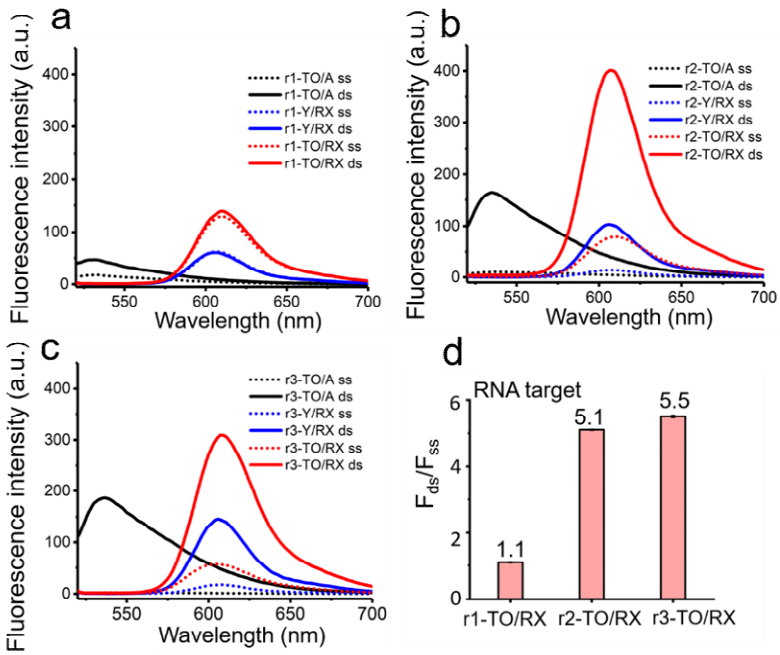

Figure S 4. Fluorescence spectra of TO, RX or TO/RX-functionalised 2′-OMe RNA probes to RNA target when excitation wavelength was 510 nm. (a) Fluorescence spectra of 0.25 μM single TO, RX or TO/RX-functionalised 2′-OMe RNA probes to 0.275 μM RNA target. (b) Fluorescence spectra of 0.25 μM double TO, RX or TO/RX-functionalised 2′-OMe RNA probes to 0.275 μM RNA target. (c) Fluorescence spectra of 0.25 μM triple TO, RX or TO/RX-functionalised 2′-OMe RNA probes to 0.275 μM RNA target. (d) Ratios of fluorescence intensity of TO/RX-functionalised 2′-OMe RNA probes before and after hybridization with RNA target. Conditions: 10 mM Na-phosphate buffer, 200 mM NaCl, pH 7.0. Data points were measured in triplicate.

Table S. 6. Fluorescence emission data for DNA probes against DNA target. F_{ds}/F_{ss} – ratio of fluorescence emission at $\lambda_{em, max}$ of oligonucleotide duplexes to single-stranded, $I_{0, max}$– fluorescence emission intensity at $\lambda_{em, max}$ of single-stranded oligonucleotides probes, I_{max} – fluorescence emission intensity at $\lambda_{em, max}$ of probe-target duplexes. [a] – saturation of detector. Conditions: Probe concentration 0.25 μM, target concentration 0.275 μM in 10 mM Na-phosphate buffer, 200 mM NaCl, pH 7.0. Data points were measured in triplicate.

λ_{ex}	Probe	F_{ds}/F_{ss} at $\lambda_{em, max}$	$I_{0, max}$	I_0 error	I_{max}	I_{max} error	$\lambda_{em, max}$ probe-target
484 nm	d1-TO/A	2.4	73.7	0.2	178.1	0.9	528
	d1-Y/RX	0.9	36.6	0.6	32.8	0.4	607
	d1-TO/RX	1.4	174.4	2.5	236.0	1.7	606
	d2-TO/A	3.5	86.8	1.6	307.9	0.1	528
	d2-Y/RX	1.5	37.8	1.6	58.2	0.9	607
	d2-TO/RX	3.2	178.6	0.7	567.7	0.7	607
	d3-TO/A	10.0	43.0	0.1	428.7	3.9	531
	d3-Y/RX	2.5	31.4	0.0	78.5	1.6	608
	d3-TO/RX	7.4	104.2	0.4	772.9	3.6	606
510 nm	d1-TO/A	2.4	103.3	0.6	249.8	0.1	527
	d1-Y/RX	0.9	74.5	0.4	68.9	0.8	607
	d1-TO/RX	1.5	240.9	2.5	353.4	8.5	605
	d2-TO/A	4.6	93.0	0.8	424.8	1.8	528
	d2-Y/RX	1.5	75.9	1.5	116.5	2.2	607
	d2-TO/RX	5.9	135.9	2.4	804.3	4.1	606
	d3-TO/A	13.5	42.4	0.1	571.9	8.1	530
	d3-Y/RX	2.5	62.5	1.7	153.2	5.8	606
	d3-TO/RX	>16.7	59.8	0.5	1000.0[a]	0.0	601
570 nm	d1-TO/A	0.6	4.4	0.9	2.5	0.0	578
	d1-Y/RX	0.9	347.8	3.0	322.2	0.5	605
	d1-TO/RX	1.8	136.6	0.1	249.1	0.9	605
	d2-TO/A	1.3	2.7	0.3	3.5	0.8	578
	d2-Y/RX	1.5	343.1	5.2	525.8	8.2	606
	d2-TO/RX	5.5	103.5	1.1	564.3	1.8	606
	d3-TO/A	3.0	2.7	0.4	8.1	1.6	578
	d3-Y/RX	2.4	277.5	5.5	668.4	11.2	607
	d3-TO/RX	13.2	58.3	0.7	772.3	6.1	605

Table S. 7. Fluorescence emission data for DNA probes against RNA target. F_{ds}/F_{ss} – ratio of fluorescence emission at $\lambda_{em,\ max}$ of oligonucleotide duplexes to single-stranded, $I_{0,\ max}$– fluorescence emission intensity at $\lambda_{em,\ max}$ of single-stranded oligonucleotides probes, I_{max} – fluorescence emission intensity at $\lambda_{em,\ max}$ of probe-target duplexes. Conditions: Probe concentration 0.25 μM, target concentration 0.275 μM in 10 mM Na-phosphate buffer, 200 mM NaCl, pH 7.0. Data points were measured in triplicate.

λ_{ex}	Probe	F_{ds}/F_{ss} at $\lambda_{em,\ max}$	$I_{0,\ max}$	I_0 error	I_{max}	I_{max} error	$\lambda_{em,\ max}$ probe-target
484 nm	d1-TO/A	3.1	80.8	0.4	251.5	6.3	531
	d1-Y/RX	0.9	42.1	1.4	37.8	1.6	607
	d1-TO/RX	1.3	188.9	1.4	248.4	0.2	608
	d2-TO/A	4.1	84.0	1.6	347.4	8.8	531
	d2-Y/RX	1.9	36.7	2.7	70.6	1.5	607
	d2-TO/RX	2.1	215.7	0.3	449.4	4.8	605
	d3-TO/A	11.5	48.1	0.2	551.6	0.6	532
	d3-Y/RX	2.2	32.2	2.9	72.2	1.2	607
	d3-TO/RX	6.2	92.0	0.1	569.0	10.0	607
510 nm	d1-TO/A	3.4	111.1	0.9	372.5	5.1	531
	d1-Y/RX	0.9	83.3	2.3	77.9	1.8	605
	d1-TO/RX	1.5	260.1	2.0	386.6	1.3	609
	d2-TO/A	5.1	94.2	2.3	484.5	8.9	532
	d2-Y/RX	1.6	91.2	2.0	142.9	3.3	606
	d2-TO/RX	3.6	180.2	3.3	656.5	6.2	604
	d3-TO/A	13.6	56.9	1.8	776.1	2.4	532
	d3-Y/RX	2.3	63.2	1.6	142.4	3.7	608
	d3-TO/RX	12.8	62.6	2.1	801.2	6.4	606
570 nm	d1-TO/A	1.0	3.1	0.3	3.1	0.6	578
	d1-Y/RX	0.9	387.2	6.3	358.7	2.0	607
	d1-TO/RX	1.3	156.3	0.4	204.1	0.4	607
	d2-TO/A	1.6	3.4	0.1	5.5	0.0	578
	d2-Y/RX	1.6	406.8	8.1	646.6	16.3	606
	d2-TO/RX	2.7	166.2	6.3	445.5	4.4	604
	d3-TO/A	2.1	4.3	0.4	9.0	0.5	578
	d3-Y/RX	2.3	266.1	7.0	601.3	16.2	607
	d3-TO/RX	9.4	59.8	5.3	564.6	3.1	606

Table S. 8. Fluorescence emission data for 2′-OMe long RNA probes against DNA target. F_{ds}/F_{ss} – ratio of fluorescence emission at $\lambda_{em, max}$ of oligonucleotide duplexes to single-stranded, $I_{0, max}$– fluorescence emission intensity at $\lambda_{em, max}$ of single-stranded oligonucleotides probes, I_{max} – fluorescence emission intensity at $\lambda_{em, max}$ of probe-target duplexes. Conditions: Probe concentration 0.25 μM, target concentration 0.275 μM in 10 mM Na-phosphate buffer, 200 mM NaCl, pH 7.0. Data points were measured in triplicate.

λ_{ex}	Probe	F_{ds}/F_{ss} at $\lambda_{em, max}$	$I_{0, max}$	I_0 error	I_{max}	I_{max} error	$\lambda_{em, max}$ probe-target
484 nm	r1-TO/A	3.4	12.5	0.2	42.5	0.1	529
	r1-Y/RX	1.1	32.2	0.1	34.6	0.3	603.5
	r1-TO/RX	1.6	116.8	3.7	181.7	2.8	608
	r2-TO/A	9.0	12.1	0.5	109.4	2.4	533
	r2-Y/RX	3.6	6.0	0.5	21.9	0.2	605.5
	r2-TO/RX	2.4	116.3	2.0	280.4	0.7	608
	r3-TO/A	36.0	3.5	0.0	127.4	2.1	531.5
	r3-Y/RX	1.2	7.3	0.4	8.3	0.4	608
	r3-TO/RX	1.4	57.1	3.3	82.7	0.8	611
510 nm	r1-TO/A	3.9	15.5	0.7	59.9	1.1	527.5
	r1-Y/RX	1.1	67.5	0.5	71.1	0.2	605
	r1-TO/RX	1.8	144.8	5.6	253.6	3.4	608
	r2-TO/A	14.2	10.9	0.3	154.3	2.2	531.5
	r2-Y/RX	3.9	11.9	0.0	46.9	0.0	605.5
	r2-TO/RX	4.5	82.7	1.3	374.2	5.5	607.5
	r3-TO/A	64.4	2.8	0.1	180.4	3.4	533.5
	r3-Y/RX	1.2	14.6	0.9	17.0	0.8	606.5
	r3-TO/RX	1.5	59.8	1.7	92.4	3.1	606.5
570 nm	r1-TO/A	0.9	5.1	1.4	4.8	1.4	578
	r1-Y/RX	1.1	318.4	5.4	341.8	4.1	604
	r1-TO/RX	1.7	79.1	2.3	136.1	0.5	606
	r2-TO/A	1.4	2.8	0.6	3.7	0.8	578
	r2-Y/RX	3.5	62.3	0.1	219.6	8.0	605.5
	r2-TO/RX	3.1	71.1	1.1	223.8	3.7	604.5
	r3-TO/A	2.9	11.7	1.7	33.4	10.1	578
	r3-Y/RX	1.2	65.2	4.2	75.6	4.8	607
	r3-TO/RX	1.1	208.9	0.7	228.0	2.3	601.5

Table S. 9. Fluorescence emission data for 2′-OMe long RNA probes against RNA target. F_{ds}/F_{ss} – ratio of fluorescence emission at $\lambda_{em, max}$ of oligonucleotide duplexes to single-stranded, $I_{0, max}$– fluorescence emission intensity at $\lambda_{em, max}$ of single-stranded oligonucleotides probes, I_{max} – fluorescence emission intensity at $\lambda_{em, max}$ of probe-target duplexes. Conditions: Probe concentration 0.25 μM, target concentration 0.275 μM in 10 mM Na-phosphate buffer, 200 mM NaCl, pH 7.0. Data points were measured in triplicate.

λ_{ex}	Probe	F_{ds}/F_{ss} at $\lambda_{em, max}$	$I_{0, max}$	I_0 error	I_{max}	I_{max} error	$\lambda_{em, max}$ probe-target
484 nm	r1-TO/A	2.6	13.2	0.0	33.6	0.2	530
	r1-Y/RX	1.0	29.7	0.3	30.3	0.5	607
	r1-TO/RX	1.0	105.6	0.6	107.7	0.2	612.5
	r2-TO/A	9.6	11.3	0.5	108.8	0.2	534.5
	r2-Y/RX	7.1	6.8	0.3	48.3	3.1	607
	r2-TO/RX	2.5	107.9	3.0	269.5	7.4	607
	r3-TO/A	45.0	2.9	0.3	129.3	1.1	537.5
	r3-Y/RX	8.2	8.6	0.1	70.4	0.1	607.5
	r3-TO/RX	4.4	52.8	1.2	232.3	2.5	610
510 nm	r1-TO/A	2.7	17.2	0.1	47.2	0.4	531.5
	r1-Y/RX	1.0	63.4	1.5	61.8	1.3	606.5
	r1-TO/RX	1.1	130.4	1.1	140.4	1.0	610
	r2-TO/A	15.6	10.4	0.1	162.4	2.0	535
	r2-Y/RX	7.9	13.6	0.2	108.0	4.9	606
	r2-TO/RX	5.1	75.6	3.0	387.0	14.5	607.5
	r3-TO/A	79.3	2.3	0.1	186.3	0.2	536.5
	r3-Y/RX	8.5	17.1	0.1	144.9	0.9	606
	r3-TO/RX	5.5	56.3	0.4	309.9	0.7	608
570 nm	r1-TO/A	1.6	3.1	0.4	4.8	0.4	578
	r1-Y/RX	1.0	300.8	5.8	296.8	5.6	606
	r1-TO/RX	0.9	71.0	0.9	63.9	0.6	605.5
	r2-TO/A	2.3	2.5	0.5	5.8	0.1	578
	r2-Y/RX	8.2	62.8	0.2	517.4	13.0	606.5
	r2-TO/RX	3.5	66.9	2.5	232.4	9.9	607
	r3-TO/A	1.1	10.0	3.4	10.8	3.2	578
	r3-Y/RX	7.5	78.3	0.9	588.0	8.2	607.5
	r3-TO/RX	1.7	202.8	4.5	340.4	3.0	603.5

Table S. 10. Fluorescence emission data for 2′-OMe short RNA probes against DNA target. F_{ds}/F_{ss} – ratio of fluorescence emission at $\lambda_{em,\ max}$ of oligonucleotide duplexes to single-stranded, $I_{0,\ max}$– fluorescence emission intensity at $\lambda_{em,\ max}$ of single-stranded oligonucleotides probes, I_{max} – fluorescence emission intensity at $\lambda_{em,\ max}$ of probe-target duplexes. Conditions: Probe concentration 0.25 μM, target concentration 0.275 μM in 10 mM Na-phosphate buffer, 200 mM NaCl, pH 7.0. Data points were measured in triplicate.

λ_{ex}	Probe	F_{ds}/F_{ss} at $\lambda_{em,\ max}$	I_0 max	I_0 error	I_{max}	I_{max} error	$\lambda_{em,\ max}$ ds
484 nm	s-r1-TO/A	17.9	10.9	0.1	194.4	2.8	532.3
	s-r1-Y/RX	1.1	28.9	0.3	30.6	0.1	600.8
	s-r1-TO/RX	1.4	116.0	1.6	167.8	1.6	607.8
	s-r1-Y/TO	10.2	7.2	0.1	72.7	0.9	531.3
	s-r1-RX/A	1.0	22.8	0.1	23.5	0.1	612.0
	s-r1-RX/TO	1.6	125.1	2.9	202.0	5.5	614.0
	s-r1^a-TO/A	20.5	9.0	0.3	185.6	2.4	533.0
	s-r1^a-Y/RX	1.1	28.5	1.7	31.3	1.7	607.0
	s-r1^a-TO/RX	2.9	106.2	0.9	305.1	4.9	607.0
	s-r1^a-Y/TO	20.0	6.7	0.2	133.0	2.3	529.5
	s-r1^a-RX/A	1.0	24.6	1.4	25.5	1.0	613.0
	s-r1^a-RX/TO	1.5	145.5	0.6	220.7	2.7	613.3
510 nm	s-r1-TO/A	21.8	13.1	0.9	283.7	3.0	532.8
	s-r1-Y/RX	1.2	49.0	1.3	57.8	0.2	601.8
	s-r1-TO/RX	1.9	124.8	2.8	232.6	2.4	608.3
	s-r1-Y/TO	13.1	8.3	0.1	108.5	2.9	531.0
	s-r1-RX/A	1.1	42.1	0.6	47.7	0.6	611.5
	s-r1-RX/TO	2.3	131.5	0.7	302.6	5.4	615.3
	s-r1^a-TO/A	26.7	10.2	0.2	271.4	4.5	535.5
	s-r1^a-Y/RX	1.3	47.8	3.2	61.5	3.0	605.5
	s-r1^a-TO/RX	4.0	115.2	0.6	465.8	6.9	607.3
	s-r1^a-Y/TO	24.0	8.4	0.3	200.5	2.3	530.0
	s-r1^a-RX/A	1.2	40.8	1.1	50.4	0.7	611.8
	s-r1^a-RX/TO	2.1	158.9	0.7	331.6	7.3	613.3
570 nm	s-r1-Y/RX	1.0	196.5	4.8	197.0	4.1	604.5
	s-r1-TO/RX	1.5	87.9	3.4	136.0	1.9	605.3
	s-r1-RX/A	1.0	216.8	0.4	216.2	0.3	612.5
	s-r1-RX/TO	1.8	90.7	0.5	165.5	2.3	612.5

s-r1[a]-Y/RX	1.0	256.4	9.4	248.9	4.5	606.5
s-r1[a]-TO/RX	2.5	96.2	2.2	239.8	0.5	607.0
s-r1[a]-RX/A	1.1	214.7	0.4	226.2	1.2	611.5
s-r1[a]-RX/TO	1.6	112.7	1.5	183.9	3.8	612.3

Table S. 11. Fluorescence emission data for 2′-OMe short RNA probes against DNA target. F_{ds}/F_{ss} – ratio of fluorescence emission at $\lambda_{em,\ max}$ of oligonucleotide duplexes to single-stranded, $I_{0,\ max}$– fluorescence emission intensity at $\lambda_{em,\ max}$ of single-stranded oligonucleotides probes, I_{max} – fluorescence emission intensity at $\lambda_{em,\ max}$ of probe-target duplexes. Conditions: Probe concentration 0.25 μM, target concentration 0.275 μM in 10 mM Na-phosphate buffer, 200 mM NaCl, pH 7.0. Data points were measured in triplicate.

λ_{ex}	Probe	F_{ds}/F_{ss} at $\lambda_{em,\ max}$	I_0 max	I_0 error	I_{max}	I_{max} error	$\lambda_{em,\ max}$ ds
484 nm	s-r1-TO/A	23.8	10.9	0.1	217.5	3.3	534.8
	s-r1-Y/RX	1.2	28.9	0.3	33.2	0.3	601.8
	s-r1-TO/RX	1.5	116.0	1.6	171.6	0.2	609.0
	s-r1-Y/TO	8.8	7.2	0.1	62.2	0.6	534.8
	s-r1-RX/A	1.1	22.8	0.1	26.7	0.4	611.0
	s-r1-RX/TO	1.7	125.1	2.9	215.7	2.1	612.5
	s-r1[a]-TO/A	14.4	9.0	0.3	133.8	0.1	534.8
	s-r1[a]-Y/RX	1.1	28.5	1.7	31.7	0.1	606.0
	s-r1[a]-TO/RX	1.7	106.2	0.9	171.2	1.4	608.0
	s-r1[a]-Y/TO	17.3	6.7	0.2	108.4	3.7	533.3
	s-r1[a]-RX/A	1.1	24.6	1.4	27.2	0.2	611.5
	s-r1[a]-RX/TO	1.8	145.5	0.6	264.7	1.3	611.8
510 nm	s-r1-TO/A	26.9	13.1	0.9	327.8	5.9	533.5
	s-r1-Y/RX	1.3	49.0	1.3	63.8	0.4	599.8
	s-r1-TO/RX	2.0	124.8	2.8	245.3	1.5	608.3
	s-r1-Y/TO	11.1	8.3	0.1	90.4	1.0	534.8
	s-r1-RX/A	1.3	42.1	0.6	52.3	0.4	611.5
	s-r1-RX/TO	2.0	131.5	0.7	308.2	1.6	611.8
	s-r1[a]-TO/A	18.4	10.2	0.2	197.8	0.5	534.5
	s-r1[a]-Y/RX	1.3	47.8	3.2	63.0	0.6	605.5
	s-r1[a]-TO/RX	2.2	115.2	0.6	247.4	6.3	607.5
	s-r1[a]-Y/TO	22.2	8.4	0.3	161.9	4.1	533.8
	s-r1[a]-RX/A	1.4	40.8	1.1	54.2	0.6	611.5
	s-r1[a]-RX/TO	2.6	158.9	0.7	411.5	0.8	611.0
570 nm	s-r1-Y/RX	1.2	196.5	4.8	228.6	2.9	602.5
	s-r1-TO/RX	1.7	87.9	3.4	145.9	1.1	604.8
	s-r1-RX/A	1.1	216.8	0.4	236.8	1.6	611.8
	s-r1-RX/TO	1.7	90.7	0.5	171.2	1.2	611.0
	s-r1[a]-Y/RX	1.1	256.4	9.4	267.8	0.5	606.3

	s-r1[a]-TO/RX	1.6	96.2	2.2	156.0	3.4	605.0
	s-r1[a]-RX/A	1.1	214.7	0.4	242.5	2.6	611.5
	s-r1[a]-RX/TO	2.1	112.7	1.5	230.7	1.0	611.3

Table S. 12. Time-resolved fluorescence data for d1- to d3-TO/A, r1- to r3-TO/A and r1 to r3-TO/RX probes against DNA and RNA targets. Excitation wavelength was 475 nm. Emission wavelength is 530 nm for d/r1- to d/r3-TO/A probes and is 610 nm for r1- to r3-TO/RX probes. Samples were made up to 1 μM of each probe with 1.1 μM of DNA and RNA targets in buffer (10 mM Na-phosphate, 200 mM NaCl, pH = 7.0). Data points were measured in triplicate.

Probe:Target	**τ_1 (ns)**	**a_1**	**τ_2 (ns)**	**a_2**	**$\langle\tau\rangle$ (ns)**	**$\langle\tau\rangle_{ds/ss}$**
d1-TO/A	1.10	0.67	3.73	0.33	1.97	
d1-TO/A:DNA	1.49	0.50	4.37	0.50	2.93	1.48
d1-TO/A:RNA	1.50	0.33	4.56	0.67	3.54	1.79
d2-TO/A	1.11	0.67	4.29	0.33	2.17	
d2-TO/A:DNA	1.23	0.50	3.90	0.50	2.56	1.18
d2-TO/A:RNA	1.27	0.33	4.27	0.67	3.27	1.50
d3-TO/A	0.88	0.67	4.04	0.33	1.93	
d3-TO/A:DNA	1.10	0.43	3.88	0.57	2.69	1.39
d3-TO/A:RNA	1.09	0.33	4.55	0.67	3.39	1.75
r1-TO/A	0.18	0.26	2.73	0.74	2.08	
r1-TO/A:DNA	0.62	0.33	3.50	0.67	2.56	1.23
r1-TO/A:RNA	0.24	0.16	2.61	0.84	2.24	1.08
r2-TO/A	0.19	0.24	3.14	0.76	2.44	
r2-TO/A:DNA	0.25	0.13	3.15	0.87	2.76	1.13
r2-TO/A:RNA	0.23	0.10	3.44	0.90	3.11	1.27
r3-TO/A	0.15	0.28	2.07	0.72	1.53	
r3-TO/A:DNA	0.22	0.19	2.92	0.81	2.40	1.57
r3-TO/A:RNA	0.22	0.18	3.39	0.82	2.81	1.83

Table S 13. Mass data on FIP and BIP with the AP-C6 dT modification labelled with dyes.

Sequence	X =	Probe	Mass calculated	Mass found
5′-TCAGTACTAGTGCCXGTGCCCACAATCGTTTTTAAACGGGT	AP-C6-(TO_{B6}-NHS)	F-d1-Y/TO	13130	13130
	AP-C6-(TAMRA-N_3/TO_{B6}-NHS)	F-d1-TA/TO	13642	13642
5′-TCAGXACTAGTGCCXGTGCCCACAATCGTTTTTAAACGGGT	AP-C6-(TO_{B6}-NHS)	F-d2-Y/TO	13693	13694
	AP-C6-(TAMRA-N_3/TO_{B6}-NHS)	F-d2-TA/TO	14717	14718
	AP-C6-(TO_{B6}-N_3)	F-d2-TO/A	13751	13752
5′-TCGTATACAGGGCXTTTGACATCTATCTTGGAAGCGACAACAA	AP-C6-(TO_{B6}-NHS)	B-d1-Y/TO	13789	13789
	AP-C6-(TAMRA-N_3/TO_{B6}-NHS)	B-d1-TA/TO	14301	14301
5′-TCGXATACAGGGCXTTTGACATCTATCTTGGAAGCGACAACAA	AP-C6-(TO_{B6}-NHS)	B-d2-Y/TO	14353	14352
	AP-C6-(TAMRA-N_3/TO_{B6}-NHS)	B-d2-TA/TO	15377	15377
	AP-C6-(TO_{B6}-N_3)	B-d2-TO/A	14411	14409

Note: in probe names, d = DNA oligo, number = probe number, F= forward primer, B= backward primer, A = unlabelled amine, Y = unlabelled alkyne, TO = labelled with thiazole orange, TA = labelled with TAMRA, TA/TO = labelled with thiazole orange and TAMRA.

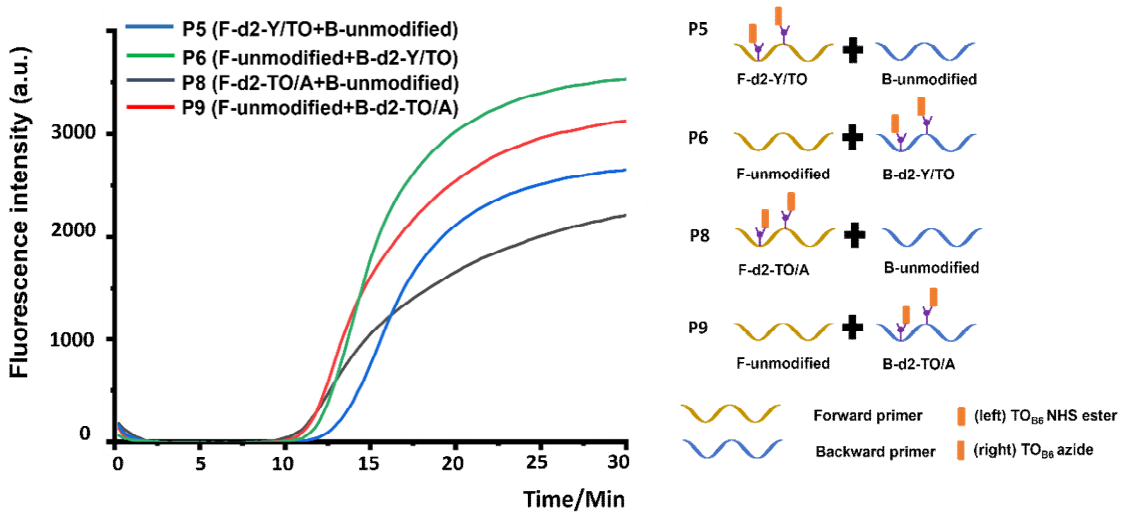

Figure S 5. LAMP amplification of P5-P6 (blue line, green line) and P8-P9 (black line, red line). 5.0 µL extracted RNA template was added in the mixture of 7.5 µL of 2X LAMP master mix (a blend of dNTPs, Bst 2.0 WarmStart DNA Polymerase and WarmStart RTx Reverse Transcriptase in an optimized LAMP buffer solution), 1.5 µL of 10X primer mix (16 µM), 1.5 µL of FIP (16 µM), BIP (16 µM) and 2 µL H_2O into 50 µL PCR tubes. Vortex the mixture and centrifuge it for 30 seconds. Incubate the PCR tubes at 65 °C. LAMP was undertaken using a BioRad CFX96 Real-Time PCR Instrument, with CFX Manager software (BioRad), monitoring in the following channels: TET channel (excitation range 515–535 nm, detector range 560–580 nm), Primers' sequences were shown in Table S13. Data points were measured in triplicate.

References

References

(1) Belmont, P.; Constant, J. F.; Demeunynck, M. Nucleic acid conformation diversity: from structure to function and regulation. *Chem. Soc. Rev.* **2001**, *30* (1), 70-81.

(2) Blackburn, G. M.; Gait, M. J.; Loakes, D.; Williams, D. M. Chapter 2. DNA and RNA Structure. *Nucleic Acids in Chemistry and Biology*. **2007**; 13-76.

(3) Chargaff, E.; Lipshitz, R.; Green, C. Composition of the Desoxypentose Nucleic Acids of Four Genera of Sea-Urchin. *J.Biol.Chem.* **1952**, *195* (1), 155-160.

(4) Franklin, R. E.; Gosling, R. G. Molecular Configuration in Sodium Thymonucleate. *Nature* **1953**, *171* (4356), 740-741.

(5) Wilkins, M. H. F.; Seeds, W. E.; Stokes, A. R.; Wilson, H. R. Helical Structure of Crystalline Deoxypentose Nucleic Acid. *Nature* **1953**, *172* (4382), 759-762.

(6) Waston, J. D.; Crick, F. H. C. Molecular Structure of Nucleic Acids: A Structure for Deoxyribose Nucleic Acid. *Nature* **1953**, *171*, 737-738.

(7) Hoogsteen, K. The crystal and molecular structure of a hydrogen-bonded complex between 1-methylthymine and 9-methyladenine. *Acta Cryst.* **1963**, *16*, 907.

(8) Wang, A.; Quigley, G. J.; Kolpak, F. J.; Crawford, J. L.; van Boom, J. H.; van der Marel, G.; Rich, A. Molecular structure of a left-handed double helical DNA fragment at atomic resolution. *Nature* **1979**, *282*, 680-686.

(9) Hamilton, P. L.; Arya, D. P. Natural product DNA major groove binders. *Nat Prod Rep* **2012**, *29* (2), 134-143.

(10) Baraldi, P. G.; Bovero, A.; Fruttarolo, F.; Preti, D.; Tabrizi, M. A.; Pavani, M. G.; Romagnoli, R. DNA minor groove binders as potential antitumor and antimicrobial agents. *Med Res Rev* **2004**, *24* (4), 475-528.

(11) Kopka, M. L.; Dickerson, R. E.; Drew, R. H.; Conner, B. N.; Wing, R. M.; Fratini, A. V. The Anatomy of A-, B-, and Z-DNA. *Science* **1982**, *216* (4545), 475-485.

(12) Brown, T. *Nucleic acids book*, https://atdbio.com/nucleic-acids-book.

(13) Hall, R. H.; Todd, A.; Webb, R. F. Nucleotides. Part XLI. Mixed anhydrides as intermediates in the synthesis of dinucleoside phosphates. *J. Chem. Soc.* **1957**, 3291-3296.

(14) Michelson, A. M.; Todd, A.; Nucleotides part XXXII. Synthesis of a dithymidine dinucleotide containing a 3′: 5′-internucleotidic linkage. *J. Chem. Soc.* **1955**, 2632-2638.

(15) Letsinger, R. L.; Mahadevan, V. Stepwise Synthesis of Oligodeoxyribonucleotides on an Insoluble Polymer Support. *J. Am. Chem. Soc.* **1966**, *88*, 5319-5324.

(16) Beaucage, S. L.; Caruthers, M. H. Deoxynucleoside phosphoramidites—A new class of key intermediates for deoxypolynucleotide synthesis. *Tetrahedron Lett.* **1981**, *22*, 1859-1862.

(17) McBride, L. J.; Caruthers, M. H. An investigation of several deoxynucleoside phosphoramidites useful for synthesizing deoxyoligonucleotides. *Tetrahedron Lett.* **1983**, *24*, 245-248.

(18) Beaucage, S. L.; Iyer, R. P. The Functionalization of Oligonucleotides Via Phosphoramidite Derivatives. *Tetrahedron* **1993**, *49*, 1925-1963.

(19) Thorpe, C.; Epple, S.; Woods, B.; El-Sagheer, A. H.; Brown, T. Synthesis and biophysical properties of carbamate-locked nucleic acid (LNA) oligonucleotides with potential antisense applications. *Org. Biomol. Chem.* **2019**, *17* (21), 5341-5348.

(20) Kumar, P.; Truong, L.; Baker, Y. R.; El-Sagheer, A. H.; Brown, T. Synthesis, Affinity for Complementary RNA and DNA, and Enzymatic Stability of Triazole-Linked Locked Nucleic Acids (t-LNAs). *ACS Omega* **2018**, *3* (6), 6976-6987.

(21) El-Sagheer, A. H.; Sanzone, A. P.; Gao, R.; Tavassoli, A.; Brown, T. Biocompatible artificial DNA linker that is read through by DNA polymerases and is functional in Escherichia coli. *Proceedings of the National Academy of Sciences* **2011**, *108* (28), 11338-11343.

(22) Wu, P. The Nobel Prize in Chemistry 2022: Fulfilling Demanding Applications with Simple Reactions. *ACS Chem. Biol.* **2022**, *17* (11), 2959-2961.

(23) Kolb, H. C.; Finn, M. G.; Sharpless, K. B. Click Chemistry: Diverse Chemical Function from a Few Good Reactions. *Angew. Chem.* **2001**, *40*, 2004-2021.

(24) Rostovtsev, V. V.; Green, L. G.; Fokin, V. V.; Sharpless, K. B. A Stepwise Huisgen Cycloaddition Process: Copper(I)-Catalyzed Regioselective "Ligation" of Azides and Terminal Alkynes. *Angew. Chem.* **2002**, *41*, 2596-2599.

(25) Sheehan, J. C.; Hess, G. P. A New Method of Forming Peptide Bonds. *J. Am. Chem. Soc.* **1955,** *77* 1067–1068.

(26) Carpino, L. A. 1-Hydroxy-7-Azabenzotriazole. An Efficient Peptide Coupling Additive. *J. Am. Chem. Soc.* **1993**, *115 (10)*, 4397–4398.

(27) Coste, J.; Nguyen, D. L.; Castro, B. PyBOP®: A New Peptide Coupling Reagent Devoid of Toxic by-Product. *Tetrahedron Lett.* **1990**, *31 (2)*, 205–208.

(28) Kasha, M. Characterization of Electronic Transitions in Complex Molecules. *Discuss. Faraday Soc.* **1950**, *9*, 14–19.

(29) Lakowicz, J. R. *Principles of Fluorescence Spectroscopy*; **2006**.

(30) Yuan, L.; Lin, W.; Zheng, K.; Zhu, S. FRET-Based Small-Molecule Fluorescent Probes: Rational Design and Bioimaging Applications. *Acc. Chem. Res.* **2013**, *46*, 1462–1473.

(31) Didenko, V. V. DNA probes using fluorescence resonance energy transfer (FRET): designs and applications. *Biotechniques* **2001**, *31*, 1106-1121.

(32) Dale, R. E.; Eisinger, J.; Blumberg, W. E. The orientational freedom of molecular probes. The orientation factor in intramolecular energy transfer. *Biophys. J.* **1979**, *26*, 161-193.

(33) Iqbal, A.; Arslan, S.; Okumus, B.; Wilson, T. J.; Giraud, G.; Norman, D. G.; Ha, T.; Lilley, D. M. Orientation dependence in fluorescent energy transfer between Cy3 and Cy5 terminally attached to double-stranded nucleic acids. *Proc. Natl. Acad. Sci.* **2008**, *105* (32), 11176-11181.

(34) Lewis, F. D.; Zhang, L.; Zuo, X. Orientation control of fluorescence resonance energy transfer using DNA as a helical scaffold. *J. Am. Chem. Soc.* **2005**, *127*, 10002-10003.

(35) Kwok, P. Methods for Genotyping Single Nuclotide Polymorphism. *Annu. Rev.Genomics Hum. Genet.* **2001**, *2*, 235–258.

(36) Ranasinghe, R. T.; Brown, T. Fluorescence based strategies for genetic analysis. *Chem Comm.* **2005**, (44), 5487-5502.

(37) Garcia, E.; Lebruska, L.; Laurent, M.; Shen, R.; Barker, D. Illumina universal bead arrays. *Meth. Enzymol* **2006**, *410* (5773), 58

(38) Didenko, V. V. *Fluorescent energy transfer nucleic acid probes: designs and protocols*. Springer Science & Business Media, **2006**.

(39) Tyagi, S.; Kramer, F. R. Molecular Beacon Probes That Fluoresce on Hybridization. *Nat. Biotechnol.* **1996**, *14 (3)*, 303–308.

(40) Tyagi, S.; Bratu, D. P.; Kramer, F. R. Multicolor Molecular Beacons for Allele Discrimination. . *Nat. Biotechnol.* **1996**, *16*, 49–53.

(41) Richardson, J. A.; Gerowska, M.; Shelbourne, M.; French, D.; Brown, T. Six-colour HyBeacon probes for multiplex genetic analysis. *Chembiochem* **2010**, *11* (18), 2530-2533.

(42) French, D. J.; Archard, C. L.; Andersen, M. T.; McDowell, D. G. Ultra-rapid DNA analysis using HyBeacon™ probes and direct PCR amplification from saliva. *Mol. Cell. Probes* **2002**, *16* (5), 319-326.

(43) French, D. J.; Archard, C. L.; Brown, T.; McDowell, D. G. HyBeaconTM probes: a new tool for DNA sequence detection and allele discrimination. *Mol. Cell. Probes* **2001**, *15* (6), 363-374.

(44) Marras, S. A. E. Selection of Fluorophore and Quencher Pairs for Fluorescent Nucleic Acid Hybridization Probes. *Fluorescent Energy Transfer Nucleic Acid Probes: Designs and Protocols* Humana Press, **2006**, 3-16.

(45) Tsourkas, A.; Behlke, M. A.; Rose, S. D.; Bao, G. Hybridization kinetics and thermodynamics of molecular beacons. *Nucleic Acids Res.* **2003**, *31* (4), 1319-1330.

(46) Tsourkas, A.; Behlke, M. A.; Bao, G. Structure–function relationships of shared-stem and conventional molecular beacons. *Nucleic Acids Res.* **2002**, *30* (19), 4208-4215.

(47) Hall, L. M.; Gerowska, M.; Brown, T. A highly fluorescent DNA toolkit: synthesis and properties of oligonucleotides containing new Cy3, Cy5 and Cy3B monomers. *Nucleic Acids Res.* **2012**, *40* (14), e108.

(48) Svanvik, N.; Westman, G.; Wang, D.; Kubista, M. Light-up probes: thiazole orange-conjugated peptide nucleic acid for detection of target nucleic acid in homogeneous solution. *Anal. Biochem.* **2000**, *281* (1), 26-35.

(49) Okamoto, A. ECHO probes: a concept of fluorescence control for practical nucleic acid sensing. *Chem. Soc. Rev.* **2011**, *40* (12), 5815-5828.

(50) Privat, E.; Melvin, T.; Mérola, F.; Schweizer, G.; Prodhomme, S.; Asseline, U.; Vigny, P. Fluorescent Properties of Oligonucleotide-conjugated Thiazole Orange Probes. *Photochem. Photobiol.* **2002**, *75* (3), 201-210.

(51) Hövelmann, F.; Seitz, O. DNA stains as surrogate nucleobases in fluorogenic hybridization probes. *Acc. Chem. Res.* **2016**, *49* (4), 714-723.

(52) Sato, T.; Sato, Y.; Nishizawa, S. Triplex-forming peptide nucleic acid probe having thiazole orange as a base surrogate for fluorescence sensing of double-stranded RNA. *J. Am. Chem. Soc.* **2016**, *138* (30), 9397-9400.

(53) Sato, T.; Sato, Y.; Nishizawa, S. Optimization of the Alkyl Linker of TO Base Surrogate in Triplex-Forming PNA for Enhanced Binding to Double-Stranded RNA. *Chem. Eur. J.* **2017**, *23* (17), 4079-4088.

(54) Walsh, S.; El-Sagheer, A. H.; Brown, T. Fluorogenic thiazole orange TOTFO probes stabilise parallel DNA triplexes at pH 7 and above. *Chem. Sci.* **2018**, *9* (39), 7681-7687.

(55) Lu, Y. J.; Deng, Q.; Hou, J. Q.; Hu, D. P.; Wang, Z. Y.; Zhang, K.; Luyt, L. G.; Wong, W. L.; Chow, C. F. Molecular engineering of thiazole orange dye: Change of fluorescent signaling from universal to specific upon binding with nucleic acids in bioassay. *ACS Chem. Biol.* **2016**, *11* (4), 1019-1029.

(56) Lubitz, I.; Zikich, D.; Kotlyar, A. Specific high-affinity binding of thiazole orange to triplex and G-quadruplex DNA. *Biochemistry* **2010**, *49* (17), 3567-3574.

(57) Isacsson, J.; Westman, G. Solid-phase synthesis of asymmetric cyanine dyes. *Tetrahedron Lett.* **2001**, *42* (18), 3207-3210.

(58) Lartia, R.; Asseline, U. New cyanine–oligonucleotide conjugates: relationships between chemical structures and properties. *Chem. Eur. J.* **2006**, *12* (8), 2270-2281.

(59) Rye, H. S.; Yue, S.; Wemmer, D. E.; Quesada, M. A.; Haugland, R. P.; Mathies, R. A.; Glazer, A. N. Stable fluorescent complexes of double-stranded DNA with bis-intercalating asymmetric cyanine dyes: properties and applications. *Nucleic Acids Res.* **1992**, *1992* (20), 2803-2812.

(60) Nygren, J.; Svanvic, N.; Kubista, M. The Interactions Between the Orange and DNA. *Biopolymers* **1998**, *46* (1), 39-51.

(61) Carreon, J. R.; Mahon, K. P.; Kelley, S. O. Thiazole orange− peptide conjugates: sensitivity of DNA binding to chemical structure. *Org. Lett.* **2004**, *6* (4), 517-519.

(62) Privat, E.; Asseline, U. Synthesis and Binding Properties of Oligo-2′-deoxyribonucleotides Covalently Linked to a Thiazole Orange Derivative. *Bioconjugate Chem.* **2001**, *12* (5), 757-769.

(63) Stadler, A. L.; Delos Santos, J. O.; Stensrud, E. S.; Dembska, A.; Silva, G. L.; Liu, S.; Shank, N. I.; Kunttas-Tatli, E.; Sobers, C. J.; Gramlich, P. M. Fluorescent DNA nanotags featuring covalently attached intercalating dyes: Synthesis, antibody conjugation, and intracellular imaging. *Bioconjugate Chem.* **2011**, *22* (8), 1491-1502.

(64) Spielmann, H. P.; Wemmer, D. E.; Jacobsen, J. P. Solution structure of a DNA complex with the fluorescent bis-intercalator TOTO determined by NMR spectroscopy. *Biochemistry* **1995**, *34* (27), 8542-8553.

(65) Ikeda, S.; Okamoto, A. Hybridization-Sensitive On–Off DNA Probe: Application of the Exciton Coupling Effect to Effective Fluorescence Quenching. *Chem.Asian J.* **2008**, *3* (6), 958-968.

(66) Ikeda, S.; Kubota, T.; Yuki, M.; Okamoto, A. Exciton-controlled hybridization-sensitive fluorescent probes: multicolor detection of nucleic acids. *Angew. Chem.* **2009**, *121* (35), 6602-6606.

(67) Sugizaki, K.; Okamoto, A. ECHO-LNA conjugates: hybridization-sensitive fluorescence and its application to fluorescent detection of various RNA strands. *Bioconjugate Chem.* **2010**, *21* (12), 2276-2281.

(68) Ikeda, S.; Yuki, M.; Yanagisawa, H.; Okamoto, A. Doubly thiazole orange-labeled cytidine for functional expansion of a hybridization-sensitive probe. *Tetrahedron Lett.* **2009**, *50* (51), 7191-7195.

(69) Qiu, J.; Wilson, A.; El-Sagheer, A. H.; Brown, T. Combination probes with intercalating anchors and proximal fluorophores for DNA and RNA detection. *Nucleic Acids Res.* **2016**, *44* (17), e138

(70) Hövelmann, F.; Bethge, L.; Seitz, O. Single Labeled DNA FIT Probes for Avoiding False-Positive Signaling in the Detection of DNA/RNA in qPCR or Cell Media. *ChemBioChem* **2012**, *13* (14), 2072-2081.

(71) Steinmeyer, J.; Walter, H. K.; Bichelberger, M. A.; Schneider, V.; Kubař, T.; Rönicke, F.; Olshausen, B.; Nienhaus, K.; Nienhaus, G. U.; Schepers, U. "siRNA traffic lights": arabino-configured 2′-anchors for fluorescent dyes are key for dual color readout in cell imaging. *Org. Biomol. Chem.* **2018**, *16* (20), 3726-3731.

(72) Wang, X.; Krull, U. J. Synthesis and fluorescence studies of thiazole orange tethered onto oligonucleotide: development of a self-contained DNA biosensor on a fiber optic surface. *Bioorg. Med.l Chem. Lett.* **2005**, *15* (6), 1725-1729.

(73) Micklefield, J. Backbone modification of nucleic acids: synthesis, structure and therapeutic applications. *Curr. Med. Chem.* **2001**, *8* (10), 1157-1179.

(74) Wang, X.; Feng, M.; Xiao, L.; Tong, A.; Xiang, Y. Postsynthetic modification of DNA phosphodiester backbone for photocaged DNAzyme. *ACS Chem. Biol.* **2016**, *11* (2), 444-451.

(75) Grünweller, A.; Wyszko, E.; Bieber, B.; Jahnel, R.; Erdmann, V. A.; Kurreck, J. Comparison of different antisense strategies in mammalian cells using locked nucleic acids, 2′-O-methyl RNA, phosphorothioates and small interfering RNA. *Nucleic Acids Res.* **2003**, *31* (12), 3185-3193.

(76) Murray, A. W.; Atkinson, M. R. Biochemistry. **1968**, *7*, 4023–4029.

(77) Potter, B. V.; Connolly, B. A.; Eckstein, F. Synthesis and configurational analysis of a dinucleoside phosphate isotopically chiral at phosphorus. Stereochemical course of Penicillium citrinum nuclease P1 reaction. *Biochemistry* **1983**, *22* (6), 1369-1377.

(78) Wan, W. B.; Migawa, M. T.; Vasquez, G.; Murray, H. M.; Nichols, J. G.; Gaus, H.; Berdeja, A.; Lee, S.; Hart, C. E.; Lima, W. F. Synthesis, biophysical properties and biological activity of second generation antisense oligonucleotides containing chiral phosphorothioate linkages. *Nucleic Acids Res.* **2014**, *42* (22), 13456-13468.

(79) Nukaga, Y.; Yamada, K.; Ogata, T.; Oka, N.; Wada, T. Stereocontrolled solid-phase synthesis of phosphorothioate oligoribonucleotides using 2′-O-(2-cyanoethoxymethyl)-nucleoside 3′-O-oxazaphospholidine monomers. *J. Org. Chem.* **2012**, *77* (18), 7913-7922.

(80) Iwamoto, N.; Butler, D.; Svrzikapa, N.; Mohapatra, S.; Zlatev, I.; Sah, D. W. Y.; Meena; Standley, S. M.; Lu, G.; Apponi, L. H.; Frank-Kamenetsky, M.; Zhang, J.; Vargeese, C.; Verdine. G. L. Control of phosphorothioate stereochemistry substantially increases the efficacy of antisense oligonucleotides. *Nat. Biotechnol.* **2017**, *35*, 845-851.

(81) Lochmann, D.; Jauk, E.; Zimmer, A. Drug delivery of oligonucleotides by peptides. *Eur. J. Pharm. Biopharm.* **2004**, *58* (2), 237-251.

(82) Yèagle, P. L. Lipid regulation of cell membrane structure and function. *The FASEB J.* **1989**, *3* (7), 1833-1842.

(83) Baker, Y. R.; Thorpe, C.; Chen, J.; Poller, L. M.; Cox, L.; Kumar, P.; Lim, W. F.; Lie, L.; McClorey, G.; Epple, S.; et al. An LNA-amide modification that enhances the cell uptake and activity of phosphorothioate exon-skipping oligonucleotides. *Nat. Comm.* **2022**, *13* (1), 4036.

(84) Fujino, T.; Yamazaki, N.; Isobe, H. Convergent synthesis of oligomers of triazole-linked DNA analogue (TLDNA) in solution phase. *Tetrahedron Lett.* **2009**, *50* (28), 4101-4103.

(85) Isobe, H.; Fujino, T.; Yamazaki, N.; Guillot-Nieckowski, M.; Nakamura, E. Triazole-linked analogue of deoxyribonucleic acid (TLDNA): Design, synthesis, and double-strand formation with natural DNA. *Org. Lett.* **2008**, *10* (17), 3729-3732.

(86) El-Sagheer, A. H.; Brown, T. A triazole linkage that mimics the DNA phosphodiester group in living systems. *Q. Rev. Biophys.* **2015**, *48* (4), 429-436.

(87) Birts, C. N.; Sanzone, A. P.; El-Sagheer, A. H.; Blaydes, J. P.; Brown, T.; Tavassoli, A. Transcription of click-linked DNA in human cells. *Angew. Chem.* **2014**, *53* (9), 2362-2365.

(88) El-Sagheer, A. H.; Brown, T. Efficient RNA synthesis by in vitro transcription of a triazole-modified DNA template. *Chem. Comm.* **2011**, *47* (44), 12057-12058.

(89) Kukwikila, M.; Gale, N.; El-Sagheer, A. H.; Brown, T.; Tavassoli, A. Assembly of a biocompatible triazole-linked gene by one-pot click-DNA ligation. *Nat. Chem.* **2017**, *9* (11), 1089-1098.

(90) Taemaitree, L.; Shivalingam, A.; El-Sagheer, A. H.; Brown, T. An artificial triazole backbone linkage provides a split-and-click strategy to bioactive chemically modified CRISPR sgRNA. *Nat. Comm.* **2019**, *10* (1), 1-8.

(91) Crooke, S. T.; Geary, R. S. Clinical pharmacological properties of mipomersen (Kynamro), a second generation antisense inhibitor of apolipoprotein B. *Br. J. Clin. Pharmacol.* **2013**, *76* (2), 269-276.

(92) Obika, S.; Onoda, M.; Morita, K.; Andoh, J.-i.; Koizumi, M.; Imanishi, T. 3′-Amino-2′, 4′-BNA: novel bridged nucleic acids having an N3′→ P5′ phosphoramidate linkage. *Chem. Comm.* **2001**, (19), 1992-1993.

(93) Obika, S.; Nanbu, D.; Hari, Y.; Morio, K.-i.; In, Y.; Ishida, T.; Imanishi, T. Synthesis of 2′-O, 4′-C-methyleneuridine and-cytidine. Novel bicyclic nucleosides having a fixed C3,-endo sugar puckering. *Tetrahedron Lett.* **1997**, *38* (50), 8735-8738.

(94) Koshkin, A. A.; Singh, S. K.; Nielsen, P.; Rajwanshi, V. K.; Kumar, R.; Meldgaard, M.; Olsen, C. E.; Wengel, J. LNA (Locked Nucleic Acids): Synthesis of the adenine, cytosine, guanine, 5-methylcytosine, thymine and uracil bicyclonucleoside monomers, oligomerisation, and unprecedented nucleic acid recognition. *Tetrahedron* **1998**, *54* (14), 3607-3630.

(95) Singh, S. K.; Koshkin, A. A.; Wengel, J.; Nielsen, P. LNA (locked nucleic acids): synthesis and high-affinity nucleic acid recognition. *Chem. Comm.* **1998**, (4), 455-456.

(96) Petersen, M.; Nielsen, C. B.; Nielsen, K. E.; Jensen, G. A.; Bondensgaard, K.; Singh, S. K.; Rajwanshi, V. K.; Koshkin, A. A.; Dahl, B. M.; Wengel, J. The conformations of locked nucleic acids (LNA). *J. Mol. Recognit.* **2000**, *13* (1), 44-53.

(97) Petersen, M.; Bondensgarrd, K.; Wengel, J; Jacobsen, J. P. Locked Nucleic Acid (LNA) Recognition of RNA: NMR Solution Structures of LNA:RNA Hybrids. *J. Am. Chem. Soc.* **2002**, *124* (21), 5874-5982.

(98) Burel, S. A.; Hart, C. E.; Cauntay, P.; Hsiao, J.; Machemer, T.; Katz, M.; Watt, A.; Bui, H.-h.; Younis, H.; Sabripour, M. Hepatotoxicity of high affinity gapmer antisense oligonucleotides is mediated by RNase H1 dependent promiscuous reduction of very long pre-mRNA transcripts. *Nucleic Acids Res.* **2016**, *44* (5), 2093-2109.

(99) Wahlestedt, C.; Salmi, P.; Good, L.; Kela, J.; Johnsson, T.; Hökfelt, T.; Broberger, C.; Porreca, F.; Lai, J.; Ren, K. Potent and nontoxic antisense oligonucleotides containing locked nucleic acids. *Proc. Natl. Acad. Sci.* **2000**, *97* (10), 5633-5638.

(100) Fluiter, K.; Mook, O. R.; Vreijling, J.; Langkjær, N.; Højland, T.; Wengel, J.; Baas, F. Filling the gap in LNA antisense oligo gapmers: the effects of unlocked nucleic acid (UNA) and 4′-C-hydroxymethyl-DNA modifications on RNase H recruitment and efficacy of an LNA gapmer. *Mol. BioSyst.* **2009**, *5* (8), 838-843.

(101) Ørum, H.; Wolter, A.; Kongsbak, L. Locked nucleic acids (LNA) and medical applications. *Lett. Pept. Sci.***2003**, *10* (3), 325-334.

(102) Kuwahara, M.; Obika, S.; Nagashima, J. i.; Ohta, Y.; Suto, Y.; Ozaki, H.; Sawai, H.; Imanishi, T. Systematic analysis of enzymatic DNA polymerization using oligo-DNA templates and triphosphate analogs involving 2′, 4′-bridged nucleosides. *Nucleic Acids Res.* **2008**, *36* (13), 4257-4265.

(103) Cromwell, C. R.; Sung, K.; Park, J.; Krysler, A. R.; Jovel, J.; Kim, S. K.; Hubbard, B. P. Incorporation of bridged nucleic acids into CRISPR RNAs improves Cas9 endonuclease specificity. *Nat. Comm.* **2018**, *9* (1), 1-11.

(104) Askari, F. K.; McDonnell, W. M. Antisense-oligonucleotide therapy. *N. Engl. J. Med.* **1996**, *334* (5), 316-318.

(105) Rossor, A. M.; Reilly, M. M.; Sleigh, J. N. Antisense oligonucleotides and other genetic therapies made simple. *Pract. Neurol.* **2018**, *18* (2), 126-131.

(106) Bajan, S.; Hutvagner, G. RNA-based therapeutics: from antisense oligonucleotides to miRNAs. *Cells* **2020**, *9* (1), 137.

(107) Kurreck, J. Antisense technologies: improvement through novel chemical modifications. *Eur. J. Biochem.* **2003**, *270* (8), 1628-1644.

(108) Zamecnik, P. C.; Stephenson, M. L. Inhibition of Rous sarcoma virus replication and cell transformation by a specific oligodeoxynucleotide. *Proc. Natl. Acad. Sci.* **1978**, *75* (1), 280-284.

(109) Elbashir, S. M.; Harborth, J.; Lendeckel, W.; Yalcin, A.; Weber, K.; Tuschl, T. Duplexes of 21-nucleotide RNAs mediate RNA interference in cultured mammalian cells. *nature* **2001**, *411* (6836), 494-498.

(110) Kole, R.; Krainer, A. R.; Altman, S. RNA therapeutics: beyond RNA interference and antisense oligonucleotides. *Nat. Rev. Drug Discov.* **2012**, *11* (2), 125-140.

(111) Stein, C. The experimental use of antisense oligonucleotides: a guide for the perplexed. *J. Clin. Investig.* **2001**, *108* (5), 641-644.

(112) Johnson, R. E.; Prakash, L.; Prakash, S. Biochemical evidence for the requirement of Hoogsteen base pairing for replication by human DNA polymerase ι. *Proc. Natl. Acad. Sci.* **2005**, *102* (30), 10466-10471.

(113) Dove, A. Antisense and sensibility. *Nat. Biotechnol.* **2002**, *20* (2), 121-124.

(114) Deleavey, Glen F.; Damha, Masad J. Designing Chemically Modified Oligonucleotides for Targeted Gene Silencing. *Chem.Biol.* **2012**, *19* (8), 937-954.

(115) Mutisya, D.; Selvam, C.; Lunstad, B. D.; Pallan, P. S.; Haas, A.; Leake, D.; Egli, M.; Rozners, E. Amides are excellent mimics of phosphate internucleoside linkages and are well tolerated in short interfering RNAs. *Nucleic Acids Res.* **2014**, *42* (10), 6542-6551.

(116) Janas, M. M.; Schlegel, M. K.; Harbison, C. E.; Yilmaz, V. O.; Jiang, Y.; Parmar, R.; Zlatev, I.; Castoreno, A.; Xu, H.; Shulga-Morskaya, S. Selection of GalNAc-conjugated siRNAs with limited off-target-driven rat hepatotoxicity. *Nat. Comm.* **2018**, *9* (1), 1-10.

(117) De Clercq, E.; Eckstein, F.; Merigan, T. Interferon induction increased through chemical modification of a synthetic polyribonucleotide. *Science* **1969**, *165* (3898), 1137-1139.

(118) Eckstein, F. Phosphorothioate oligodeoxynucleotides: what is their origin and what is unique about them? *Antisense Nucleic Acid Drug Dev.* **2000**, *10* (2), 117-121.

(119) Stec, W. J.; Zon, G.; Uznański, B. Reversed-phase high-performance liquid chromatographic separation of diastereomeric phosphorothioate analogues of oligodeoxyribonucleotides and other backbone-modified congeners of DNA. *J. Chromatogr. A.* **1985**, *326*, 263-280.

(120) Cruse, W.; Salisbury, S.; Brown, T.; Cosstick, R.; Eckstein, F.; Kennard, O. Chiral phosphorothioate analogues of B-DNA: The crystal structure of Rp-d¦ Gp (S) CpGp (S) CpGp (S) C¦. *J. Mol. Biol* **1986**, *192* (4), 891-905.

(121) Bachelin, M.; Hessler, G.; Kurz, G.; Hacia, J.; Dervan, P.; Kessler, H. Structure of a stereoregular phosphorothioate DNA/RNA duplex. *Nat. Struct. Biol* **1998**, *5* (4), 271-276.

(122) Furrer, P.; Billeci, T. M.; Donati, A.; Kojima, C.; Karwowski, B.; Sierzchala, A.; Stec, W.; James, T. L. Structural effect of complete [Rp]-phosphorothioate and phosphorodithioate substitutions in the DNA strand of a model antisense inhibitor-target RNA complex. *J. Mol. Biol* **1999**, *285* (4), 1609-1622.

(123) Agrawal, S.; Goodchild, J.; Civeira, M. P.; Thornton, A. H.; Sarin, P. S.; Zamecnik, P. C. Oligodeoxynucleoside phosphoramidates and phosphorothioates as inhibitors of human immunodeficiency virus. *Proc. Natl. Acad. Sci.* **1988**, *85* (19), 7079-7083.

(124) Matsukura, M.; Shinozuka, K.; Zon, G.; Mitsuya, H.; Reitz, M.; Cohen, J. S.; Broder, S. Phosphorothioate analogs of oligodeoxynucleotides: inhibitors of replication and cytopathic effects of human immunodeficiency virus. *Proc. Natl. Acad. Sci.* **1987**, *84* (21), 7706-7710.

(125) Spitzer, S.; Eckstein, F. Inhibition of deoxyribonucleases by phosphorothioate groups in oligodeoxyribonucleotides. *Nucleic Acids Res.* **1988**, *16* (24), 11691-11704.

(126) Crooke, S. T. Progress in antisense technology: the end of the beginning. *Meth. Enzymol.* **2000**, *313*, 3-45.

(127) Brautigam, C. A.; Steitz, T. A. Structural principles for the inhibition of the 3′-5′ exonuclease activity of Escherichia coli DNA polymerase I by phosphorothioates. *J. Mol. Biol.* **1998**, *277* (2), 363-377.

(128) LEE, M.; SIMON, A. D.; Stein, C.; RABBANI, L. E. Antisense strategies to inhibit restenosis. *Antisense Nucleic Acid Drug Dev.* **1999**, *9* (5), 487-492.

(129) Campbell, J. M.; Bacon, T. A.; Wickstrom, E. Oligodeoxynucleoside phosphorothioate stability in subcellular extracts, culture media, sera and cerebrospinal fluid. *J. Biochem. Biophys. Methods* **1990**, *20* (3), 259-267.

(130) Yang, L.; Niu, H.; Gao, X.; Wang, Q.; Han, G.; Cao, L.; Cai, C.; Weiler, J.; Yin, H. Effective exon skipping and dystrophin restoration by 2′-*O*-methoxyethyl antisense oligonucleotide in dystrophin-deficient mice. *PLoS One* **2013**, *8* (4), e61584.

(131) Maruyama, R.; Yokota, T. Knocking down long noncoding RNAs using antisense oligonucleotide gapmers. *Gapmers* **2020**, 49-56.

(132) Crooke, S. T.; Lemonidis, K. M.; Neilson, L.; Griffey, R.; Lesnik, E. A.; Monia, B. P. Kinetic characteristics of Escherichia coli RNase H1: cleavage of various antisense oligonucleotide-RNA duplexes. *Biochem. J.* **1995**, *312* (2), 599-608.

(133) Zamaratski, E.; Pradeepkumar, P.; Chattopadhyaya, J. A critical survey of the structure-function of the antisense oligo/RNA heteroduplex as substrate for RNase H. *J. Biochem. Biophys. Methods* **2001**, *48* (3), 189-208.

(134) Monia, B. P.; Lesnik, E.; Gonzalez, C.; Lima, W. F.; McGee, D.; Guinosso, C. J.; Kawasaki, A. M.; Cook, P. D.; Freier, S. M. Evaluation of 2′-modified oligonucleotides containing 2′-deoxy gaps as antisense inhibitors of gene expression. *J. Biol. Chem.* **1993**, *268* (19), 14514-14522.

(135) Narenji, H.; Gholizadeh, P.; Aghazadeh, M.; Rezaee, M. A.; Asgharzadeh, M.; Kafil, H. S. Peptide nucleic acids (PNAs): currently potential bactericidal agents. *Biomed. Pharmacother.* **2017**, *93*, 580-588.

(136) Gao, X.; Shen, X.; Dong, X.; Ran, N.; Han, G.; Cao, L.; Gu, B.; Yin, H. Peptide Nucleic Acid Promotes Systemic Dystrophin Expression and Functional Rescue in Dystrophin-deficient mdx Mice. *Mol. Ther. Nucleic Acids* **2015**, *4* (10), e255.

(137) Matray, T. J.; Gryaznov, S. M. Synthesis and properties of RNA analogs—oligoribonucleotide N3′→ P5′ phosphoramidates. *Nucleic Acids Res.* **1999**, *27* (20), 3976-3985.

(138) Gryaznov, S.; Chen, J.-K. Oligodeoxyribonucleotide N3'. fwdarw. P5'Phosphoramidates: synthesis and Hybridization Properties. *J. Am. Chem. Soc.* **1994**, *116* (7), 3143-3144.

(139) Skorski, T.; Perrotti, D.; Nieborowska-Skorska, M.; Gryaznov, S.; Calabretta, B. Antileukemia effect of c-myc N3′→ P5′ phosphoramidate antisense oligonucleotides in vivo. *Proc. Natl. Acad. Sci.* **1997**, *94* (8), 3966-3971.

(140) Nielsen, P. E.; Egholm, M.; Berg, R. H.; Buchardt, O. Sequence-selective recognition of DNA by strand displacement with a thymine-substituted polyamide. *Science* **1991**, *254* (5037), 1497-1500.

(141) Nielsen, P. E. PNA technology. *Mol. Biotechnol.* **2004**, *26* (3), 233-248.

(142) Dueholm, K. L.; Egholm, M.; Behrens, C.; Christensen, L.; Hansen, H. F.; Vulpius, T.; Petersen, K. H.; Berg, R. H.; Nielsen, P. E.; Buchardt, O. Synthesis of peptide nucleic acid monomers containing the four natural nucleobases: thymine, cytosine, adenine, and guanine and their oligomerization. *J. Org. Chem.* **1994**, *59* (19), 5767-5773.

(143) Christensen, L.; Fitzpatrick, R.; Gildea, B.; Petersen, K. H.; Hansen, H. F.; Koch, T.; Egholm, M.; Buchardt, O.; Nielsen, P. E.; Coull, J. Solid-phase synthesis of peptide nucleic acids. *J. Pept. Sci.* **1995**, *1* (3), 175-183.

(144) Egholm, M.; Buchardt, O.; Christensen, L.; Behrens, C.; Freier, S. M.; Driver, D. A.; Berg, R. H.; Kim, S. K.; Norden, B.; Nielsen, P. E. PNA hybridizes to complementary oligonucleotides obeying the Watson–Crick hydrogen-bonding rules. *Nature* **1993**, *365* (6446), 566-568.

(145) Wittung, P.; Nielsen, P. E.; Buchardt, O.; Egholm, M. DNA-like double helix formed by peptide nucleic acid. *Nature* **1994**, *368* (6471), 561-563.

(146) Koppelhus, U.; Awasthi, S. K.; Zachar, V.; Holst, H. U.; Ebbesen, P.; Nielsen, P. E. Cell-dependent differential cellular uptake of PNA, peptides, and PNA-peptide conjugates. *Antisense Nucleic Acid Drug Dev.* **2002**, *12* (2), 51-63.

(147) Pooga, M.; Soomets, U.; Hällbrink, M.; Valkna, A.; Saar, K.; Rezaei, K.; Kahl, U.; Hao, J. X.; Xu, X. J.; Wiesenfeld-Hallin, Z. Cell penetrating PNA constructs regulate galanin receptor levels and modify pain transmission in vivo. *Nat. Biotechnol.* **1998**, *16* (9), 857-861.

(148) Cutrona, G.; Carpaneto, E. M.; Ulivi, M.; Roncella, S.; Landt, O.; Ferrarini, M.; Boffa, L. C. Effects in live cells of a c-myc anti-gene PNA linked to a nuclear localization signal. *Nat. Biotechnol.* **2000**, *18* (3), 300-303.

(149) Karras, J. G.; Maier, M. A.; Lu, T.; Watt, A.; Manoharan, M. Peptide nucleic acids are potent modulators of endogenous pre-mRNA splicing of the murine interleukin-5 receptor-α chain. *Biochemistry* **2001**, *40* (26), 7853-7859.

(150) Herbert, B.-S.; Pitts, A.; Baker, S.; Hamilton, S.; Wright, W.; Shay, J.; Corey, D. Inhibition of human telomerase in immortal human cells leads to progressive telomere shortening and cell death. *Proc. Natl. Acad. Sci.* **1999**, *96* (25), 14276-14281.

(151) Knudsen, H.; Nielsen, P. E. Antisense properties of duplex-and triplex-forming PNAs. *Nucleic Acids Res.* **1996**, *24* (3), 494-500.

(152) Sazani, P.; Kang, S.-H.; Maier, M. A.; Wei, C.; Dillman, J.; Summerton, J.; Manoharan, M.; Kole, R. Nuclear antisense effects of neutral, anionic and cationic oligonucleotide analogs. *Nucleic Acids Res.* **2001**, *29* (19), 3965-3974.

(153) McMahon, B. M.; Mays, D.; Lipsky, J.; Stewart, J. A.; Fauq, A.; Richelson, E. Pharmacokinetics and tissue distribution of a peptide nucleic acid after intravenous administration. *Antisense Nucleic Acid Drug Dev.* **2002**, *12* (2), 65-70.

(154) Sazani, P.; Gemignani, F.; Kang, S.-H.; Maier, M. A.; Manoharan, M.; Persmark, M.; Bortner, D.; Kole, R. Systemically delivered antisense oligomers upregulate gene expression in mouse tissues. *Nat. Biotechnol.* **2002**, *20* (12), 1228-1233.

(155) Summerton, J.; Weller, D. Morpholino antisense oligomers: design, preparation, and properties. *Antisense Nucleic Acid Drug Dev.* **1997**, *7* (3), 187-195.

(156) Kang, H.; Chou, P. J.; Johnson JR, W. C.; Weller, D.; Huang, S. B.; Summerton, J. E. Stacking interactions of ApA analogues with modified backbones. *Biopolymers* **1992**, *32* (10), 1351-1363.

(157) Taylor, M. F.; Paulauskis, J. D.; Weller, D. D.; Kobzik, L. In vitro efficacy of morpholino-modified antisense oligomers directed against tumor necrosis factor-α mRNA. *J. Biol. Chem.* **1996**, *271* (29), 17445-17452.

(158) Heasman, J. Morpholino oligos: making sense of antisense? *Dev. Biol.* **2002**, *243* (2), 209-214.

(159) Chiba, A.; Kusunoki, S.; Obata, H.; Machinami, R.; Kanazawa, I. Serum anti-GQ1b IgG antibody is associated with ophthalmoplegia in Miller Fisher syndrome and Guillain-Barré syndrome: clinical and immunohistochemical studies. *Neurology* **1993**, *43* (10), 1911-1911.

(160) Geary, R. S.; Baker, B. F.; Crooke, S. T. Clinical and preclinical pharmacokinetics and pharmacodynamics of mipomersen (Kynamro®): a second-generation antisense oligonucleotide inhibitor of apolipoprotein B. *Clin. Pharmacokinet.* **2015**, *54* (2), 133-146.

(161) Goldberg, E. W. a. T. Mipomersen (Kynamro)

A Novel Antisense Oligonucleotide Inhibitor for the Management of Homozygous Familial Hypercholesterolemia. *Drug Forecast* **2014**, *39*, 119–122.

(162) Aartsma-Rus, A. FDA approval of nusinersen for spinal muscular atrophy makes 2016 the year of splice modulating oligonucleotides. *Nucleic Acid Ther.* **2017**, *27* (2), 67-69.

(163) Edinoff, A. N.; Nguyen, L. H.; Odisho, A. S.; Maxey, B. S.; Pruitt, J. W.; Girma, B.; Cornett, E. M.; Kaye, A. M.; Kaye, A. D. The Antisense Oligonucleotide Nusinersen for Treatment of Spinal Muscular Atrophy. *Orthop Rev. (Pavia)* **2021**, *13* (2), 24934.

(164) Keam, S. J. Inotersen: first global approval. *Drugs* **2018**, *78* (13), 1371-1376.

(165) Aartsma-Rus, A.; Krieg, A. M. FDA approves eteplirsen for Duchenne muscular dystrophy: the next chapter in the eteplirsen saga. *Nucleic Acid Ther.* **2017**, *27* (1), 1-3.

(166) Lim, K. R. Q.; Maruyama, R.; Yokota, T. Eteplirsen in the treatment of Duchenne muscular dystrophy. *Drug Des. Devel. Ther.***2017**, *11*, 533-545.

(167) Urits, I.; Swanson, D.; Swett, M. C.; Patel, A.; Berardino, K.; Amgalan, A.; Berger, A. A.; Kassem, H.; Kaye, A. D.; Viswanath, O. A Review of Patisiran (ONPATTRO®) for the Treatment of Polyneuropathy in People with Hereditary Transthyretin Amyloidosis. *Neurol. Ther.* **2020**, *9* (2), 301-315.

(168) Weng, Y.; Xiao, H.; Zhang, J.; Liang, X. J.; Huang, Y. RNAi therapeutic and its innovative biotechnological evolution. *Biotechnol. Adv.* **2019**, *37* (5), 801-825.

(169) Dong, Y.; Siegwart, D. J.; Anderson, D. G. Strategies, design, and chemistry in siRNA delivery systems. *Adv. Drug Deliv. Rev.* **2019**, *144*, 133-147.

(170) Setten, R. L.; Rossi, J. J.; Han, S. P. The current state and future directions of RNAi-based therapeutics. *Nat. Rev. Drug Discov.* **2019**, *18* (6), 421-446.

(171) Migliorati, J. M.; Jin, J.; Zhong, X. b. siRNA drug Leqvio (inclisiran) to lower cholesterol. *Trends Pharmacol. Sci.* **2022**, *43* (5), 455-456.

(172) Lamb, Y. N. Inclisiran: First Approval. *Drugs* **2021**, *81* (3), 389-395.

(173) Nair, J. K.; Willoughby, J. L.; Chan, A.; Charisse, K.; Alam, M. R.; Wang, Q.; Hoekstra, M.; Kandasamy, P.; Kel'in, A. V.; Milstein, S. Multivalent N-acetylgalactosamine-conjugated siRNA localizes in hepatocytes and elicits robust RNAi-mediated gene silencing. *J. Am. Chem. Soc.* **2014**, *136* (49), 16958-16961.

(174) Team, R. Inclisiran (Leqvio). *Can. J. Health Technol.* **2022**, *2* (4).

(175) Shendure, J.; Ji, H. Next-generation DNA sequencing. *Nat. Biotechnol.* **2008**, *26* (10), 1135-1145.

(176) Lee, L. G.; Chen, C. H.; Chiu, L. A. Thiazole orange - A new dye for reticulocyte analysis. *Cytometry* **1986**, *7* (6), 508-517

(177) Nygren, J.; Svanvik, N.; Kubista, M. The interactions between the fluorescent dye thiazole orange and DNA. *Biopolymers* **1998**, *46* (1), 39-51.

(178) Hövelmann, F.; Gaspar, I.; Ephrussi, A.; Seitz, O. Brightness Enhanced DNA FIT-Probes for Wash-Free RNA Imaging in Tissue. *J. Am. Chem. Soc.* **2013**, *135* (50), 19025-19032.

(179) Socher, E.; Knoll, A.; Seitz, O. Dual fluorophore PNA FIT-probes--extremely responsive and bright hybridization probes for the sensitive detection of DNA and RNA. *Org. Biomol. Chem.* **2012**, *10* (36), 7363-7371.

(180) Fang, G. M.; Chamiolo, J.; Kankowski, S.; Hovelmann, F.; Friedrich, D.; Lower, A.; Meier, J. C.; Seitz, O. A bright FIT-PNA hybridization probe for the hybridization state specific analysis of a C --> U RNA edit via FRET in a binary system. *Chem. Sci.* **2018**, *9* (21), 4794-4800.

(181) Holzhauser, C.; Liebl, R.; Goepferich, A.; Wagenknecht, H.-A.; Breunig, M. RNA "Traffic Lights": An Analytical Tool to Monitor siRNA Integrity. *ACS Chem. Biol.* **2013**, *8* (5), 890-894.

(182) Ikeda, S.; Kubota, T.; Wang, D. O.; Yanagisawa, H.; Yuki, M.; Okamoto, A. Emission control by binary energy transfer processes on oligouridine. *Org. Biomol. Chem.* **2011**, *9* (19), 6598-6603.

(183) Klimkowski, P.; De Ornellas, S.; Singleton, D.; El-Sagheer, A. H.; Brown, T. Design of thiazole orange oligonucleotide probes for detection of DNA and RNA by fluorescence and duplex melting. *Org. Biomol. Chem.* **2019**, *17* (24), 5943-5950.

(184) Karunakaran, V.; Pérez Lustres, J. L.; Zhao, L.; Ernsting, N. P.; Seitz, O. Large Dynamic Stokes Shift of DNA Intercalation Dye Thiazole Orange has Contribution from a High-Frequency Mode. *J. Am. Chem. Soc.* **2006**, *128* (9), 2954-2962.

(185) Suss, O.; Motiei, L.; David. Broad Applications of Thiazole Orange in Fluorescent Sensing of Biomolecules and Ions. *Molecules* **2021**, *26* (9).

(186) Lu, Q.; Zhou, Z.; Mei, Y.; Wei, W.; Liu, S. Detection of DNA damage by thiazole orange fluorescence probe assisted with exonuclease III. *Talanta* **2013**, *116*, 958-963.

(187) Kimura, Y.; Hanami, T.; Tanaka, Y.; de Hoon, M. J. L.; Soma, T.; Harbers, M.; Lezhava, A.; Hayashizaki, Y.; Usui, K. Effect of Thiazole Orange Doubly Labeled Thymidine on DNA Duplex Formation. *Biochemistry* **2012**, *51* (31), 6056-6067.

(188) Bethge, L.; Singh, I.; Seitz, O. Designed thiazole orange nucleotides for the synthesis of single labelled oligonucleotides that fluoresce upon matched hybridization. *Org. Biomol. Chem.* **2010**, *8* (10), 2439-2448.

(189) Berndl, S.; Wagenknecht, H. A. Fluorescent Color Readout of DNA Hybridization with Thiazole Orange as an Artificial DNA Base. *Angew. Chem. Int. Ed.* **2009**, *48* (13), 2418-2421.

(190) Ikeda, S.; Kubota, T.; Kino, K.; Okamoto, A. Sequence dependence of fluorescence emission and quenching of doubly thiazole orange labeled DNA: Effective design of a hybridization-sensitive probe. *Bioconjugate Chem.* **2008**, *19* (8), 1719-1725.

(191) Kohler, O.; Venkatrao, D.; Jarikote, D. V.; Seitz, O. Forced intercalation probes (FIT probes): Thiazole orange as a fluorescent base in peptide nucleic acids for homogeneous single-nucleotide-polymorphism detection. *Chembiochem* **2005**, *6* (1), 69-77.

(192) Jarikote, D. V.; Kohler, O.; Socher, E.; Seitz, O. Divergent and linear solid-phase synthesis of PNA containing thiazole orange as artificial base. *Eur. J. Org. Chem.* **2005**, (15), 3187-3195.

(193) Privat, E.; Melvin, T.; Merola, F.; Schweizer, G.; Prodhomme, S.; Asseline, U.; Vigny, P. Fluorescent properties of oligonucleotide-conjugated thiazole orange probes. *Photochem. Photobiol.* **2002**, *75* (3), 201-210.

(194) Fang, G. M.; Chamiolo, J.; Kankowski, S.; Hovelmann, F.; Friedrich, D.; Lower, A.; Meier, J. C.; Seitz, O. A bright FIT-PNA hybridization probe for the hybridization state specific analysis of a C -> U RNA edit via FRET in a binary system. *Chem. Sci.* **2018**, *9* (21), 4794-4800.

(195) Qiu, J. Q.; Wilson, A.; El-Sagheer, A. H.; Brown, T. Combination probes with intercalating anchors and proximal fluorophores for DNA and RNA detection. *Nucleic Acids Res.* **2016**, *44* (17).

(196) Chamiolo, J.; Fang, G. M.; Hovelmann, F.; Friedrich, D.; Knoll, A.; Loewer, A.; Seitz, O. Comparing Agent-Based Delivery of DNA and PNA Forced Intercalation (FIT) Probes for Multicolor mRNA Imaging. *Chembiochem* **2019**, *20* (4), 595-604.

(197) Bai, C.; Klimkowski, P.; Jin, C.; Kuchlyan, J.; El-Sagheer, A. H.; Brown, T. A new phosphoramidite enables orthogonal double labelling to form combination oligonucleotide probes. *Org. Biomol. Chem.* **2022**, *20* (44), 8618-8622.

(198) Milelli, A.; Marchetti, C.; Greco, M. L.; Moraca, F.; Costa, G.; Turrini, E.; Catanzaro, E.; Betari, N.; Calcabrini, C.; Sissi, C.; et al. Naphthalene diimide-polyamine hybrids as antiproliferative agents: Focus on the architecture of the polyamine chains. *Eur. J. Med. Chem.* **2017**, *128*, 107-122.

(199) Franzini, R. M.; Kool, E. T. Efficient Nucleic Acid Detection by Templated Reductive Quencher Release. *J. Am. Chem. Soc.* **2009**, *131* (44), 16021.

(200) Blommers, M. J.; Natt, F.; Jahnke, W.; Cuenoud, B. Dual recognition of double-stranded DNA by 2 ‘-aminoethoxy-modified oligonucleotides: the solution structure of an intramolecular triplex obtained by NMR spectroscopy. *Biochemistry* **1998**, *37* (51), 17714-17725.

(201) Uhlmann, E.; Peyman, A. Antisense oligonucleotides: a new therapeutic principle. *Chem. Rev.* **1990**, *90* (4), 543-584.

(202) Maruyama, R.; Yokota, T. J. G. Knocking down long noncoding RNAs using antisense oligonucleotide. *Gapmers* **2020**, 49-56.

(203) Chen, S.; Le, B. T.; Chakravarthy, M.; Kosbar, T. R.; Veedu, R. N. J. S. r. Systematic evaluation of 2′-Fluoro modified chimeric antisense oligonucleotide-mediated exon skipping in vitro. *Sci. Rep.* **2019**, *9* (1), 1-10.

(204) Socher, E.; Seitz, O. FIT-Probes in Real-Time PCR. *Molecular Beacons: Signalling Nucleic Acid Probes, Methods, and Protocols* **2008**, 187-197.

(205) Milelli, A.; Marchetti, C.; Greco, M. L.; Moraca, F.; Costa, G.; Turrini, E.; Catanzaro, E.; Betari, N.; Calcabrini, C.; Sissi, C. J. E. J. o. M. C. Naphthalene diimide-polyamine hybrids as antiproliferative agents: Focus on the architecture of the polyamine chains. *Eur. J. Med. Chem.* **2017**, *128*, 107-122.

(206) Velavan, T. P.; Meyer, C. G. The COVID-19 epidemic. *Trop. Med. Int. Health* **2020**, *25* (3), 278.

(207) Francois, P.; Tangomo, M.; Hibbs, J.; Bonetti, E.-J.; Boehme, C. C.; Notomi, T.; Perkins, M. D.; Schrenzel, J. Robustness of a loop-mediated isothermal amplification reaction for diagnostic applications. *FEMS Immunol. Med. Microbiol.* **2011**, *62* (1), 41-48.

(208) Tsugunori Notomi, H. O., Harumi Masubuchi, Toshihiro Yonekawa, Keiko Watanabe, Nobuyuki Amino, Tetsu Hase. Loop-mediated isothermal amplification of DNA. *Nucleic Acids Res.* **2000**, *28* (12), e63.

(209) Hardinge, P.; Murray, J. A. H. Full Dynamic Range Quantification using Loop-mediated Amplification (LAMP) by Combining Analysis of Amplification Timing and Variance between Replicates at Low Copy Number. *Sci. Rep.* **2020**, *10* (1), 916.

(210) Carter, J. G.; Orueta Iturbe, L.; Duprey, J. L. H. A.; Carter, I. R.; Southern, C. D.; Rana, M.; Whalley, C. M.; Bosworth, A.; Beggs, A. D.; Hicks, M. R.; et al. Ultrarapid detection of SARS-CoV-2 RNA using a reverse transcription–free exponential amplification reaction, RTF-EXPAR. *Proc. Natl. Acad. Sci.* **2021**, 118 (35).

(211) El-Tholoth, M.; Bau, H. H.; Song, J. A single and two-stage, closed-tube, molecular test for the 2019 novel coronavirus (COVID-19) at home, clinic, and points of entry. *Anal. Chem.* **2021**, 93, 38, 13063–13071.

(212) Roundtree, I. A.; Evans, M. E.; Pan, T.; He, C. Dynamic RNA modifications in gene expression regulation. *Cell* **2017**, *169* (7), 1187-1200.

(213) Cummins, L.; Owens, S.; Risen, L.; Lesnik, E.; Freier, S.; McGee, D.; Guinosso, C.; Cook, P. Characterization of fully 2′-modified oligoribonucleotide hetero- and homoduplex hybridization and nuclease sensitivity. *Nucleic Acids Res.*, **1995**, *23* (11), 2019–2024

(214) Monia, B. P.; Johnston, J. F.; Sasmor, H.; Cummins, L. L. Nuclease resistance and antisense activity of modified oligonucleotides targeted to Ha-ras. *J. Biol. Chem.* **1996**, *271* (24), 14533-14540.

(215) Martin, P. Ein neuer Zugang zu 2′-O-Alkylribonucleosiden und Eigenschaften deren Oligonucleotide. *Helv. Chim. Acta.* **1995**, *78* (2), 486-504.

(216) El-Sagheer, A. H.; Brown, T. Click chemistry with DNA. *Chem. Soc. Rev.* **2010**, *39* (4), 1388-1405.

(217) Kumar, P.; El-Sagheer, A. H.; Truong, L.; Brown, T. Locked nucleic acid (LNA) enhances binding affinity of triazole-linked DNA towards RNA. *Chem. Comm.* **2017**, *53* (63), 8910-8913.

(218) Baker, Y. R.; Traoré, D.; Wanat, P.; Tyburn, A.; El-Sagheer, A. H.; Brown, T. Searching for the ideal triazole: Investigating the 1,5-triazole as a charge neutral DNA backbone mimic. *Tetr9hedron* **2020**, *76* (7).

(219) Lucas, R.; Neto, V.; Bouazza, A. H.; Zerrouki, R.; Granet, R.; Krausz, P.; Champavier, Y. Microwave-assisted synthesis of a triazole-linked 3′–5′ dithymidine using click chemistry. *Tetrahedron Lett.* **2008**, *49* (6), 1004-1007.

(220) Shivalingam, A.; Tyburn, A. E.; El-Sagheer, A. H.; Brown, T. Molecular requirements of high-fidelity replication-competent DNA backbones for orthogonal chemical ligation. *J. Am. Chem. Soc.* **2017**, *139* (4), 1575-1583.

(221) Varizhuk, A. M.; Kaluzhny, D. N.; Novikov, R. A.; Chizhov, A. O.; Smirnov, I. P.; Chuvilin, A. N.; Tatarinova, O. N.; Fisunov, G. Y.; Pozmogova, G. E.; Florentiev, V. L. Synthesis of triazole-linked oligonucleotides with high affinity to DNA complements and an analysis of their compatibility with biosystems. *J. Org. Chem.* **2013**, *78* (12), 5964-5969.

(222) Kauppinen, S.; Vester, B.; Wengel, J. Locked Nucleic Acid: High-Affinity Targeting of Complementary RNA for RNomics *RNA Towards Medicine* **2006**, 405-422.

(223) Nielsen, K. E.; Rasmussen, J.; Kumar, R.; Wengel, J.; Jacobsen, J. P.; Petersen, M. NMR Studies of Fully Modified Locked Nucleic Acid (LNA) Hybrids: Solution Structure of an LNA:RNA Hybrid and Characterization of an LNA:DNA Hybrid. *Bioconjugate Chem.* **2004**, *15* (3), 449–457.

(224) Kurreck, J.; Wyszko, E.; Gillen, C.; Erdmann, V. A. Design of antisense oligonucleotides stabilized by locked nucleic acids. *Nucleic Acids Res.* **2002**, *30* (9), 1911-1918.

(225) Braasch, D. A.; Jensen, S.; Liu, Y.; Kaur, K.; Arar, K.; White, M. A.; Corey, D. R. RNA interference in mammalian cells by chemically-modified RNA. *Biochemistry* **2003**, *42* (26), 7967-7975.

(226) Dess, D. B.; Martin, J. C. Readily accessible 12-I-5 oxidant for the conversion of primary and secondary alcohols to aldehydes and ketones. *J. Org. Chem.* **1983**, *48* (22), 4155-4156.

(227) Boeckman, R. J. 1,1,1-Triacetoxy-1,1-dihydro-1,2-benziodoxol-3(1*H*)-one. *Encyclopedia of Reagents for Organic Synthesis* **2009**.

(228) Varizhuk, A.; Chizhov, A.; Florentiev, V. Synthesis and hybridization data of oligonucleotide analogs with triazole internucleotide linkages, potential antiviral and antitumor agents. *Bioorg. Chem.* **2011**, *39* (3), 127-131.

(229) Koshkin, A. A.; Fensholdt, J.; Pfundheller, H. M.; Lomholt, C. A simplified and efficient route to 2′-O, 4′-C-methylene-linked bicyclic ribonucleosides (locked nucleic acid). *J. Org. Chem.* **2001**, *66* (25), 8504-8512.

(230) Vorbrüggen, H.; Krolikiewicz, K.; Bennua, B. Nucleoside syntheses, XXII1) Nucleoside synthesis with trimethylsilyl triflate and perchlorate as catalysts. *Chem. Ber.* **1981**, *114* (4), 1234-1255.

(231) Vorbrüggen, H.; Höfle, G. Nucleoside Syntheses, XXIII1) On the Mechanism of Nucleoside Synthesis. *Chem. Ber.* **1981**, *114* (4), 1256-1268.

(232) Vorbrüggen, H. Some recent trends and progress in nucleoside synthesis. *Acta. Biochim.Pol* **1996**, *43* (1), 25-36.

(233) Saudi, M.; Zmurko, J.; Kaptein, S.; Rozenski, J.; Neyts, J.; Van Aerschot, A. In search of Flavivirus inhibitors part 2: tritylated, diphenylmethylated and other alkylated nucleoside analogues. *Eur. J. Med. Chem.* **2014**, *76*, 98-109.

(234) Bürckstümmer, E.; Carell, T. Synthesis and properties of DNA containing a spore photoproduct analog. *Chem. Comm.* **2008**, (34), 4037-4039.